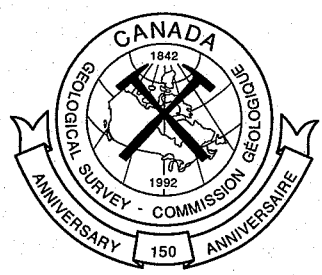

GEOLOGICAL SURVEY OF CANADA

OPEN FILE 2598

The failure behaviour of large rockslides in mountainous regions

O. Hungr, S.G. Evans

1993

Energy, Mines and Resources Canada
Énergie, Mines et Ressources Canada

Canada

THE FAILURE BEHAVIOUR OF LARGE ROCKSLIDES IN MOUNTAINOUS REGIONS

O. Hungr[1] and S.G. Evans[2]

[1] Thurber Engineering Ltd.
Vancouver, British Columbia

[2] Geological Survey of Canada
Ottawa, Ontario

PREFACE

An important element of the scientific program of the Geological Survey of Canada concerns evaluation of the risks to society posed by active geological process. In the geologically relatively young environment of Canada, the hazard of the failure of unstable slopes and resulting landslides is significant, particularly in the mountainous region of the Cordillera, in British Columbia, Yukon and Alberta.

The key to evaluating the hazard posed by landslides is the development of a thorough understanding of the geological processes that cause slopes to become unstable, and of the actual process of landsliding. One measure of our level of understanding of such complex processes is our ability to create models of them. In engineering geomorphology, such models are then tested against new case histories, in order to validate the models and to determine how robust they are.

The present report presents an examination of the behaviour of large rockslides. This work follows an earlier collaborative project in which the process of rockfall was modelled successfully (Hungr and Evans, 1989).

Reference

Hungr, O. and S.G. Evans
1989: Engineering aspects of rockfall hazards in Canada; Geological Survey of Canada, Open File Report 2061, 102 pp.

ACKNOWLEDGMENTS

The initial stages of the study were guided a steering committee, comprising A.S. Imrie and D.P. Moore (B.C. Hydro), J.A. Heginbottom (Geological Survey of Canada), G.C. Morgan (B.C. Ministry of Environment) and D. Smith (Thurber Engineering Ltd.).

Funding for the study was provided by B.C. Hydro and by the Government of Canada through the Geological Survey of Canada, Department of Energy, Mines and Resources, and through Emergency Preparedness Canada, Department of National Defence (both under DSS Contract 23397-9-0749/01-SZ, J.A. Heginbottom, scientific authority, A. Toren, DSS contracting officer).

The authors acknowledge the direct assistance of B.C. Hydro in providing case history data from its files. O. Hungr also acknowledges the contribution of valuable data and discussion provided by J.P. Aste, P. Antoine, J. Follacci, A. Malatrait and L. Selmi, of the Bureau de Recherches Géologiques et Minières, Lyon, France, and H. Moriwaki and N. Oyagi of National Institute for Disaster Prevention, Tsukuba City, Japan.

D. Smith, Thurber Engineering Ltd., as review principal read the whole report in draft and made many useful suggestions.

3

TABLE OF CONTENTS

ABSTRACT

A research project has been carried out to review the problematics of prediction of failure behaviour of large rockslides. Regional inventories of rock avalanches from various parts of the world are reviewed, indicating frequencies of occurrence of the order of 0.0002 to 0.002 cases per year per 10,000 km^2 of mountainous terrain. A tentative frequency-magnitude relationship is shown.

A comprehensive data base of the physical characteristics of large rockslides has been compiled. A description and User's Manual is presented in Appendix A. The purpose of the data base is to compile parameters describing rockslide case histories and their behaviour, and make them accessible to quantitative queries using relational data base technology. At present, there are 57 case histories in the data base and 240 bibliographic references.

A classification of rockslide failure mechanisms is proposed, which recognizes structural relationships controlling detachment. Together with the data base, this offers a framework for the empirical recognition of capability for catastrophic failure.

Descriptions of thirteen rockslide sites are given, which were examined in course of the project. The fieldwork involved a detailed re-examination of the Avalanche Lake case history in the Northwest Territories (Appendix C).

Dependence of rock avalanche runout on volume and the degree of lateral confinement is shown to result from geometrical similarities.

It is shown that dynamic block models of rock avalanche runout must be referenced to the centre of gravity of the moving mass. A new dynamic model based on the principles of both fluid mechanics and plasticity is described.

A detailed summary of conclusions and recommendations is presented in Chapter 5.

1. INTRODUCTION

1.1 Purpose

Large scale failures of mountain slopes are spectacular but rare accidents. Their potential for destruction of life and property is difficult to evaluate from historical records. For example, ten of the largest historic rockslide events in the Alps account for a total life loss of 7,000 to 10,000 (Eisbacher and Clague, 1984)*. But as many as 5,000 within those numbers are due to a single event (Mont Granier, France) which took place in 1248. A single rock avalanche event at Mount Huascaran, Peru in 1970 was the direct cause of as many as 18,000 deaths.

Material costs of individual rockslide disasters can be as high as $200 million (the 1987 cost of the Val Pola slide in Valtellina, Italy - French Ministry of Environment, unpublished). But many major events occur in unpopulated regions, without significant economic impact. The 1959 Pandemonium Creek slide in the Coast Ranges of British Columbia travelled for 8 km and devastated some 200 ha of valley floor area but remained virtually unnoticed by either the population or authorities (Evans et al., 1989).

The economic and social significance of large rockslide hazards in any area thus depends on population density and the presence of vulnerable reservoirs, plants and transportation lines. Both of these factors are rapidly changing in many parts of the world and this is certain to increase the future impact of rockslide hazards.

A variety of measures have been implemented around the world to reduce the damage from potential rockslide hazards (Table 1.1). Their costs have ranged as high as $50 million per site.

---

* See Bibliography in Appendix D.

Realistically, a prediction of large scale instability of a mountain slope can only be made when there are some signs that failure is already in progress. As a result, the design and implementation of remedial measures usually takes place within a limited time frame, if not under emergency conditions. For example, the highly successful evacuation of the runout zone of the Valtellina rock avalanche was carried out during only three days (Govi, 1989). Drainage of a rockslide along the Grande Maison reservoir in the French Alps by means of an adit and a network of drill holes was achieved in a period of only three months during reservoir filling (Prof. P. Antoine, pers. comm.). In British Columbia, a comprehensive investigation of slope movements at the Wahleach power station, and the consequent design of a relocated power tunnel took only 18 months.

Such remedial projects rely on an ability to predict the ultimate behaviour of the incipient landslide. As pointed out by Professor Govi (1989), this requires the knowledge of similar case histories which could serve as precedents, and the availability of reasonably reliable empirical or analytical models.

The present research project has an objective to synthesize the available means for practical prediction of the failure behaviour of large rockslides, including probability of occurrence, temporal predictability, potential for catastrophic failure and failure velocity and runout.

1.2 Scope and Definitions

The present project is concerned with well-defined gravitational movements of slopes in rock with magnitudes (volumes) of at least 1 million m^3 or deposit areas of at least 0.1 km^2 (c.f. Abele, 1974, p. 5). The geographic range is unlimited, because well-documented case histories are rare even in the worldwide context.

Slope deformations of uncertain origin or immature development are not considered. The selection criterion here is that a rockslide should have a distinct back scarp and lateral limits. Also excluded are failures

concurrent with volcanic eruptions and those dominated by glacial ice.

"Failure" is defined here as the single movement episode in the history of a landslide which had the highest velocities.

Rockslides whose failure involved high velocity motion as well as total disintegration of the rock mass are referred to as "rock avalanches" (simplified from Varnes, 1978). Cases which have not experienced high velocities or long displacements may either belong to the "slow rockslides" category, or may still be in a pre-failure stage. Distinction between the two alternatives is a major concern of this study. A few rare rockslide cases involved very high velocities with limited disintegration (e.g. the Vaiont slide of 1963). These may be termed simply "rapid rockslides".

Other terms are defined in the Glossary, Appendix E.

1.3 Method

The study consisted of the following tasks:

- Compilation of a data base suitable for the systematic collection, processing and retrieval of parameters associated with rockslide behaviour.
- Review of literature, to locate data describing case histories of large rockslides and review existing empirical/analytical models which could be used to make practical predictions of rockslide behaviour.
- Compilation of a computerized bibliography.
- Visits to fourteen sites of major rockslides in Canada and Europe in order to observe factors determining failure behaviour of typical rockslide cases.
- Definition of quantitative and descriptive parameters and classifications and investigation of correlations which connect these to predictions of failure and runout.

- Development of a dynamic model of rock avalanche runout.

1.4 Data Base of Rockslide Parameters

The purpose of the data base is to retain data which could have bearing on the failure behaviour of a rockslide and make it accessible to systematic queries, using quantitatively defined filter conditions.

Rockslide failure is a very complex, multi-dimensional process. Its full description requires a large number of parameters which cannot be easily reduced, without pre-judging their importance. The data base was therefore designed to allow as complete coverage of the full range of parameters as possible. At the same time, it is recognized that few case histories will provide a complete set of parameters and many data records may thus be only fractionally completed. A provision for recording the precision of numerical values has been incorporated.

A detailed description of the data base is given in the User's Manual, Appendix A. The manual is designed as a self-contained document, suitable for use by persons who may wish to use the data base without reading this report.

The data base consists of three parts:

1) The bibliography file (REFS.DBF), used to maintain, sort and query rockslide literature.

2) File of parameters used to describe the source areas of rockslides (ROCKS.DBF).

3) File describing the failure scenario, path and deposits of rock avalanches (STURZ.DBF).

The latter two files have 203 parameters, most of which are either quantitative, or related to defined scales. The parameters cover geometry, geology and structure of the source area, pre-failure history, failure triggers and velocity, path and deposit dimensions and character. The input features of DBase IV permit a structured access to this data through user-oriented forms. A

set of complete forms and short forms (for less detailed input) are included with the database. The user can easily produce special forms to focus only on parameters of particular interest. Individual parameters can also be extracted or combined using the query and form design features of DBase IV. At this stage, the data bases include 57 case histories, in varying degrees of completeness. A list of the case histories is given in Table 1.2 The bibliographic file contains 240 references. It is proposed to distribute copies of the data base to researchers in Canada and abroad, in return for their supplying additional case history data.

Table 1.1

MEASURES THAT HAVE BEEN USED TO REDUCE
DAMAGE FROM MAJOR POTENTIAL ROCKSLIDE HAZARDS
(Numbers refer to the Bibliography, Appendix D)

- Stabilization (usually by drainage) - 22,45,74,145,171
- Prohibition of development in hazard areas - 47,148,160
- Monitoring of landslide behaviour - 22,24,53,70,77,114, 133,139,140,153,171,183,203,221,223,224
- Evacuation of residents - 35,139,140,141,221
- Removal of existing housing and installations - 114
- Re-routing of transportation lines - 114
- Reduction of reservoir operating levels - 120,171
- Reinforcement of dams to resist overtopping - 203
- Drainage bypass channels or tunnels - 70,114,149
- Protective berms - 23,139,224

Table 1.2, Case Histories of Large Rockslides in the Data Base

No.	Location	Source Volume (10^6 m^3)	Lithology Group *	Velocity Class **	References ***
1	Frank	29	CA	7	31,33,99,11,64,183,184,186
2	Elm	10	ML	7	7,23,27,51,56
3	Gross Ventre	40	SC	7	91
4	Madison Canyon	21	MH	7	43,143,111
5	Little Tahoma Peak	0	VO	7	37,146
6	Sherman Glacier	12	ML	7	65, 147
7	Hope	47	ML	7	63,144,26,55
8	Huascaran, 1970	75	IN	7	25,56,73,75
9	Huascaran, 1962	13	IN	7	25,73,75
10	Mayunmarca	1000	SC	7	58,130
11	Blackhawk	300	ML	7	52,82
12	North Nahanni	6	CA	7	106,199
13	Beaver Flats	0	CA	7	108
14	Brazeau Lake	5	CA	7	107
15	Downie	1500	MH	1	74,145
16	Goldau	43	SC	7	7,21,23,213
17	Diablerets	50	ML	7	7,21,23,213
18	Granier	215	CA	7	7,23,39,212,213
19	Clapiere	50	ML	3	6,144,223
20	Sechillienne	25	MH	2	133,224
21	Massif de Plate	20	CA	5	23,225
22	Valtellina	33	ML	7	35,149,221
23	Lake of the Woods	24	IN	7	148
24	Mt. Breakenridge	200	ML	1	153
25	Glen Pean	40	MH	1	5
26	Pandemonium Creek	5	IN	7	193
27	Vaiont	250	CA	7	10,23,29,54,67,70,71,76,85
28	Rockslide Pass	450	CA	7	34,196,219
29	Avalanche Lake	500	CA	7	34,127,194
30	Scatter River South	300	SC	1	226
31	Scatter River North	4	SC	1	226
32	East Culebra	7	SC	5	227
33	Rubble Creek	25	VO	7	47,197
34	Kennedy River	3	IN	7	225
35	Torreggio	6	MH	5	
36	Maligne Lake	500	CA	7	68,108
37	Martinez Mountain	380	MH	7	151
38	Bonneville	0	VO	7	72
39	Devastation Glacier	29	VO	7	47,118
40	Antelao	5	CA	7	23
41	Antropiana	12	MH	7	23,211

* Lithology types: IN - Igneous, intrusive
VO - Volcanic
SC - Sedimentary, clastic
CA - Carbonate
MH - Metamorphic, medium to high grade
ML - Metamorphic, low grade

** Velocity classes defined in Table 12 of Appendix A (after Varnes, 197

*** Refer to numbered list of references, Appendix D.

Table 1.2, Case Histories of Large Rockslides in the Data Base

42	Bec Rouge	3	ML	4	23
43	Biasca	15	MH	7	7,23,211
44	Clavans	3	MH	7	23
45	Campo	120	MH	2	7,23
46	Disentis (Muster)	15	MH	7	23
47	Dobratsch	30	CA	7	23,213
48	Ganderberg	0	MH	4	23
49	Lago di Alleghe	20	CA	7	23
50	Lavini di Marco	200	CA	7	23
51	Linthal	0	ML	5	7,23
52	Mottec	2	MH	7	23
53	Motto d'Arbino	35	MH	7	7,23
54	Piuro	4	MH	7	23
55	Spriana	0	MH	2	23
56	St. Sorlin D'Arves	500	ML	2	219
57	Ontake	33	VO	7	38,125,171,177

---

* Lithology types: IN - Igneous, intrusive
VO - Volcanic
SC - Sedimentary, clastic
CA - Carbonate
MH - Metamorphic, medium to high grade
ML - Metamorphic, low grade

** Velocity classes defined in Table 12 of Appendix A

*** Refer to numbered list of references, Appendix D.

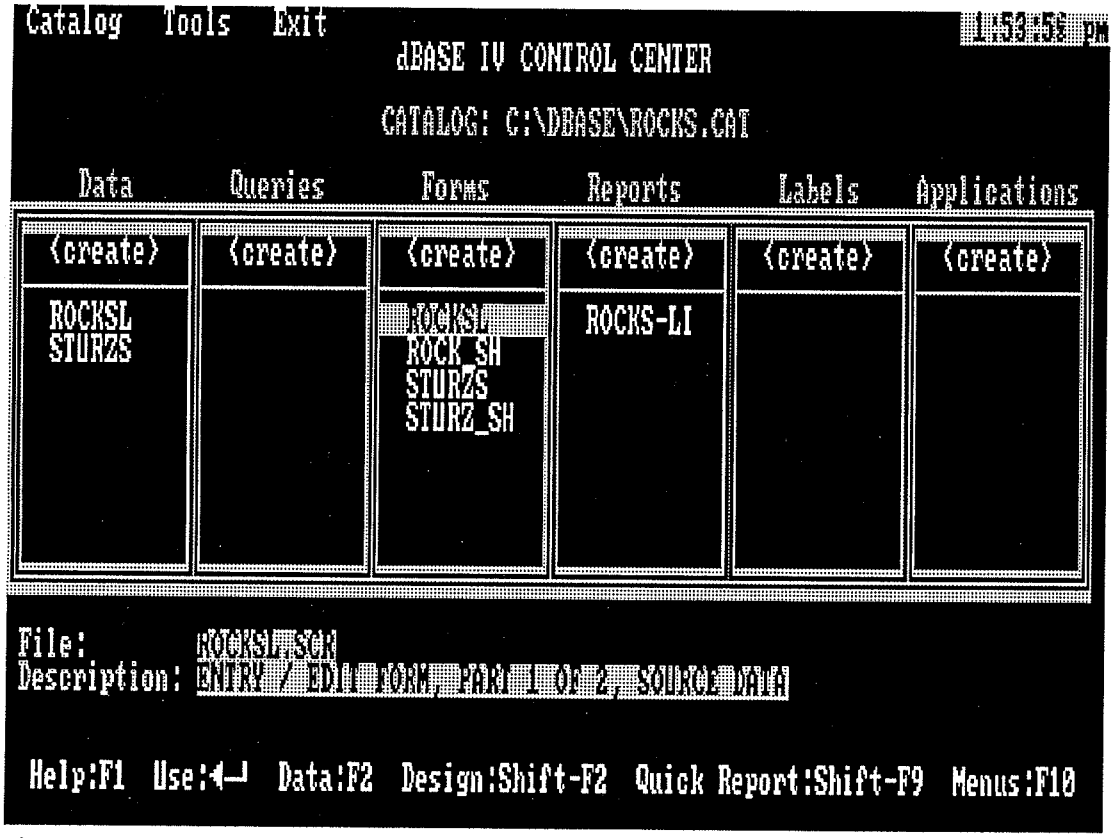

Figure 1.1 Control centre, rockslide data base.

2. PROBABILITY OF OCCURRENCE

2.1 Background Probability

Large landslides are not, in general, cyclic phenomena at any given location. But they can be considered as cyclic on a regional basis. Landslide occurrence inventories can be compiled in two ways:

Method 1)

A count of recognized landslide deposits in an area of mountainous terrain is prepared, based on airphoto and field studies. A period of time is then assumed, over which these deposits are likely to have accumulated (e.g. the period following deglaciation).

Method 2

A count of landslide cases reported over a given historic period in a study region is compiled.

Method 1 has the important advantage of allowing long time periods to be sampled. On the other hand, it suffers from inaccuracies since it is difficult to guess for how long deposits may remain recognizable. Very old deposits may be overlooked, leading to underestimation of frequencies. To calculate frequencies, it is necessary to assume them to be constant. It is a common assumption that present rockslide frequencies are less than those in Early Holocene (e.g. Abele, 1974, Cruden 1985). This should lead to overestimation of frequencies.

Method 2 is potentially more accurate, but is limited to the length of the historical period, often little more than 100 years. Dating of prehistoric landslides is at present of limited use statistically, as only a small fraction of known deposits can be reliably dated.

Table 2.1 summarizes several regional inventories of rock avalanches and rapid rockslides, belonging to both types. Only events with magnitudes greater than 20 million m^3 have been included in the data, since both Abele (1974) and Whitehouse and Griffiths (1983)

argue that inventories of smaller events are incomplete. Two types of limiting criteria (by deposit area and by the minimum dimension of a deposit) had to be converted into magnitude as described in the Notes of the table.

The inventories cover a wide range of mountainous environments and tectonic settings and it is, perhaps, surprising that the calculated frequencies show a reasonable degree of consistency within the three geological domains. Even unequal earthquake exposure in the various mountain ranges represented does not seem to have a noticeable effect (cf. Inventories 2, 3, 4 and 5).

It is remarkable that Inventories 8 and 9 suggest practically the same frequency, although the former covers the entire post-glacial period, while the latter is based in the historic time only. This contradicts the hypothesis of decreasing postglacial rates mentioned previously.

Magnitude-frequency relationships for rock avalanches have been described by Gardner (1980), Hsu (1983), Whitehouse and Griffiths (1983) and Cruden (1985). All show approximately a tenfold increase in frequency for an order of magnitude reduction near 20M m^3. Consequently, the frequency-magnitude curves should have a negative 45° slope in a log-log plot, as shown in Figure 2.1.

In order to fix the position of the M/F curves relative to the coordinate axes, we can make use of the data provided in Table 2.1. However, this data is expressed in terms of cumulative frequencies of events greater than 20 million m^3. It is necessary first to derive cumulative frequency curves corresponding to the linear function of Figure 2.1. The equation of a line in Figure 2.1 is:

$$\log f - \log f_{20} = C\ (\log M_{20} - \log M) \qquad (1)$$

where f and M are frequency and magnitude, f_{20} and M_{20} are the frequency and magnitude of a 20 million m^3 event and C is a constant expressing the slope of the line, which should approach 1.0. The equation can be rewritten as:

$$f = f_{20}\ (M_{20}/M)^C \qquad (2)$$

The cumulative frequency of events greater than M′ and up to a maximum magnitude M_{max} equals:

$$f_c = \int_{M'}^{M_{max}} f \, dM = f_{20} \, M_{20}^{c} \int_{M'}^{M_{max}} M^{-c} \, dM =$$

$$= f_{20} \, M_{20}^{c} \, [M_{max}^{(1-c)} - M'^{(1-c)}]/(1-c) \qquad (3)$$

Figure 2.2 shows the cumulative frequencies derived using Equation (3), with a c = 0.999, M_{max} = 500 million m^3 and f_{20} adjusted empirically so that the cumulative curves meet the reference points for M = 20 million m^3, from Table 2.1. The back-calculated f_{20} frequencies were then used to position the two lines in Figure 2.1.

The cumulative frequency relationships are theoretically linear on the semi-log plot (Figure 2.2). However, it is probable that the line shown for the crystalline and metamorphic rocks curves upwards at magnitudes less than 20 million m^3, as it is known qualitatively that the relative frequency of small failures is large for this type of rocks (Abele, 1974).

Somewhat higher average rock avalanche frequencies occur on volcanoes. Inokuchi (1988) estimates that major rock avalanches occur on Japanese volcanoes every 100 to 200 years. Given the total area of 24,000 km^2 covered by quaternary volcanoes on the Japanese Islands, the average frequency is 0.002 to 0.004 events per year for 10,000 km^2. Some individual volcanoes, however, have had two to three recognized events, which could be translated to a local frequency about one order of magnitude above the average.

The use of the magnitude-frequency diagram is illustrated by the following example: The combined length of railway lines in the sedimentary Rocky Mountains of Canada is approximately 1,000 km. The area of a tributary corridor 5 km wide is 5,000 km^2. The rail lines would be expected to be interrupted by a major (greater than 10M m^3) rock avalanche every 800 years, using the top line in Figure 2.2. In fact, there is one

recorded interruption (Frank Slide in 1903). The remaining 1,500 km approximately of railway corridors in Western Canadian mountains have also been disrupted once, by a rock avalanche deriving from a volcanic centre (Rubble Creek in 1855).

The above frequencies are broad averages only. Local concentrations of rockslide occurrence can be important. For example, Eisbacher and Clague (1984, page 79) show a location in northern Italy where seven major prehistoric rock avalanche deposits are clustered in an area of 1,000 km^2. Consequently, the relationship of Figure 2.2 should be used for practical predictions only in combination with a "Safety Factor" of about 5. Using such an approach, the probability of a 10M m^3 or greater rock avalanche reaching a 200 km long reservoir in sedimentary mountains is predicted as 1:800 annually. This is not a negligible risk.

There is not sufficient data to examine the frequency of rockslides other than rock avalanches.

2.2 Specific Probabilities

Application of the average frequencies to a specific site will result in negligible probabilities. For example, a valley community may have a "tributary area" of 20 km^2, and an annual rock avalanche probability of 1:40,000 even when considering the highest frequency and an uncertainty factor of 5. This is what perhaps explains the long and peaceful existence of many towns and villages in high mountains. It is only when signs of an incipient failure are observed that a large increase of the background probability is required. The means of doing this lie in the concept of "Bayesian updating" described by Einstein (1988). Unfortunately, the method is presently based entirely on subjective judgement and can thus be regarded as not more than informed guesswork.

The first step is to decide whether a given site is "capable" of producing a slide large and mobile enough to endanger the site of interest. Methods of estimating failure speed and runout, described in the subsequent

sections, should be used. Their application is, however, connected with a degree of uncertainty which could be expressed by a subjectively estimated coefficient X. Thus, a source judged "not capable" may still have a probability of X producing an unexpectedly rapid failure.

Should an identified source be considered capable, the next step is to update the background probability. A "likelihood function" (Einstein, 1988) can be formulated by assuming that the next large rock avalanche in the surrounding region will occur at one of N capable sites showing symptoms of impending failure as severe as the site in consideration. Such symptoms may include cracks, subsidence, bulging or previous failures from the same or adjacent source location. The annual failure probability, p, in the absence of active movements can then be estimated as:

$$p = \frac{P_b \, X}{N} \qquad (4)$$

where P_b is the background probability for the region, derived from Figure 2.2 as described in the previous section. While P_b may be accurate to an order of magnitude, both X and N are of course not more than subjective guesses. Nevertheless, this approach allows us to correlate an estimate of a relative degree of disturbance with an estimate of probability.

2.3 Failure Prediction

Total displacement is not a suitable criterion for failure prediction. For example, the rock mass involved in the 1987 Valtellina rock avalanche underwent about 100 m of slow displacement in prehistoric time, as shown by a prominent crown scarp (see Appendix C). On the other hand, the 1964 Hope Slide in British Columbia failed without a previous displacement of more than a few metres.

The process of rockslide risk assessment enters a new stage when active movements are recognized. Monitoring of displacements, strains, piezometric pressures or

rock noise has been used to gauge deterioration in stability and signal the onset of failure.

When displacement or displacement rate (velocity) is plotted against time, steep hyperbolic curves result which are difficult to extrapolate forward in an attempt to predict the time of failure (Voight and Kennedy, 1978). Fukuzono (1985) suggested plotting the inverse of velocity (1/v) as shown by three examples in Figure 2.3. Many landslides exhibit a nearly linear relationship between 1/v and time shortly before failure, as shown by the Vaiont Slide record. This form, shown schematically as No. 1 in Figure 2.4, was called by Fukuzono (1985) a "Saito type record" because it bears resemblance to the empirical procedures for failure prediction pioneered in Saito's work on the Japanese railways (Saito, 1965).

Another large group of pre-failure velocity records approximates to an exponential model, concave on the 1/v vs. time plot, as shown by No. 2 in Figure 2.4. The Liberty Pit failure record in Figure 2.3 shows such a trend, when short-term fluctuations are neglected. According to Fukuzono (1990), <80% of all slope failures have curves less concave than the exponential curve, while 50% are of the Saito type.

Prediction of failure time can be made graphically, by extending the trend of the 1/v vs. time relationship to the horizontal axis, or close enough to it to attain a pre-determined failure velocity limit x_f.

A convenient parameter for evaluation of failure velocity records is the inverse slope of the 1/v vs. time curve, with a dimension of length (Figure 2.4):

$$S_f = [d(1/v)/dt]^{-1} \qquad (5)$$

For a Saito record, S_f is a constant. For example, for the Vaiont record of the last 40 days before failure, S_f equals approximately 40/0.18 = 220 mm. A prediction of the time to failure is obtained simply by dividing S_f by the current velocity. Such a prediction will be conservative, if a concave trend persists up to failure.

Average S_f values for the last 20 to 60 days before failure have been collected from seven rockslides, monitored to failure, with volumes ranging from several hundred thousands to hundreds of millions m^3 (Table 2.2). The S_f coefficient varies from 150 to 700 mm for the seven cases. These values indicate that a limiting slide velocity of 50 mm/day, suggested by Salt (1988) as a critical pre-failure limit, represents 3 to 14 days to failure.

One example of a non-catastrophic failure, the Tripp Mine slide in Figure 2.3, had an S_f of approximately 1200 mm prior to attaining its peak velocity of 22 mm/day.

Acceleration is an increasing variable in both the Saito and exponential records, related to S_f by:

$$a = v^2/s_f \quad (mm/day^2) \tag{6}$$

where v is the current velocity in mm/day.

Using the critical pre-failure values of velocity and acceleration (50 mm/day, 5 mm/day^2) suggested by Salt (1988) in Eqn. 6, we obtain S_f(critical) = 500 mm.

Based on this rather limited collection of data, an S_f of less than 1000 mm can be used as an indicator of impending failure for large rockslides.

A general mathematical expression for pre-failure rate changes of observed parameters was presented by Voight (1989):

$$(t_f - t) = (x^{(1-m)} - x_f^{(1-m)})/A(m-1) \tag{7}$$

where T and x are the current time and rate (velocity), t_f and x_f are time and rate at failure and A and m are constants.

When m equals 2 and x_f is infinite, Equation 7 describes the Saito model (Fukuzono, 1985). With an m = 1, the equation must be replaced with an exponential

relationship. For m = 0, the equation reduces to a velocity equation with a constant acceleration equal to A, plotted as No. 3 in Figure 2.4.

Mathematical curve fitting is, however, difficult and dangerous for records of the kind shown by 2 in Figure 2.3 and a judicious application of graphical smoothing is preferable.

The best use of curve fitting techniques would be to improve the method of numerical differentiation by which velocity is derived from the displacement record. Fukuzono (1985) uses a simple first order Lagrangian differential formula:

$$v' = \frac{s - s'}{t - t'} \qquad (8)$$

where t is time, s displacement (or strain or other changing parameter) and the prime sign denotes the time step immediately preceding the current one. A wide choice of higher order regression differentiation techniques exists, which could be used to reduce the interference of short-term fluctuations and random error. It is advisable to process displacement records by several regression formulas simultaneously, to see which one will produce the most stable trend.

Empirical failure prediction techniques work poorly for long term predictions, when landslide movement rates are controlled by the fluctuation of pore pressures and other variables. This was most clearly shown by the displacement history of the Vaiont Slide during the last three years prior to failure, when movement was apparently controlled by the reservoir water level (Mueller, 1964). Similarly, the recent record of the La Clapiére rockslide in France (Figure 2.5) appears to be controlled mainly by precipitation. An average trend indicating a 1989 failure date with an S_f of 16,000 mm seems to have changed in recent years. The total displacement of parts of the rockslide has now exceeded 100 m (J. Follacci, pers. comm).

Displacement monitoring cannot be used to predict failures triggered by seismic events. Thus, the 1980 failure of 2,700 million m^3 from Mount St. Helens was triggered by a Magnitude 5 volcanic earthquake and was not preceded by accelerated movements (Voight, 1989).

Table 2.1

FREQUENCY OF OCCURRENCE OF ROCK AVALANCHES
EXCEEDING 20M m^3 IN MAGNITUDE

No.	Reference	Study Area Location	Area (10^3 km^2)	Geology	Method (see text)	Study Period Dates	Study Period Years	Basis of Selection	Number of cases	Rock Avalanche Frequency (cases/year/ 10,000 km^2 (4)
1)	Abele (1974)	North calcareous Alps	61	sedimentary	1	postglacial	11,000	deposit area>1 km^2(1)	40	0.0006
2)	Abele (1974)	South calcareous Alps	28	sedimentary	1	postglacial	11,000	deposit area>1 km^2(1)	32	0.0010
3)	Whitehouse and Griffiths (1983)	Central New Zealand	10	sedimentary	1	postglacial	10,250	volume>20M m^3	14	0.0014
4)	Cruden (1985)	Alberta Rockies	60	sedimentary	1	postglacial	11,000	min.dimension>700 m(2)	129	0.0019
5)	Eisbacher (1979)	Mackenzies, N.W.T. Canada	27	sedimentary	1	postglacial	11,000	volume >20M m^3	14	0.0005
6)	Abele (1974)	Central Alps	82	metam. & crystall.	1	postglacial	11,000	deposit area>1 km^2	21	0.0002
7)	Evans (unpubl.)	Coast Range, B.C.	12	metam. & crystall.	2	2,000 B.P.	2,000	volume>20 M m^3	3	0.0012
8)	Abele (1974)	The Alps	176	mixed	1	postglacial	11,000	deposit area>1 km^2	93	0.0005
9)	Eisbacher and Clague (1984)	The Alps	176	mixed	2	1200-1987	787	volume>20 M m^3	8(3)	0.0006

Notes:

(1) Conversion of deposit area to magnitude was made using Figure 4.10
(2) Conversion of "minimum deposit dimension magnitude" was made using a width to length ratio of 0.5 and Figure 4.10.
(3) The 1987 Valtellina case has been included.
(4) Frequency per 10,000 km^2 of mountainous terrain (>1,000 m relief).

Table 2.2

COEFFICIENT S_f PRECEDING MONITORED ROCKSLIDE FAILURES

Case	Source	Volume (m^3)	Time Interval Before Failure (days)	S_f (mm)
Vaiont	Mueller (1964)	200 M	40	220
Mt.St.Helens (1982 eruption)	Voight (1989)	--	40	210*
Ruahihi	Salt (1988)	?	30	161
Abbotsford	Salt (1988)	2M	30	300-700
Chiquicamata	Kennedy and Niermeger (1971)	800,000	65	700
Hogarth Pit	Brawner et al. (1975)	200,000	50	550
Liberty Pit	Zavodni and Broadbent (1980)	400,000	20	554

* Crack displacements preceding volcanic eruption.

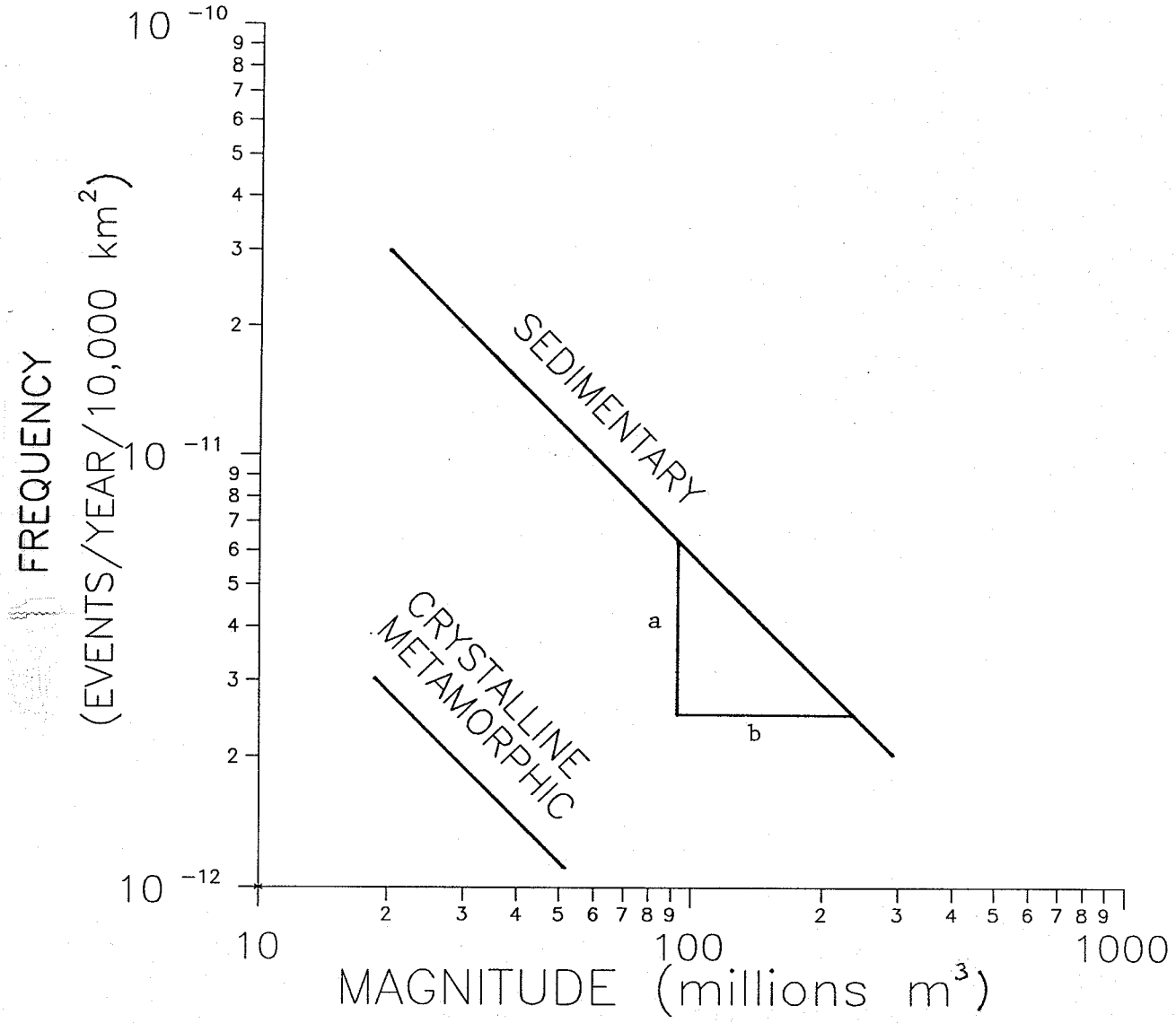

Figure 2.1

Suggested magnitude-frequency relationship for large rock avalanches. ($a \simeq b$)

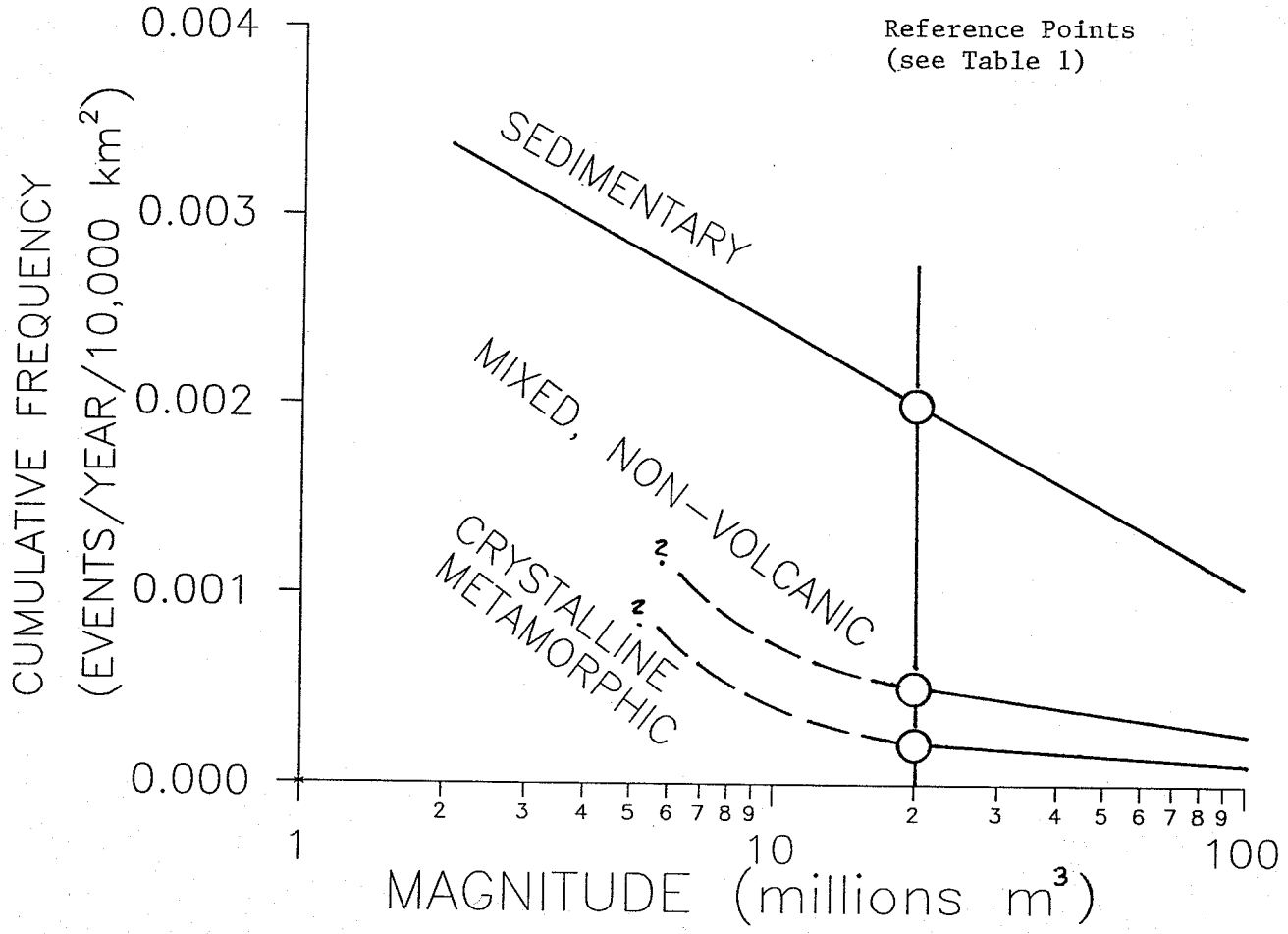

Figure 2.2

Cumulative frequency of rock avalanches greater than a given magnitude (and smaller than 500 million m^3).

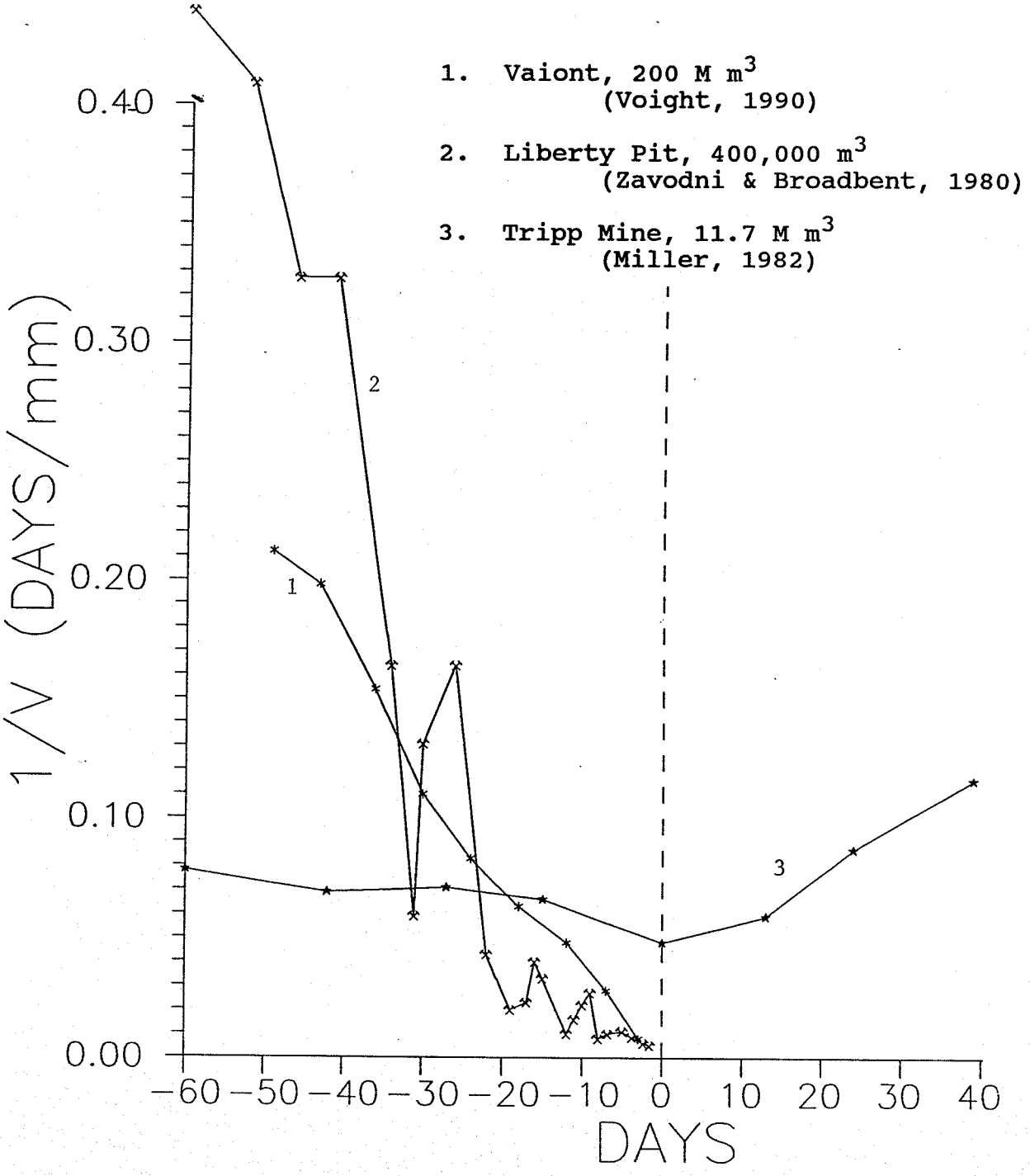

Figure 2.3

Examples of pre-failure displacement rates for large rockslides.

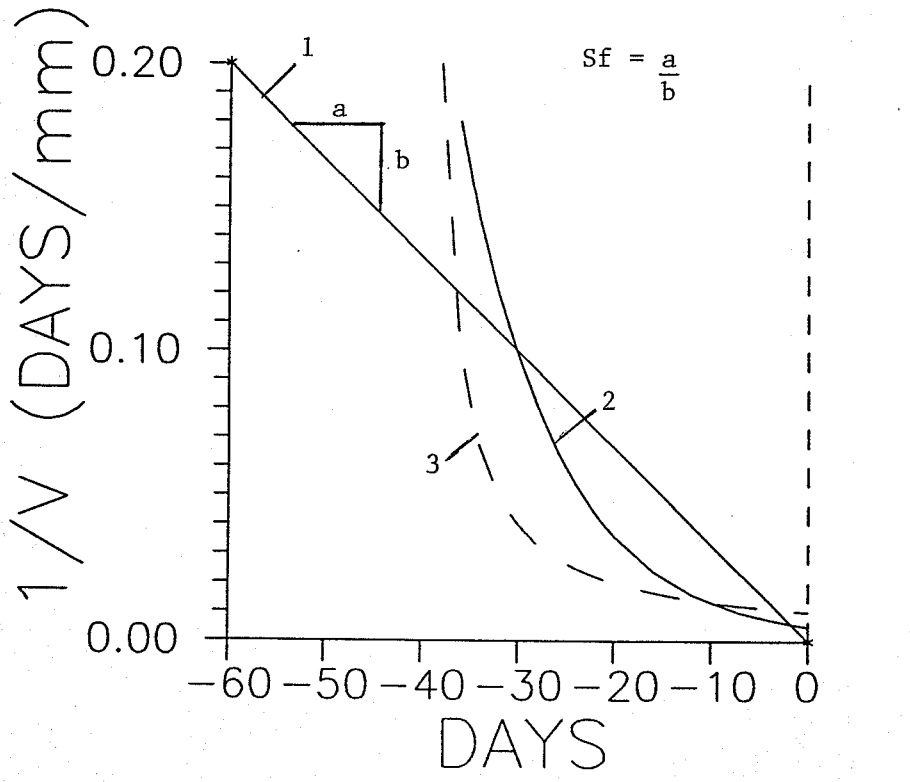

Figure 2.4

Typical relationships between inverse velocity and time (after Fukuzono, 1985).

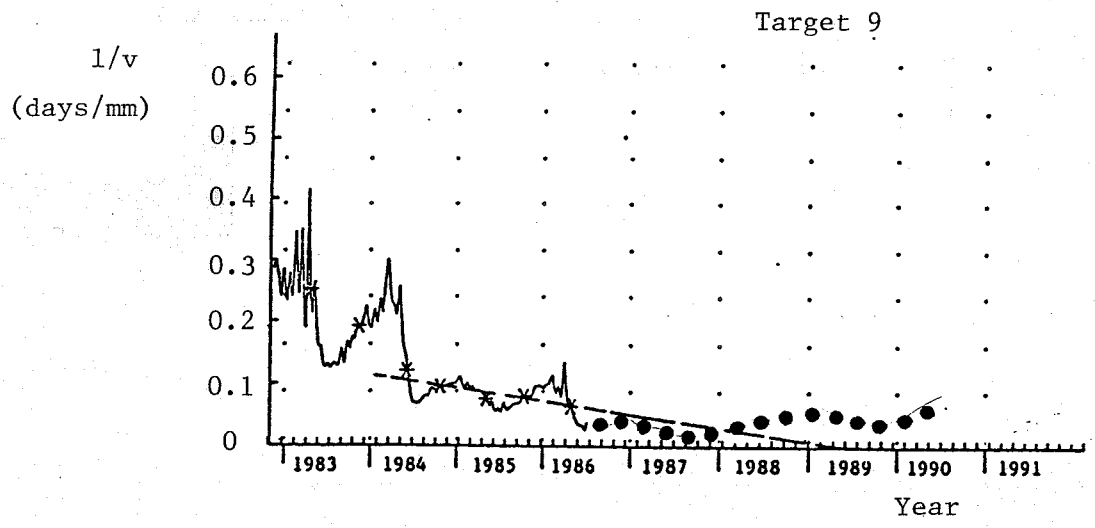

Figure 2.5

Inverse velocity - time diagram for an optical displacement target on the La Clapiere Slide (from Vibert et al., 1988). The dashed line indicates a July, 1986 prediction trend. The large dots show the approximate post 1986 development (French Dept. of Public Works, pers.comm.).

3. CATASTROPHIC FAILURE POTENTIAL

3.1 Failure Dynamics

To conceptualize the process of slope failure, it is useful to think in terms of the resultant driving and resisting forces acting on the failing mass. Their possible change with displacement is shown in Figure 3.1a.

The driving force is a component of gravity and depends on the mean inclination of the current velocity vector field. Self-stabilizing mechanisms are those in which the velocity field has a concave shape, as in a rotational slump. The driving force will then be reduced with displacement, as is the case in Figure 3.1a. The force may also remain constant, as in the case of a translational slide, or increase due to detachment of material from the slide toe (retrogressive sliding).

Self-stabilizing mechanisms have more chance to remain slow, and more so the greater their depth ratio. Translational or retrogressive mechanisms are more likely to be rapid.

The resisting force will equal the driving force at the onset of displacement, then reduce as a result of brittleness. The vertical distance between the resisting and driving force curves gives the net unbalanced force, F, available to cause acceleration of the slide. From the work-energy theorem, the kinetic energy developed by the slide at any value of displacement will equal the work done by the unbalanced force $\int F\,dx$, i.e. the shaded area between the two curves.

The static resisting force derives from two sources: 1) strength developed on the sliding surface ("boundary strength") and 2) stress re-distribution caused by the internal distortion of the sliding body ("internal strength"). The overall brittleness of the resisting force will be a combination of the two. Thus, a slide controlled by a ductile sliding surface may still develop brittleness as a result of brittle internal strength. This appears to have been the case in the Vaiont Slide (Hutchinson, 1988, Hungr et al., 1989).

The role of internal strength is most important where the ratio between internal and boundary strength is large and where the toe region of the sliding body is stable relative to the head region (Hungr et al., 1989).

The shape of the resisting force curve may be velocity dependent. Figure 3.1b shows the case of a viscous response, where a strength increase results from increasing velocity. The velocity is then severely limited, as the width of the shaded area is determined by the viscous relationship.

The viscosity increase may be a material property. For example, Salt (1988) conducted high velocity ring shear tests on clay gouge and measured a 2 to 3% increase of residual strength per log cycle increase of shearing rate at rates exceeding 10 mm/day.

A macroscopic viscous effect could also result from large scale dilatancy of uneven or developing sliding surfaces. As dilation occurs, a reduction of pore pressure near the shear band will temporarily increase strength. Motion will then be restricted in a viscous manner, to allow time for pore pressure equalization. Such an effect cannot be reproduced in the laboratory, as it derives from large scale volume changes at the boundaries of the moving mass and it can only be quantified by means of back analysis.

The viscous response is likely to be dominant in weak, low permeability rocks under low to moderately high stresses (e.g. shales).

A rate-softening effect opposite to viscosity can also occur (Figure 3.1c). A velocity-dependent strength reduction can result from frictional heating and expansion of the pore fluid, as shown theoretically by Lachenbruch (1980) and Voight and Faust (1982). The strength reduction is enhanced by increasing velocity, normal stress and friction angle and by decreasing thickness of the sliding zone. The high failure velocity of the Vaiont slide was ascribed to this process by several authors (Voight and Faust, 1982, Hendron and Patton, 1985).

At extremely high normal stress values, the frictional heating may become as strong as to vaporize the pore fluid (e.g. Goguel and Pachoud, 1972, Habib, 1975) or even melt the rock contacts of the sliding surface (Erismann, 1979).

The rate-softening frictional heating process is important in deep landslides, with high stress levels and well defined, thin shear zones.

It is practically not possible at present to describe a relationship such as shown in Figure 3.1 quantitatively. This is because of lack of knowledge concerning post-failure decay of strength, the various types of velocity dependence as well as stress, strain and pore pressure distributions in the deforming body. The only feasible, if not exact, method to predict that a rockslide is capable of catastrophic failure is by recognizing typical failure mechanisms, and outlining their characteristic behaviour from precedent.

3.2 Failure Mechanisms

Fifty-seven case histories of large rockslides from various parts of the world have been compiled in the data base and reviewed, in an attempt to isolate factors determining failure behaviour. The crucial point is to recognize cases which are capable of developing catastrophic failure, involving mean velocities in excess of 3 m/sec. Such failure is directly life-threatening, it generates waves in water bodies and it contains an inertial component allowing extended runout, beyond the residual equilibrium slope.

Velocity depends primarily on the failure mechanism. Structural control appears to be of prime importance. Rockslide detachment may involve the following components:

1) Tensile failure of jointed rock mass, which contributes little to the resisting forces.

2) Shear failure of rock mass, without preferred direction.

3) Shearing along randomly oriented discontinuities, involving relatively high roughness, curvature and limited persistence (presence of "rock bridges").

4) Shear failure along penetrative weakness surfaces including weak directions of anisotropic rock masses (e.g. bedding or schistosity), weak layers, major joints or faults. The surfaces may be planar or curved and several different types may participate in a given failure.

5) Rotational instability (toppling) of closely jointed or anisotropic rock masses.

The classification system shown in Figure 3.2 reflects the participation of the five components in the failure mechanism. Nine classes of detachment are shown, each of which can possess a significant three-dimensional component.

Tables 3.2 through 3.10 summarize quantitative parameters of typical source areas in the nine classes, derived from the data base described in Section 1.4. Definitions of the parameters are presented in Table 3.1.

Type A, Rock Slump

In the absence of favourably oriented discontinuities, rock fails by rotational shearing as if it were a strong, cohesive soil (Figure 3.3). Only the weakest rock masses are subject to slumping failure: theoretically, a 100 m high vertical cliff would fail only if the large scale uniaxial compressive strength of the rock mass was less than about 1.5 MPa. Frequently the crest of the source cliff contains a layer of stronger cap rock, which separates by means of tensile failure. The failure mechanism is self-stabilizing, especially so if the failure surface passes beneath the slope toe or if the slope angle decreases in the toe region.

Slump failures are non-catastrophic, although they may involve large displacements. A graphic description of a major slump acceleration in Cretaceous marls at the Massif de Plate near Chamonix in the Savoy Alps was

quoted by Eisbacher and Clague (1984, p. 142), based on eighteenth century sources. The 1751 failure of the 20° slope capped by limestone involved some 20 million m^3 and continued for more than a month. Only local toppling of limestone columns created high velocity movements. The slide debris shifted into the river channel at the foot of the slope, but remained standing at an angle only a few degrees below the original slope angle and did not run up the opposite side of the valley or dam the river. Many smaller examples of slow to moderately rapid slump movements in weak rocks or overconsolidated clays have been described in the literature (e.g. Hamel, 1972).

Rock slump occurs in weak rocks such as shale, marl or tuff, which are isotropic, or structured so that the weak direction is horizontal or dips gently opposite to the slope direction.

Typical parameters of rock slump source areas are given in Table 3.2. The three cases involved sedimentary rocks of relatively low strength, flat and favourably oriented rock fabric and a lack of weak structures. Two of the failures were seated high above the valley. Movement velocities were non-catastrophic.

Type B - Rock Collapse

Many languages have a specific term for a rockslide which occurs on a steep slope in relatively strong rock, involving an apparently random collapse of the rock mass structure: "Bergsturz" in German, "écroulement" in French, "frane di crollo" in Italian or "zriceni" in Czech. The main meaning of these terms relates to rapid, catastrophic rate of movement. However, in a more narrow interpretation, a lack of dominant sliding surface and a corresponding lack of coherence from the first moment of detachment are also implied.

Rock collapse is defined here as a failure of a steep slope in a strong rock mass, controlled primarily by shearing along random discontinuities of limited persistence (Figure 3.4). The rock mass tends to be isotropic, or dipping into the slope. Downslope oriented stress relief joints often play an important role (e.g. Huascaran, Plafker and Ericksen, 1978).

Block toppling may be a component of the detachment mechanism and there may be a significant amount of intact rock crushing, shearing or tensile failure. The detachment surface is steep and irregular.

The original slope is generally steeper than 45°, with the toe of the detachment surface placed above the toe of the slope. Ridges or buttresses appear to be especially vulnerable. Natural or artificial undermining of the slope may be critical, as shown by the 1881 failure at Elm, Switzerland, which was triggered by the mining of slate (Heim, 1932).

Rock collapse occurs most often in volcanic, plutonic or low grade metamorphic rocks but may also take place in massive sandstones or carbonates, unless another mechanism is dominant. The movement rate is invariably very rapid, leading to the formation of a rock avalanche (sturzstrom). Volumes of rock collapse failures are generally limited to less than 10 or 20 millions of m^3, although greater volumes may be found in mountain slopes of major proportions (e.g. Huascaran).

Table 3.3 gives nine examples of rock collapse failures in igneous and metamorphic rocks, with volumes ranging up to 75 million m^3. The source slopes are steeper than 45°, except for the two volcanic cases. Rock strengths are high and anisotropy low. Fabric is steep, or favourably oriented. Both ridge and re-entrant source locations are represented. All the failures are catastrophic, except No. 20 which may yet be due to fail.

Type C - Rock Glide

A simple translational sliding failure results, where major weakness planes exist dipping with or near the slope direction (Figure 3.5). The weakness plane may be a weak direction in an anisotropic rock mass, i.e. bedding or schistosity, or a unique structure such as an unusually persistent joint or a fault (e.g. Beaver Flats South, Cruden, 1976). Two planes may combine to form a wedge failure (e.g. Lake of the Woods, Thurber Consultants Ltd. 1988). The important distinction of the glide mechanism is that sliding is kinematically possible

without internal deformation and all brittleness is derived from the sliding surface.

Rock glide failures may be slow in weak rocks, if the stress levels are low and viscous effects dominate. Thus, the Panama Canal slides (Lutton et al., 1979) involved movements measured in metres per minute or hour on pre-sheared bedding surfaces inclined at less than 15°.

When the thickness of the unstable mass is relatively great, rate-softening behaviour due to frictional heating may lead to high velocities. This was postulated for the gigantic Mont Granier rock avalanche in France by Goguel and Pachoud (1972). In that case, sliding on marl bedding planes dipping at only 17° occurred under a mass up to 600 m thick. This catastrophic slide occurred in a sequence of Cretaceous strata equivalent to that which produced the moderately rapid Massif de Plate slump, discussed under Type A. The sole factor responsible for a dramatically different behaviour was the bedding orientation, with a slight dip out of the slope in the former case and into the slope in the latter (Lake of the Woods).

Another significant example of a catastrophic rock glide was the 1985 Bairaman River landslide in Papua New Guinea (King et al. 1989), which involved gently dipping limestone beds with clay intercalations. The slide was triggered by an earthquake.

In general, rock glide movements are catastrophically rapid, unless they involve structures dipping at less than 15°, combined with mass thickness of less than 100 m. They form some of the largest volumes of all rockslide mechanisms (i.e. Flims, Saidmarreh).

Rock glide movements take place most frequently in carbonates and less often in other sediments. They occasionally occur in recent volcanics, exploiting the downslope dipping contacts formed in the construction of a volcanic cone (e.g. Mt. Ontake, Japan, Inokuchi, 1985). They sometimes form in plutonic rocks, controlled by relict stratification or unusually persistent stress relief joints.

The 13 cases listed in Table 3.4 involve mostly sedimentary rocks, with volumes up to 500 million m^3. The source slope angles vary from 12 to 60°: the one case at the lower limit of this range is non-catastrophic. Rock strengths range from weak to very strong. The sliding movement is facilitated by the rock fabric in about one-half of the cases and by major structure in the remainder (anisotropy is high in the former cases). Relative thicknesses are variable, with no apparent systematic effect. Toe factors are zero (see Figure 10a, Appendix A for definition).

Type D Compound Slide

Types D to G are compound sliding failures, the kinematics of which require internal deformation of the sliding body during detachment (cf. Hutchinson, 1988). The simple compound slide, Type D, forms along a group of weak surfaces, interconnecting to form a more-less complex shape. A distinct three-dimensional form of a compound slide is shown by the 1987 Valtellina slide (Figure 3.6) involving a combination of a persistent joint set and two fault surfaces (Govi, 1989).

A common configuration leading to compound sliding is where an anisotropic mass (e.g. bedded limestone) is cut by an oblique fault. This was the case in the 1988 North Nahanni slide described by Evans et al. (1987).

Another form of a compound slide is created by strongly curved non-rotational weak surfaces, the prime example of which is Vaiont (Hendron and Patton, 1985).

Compound slides occur in moderately deformed carbonates and other sedimentary rocks, and in metamorphics. They are generally catastrophic. The participation of internal strains in the failure mechanism dramatically increases the overall brittleness (Hungr et al., 1989).

Non-catastrophic behaviour is found only in Type D slides of relatively small magnitude, occurring in very weak rocks. For example, a failure of approximately 100,000 m^3 of shale rock sliding on a curved pre-sheared bentonite seam at Luscar Mine in Alberta was

observed moving at a maximum velocity of several cm per day.

Ten examples are listed in Table 3.5 (all catastrophic). They involve a variety of sedimentary and metamorphic rock types, with a range of strengths. Nearly all the cases involve major fault structures. No. 10 involves curved bedding. Four cases involve interaction between bedding and major structures. Source slope angles have a wide range. Toe factors are zero.

Type E - Toe Slide

This type refers to a compound slide, where a weak surface (or several) forms the toe region of the detachment. The remainder of the detachment surface forms by shearing along random joints or through the rock mass.

The behaviour of a toe slide again depends on the overall steepness of the slope and strength of the rock mass. If the back scarp follows series of steep random joints in relatively strong rock, a catastrophic collapse similar to Type B can result (Figure 3.7). Both the Frank and Hope Slides appear to have occurred under similar circumstances.

Should the back scarp develop in a weak rock mass at moderate slope angles, the slide behaviour may be of a ductile type similar to Type A. Many bedrock failures in the Cretaceous rocks of the Western Canadian prairie river valleys belong to this type and are characteristically slow.

Type E could thus be considered as an extension of Types A and B, with similar behaviour patterns.

Three catastrophic cases are shown in Table 3.6, involving sedimentary and metamorphic rocks. Shearing through the rock mass accounts for 20 to 70% of the sliding surface plan area. The source slopes are steeper than 30°. The rock fabric dips between 0 and 40°. Two of the cases involve major structures in the weak toe segment.

Type F - Centre Slide

Some compound slides develop above a covered sloping weak surface, breaking through the rock mass both in the toe and crest region. Many examples of this type are slow failures, especially if the weak surface has a gentle slope and the rock is weak. A spectacular example is the slide complex at Scatter River, north-eastern British Columbia described by Hungr et al. (1984) and shown in Figure 3.8. The failure is seated on a basal weak plane inclined only 4° in the direction of movement. The slow displacements are controlled by river erosion of the toe zone, where the sliding surface cuts upwards across bedding.

The well known Downie Slide on the Columbia River (Piteau et al., 1978) has a similar mechanism, although the weak surface slopes at 18°.

Catastrophic slides of Type F appear to be rare and the authors are not aware of an example. Three non-catastrophic examples are listed in Table 3.7, including the two cases mentioned above. Toe factors range from 0.11 to 0.25.

Type G - Crest Side

The last type of compound slide develops in response to a steep weak surface cutting through the crest area, while the toe shears through the rock mass (Figure 3.9). Both the 1964 Sherman Glacier and the 1959 Madison Canyon rock avalanches contained steep faults in the crest areas. Both were triggered by earthquakes (McSaveney, 1978, Hadley, 1978).

Braun and Gillmeister (1989) reported large prehistoric slides in weak Paleozoic sediments of Virginia with similar configuration, which were apparently slow. The controlling bedding planes dip at about 30° (e.g. the Sinking creek landslide area.)

Table 3.8 shows four cases of crest slides. The first three are catastrophic. They involve relatively steep slopes and strong rocks, similar to Type B. Major

structures are also involved. The fourth is a case of a failure in weak anisotropic rock with steep original dip, approaching Type H in character. The toe factors are 0.7 and 0.8.

Type H - Flexural Toppling

Many slopes formed in steeply dipping anisotropic rocks exhibit outward rotation and reverse shearing of the rock mass, described as flexural toppling (Goodman and Bray, 1976). The dip direction is generally into the slope, but steep dip slopes have also been affected (Tabor, 1971, Riemer et al., 1988, Cruden, 1989). The rock type is predominantly schist, less commonly closely jointed gneiss or sedimentary rocks.

Some cases of flexural toppling show little sign of measurable movement, such as the Glen Pean site in Scotland, described by De Freitas and Watters (1973). Others show slow or moderate movements. A spectacular recent example of flexural toppling is the Clapiére slide in Southern France, described by Follacci (1987) and shown in Figure 3.10 (see also Figure 2.5).

The flexural toppling mechanism is self-stabilizing, because the shear stresses on the weak surfaces decrease as the beds tilt forward. This, in combination with the general low strength of rock masses involved in toppling, combines to produce ductile behaviour similar to that of Type A slump failures. Highly developed flexural toppling often transforms into a slump, as the strata break in a curved hinge zone and begin to slide. This is apparent in the crest area of the Clapiére case. There appears to be no example of such mechanism leading to catastrophic velocities, while examples of ductile behaviour are quite abundant.

All five examples shown in Table 3.9 are non-catastrophic and involve highly anisotropic rocks with steep original dips (the dip indicated in the table reflects the toppled condition). The source slopes are quite steep, ranging from 30 to 40°. Four of the five cases extend down to the floor of the valley. Major structures do not play a role in the mechanism.

Type I, Block Toppling

Block toppling is defined here as a rotational failure of steeply dipping beds in relatively massive rock, where stability is derived mostly from the base of the rock columns, rather than from friction along their sides as was the case in Type H.

Simple catastrophic toppling of a large isolated limestone tower (the "Pulverhorndl") was described from the Austrian Alps by Terzaghi (1950). Such detachments are limited in volume.

Of greater concern is catastrophic block toppling of series of massive columns separated by steeply dipping bedding or joints. An example of this kind was observed by the writer (OH) in a railway cut in steeply jointed massive quartzite, involving some 10,000 m^3. A larger example in dolomite and limestone is the prehistoric Elk Ridge rock avalanche described by Cruden and Hu (1991). The 1928 Motto d'Arbino failure in Switzerland, involving 30 to 40 million m^3 of gneiss and marble, may have had a similar mechanism (Heim, 1932, Eisbacher and Clague, 1984, p. 201 and Table 3.10). The failure was a small part at the front of a large moving mass. Heim's description of the 1928 event, and the limited runout of the deposits, indicate that the failure occurred in a piecemeal manner, with a succession of smaller falls continuing over many hours.

Obviously, the distinction between Types I and H is very important and it depends on strength and the degree of anisotropy of the rock mass. Unfortunately, no quantitative criteria exist for making such a distinction.

In summary, the proposed classification provides a framework for the recognition of failure behaviour patterns. Types A (slump) and H (flexural topple) appear to be predominantly ductile. Types B (collapse), G (crest slide) and I (block topple) are usually catastrophic and tend to involve steep slopes and strong rocks. Type C (glide) is also catastrophic, except in very weak rocks with limited slope angles and limited thickness. The compound slide and toe slide, Types D and

E, may exhibit a range of behaviour, but are probably catastrophic in all cases, except with low rock strength and limited slope angles. The centre slide, Type F, is usually ductile.

It appears from the above that, in addition to the failure mechanism, rock mass strength, anisotropy, slope height and angle are important factors determining whether a catastrophic failure can occur or not. The data base of quantitative parameters of failure case histories will help clarify the influence of these parameters, once a sufficient amount of data has been collected in it.

Table 3.1
Definition of Parameters Used to Describe Source Areas.

Case I.D.: Refer to Table 1.2 for a list of case histories.

Mean Slope Angle: Angle between toe and crest of the slope.

Scar Slope Angle: Angle between toe and crest of the slide.

Plan Radius of Pre-slide Contours (m): The radius is estimated in the centre of the source area. Ridge - positive, reentrant - negative.

Elevation - Toe of Scar Above Valley Floor (m): Elevation difference between toe of the source area and the valley.

Detachment Volume (10^6 m^3): (No bulking)

Relative Thickness: Volume/(Plan area to the power of 3/2).

Dominant Lithology:
IN - Igneous, intrusive
VO - Volcanic
SC - Sedimentary, clastic
CA - Carbonate
MH - Metamorphic, medium to high grade
ML - Metamorphic, low grade

Main Rock Unit (most abundant):
- Rock Type
- Rock Strength (see Table 6 in Appendix A)
- Strength Anisotropy (Table 10 in Appendix A)
- Structural Anisotropy (Fig. 9 in Appendix A)
- Mean Dip (of the rock fabric)
- Dip Direction

Movement Direction: Direction of movement in source area.

Percentages of the Sliding Surface Area (in plan):
- In Weak Direction (parallel with the weak direction of one or more rock units).
- On Major Structure (formed of one or more major structures, e.g. faults).
- Through Rock Mass (formed by shear through intact rock mass or along random joints).

Toe Factor: See Fig. 10a, Appendix A.

Percentage Volume Involved in Toppling Type Displacements:

Velocity Class: See Table 12 in Appendix A.

Table 3.2

MAIN PARAMETERS OF SOURCE AREA
(see definitions in Table 3.1)

TYPE A, ROCK SLUMP

Location:	M. de Plate	Linthal	Scatter R.
Case I.D.*	21	51	31
Mean Slope Angle:	21°	40°	41°
Scar Slope Angle:	21°	25°	46°
Plan Radius of Contours (m):	2500	2000	10000
Elevation - Toe of Scar Above Valley Floor:	400	890	0
Detachment Volume (10^6 m^3):	20	-	4
Relative Thickness:	-	-	0.36
Dominant Lithology:	CA	ML	SC
Main Rock Unit - Rock Type:	Marl	Sandstone	Shale
Rock Strength:	3	-	2
Strength Anisotropy:	3	-	4
Structural Anis.:	5	-	5
Mean Dip:	20°	10°	4°
Dip Direction:	350°	135°	330°
Movement Direction	185°	310°	152°
% Sliding Surface Area - In Weak Direction:	0	0	0
On Major Structure:	0	0	0
Through Rock Mass:	100	100	100
Toe Factor:	N.A.	N.A.	N.A.
% Volume in Toppling:	5	-	0
Velocity Class:	5	5	1

* Catastrophic failure cases underlined.

Table 3.3

MAIN PARAMETERS OF SOURCE AREA
(see definitions in Table 3.1)

TYPE B, ROCK COLLAPSE

Location:	Elm	Huas.	Huas. 62	Pand.	Rubble	Bonne.	Antro.	Mottec	Sech.
Case I.D.*	2	8	9	26	33	38	41	52	20**
Mean Slope Angle:	46°	72°	72°	48°	45°	38°	45°	35°	43°
Scar Slope Angle:	48°	75°	74°	49°	35°	36°	49°	45°	45°
Plan Radius of Contours (m):	1000	1000	1000	500	-600	-	-1000	10000	-1000
Elevation - Toe of Scar Above Valley Floor:	300	2900	2900	1000	550	400	900	400	160
Detachment Volume (10^6 m^3):	10	75	13	5	25	-	12	20	25
Relative Thickness:	0.27	0.94	0.57	0.45	0.10	-	-	0.03	-
Dominant Lithology:	ML	IN	IN	IN	VO	VO	MH	MH	MH
Main Rock Unit -									
Rock Type:	Slate	Gran.	Gran.	Diorite	Dacite	-	Gneiss	Gneiss	Schist
Rock Strength:	3	6	6	7	6	-	6	-	5
Strength Anisotropy:	5	1	1	-	1	-	-	-	2
Structural Anis.:	5	2	2	-	2	-	-	-	2
Mean Dip:	30°	80°	80°	84°	0°	0°	40°	30°	150°
Dip Direction:	157°	270°	270°	255°	0°	0°	280°	180°	89°
Movement Direction	2°	243°	243°	340°	310°	122°	150°	60°	90°
% Sliding Surface Area -									
In Weak Direction:	0	0	0	20	0	0	0	0	0
On Major Structure:	0	0	0	0	0	0	0	0	0
Through Rock Mass:	100	100	100	80	100	100	100	100	100
Toe Factor:	N.A.	N.A.	N.A.	N.A.	N.A.	N.A.	N.A.	N.A.	N.A.
% Volume in Toppling:	0	-	-	-	0	-	-	-	20
Velocity Class:	7	7	7	7	7	7	7	7	2**

* Catastrophic failure cases underlined.
** Possible pre-failure movements.

Table 3.4

MAIN PARAMETERS OF SOURCE AREA
(see definitions in Table 3.1)

TYPE C_1, ROCK GLIDE

Location	Q.Vent.	Beaver	Braz.	Golden	Granier	Lake of W.	Rocksl.	Aval.	Antel.	Lago di A.	Lavini di M.	Ontake	E.Culeb.
Case I.D.*	3	13	14	16	18	23	28	29	40	49	50	57	32
Mean Slope Angle:	18°	34°	31°	21°	34°	31°	60°	29°	30°	34°	23°	25°	12°
Scar Slope Angle:	19°	33°	30°	21°	16°	30°	44°	30°		34°	20°	25°	12°
Plan Radius of Contours (m):	10000	-	10000	1500	1000	1000	1500	4000	1200	700	1000	400	500
Elevation - Toe of Scar Above Valley Floor:	90	100	670	510	330	300	50	50	300	450	350	1000	0
Detachment Volume (10^6 m^3):	40	-	4.5	42	215	24	450	500	50	20	200	32	7
Relative Thickness:	0.13	-	0.11	0.06		0.05	0.34	0.14	0.11	-	0.20	0.13	0.06
Dominant Lithology:	SC	CA	CA	SC	CA	IN	CA	CA	CA	CA	CA	VO	SC
Main Rock Unit - Rock Type:	Sand.	Lime.	Dol.	Cong.	Marl	Dior.	Dol.	Dol.	Lime.	Lime.	Lime.	Tuff	Shale
Rock Strength:	5	5	5	5	3	7	6	7	6	-	6	2	2
Strength Anisotropy:	2	1	1	1	3	1	1	1	-	-	-	-	-
Structural Anis.:	3	5	3	4	5	2	4	3	-	-	-	-	-
Mean Dip:	20°	42°	27°	20°	17°	24°	12°	29°	25°	28°	18°	33°	3°
Dip Direction:	350°	225°	45°	168°	60°	180°	260°	200°	340°	110°	310°	180°	230°
Movement Direction	350°	225°	27°	180°	60°	136°	260°	200°	280°	110°	310°	155°	232°
% Sliding Surface Area - In Weak Direction:	90	0	0	0	69	0	80	100	70	100	95	0	80
On Major Structure:	0	100	100	90	0	80	0	0	0	0	0	0	0
Through Rock Mass:	10	0	0	10	31	20	20	0	30	0	0	30	20
Toe Factor:	0	0	0	0	0	0	0	0	0	0	0	0	0
% Volume in Toppling:	0	0	0	0	0	0	0	0	0	0	0	0	0
Velocity Class:	7	7	7	7	7	7	7	7	7	7	7	7	5

* Catastrophic failure cases underlined.

Table 3.5

MAIN PARAMETERS OF SOURCE AREA
(see definitions in Table 3.1)

TYPE D, COMPOUND SLIDE

Location	Mayun.	Black.	N.Nah.	Valt.	Vaiont	Malig.	Martin.	Biasca	Dobr.	Piuro
Case I.D.*	10	11	12	22	27	36	37	43	47	54
Mean Slope Angle:	19°	30°	34°	32°	33°	26°	-	38°	40°	31°
Scar Slope Angle:	17°	-	38°	33°	27°	-	-	45°	27°	28°
Plan Radius of Contours (m):	-1000	10000	10000	3000	2000	-	-	-1000	10000	-2000
Elevation - Toe of Scar Above Valley Floor:	350	-	160	600	100	-	-	700	400	300
Detachment Volume (10^6 m^3):	1000	300	6	32	250	500	380	15	30	35
Relative Thickness:	0.09	-	0.38	0.06	0.08	0.27	-	-	0.06	-
Dominant Lithology:	SC	ML	CA	ML	CA	CA	MH	MH	CA	MH
Main Rock Unit -										
Rock Type:	Sand	Marble	Lime.	Dior.	Lime.	Lime.	Gneiss	Gneiss	Lime.	Gneiss
Rock Strength:	3	-	6	6	5	6	-	6	6	6
Strength Anisotropy:	2	-	1	1	1	-	-	-	-	-
Structural Anis.:	5	-	4	4	4	-	-	-	-	-
Mean Dip:	25°	-	20°	32°	25°	32°	28°	20°	35°	80°
Dip Direction:	50°	-	45°	10°	20°	230°	70°	20°	10°	180°
Movement Direction	50°	10°	38°	70°	355°	230°	70°	280°	180°	360°
% Sliding Surface Area -										
In Weak Direction:	90	-	50	25	90	80	0	40	0	0
On Major Structure:	0	-	50	70	0	20	80	60	75	75
Through Rock Mass:	10	-	0	0	10	0	20	0	25	25
Toe Factor:	0	-	0	0	0	0	0	0	0	0
% Volume in Toppling:	0	-	0	0	0	0	0	0	0	0
Velocity Class:	7	7	7	7	7	7	7	7	7	7

* Catastrophic failure cases underlined.

Table 3.6

MAIN PARAMETERS OF SOURCE AREA
(see definitions in Table 3.1)

TYPE E, TOE SLIDE

Location:	Frank	Hope	Diablerets
Case I.D.*	1	7	17
Mean Slope Angle:	36°	33°	48°
Scar Slope Angle:	33°	33°	47°
Plan Radius of Contours (m):	10000	10000	1500
Elevation - Toe of Scar Above Valley Floor:	410	475	1300
Detachment Volume (10^6 m^3):	29	47	50
Relative Thickness:	0.10	0.02	0.20
Dominant Lithology:	CA	ML	ML
Main Rock Unit - Rock Type:	Limestone	Schist	Slate
Rock Strength:	6	6	4
Strength Anisotropy:	1	2	5
Structural Anis.:	5	3	5
Mean Dip:	10°	40°	0°
Dip Direction:	100°	240°	340°
Movement Direction	68°	240°	155°
% Sliding Surface Area - In Weak Direction:	65	20	30
On Major Structure:	15	60	0
Through Rock Mass:	20	20	70
Toe Factor:	0	0	0
% Volume in Toppling:	0	0	0
Velocity Class:	7	7	7

* Catastrophic failure cases underlined.

Table 3.7

MAIN PARAMETERS OF SOURCE AREA
(see definitions in Table 3.1)

TYPE F, CENTRE SLIDE

	Campo	Downie	Scatter R.S.
Case I.D.*	45	15	30
Mean Slope Angle:	21°	20°	20°
Scar Slope Angle:	21°	19°	12°
Plan Radius of Contours (m):	-1500	10000	2500
Elevation - Toe of Scar Above Valley Floor:	0	20	0
Detachment Volume (10^6 m^3):	120	1500	300
Relative Thickness:	0.02	0.08	0.11
Dominant Lithology:	MH	MH	SC
Main Rock Unit - Rock Type:	Schist	Gneiss	Shale
Rock Strength:	-	6	2
Strength Anisotropy:	-	2	4
Structural Anis.:	-	3	5
Mean Dip:	22°	18°	4°
Dip Direction:	160°	50°	330°
Movement Direction	160°	70°	332°
% Sliding Surface Area - In Weak Direction:	75	40	70
On Major Structure:	0	50	0
Through Rock Mass:	25	10	30
Toe Factor:	0.2	0.25	0.11
% Volume in Toppling:	0	0	0
Velocity Class:	2	1	1

* Catastrophic failure cases underlined.

Table 3.8

MAIN PARAMETERS OF SOURCE AREA
(see definitions in Table 3.1)

TYPE G, CREST SLIDE

Location:	Madison	Sherman	Kenn.	St. Sorlin
Case I.D.*	4	6	34	56
Mean Slope Angle:	33°	50°	50°	21°
Scar Slope Angle:	30°	46°	60°	21°
Plan Radius of Contours (m):	10000	1500	10000	1500
Elevation - Toe of Scar Above Valley Floor:	60	290	200	0
Detachment Volume (10^6 m^3):	21	12	3	500
Relative Thickness:	0.11	0.06	0.35	0.0
Dominant Lithology:	MH	ML	IN	ML
Main Rock Unit - Rock Type:	Gneiss	Sands.	Gran.	Slate
Rock Strength:	5	5	7	3
Strength Anisotropy:	4	1	1	5
Structural Anis.:	3	2	1	-
Mean Dip:	60°	60°	N.A.	60°
Dip Direction:	360°	270°	N.A.	100°
Movement Direction	360°	280°	210°	100°
% Sliding Surface Area - In Weak Direction:	20	0	0	30
On Major Structure:	0	75	10	0
Through Rock Mass:	80	25	90	70
Toe Factor:	0.8	0.7	0.8	0.7
% Volume in Toppling:	50	10	0	50
Velocity Class:	7	7	7	2

* Catastrophic failure cases underlined.

Table 3.9

MAIN PARAMETERS OF SOURCE AREA
(see definitions in Table 3.1)

TYPE H, FLEXURAL TOPPLE

Location:	Torr.	Clap.	Spriana	Mt.Break.	Glen Pean
Case I.D.*	35	19	55	24	25
Mean Slope Angle:	32°	40°	45°	40°	40°
Scar Slope Angle:	38°	32°	-	31°	35°
Plan Radius of Contours (m):	10000	2000	2000	1000	10000
Elevation - Toe of Scar Above Valley Floor:	0	0	0	690	0
Detachment Volume:	6	50	-	200	40
Relative Thickness:	0.09	0.08	-	0.20	0.06
Dominant Lithology:	MH	ML	MH	ML	MH
Main Rock Unit -					
Rock Type:	Gneiss	Gneiss	Gneiss	Schist	Schist
Rock Strength:	3	4	6	6	6
Strength Anisotropy:	2	3	2	2	-
Structural Anis.:	5	5	5	4	-
Mean Dip:	70°	65°	35°	45°	80°
Dip Direction:	190°	350°	60°	50°	310°
Movement Direction	10°	230°	240°	220°	150°
% Sliding Surface Area -					
In Weak Direction:	0	0	-	-	-
On Major Structure:	0	0	-	-	-
Through Rock Mass:	100	100	-	100	100
Toe Factor:	N.A.	N.A.	N.A.	N.A.	N.A.
% Volume in Toppling:	100	100	100	100	100
Velocity Class:	5	3	2	1	1

* Catastrophic failure cases underlined.

Table 3.10

MAIN PARAMETERS OF SOURCE AREA
(see definitions in Table 3.1)

TYPE I, BLOCK TOPPLE

	Motto d'Arbino
Case I.D.*	53
Mean Slope Angle:	30°
Scar Slope Angle:	20°
Plan Radius of Contours (m):	700
Elevation - Toe of Scar Above Valley Floor:	700
Detachment Volume (10^6 m^3):	35**
Relative Thickness:	0.39
Dominant Lithology:	MH
Main Rock Unit -	
Rock Type:	Gneiss
Rock Strength:	-
Strength Anisotropy:	-
Structural Anis.:	-
Mean Dip:	80°
Dip Direction:	0°
Movement Direction	15°
% Sliding Surface Area -	
In Weak Direction:	-
On Major Structure:	-
Through Rock Mass:	-
Toe Factor:	N.A.
% Volume in Toppling:	100
Velocity Class:	7

---

* Catastrophic failure cases underlined.
** Piecemeal detachment.

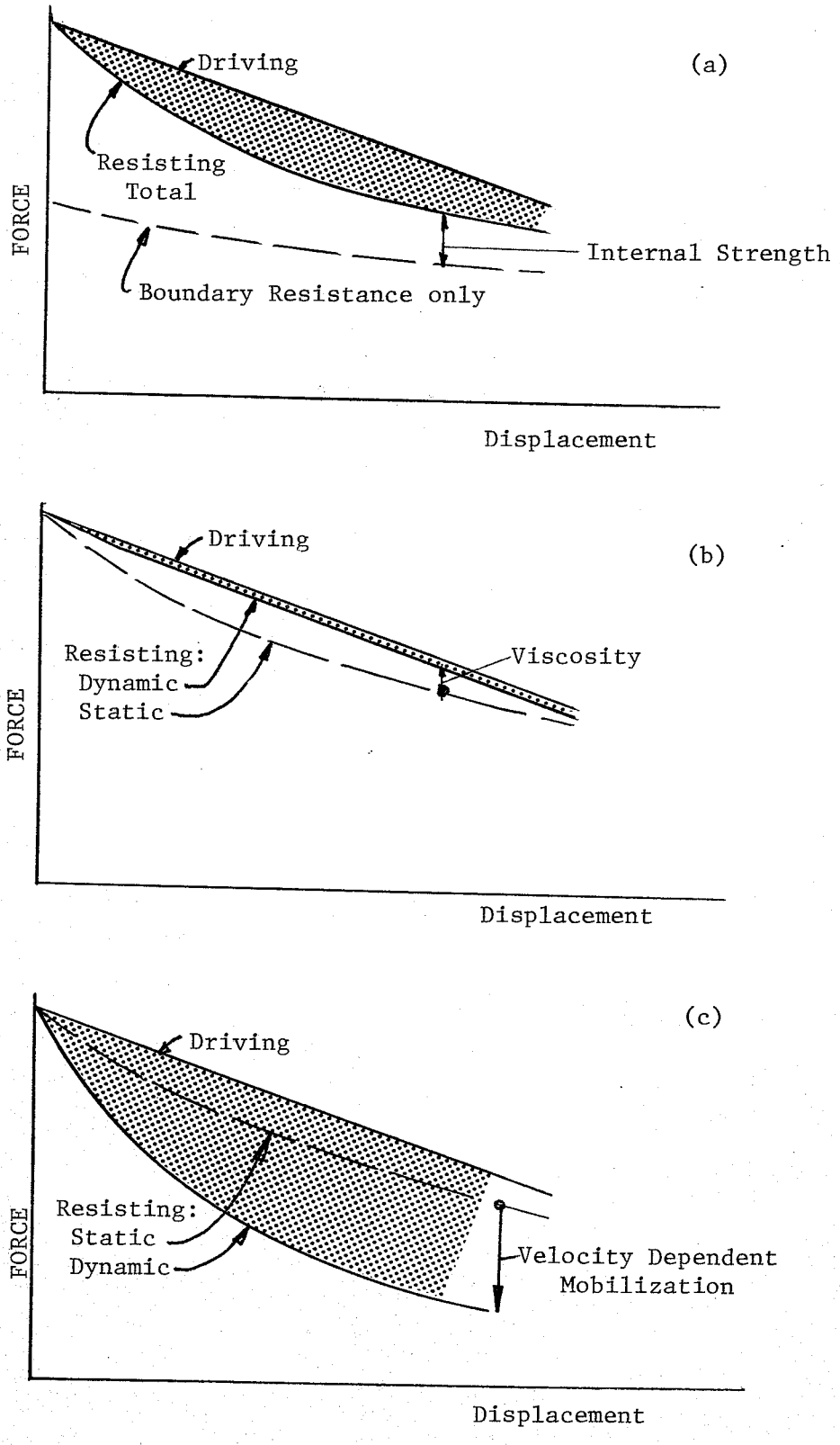

Figure 3.1 Development of force resultants: a) static conditions, b) viscous response, c) rate-softening response.

	NO STRUCTURAL CONTROL	RAN DISC TINU	TOPPLING	
		REST	FLEXURAL	BLOCK
TYPE	A		H	I
	SLUMP	COLLIDE	FLEX. TOPPLE	BLOCK TOPPLE
CATASTROPHIC (>3 m/sec) (Stronger rock, steep slope)		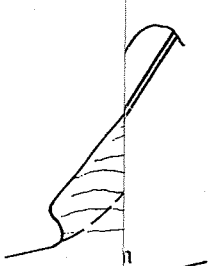 2. E ison		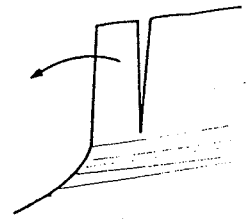 19. Pulverhorndl 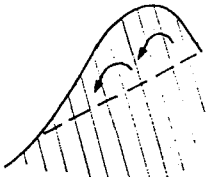 20. Elk Ridge
NON-CATASTROPHIC (Weaker rock, gentle slope)	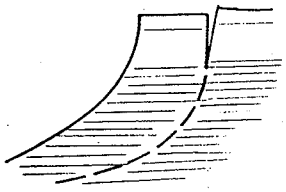 1. Massif de Plate	ek	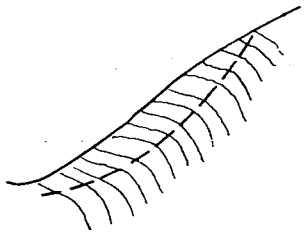 17. Clapiére 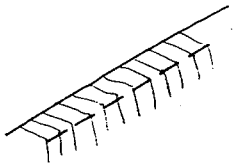 18. Glen Pean	

surface developed

LEGEND : ═══ We the rock mass

Note - references for case histo
10- Heim (1932). 4- Hungr
8- nil. 9- Cruden & Krahn (

tion of rockslide detachment
history references provided in the text)

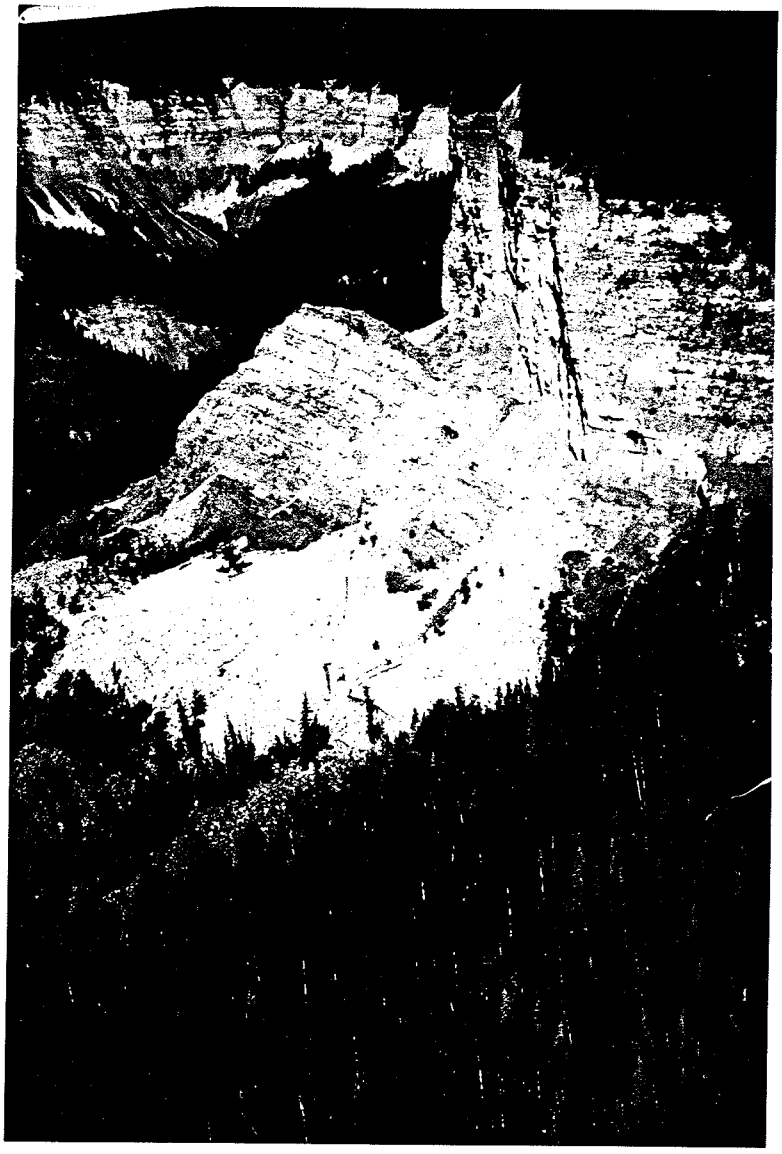

Figure 3.3

Type A, rock slump in Cretaceous shales and limestones. Scatter River, British Columbia.

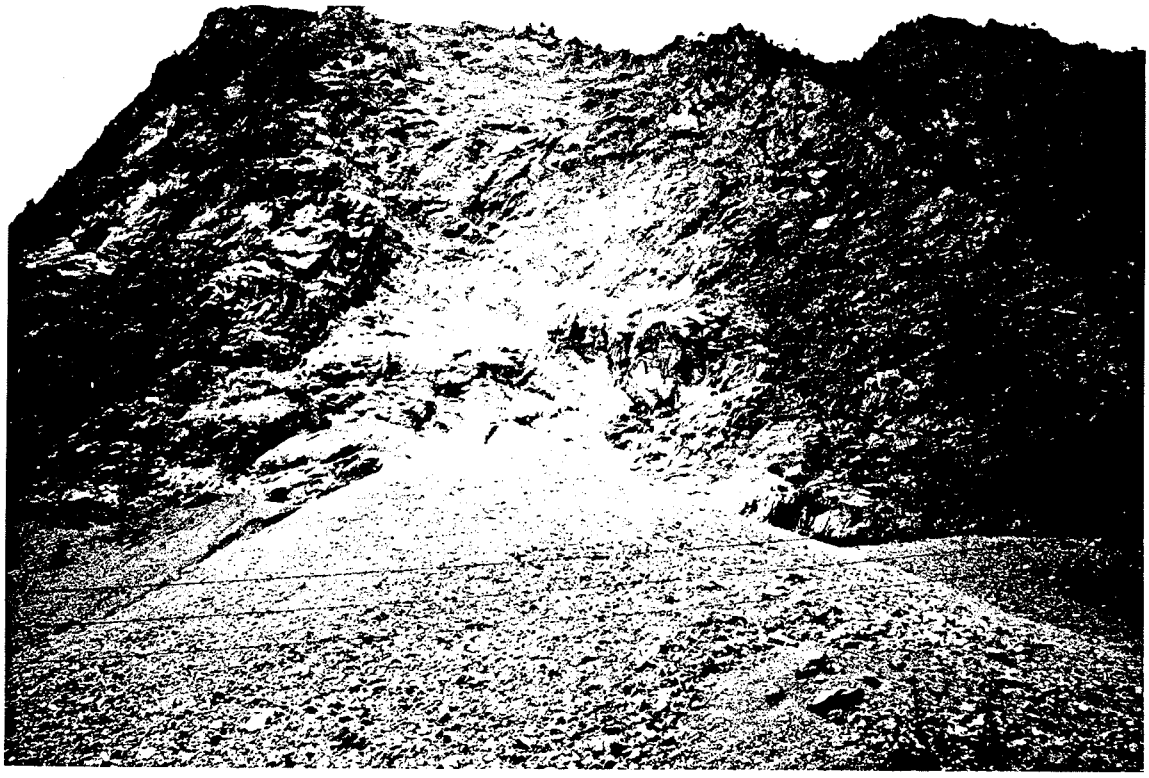

Figure 3.4

Type B, rock collapse of approximately 1 million m^3 in granitic rocks. Defile de Maupas, Isere, France.

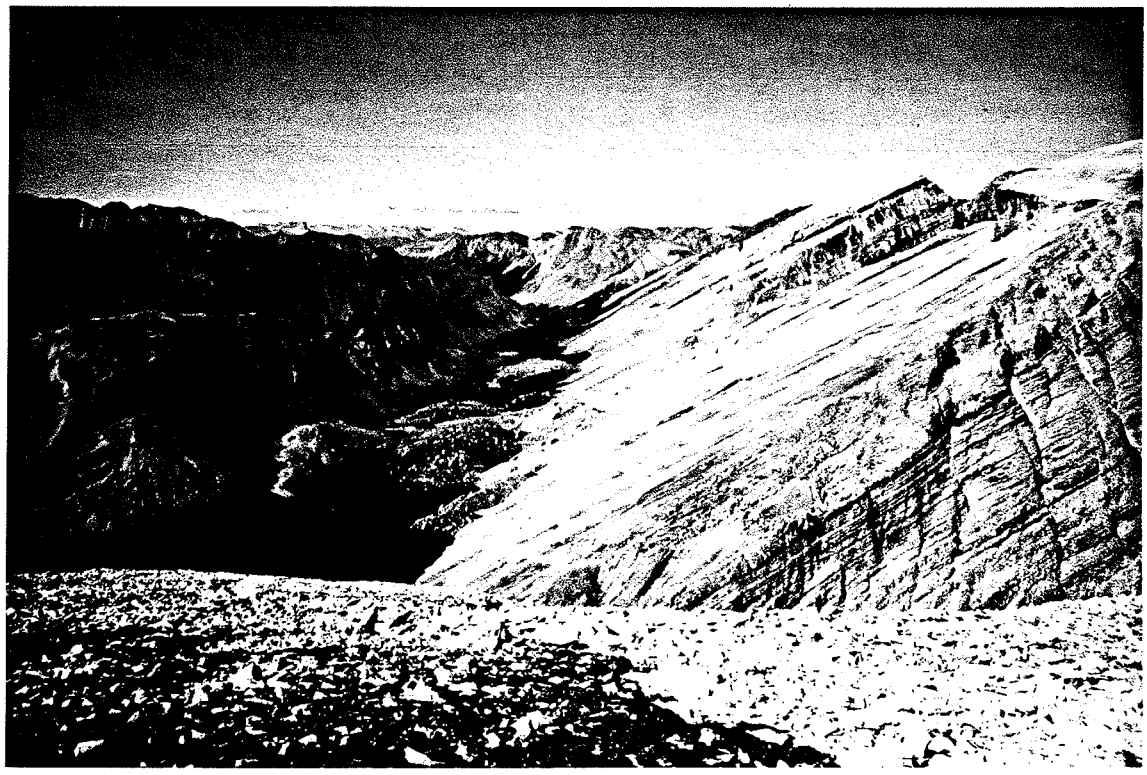

Figure 3.5

Type C, rock glide in dolomite. The slope is 1,200 m high. Avalanche Lake, Northwest Territories.

Figure 3.6

Type D, compound slide controlled by three weak surfaces in gneissic rocks. Val Pola slide, Valtellina, northern Italy.

Figure 3.7

Type E, compound slide controlled by a weak surface in the toe area in limestone. The source of the slide is the area in shadow. The toe weakness is a near-horizontal fault (Arrow). The Diablerets Slide, Bernese Alps, Switzerland.

Figure 3.8

Type F, compound slide with a near-horizontal weak surface beneath its centre, in Cretaceous shales and limestone. The valley is 1 km wide. Scatter River, north-eastern British Columbia.

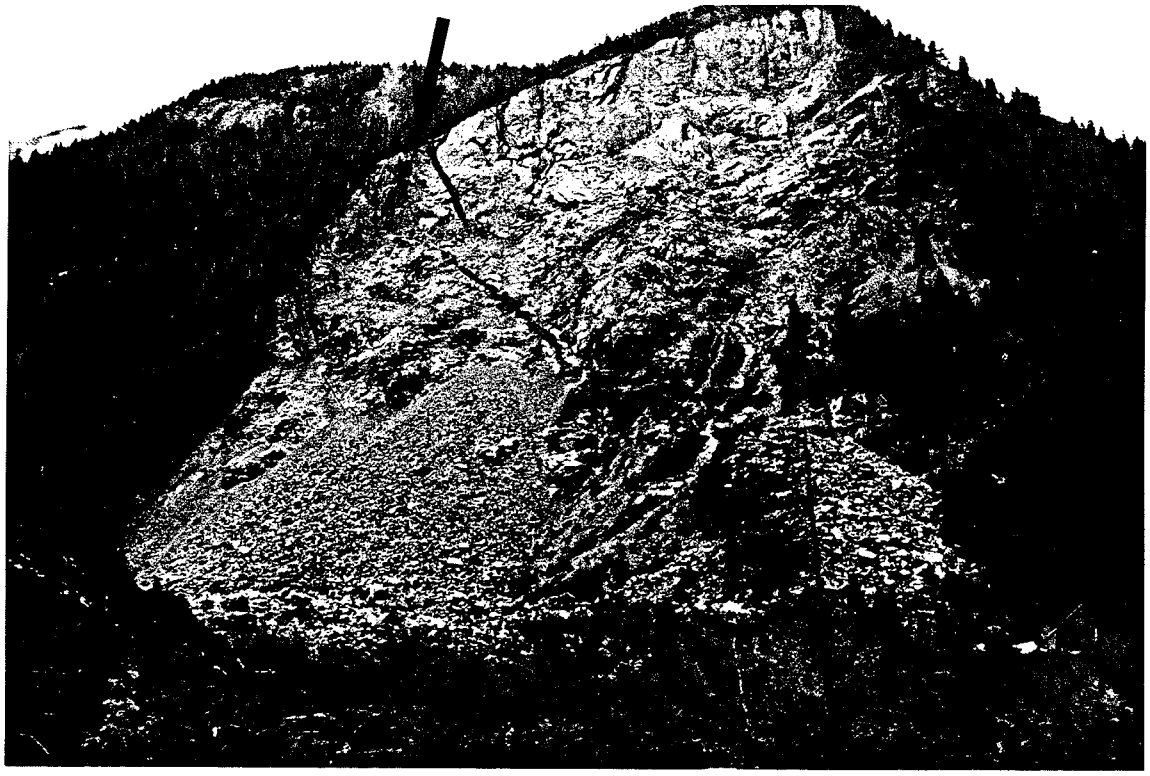

Figure 3.9

Type G, compound slide, controlled by a steep fault (shown by arrow) in the crest area. Quartz diorite, Kennedy River, Vancouver Island.

Figure 3.10

Type H, Flexural toppling failure in schist and gneiss, which developed into a slump. La Clapiere, Maritime Alps, France.

4. ROCK AVALANCHE VELOCITY AND RUNOUT

4.1 Introduction

Rockslides which attain catastrophic velocities generally disintegrate into masses of fragments and move in a flow-like manner. The resulting flow slides are known as rock avalanches or sturzstroms (German "collapse streams"). Rock avalanches load or impact saturated soil material in their path, liquefying it. Much evidence has now been gathered to document the presence of such liquefied basal material in rock avalanche deposits. The evidence includes layers, dykes or diapirs of basal soil in debris deposit cross-sections (Yarnold and Lombard, 1989), and areas of "splash" of liquefied mud expelled around the margins of a rock avalanche deposit (Cruden and Hungr, 1986). Some rock avalanches expel projections or "fingers" of debris flow-like character, to travel for considerable distances beyond the main deposit margins. Often, the projections travel at right angles to the direction of emplacement of the main mass (Example: North Nahanni Slide, Evans et al, 1987).

Some rock avalanches entrain sufficient liquefied material that they resemble large debris flows. These belong to the most mobile examples (e.g. Huascaran, Plafker and Ericsen, 1978).

Rock avalanches travelling over glacier ice appear to have a special character which leads to abnormally wide spreading of the deposits and great mobility (see Section 4.2).

4.2 Mobility Theories

Distances travelled by rock avalanches are much greater than what would be predicted on the assumption of purely frictional movement resistance. The following hypotheses have been proposed to explain the surprising mobility of rock avalanches.

1) Air cushion theory. Shreve (1966, 1968) suggested that a sheet of rockslide debris slides on a cushion of air, trapped when the slide is catapulted into an

air trajectory by a ramp. He presented an interpretation of certain features of deposit morphology to support the idea. Some of this interpretation has been questioned by Hsü (1975) and Cruden and Hungr (1986).

2) Fluidization by trapped air (Kent, 1966 and others). A similar air entrapment process is thought to cause a full or partial fluidization of the debris, by means of upward flow of air. Lack of physical evidence for fluidization was pointed out by Hungr (1981), Cruden and Hungr (1986) and Cassie et al. (1988).

3) Fluidization by vapor. Pautre et al. (1974) and Habib (1975) demonstrated that rock avalanche movement expends sufficient energy to vaporize pore water. The heat calculations require important assumptions concerning the thickness of the shearing zone. Also, the influence of rock mass expansion during breakage upon pore gas pressure has not been clarified.

4) Rock melting. Erismann (1979) found specimens of molten rock near the sliding surface of a rockslide near Koefels, Switzerland. He showed that sufficient frictional heat can be produced in exceptionally thick slide masses to melt basic igneous rock and showed a corresponding reduction of the friction angle in experiments.

5) Rock dissociation. Many mobile rock avalanches occurred in calcareous rocks, which do not melt when heated. Erismann (1979) suggested that such landslides may be fluidized by escaping CO_2 gas, produced by heat dissociation of limestone.

6) Fluidization by dust dispersions. Hsü (1975) that dense dispersions of rock dust act as a pore fluid among the larger clasts. The role of air in the behaviour of the dispersions was neglected, as the phenomenon was assumed to occur in the moon avalanches as well as in the terrestrial ones. Hungr and Morgenstern (1984) showed by experiment

that rock dust and sand mixtures behave frictionally, with no velocity dependence.

7) Mechanical fluidization. This hypothesis seems to have never been rigorously defined, although many authors have alluded to it (Howard, 1973, Scheidegger, 1973, Hsü, (1975) and many others). The underlying idea is that the mechanical character of shearing in a granular material changes at very high strain rates, as the grain to grain contacts change from continuous sliding to intermittent collisions. No one has succeeded so far in demonstrating a change of behaviour theoretically.

   Laboratory experiments including flume tests at velocities of up to 6 m/sec and ring shear tests at 1 m/sec failed to show any indication of a change of behaviour with increasing strain rate (Hungr, 1981, Hungr and Morgenstern, 1984, Sassa, 1988). It may be argued that still higher velocities are required to demonstrate a change in behaviour. However, in both types of test, the shearing was concentrated in a zone less than 20 mm thick, producing a shear strain rate of 5,000 to 30,000% per sec. Such a strain rate would yield a flow velocity of 25 to 150 m/sec (90 to 540 km/hour) in a shear zone only 1 m thick.

8) Acoustic fluidization. Melosh (1979, 1987) showed theoretically that vibrations produced on the sliding surface by rapid movement over uneven ground could reduce the dynamic friction angle of the granular debris. Direct shear tests of sand conducted on a vibrating table, described by Barkan (1962), showed that such a phenomenon does exist. Barkan (1962) even describes measurements of fluid behaviour characterized by a "vibro-viscosity".

   An important difference between mechanical and acoustic fluidization must be pointed out. The former process is thought to be inherent to the material itself and requires no energy input other than vigorous shearing. It should therefore be capable of duplication in the laboratory. Acoustic fluidization, on the other hand, requires vibrational energy

generated externally by the boundary conditions of the full scale movement.

9) Lubrication by liquefied saturated soil. Heim (1932) explained the high mobility of the Elm Slide by the effects of mud, entrained by the rockslide from loose valley deposits, liquefied under the weight of debris. A similar mechanism was suggested by Sassa (1984), described with the use of pore-pressure parameters, and incorporated into a dynamic model. Hutchinson (1986) and De Matos (1987) developed related models, including the effects of consolidation. No existing model accounts for the velocity dependence of pore-pressure in the liquefied layer, which may introduce important rheological effects.

Probably each of the mechanisms listed above plays a certain role in the mobilization of rock avalanches. It remains difficult to decide which is the dominant mechanism in a specific case and how it controls the dynamics of the flow.

The weight of the evidence introduced so far seems to favour lubrication by liquefied material (Hypothesis 9). This mechanism is clearly dominant in some cases and possible in all.

Acoustic fluidization (8) has a sound theoretical and experimental basis and is not contradicted by the field evidence.

The group of theories based on gas pressure (1, 2, 3 and 5) appear plausible on theoretical grounds, but are not well supported by field evidence. For example, inverse grading which is common in rock avalanche deposits points to the occurrence of vibrations, not to gas fluidization which would produce a normal grading. Also, gas escape structures such as craters, marginal fans or channelling structures have not been described in the rock avalanche literature.

The mechanical fluidization theory (7) has been disproven by experiments and should be replaced by the acoustic fluidization concept.

The two most plausible explanations of rock avalanche movement 8 and 9) both depend on the structure and the boundary conditions of the full scale flow, as much as on material properties.

As a result, it is unlikely that the standard approach of determining a constitutive relationship for the material in the laboratory and applying it to the field case by means of analysis is feasible in case of rock avalanche mobility. The constitutive relationship is in this case dependent on the boundary conditions of the full scale problem. Therefore, the analytical methods must be formulated empirically and calibrated against full scale case histories.

The selection of prototype events for calibration must be made so that the main controlling parameters (i.e. magnitude of event, degree of flow confinement and the nature of material forming the slide path are similar).

4.3 Empirical Models

Empirical models seek correlations between various parameters describing the rock avalanche path and deposit. They include the following:

Heim (1932) defined a parameter called "fahrboeschung" (travel angle), as the angle of a line extended along the centre of the flow path from the uppermost crest of the source area to the furthest point of the distal margin of the deposit. He noted that the angle has a tendency to become smaller with increasing volume of the event. He also showed that, should the resisting force during movement be frictional, the average friction coefficient must approximate the tangent of the fahrboschung or H/L, where H is the total elevation difference between the two ends of the flow path and L is the horizontal distance between them.

Scheidegger (1973) plotted H/L against the deposit volume for approximately 40 cases from various parts of the world (mostly Europe) and showed that there is an approximate linear relationship between the two quantities on a log-log scale. A version of the

Scheidegger plot incorporating an exceptionally wide range of volumes due to McEwen (1989) is shown in Figure 4.1. The trend is clear, but the scatter of the correlations is too strong to permit their use for predictions.

Abele (1974) compiled a very detailed data base of rock avalanche deposits from the Alps and produced several correlations, including:

- H/L versus volume (Figure 4.2)
- Deposit length versus volume (Figure 4.3)
- Spreading ratio versus volume (Figure 4.4)
- Spreading ratio versus maximum height of fall (Figure 4.5).

These are 4-dimensional correlations, as they are sorted with respect to the broad geological domain and the type of deposition area (see Figure 4.2). Nevertheless, they remain widely scattered.

Li (1983) replotted some of Abele's data and derived correlation equations and confidence limits for it.

Hsu (1975) questioned the "fahrboeschung" concept and argued that rock avalanches flow as a fluid, depositing on the flatter segment of the path, as shown in Figure 4.6. If a frictional model was to apply, the avalanche deposit would remain within a 32° vertical angle of the debris. The length of horizontal runout outside this angle is defined as the "excessive travel distance" L_e. This can be shown to increase with increasing event volume (Figure 4.7). Again, the trend is evident, but the scatter of the data negates practical usefulness.

Howard (1973) plotted H/L versus the total potential energy of the slide, finding a trend similar to Scheidegger's in both the sense and scatter.

Hungr (1981) repeated Scheidegger's plot, expressing "travel angle" as the vertical angle between the centres

of gravity of the source and deposit (Figure 4.8). The trend is similar and the scatter is undiminished. In addition, estimation of the position of the gravity centres is difficult in most cases.

Ui (1983, 1986) showed that rock avalanches derived from volcanic sources plot near the lower margin (most mobile) of the scatter band on a Scheidegger plot (Figure 4.9).

None of the listed correlations gives an account of the topographic configuration of the path. Obviously, channelled flows should reach further than those encountering adverse slopes or subject to lateral spreading. An attempt to account for these fundamental factors based on data collected in the rockslide data base is presented below.

With the assumption that rock avalanche deposits of various sizes are geometrically similar, the volume (V), and area (A), of the deposit should be related by the equation:

$$A = cV^{2/3} \qquad (9)$$

where c is a constant. Equation 9 is plotted by a dashed line in Figure 4.10, which also includes data points for 40 rock avalanches from the database (Section 1.4). Apart from a considerable random scatter, the general trend of the data fits Equation 9 with a c = 12.0. The assumption of geometrical similarity is therefore confirmed.

The random scatter probably results from topographic complexities such as channelling, flow obstructions and branching, but also from the influence of material forming the flow path. For example, all four of the points showing the highest degree of spreading (5,6,8 and 9) crossed glaciers in their paths.

Another source of random scatter is inaccuracy in the estimates of volume. Only a very small percentage of rock avalanche deposits has been examined in sufficient detail to provide accurate estimates of deposit thickness

and it is not uncommon to find differences of a factor of two or more between estimates by different authors.

The geometrical similarity trend leads directly to the prediction of runout distance as a function of volume, if it is assumed that rock avalanche profiles are typically bi-linear (Figure 4.6). Small scale dry rockslides run out only to the foot of cliffs and talus slopes, remaining within an angle of 32°, from the crest of the source area. Large scale rock avalanches run out beyond the toe of the source slope. Hsu's "Excessive Travel Distance" is defined as:

$$L_e = L - H/\tan 32° \qquad (10)$$

If we assume that 32° is the average angle of the source/travel segment of the path, then L_e must simply equal the length of the deposit, measured in the direction of motion. This can be expressed as a function of the deposit area A and mean width B or the mean aspect ratio R (length over mean width):

$$L_e = A/B = \sqrt{RA} \qquad (11)$$

$$\text{Where:} \quad R = \frac{L_e}{B} \qquad (12)$$

Substituting for A from Eqn. (9) (c = 12.0 from Fig. 4.10)

$$L_e = \sqrt{RcV^{2/3}} = 3.47\sqrt{R}\sqrt[3]{V} \qquad (13)$$

Figure 4.11a shows a collection of L_e values from 38 rock avalanches derived from the data base, plotted against deposit volumes. The actual Aspect Ratio of each deposit is indicated by a number inside the plotted symbols. Superimposed on this plot are curves representing the relationship of Eqn. 13, evaluated for several values of R.

The round symbol indicates cases in which the actual Excess Travel Distance falls within a 50% error margin of

the value predicted by Eqn. 13. The inverted triangles are cases which travelled further and squares are those which stopped short of the predicted distance. The case reference numbers are given on Figure 4.11b. In summary, over 50% of the cases conform to Equation 13, while 25% are more mobile and the remainder are less.

The combined assumption of geometrical similarity and bi-linear path profile therefore explains the excessive travel of most rock avalanches. In simple terms, the deposits form as soon as the inclination of the slope profile reaches close to the horizontal. This is confirmed in Figure 4.12b, which plots the path slope near the centre of each deposit (defined in Figure 4.12a) against volume. Except for rock avalanches smaller than 5 million m^3, and one case of a block toppling failure believed to have deposited in a piecemeal fashion (No. 53), all of the deposits formed at slope angles of 10° or less.

A simple preliminary method for runout prediction, given a potential detachment volume, would be to estimate the deposit area from Figure 4.10 and to distribute the deposit at the foot of the source slope where the slope inclination is less than 10°, allowing for the irregularities in the topography.

The above approach will severely underestimate the run out, however, if one or both of the following applies:

- If a part of the avalanche path crosses a glacier.

- If the avalanche enters a channel or valley infilled with stream deposits, which continues sloping steeper than about 5°.

Under the latter circumstances, one should expect the formation of a "rock avalanche-debris flow", comprising a high proportion of liquefied saturated material and capable of flowing for long distances at gentle angles. Of the nine rock avalanches in Figure 4.11 with travel distances which exceeded the general trend, four were channelized debris flow events (Huascaran, Pandemonium

Creek, Mt. Ontake), one was a thinly spread out deposit on glacier ice (Sherman) and the remaining four were widely spread over floodplain deposits.

Obviously, empirical estimation of rock avalanche runout requires knowledge not only of volume, but also the degree of channelization (Equation 13) and the character of material forming the path of the avalanche.

Lateral and longitudinal spreading of rock avalanche debris is important for the determination of runout and was investigated using the data base. Spreading Ratio was defined as the ratio between the plan areas of the deposit and the source region*. Figure 4.13 shows that the spreading generally increases with increasing relative elevation of the source toe above the floor of the valley. (It shows little dependence on the total elevation difference, see Figure 4.5). The other two factors examined - lateral confinement of the deposit in Figure 4.14 and the degree of concavity of the slide path profile in Figure 4.15 - show no systematic influence on spreading. The two principal factors controlling spreading of the slide mass therefore appear to be toe elevation of the source region and the nature of the material forming the slide path.

4.4 Block Models - Two-Dimensional

The simplest type of analytical approach is the sliding block model, which describes the rock avalanche as a dimensionless body moving down the profile of the path. Its movement is controlled by a single force resultant, representing the gravity driving force as well as all movement resistance. The correct application of this "lumped mass" approach is to consider the movement of the centroid of the displaced mass (Banks and Strohm, 1974). However, following a trend first established by

---

* This contrasts with the definition of Abele (1974), who considered areas measured in the slope direction - see Figures 4.4 and 4.5

workers in snow avalanche dynamics (Voellmy, 1955, Perla et al., 1980), most of the lumped mass models have been applied in terms of a hypothetical block travelling from the crest of the source to the extreme distal point of the deposit.

A variety of lumped models have been proposed, differing in the definition of the resisting forces as functions of velocity, distance, or both, as described below.

Banks and Strohm (1974) assumed the resisting force to be a purely frictional term, dependent on the normal component of the slide weight. This approach is probably correct for small scale rockslides and falls of limited displacement. It severely overpredicts the velocity of movement for larger rock avalanches (Koerner, 1976).

Koerner (1976) adapted the resistance equations developed by Voellmy (1955) for snow avalanches. The movement resistance of the block is assumed as composed of a frictional term and a turbulence term, dependent on the square of velocity and inversely dependent on the flow depth (this term is a measure of kinetic energy per unit volume).

Koerner took the two coefficients (friction and turbulent resistance divided by the flow depth) as constants for each flow path. An infinite number of pairs of the coefficients can be used to obtain a given total displacement. However, each pair produces a different velocity profile (Figure 4.16). The fastest velocities are produced when the frictional term is dominant, while slides controlled by turbulent resistance move over long paths with limited velocities. An appropriate choice of a unique pair can only be made if there are some independent velocity observations along the path. The Koerner approach was used by the Garibaldi Review Ranel to estimate the runout of a rockslide from the Barrier in southern British Columbia (Hardy et al., 1978).

McLellan and Kaiser (1984) attempted to find a method for assigning a pair of resistance coefficients "a priori", to determine the total runout in a given path. They found the most consistent results with a friction

coefficient equal to the tangent of the mean runout slope (Angle alpha in Figure 4.16). Problems with their method are that the runout slope is vaguely defined, the model predicts improbably large velocities and it has been tested on only six examples (from the Mackenzie Mountains). However, their general approach of calibrating the Koerner model within a select group of similar events is probably as reliable as any existing approach.

Evans et al. (1989) applied the Koerner model to the highly channelized Pandemonium Creek slide in British Columbia. They found that the initial segment of the path, down the side of the valley, had to use a larger frictional coefficient, while the runout segment along the base of the valley was more turbulent and slower. A concentrated energy loss similar to a hydraulic jump separated the two segments. This stresses the need for selecting geometrically and geologically similar events for calibration of any model.

Moriwaki et al. (1985) found a good approximation to the velocity profile of the Mt. Ontake rock avalanche using a two parameter model with a frictional (velocity independent) term, decreasing exponentially with distance. The rate of decrease becomes the second empirical constant in this case. Ouchi and Mizuyama (1989) used the same model for another volcanic rock avalanche in Japan and found it necessary to change the two input coefficients substantially.

The gradual decrease in frictional resistance is physically explained by the entrainment of increasing quantities of saturated material along the path of the flow.

Sassa (1988) defined a one parameter model, where the "apparent friction coefficient" is a function of a pore-pressure coefficient, B. This coefficient is assumed to describe the increase in pore-pressure of the partly saturated soils lying in the path of the avalanche as a result of over-riding and rapid loading by the flow front. Although Sassa suggests a laboratory testing procedure for determining B, it would seem doubtful that the pore-pressure beneath the flow front can be predicted

considering the variety of materials and geomorphic features traversed by the flow. The B-coefficient is therefore an empirical factor, best obtained by back-calculation. The form of variation of B along the path is vaguely defined as a function of the degree of saturation of the path soils.

Hutchinson (1986) and De Matos (1987) independently derived models using a frictional term, coupled with a one-dimensional consolidation algorithm to predict the gradual dissipation of excess pore pressure in an initially liquefied basal layer. The resulting resistance equation is again a two parameter scheme which is probably not dissimilar from the Koerner model. The velocities derived by De Matos (1987) for certain case histories appear unrealistically high.

None of the models based on evaluating pre-pressures in the saturated basal layer account for the probable strong connection between pore pressure and velocity under the partially-drained conditions of a high speed flow. This, in all probability, introduces important velocity dependencies which are best accounted for by an empirically based, total stress rheological model, such as that proposed by Koerner (1976).

Hungr and Evans (1991) used the Koerner model to analyse two adjacent lobes of the Avalanche Lake slide in the Northwest Territories (Case 13, Figure 14 in Appendix C). They found that the contrasting geometries of the two profiles could only be accounted for, if the model was referenced to the centre of gravity of the failed mass, not to the ends of the path as the lumped-mass models are usually applied. This is especially important in case of slides of limited displacement and large volume, such as Avalanche Lake.

The lumped-mass approach cannot account for lateral confinement and spreading of the flow and the resulting changes in flow depth. It should therefore be regarded as an empirical approach, suitable only for comparing paths which are very similar in terms of geometry and material properties.

4.5 Block Models - Three-Dimensional

Several authors have applied the lumped mass model in three dimensions, using digital representation of the path landscape. Rochet (1987) extended a rigid block trajectory and collision model by scaling the required restitution coefficients in relation to the volume of the blocks. Each is released sequentially and upon deposition, it modifies the path for the next block. Apart from this, there is no interaction between blocks. The method has not, unfortunately, been completely described in publications. However, it has been used to predict hazard zones and design remedial measures for several potential slides in France. Its calibration against case histories is apparently very limited.

Kobayashi and Kagawa (1987) derived a 3-dimensional version of the Koerner model. A series of blocks are released simultaneously on a digitally described surface. They are assumed to interact by lateral collisions with a restitution coefficient of 0.9 (about elastic). Reasonable simulation of the Mt. Ontake rock avalanche is claimed.

McEwen and Malin (1989) used a similar multi-particle model to simulate the 1980 Mt. St. Helens rock avalanche. In their case, particle collisions are assumed to be completely plastic, so that upon collision, a pair of particles continues in a direction determined by the average of their respective movement vectors (Figure 4.17). They found best representation of flow velocities using a two parameter constant-viscous resistance equation (similar to the Bingham model).

The 3-dimensional models may be useful in determining the average path (or multiple paths) of a potential slide over complex topography. They offer little advantage in cases where the travel path is well defined. Their assumptions concerning interaction between different parts of the moving mass may be quite important in controlling the movement direction. All are calibrated against a single event only.

4.6 Fluid Dynamics Models

Complex numerical procedures are required for the solution of the highly unsteady problem of flow slide movement. Two dimensional solutions based on the Bingham resistance equations have been derived by Trunk et al. (1986) and Norem and Locat (1991). An example output from the analysis of the Madison Canyon slide in the former reference is shown in Figure 4.18.

The advantage of the fluid dynamics models over the lumped mass approach is that the partition of energy into overall displacement (centre of gravity) and longitudinal spreading can be accounted for. In many events, the influence of spreading on the runout is as great, or greater than the influence of central displacement.

The conditions which determine the amount of spreading, however, introduce another indeterminate set of parameters into the analysis, which can have important consequence on the results.

Appendix B describes a simple fluid dynamics model which allows for estimating internal longitudinal strain in the flowing mass. It can be shown with this model that the longitudinal pressure gradient in a relatively dry sheet of moving rockslide debris can be much different from the hydrostatic gradient which is a standard part of fluid dynamics calculations. Allowing for the pressure gradient to be controlled by the plastic shear strength of the debris substantially reduces the degree of longitudinal spreading. This has important consequence on the predicted runout. The model has been used to describe the dynamics of the Avalanche Lake case, described in Appendix C.

Sassa (1988) developed a 3-dimensional version of his frictional model described earlier, using general fluid dynamics equations. The pressure gradient in his model is assumed to be controlled by a constant lateral "at rest" pressure coefficient. This is not a realistic assumption where the flow sheet is under compression and close to a passive plastic state (e.g. at the base of a runup slope). The flow path may be distorted as a

result. The basal resistance is again controlled by the pore pressure coefficient B, the magnitude of which excerts an overwhelming control on velocity, direction and distance of movement (Figure 4.19). His model is the only one presently available which can account for lateral confinement. However, the frictional movement equation is independent of the flow depth and, therefore, the rheological effects of confinement will not be felt.

Each of the existing fluid dynamics models has been calibrated against one event only.

4.7 Multi-block Models

Several models have been used which are based on an assumed form of the slide during movement.

Romero and Molina (1974) represented the sliding body of a series of slices, similar to a slope stability method.

BC Hydro (1981) used a coupled series of blocks deforming in a user-prescribed fashion and controlled dynamically by a single parameter frictional resistance. A similar approach was used by Hendron and Patton (1985), although their resistance term included a velocity-dependent reduction to account for the mobilizing effects of frictional heating.

The above block models are suitable for semi-coherent sliding movements along a discrete surface, such as the Vaiont Slide. It is well established that frictional models overestimate velocity in those cases where the movement is of flow-like character.

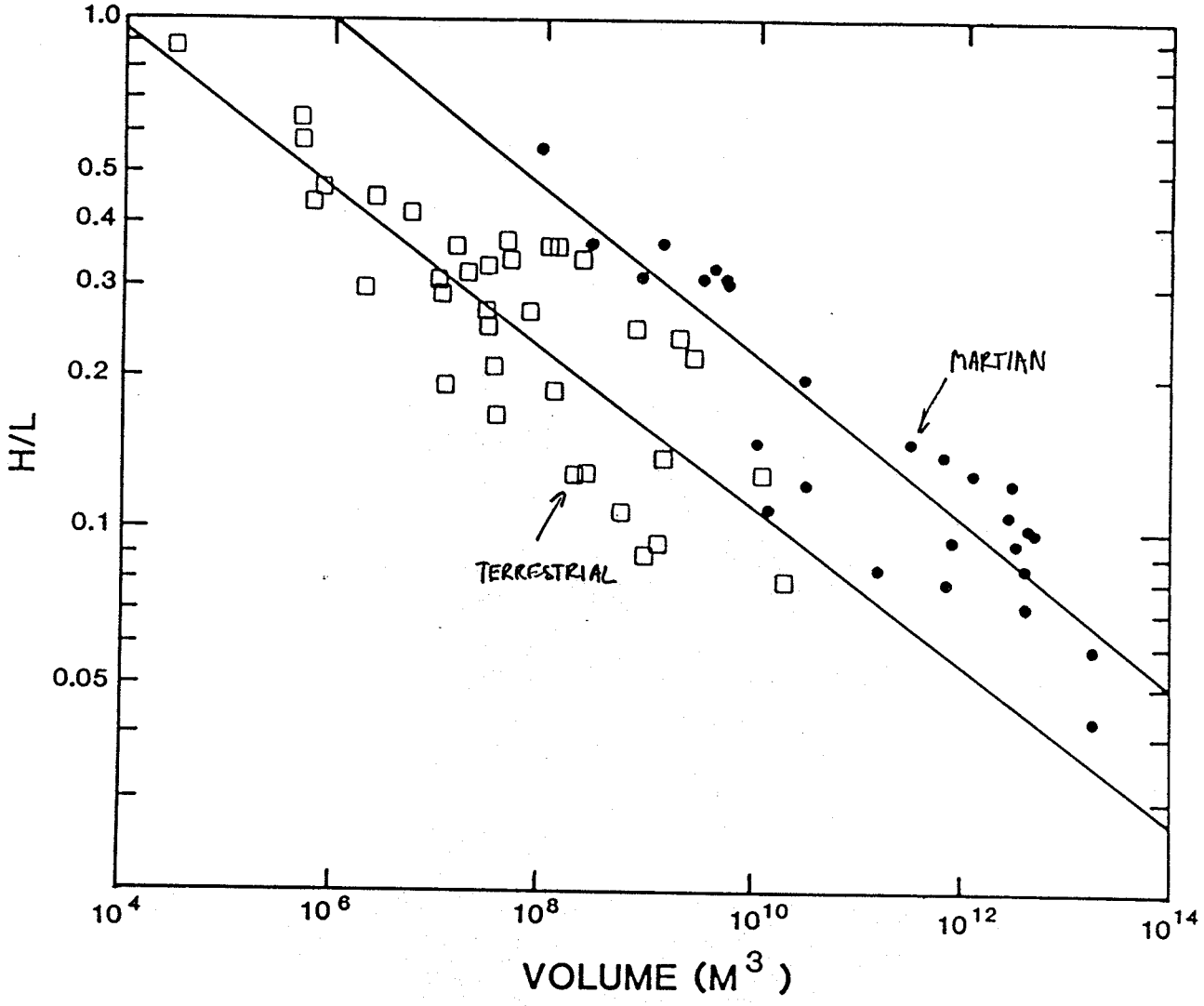

Figure 4.1

H/L versus volume for large landslides on Earth and Mars (McEwen, 1989)

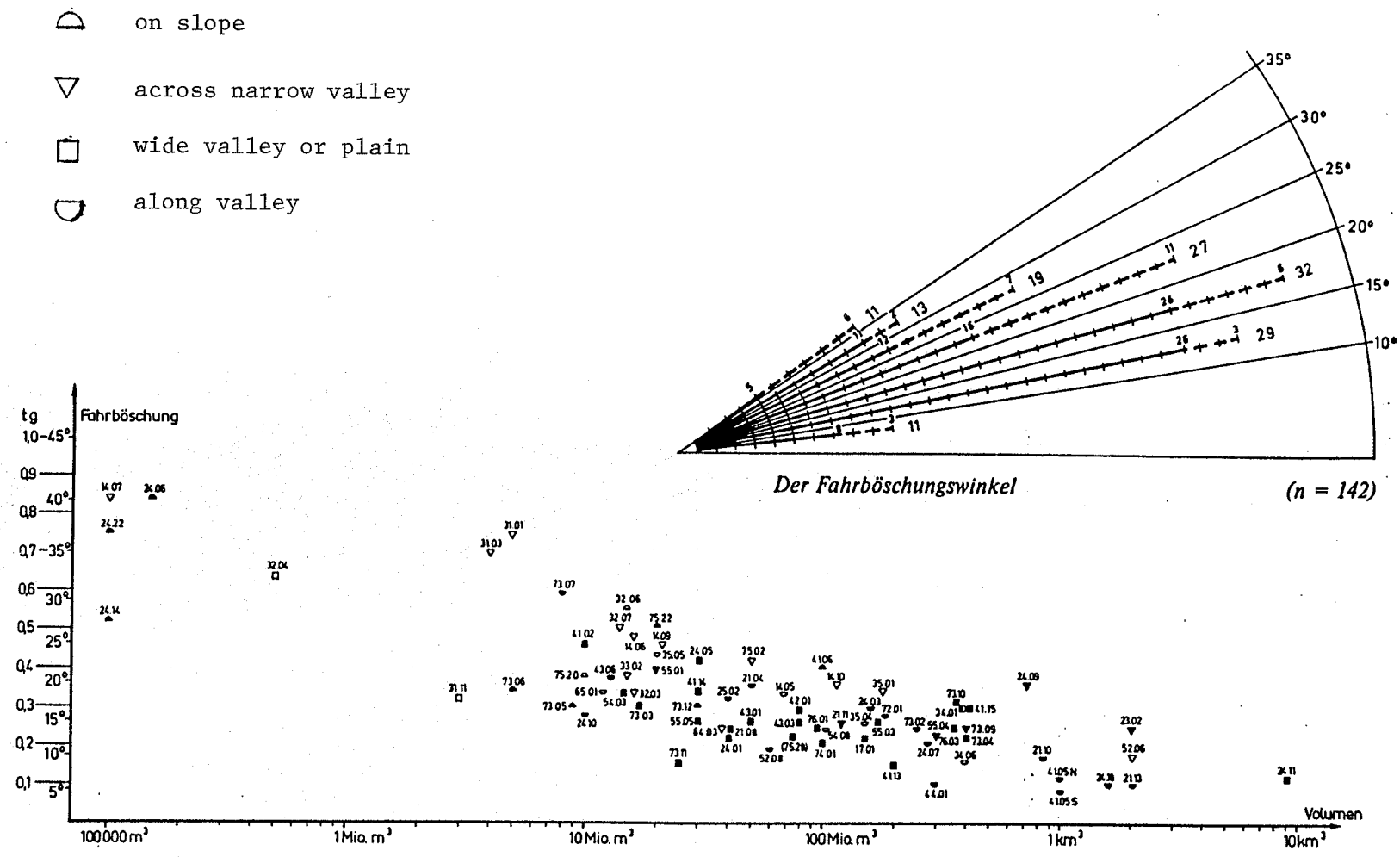

Figure 4.2

H/L versus volume (Abele, 1974). Full symbols are sedimentary rocks.

LENGTH
(km)

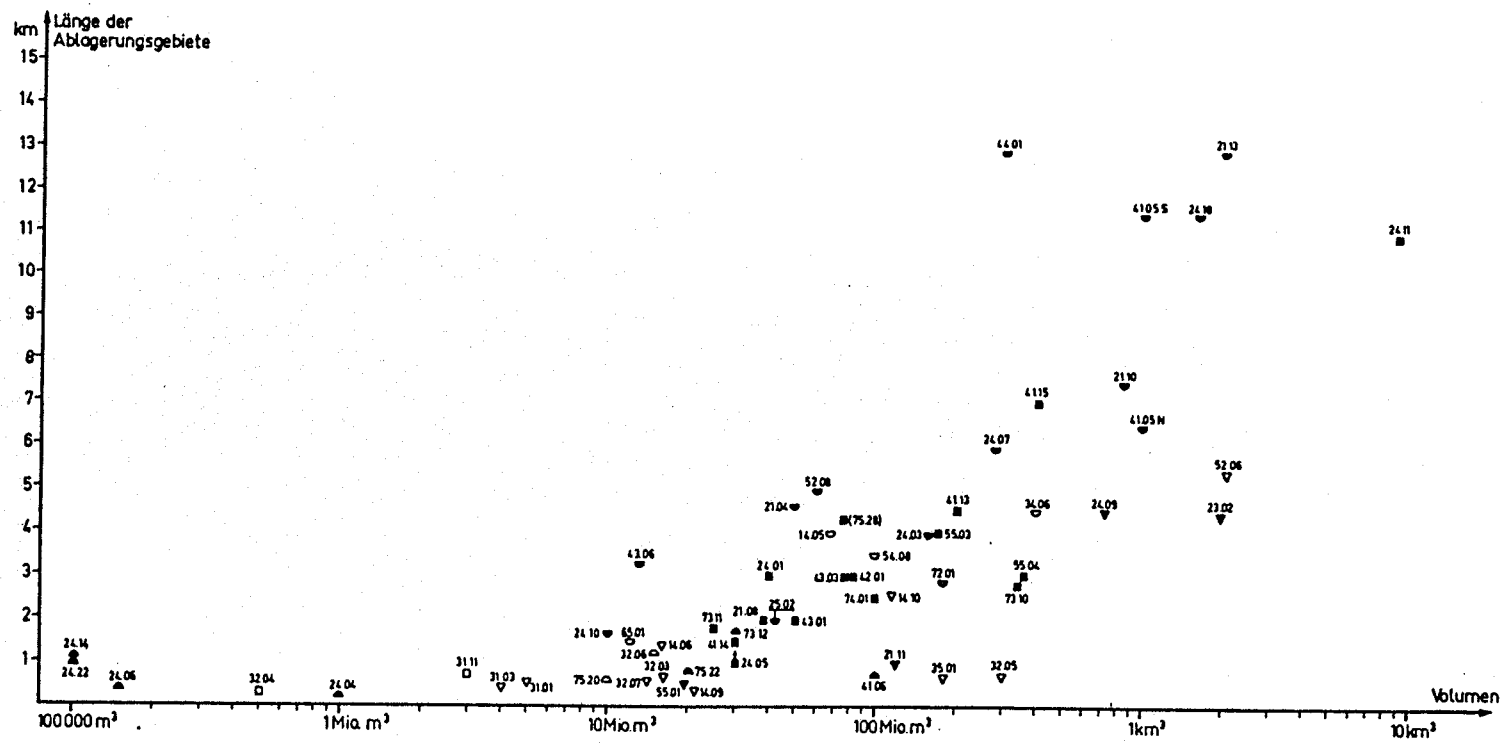

Figure 4.3

Length of deposit versus volume (Abele, 1974).

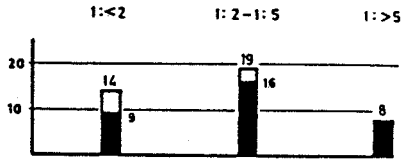

Die Streuung *(n = 41)*

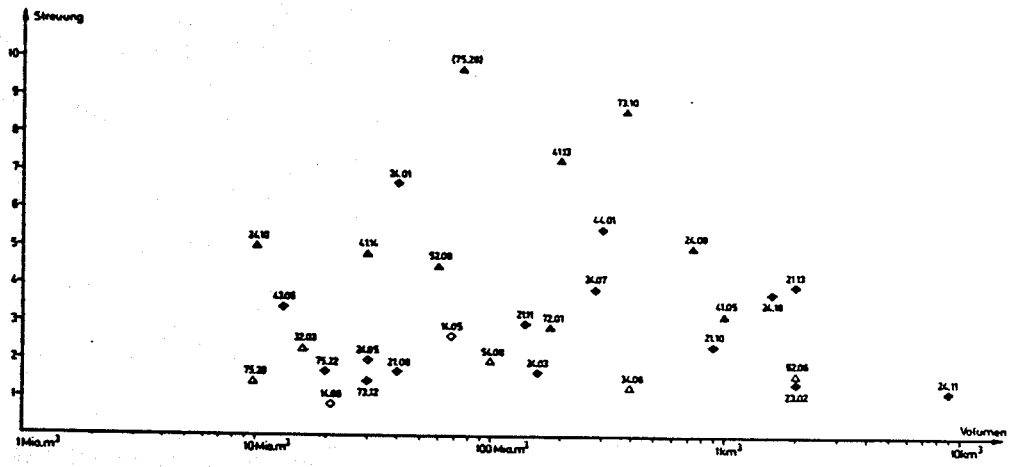

VOLUME (m^3)

Figure 4.4

Spreading ratio (deposit area/source area) versus volume (Abele, 1974).

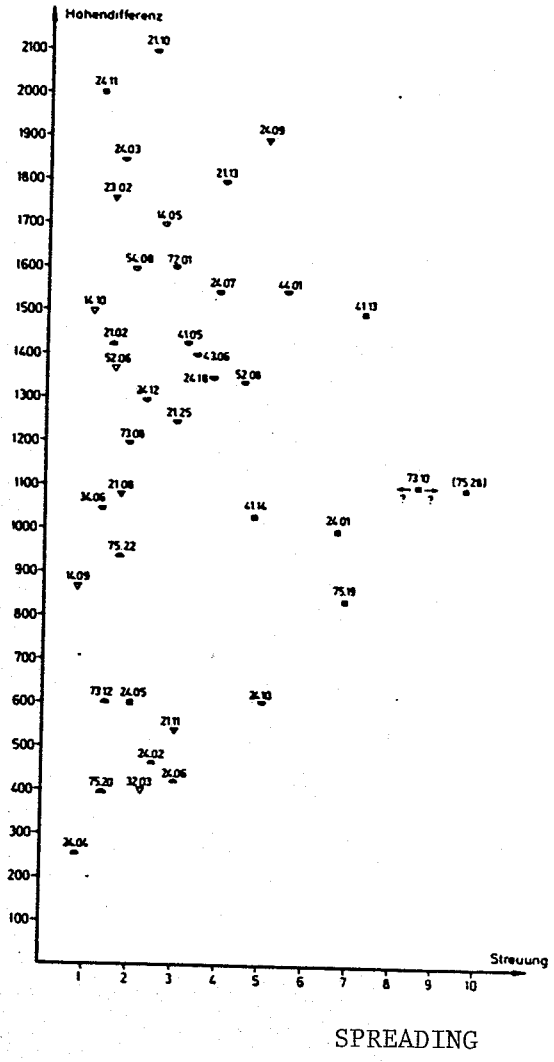

ELEVATION DIFFERENCE H (m)

SPREADING

Figure 4.5

Spreading ratio (Ad/As) versus total elevation difference (Abele, 1974).

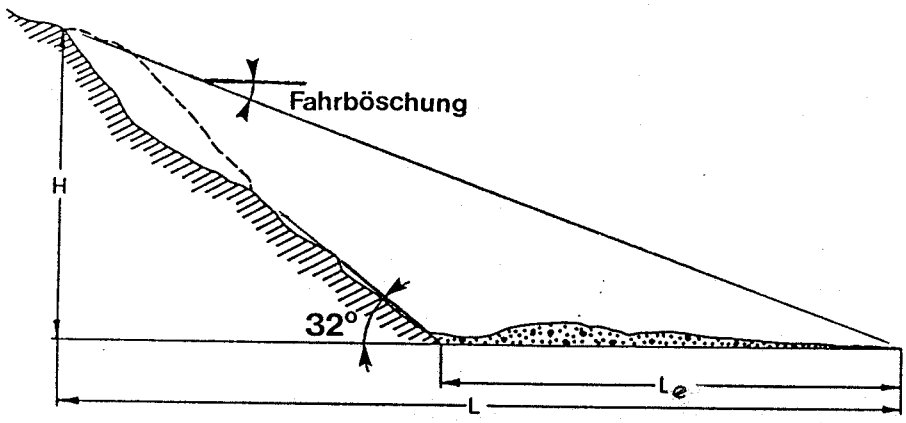

Figure 4.6

A typical profile of a rock avalanche and a definition of the geometrical terms (after Li, 1983).

Abbreviations for the rockfalls are A, Airolo; VL, Val Lagone; Hu, Huascaran; Sh, Sherman; Go, Goldau; Di, Diablerets; K, Kandertal; Bl, Blackhawk; F, Fernpass; Ta, Tamins; Si, Siders; A 17, Apollo 17 on the Moon; Va, Vaiont; En, Engelberg; Fl, Flims; Fp, Fernpass; Pa, Palmira; Sa, Saidmarreh; Ts, Tsiolkovsky on the Moon.

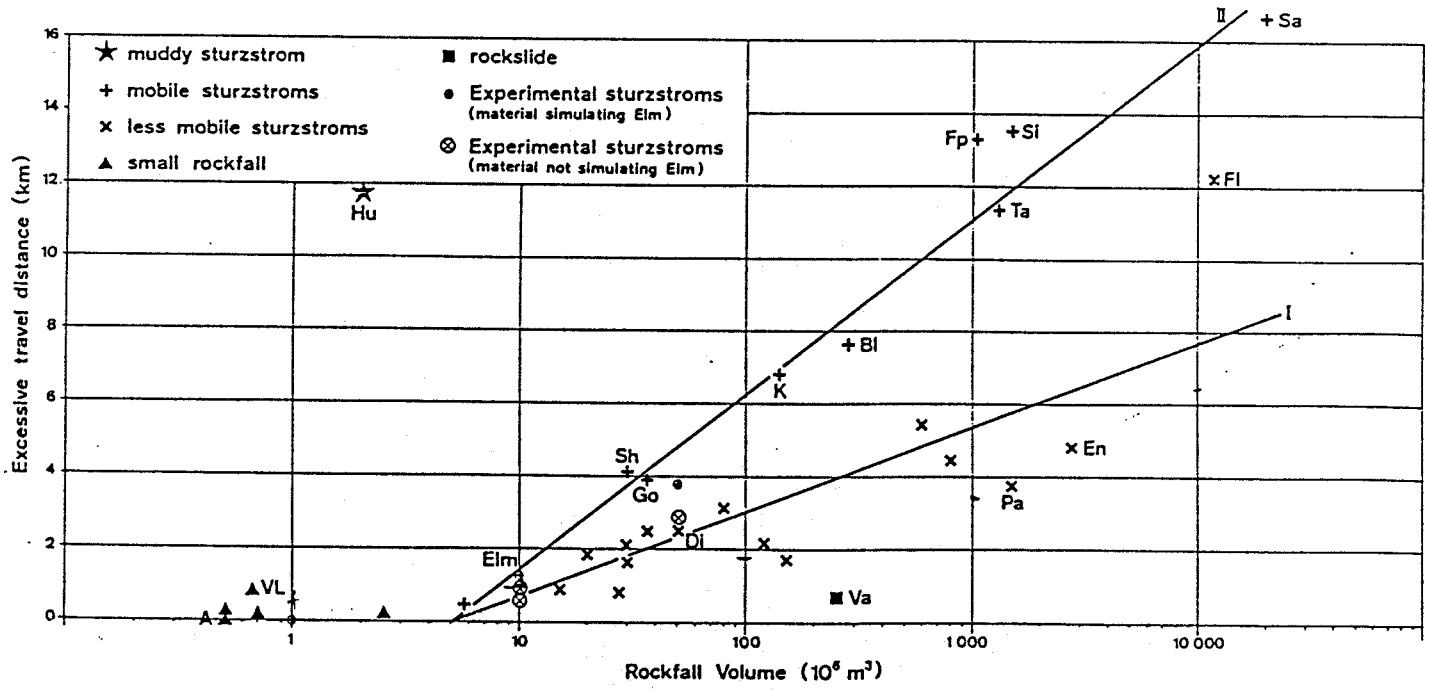

Figure 4.7

Excessive travel distance versus volume (Hsu, 1975).

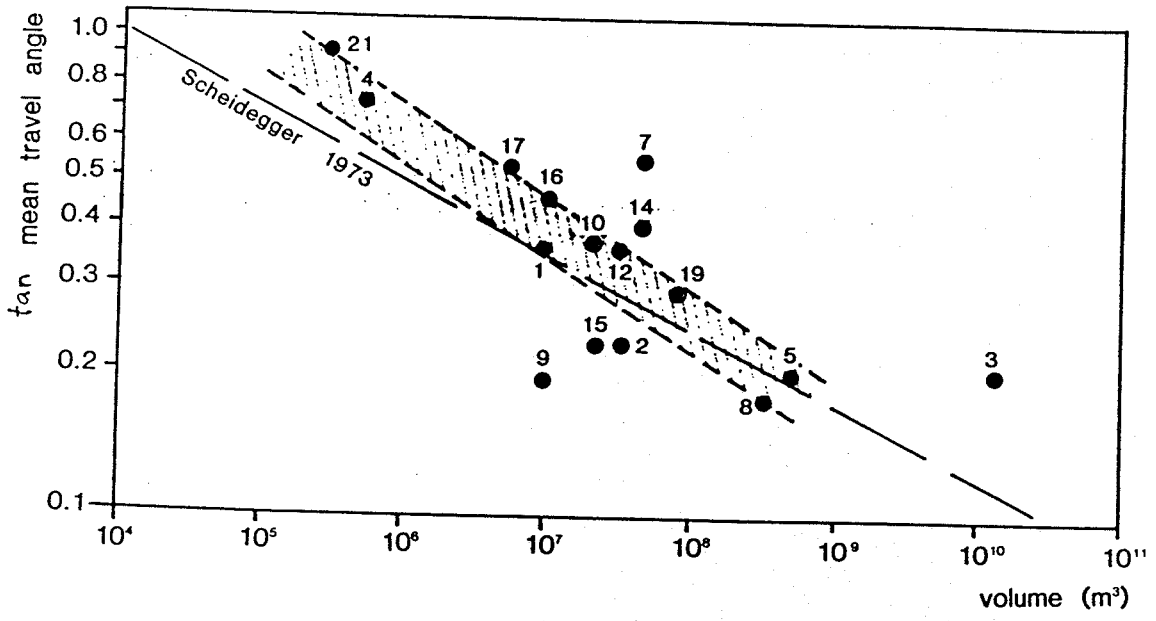

Figure 4.8

Hc/Lc versus volume (distance in terms of centres of gravity) after Hungr (1981).

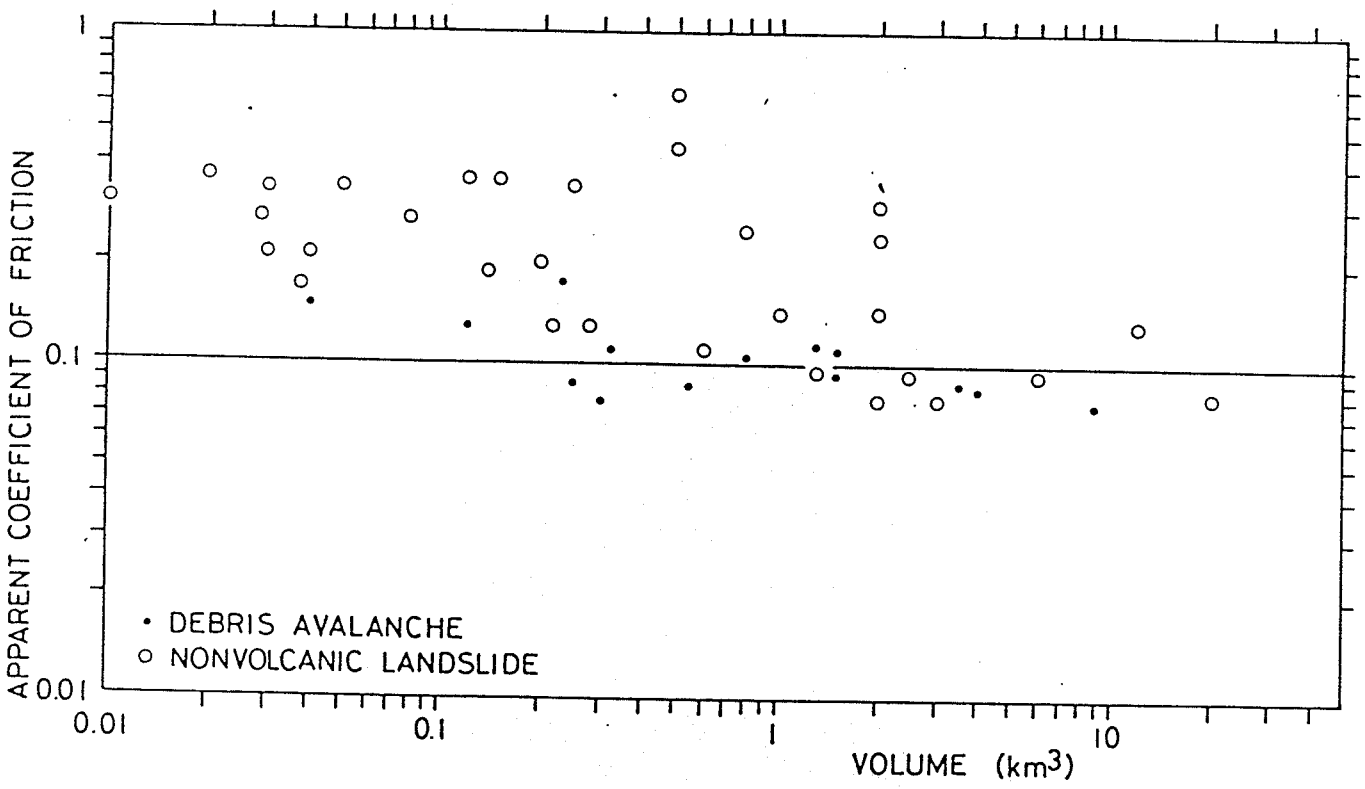

Figure 4.9

H/L versus volume, volcanic rock avalanches in Japan (Ui, 1983).

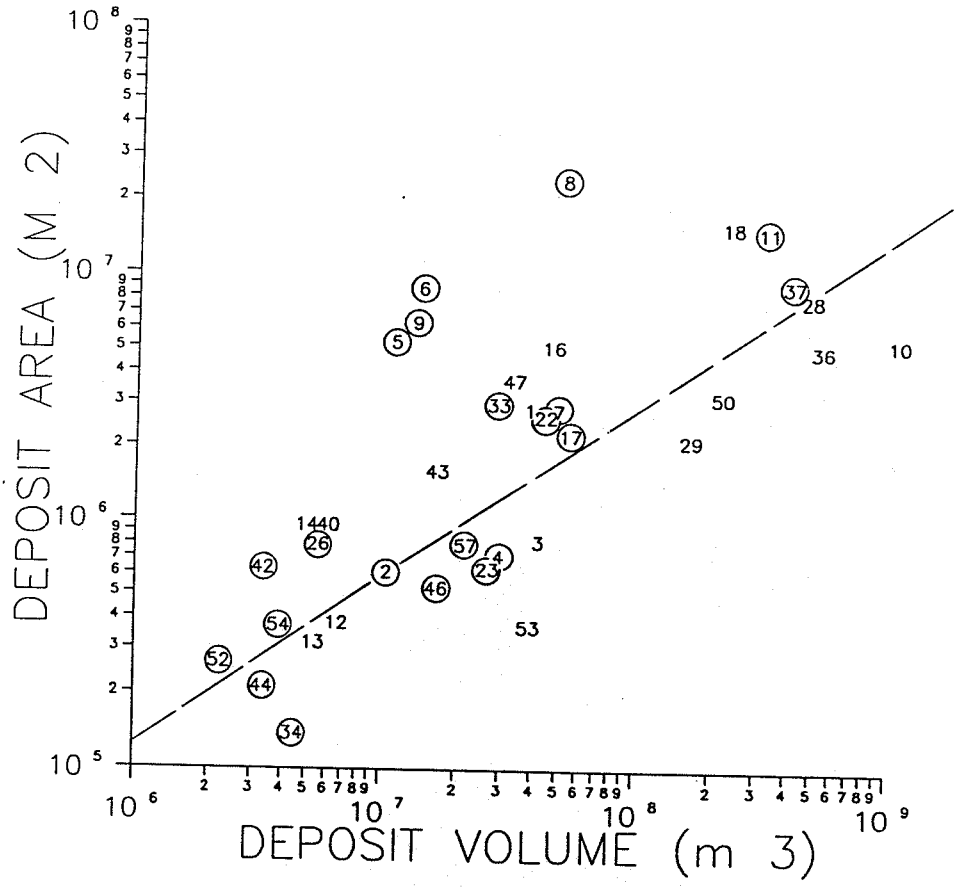

1. Frank
2. Elm
3. Gros Ventre
4. Madison Canyon
5. Little Tahoma Peak
6. Sherman Glacier
7. Hope
8. Huascaran, 1970
9. Huascaran, 1966
10. Mayunmarca
11. Blackhawk
12. North Nahanni
13. Beaver Flats
14. Brazeau Lake
16. Goldau
17. Diablerets
18. Granier
22. Valtellina
23. Lake of the Woods
26. Pandemonium Creek
27. Vaiont
28. Rockslide Pass
29. Avalanche Lake, South Lobe
33. Rubble Creek
34. Kennedy River
36. Maligne Lake
37. Martinez Mountain
40. Antelao
42. Bec Rouge
44. Clavans
46. Disentis (Muster)
47. Dobratsch
49. Lago di Alleghe
50. Lavini di Marco
52. Mottec
53. Motto d'Arbino
57. Mt. Ontake

Figure 4.10

Deposit volume versus area covered (from rockslide data base. Circled numbers are non-sedimentary events).

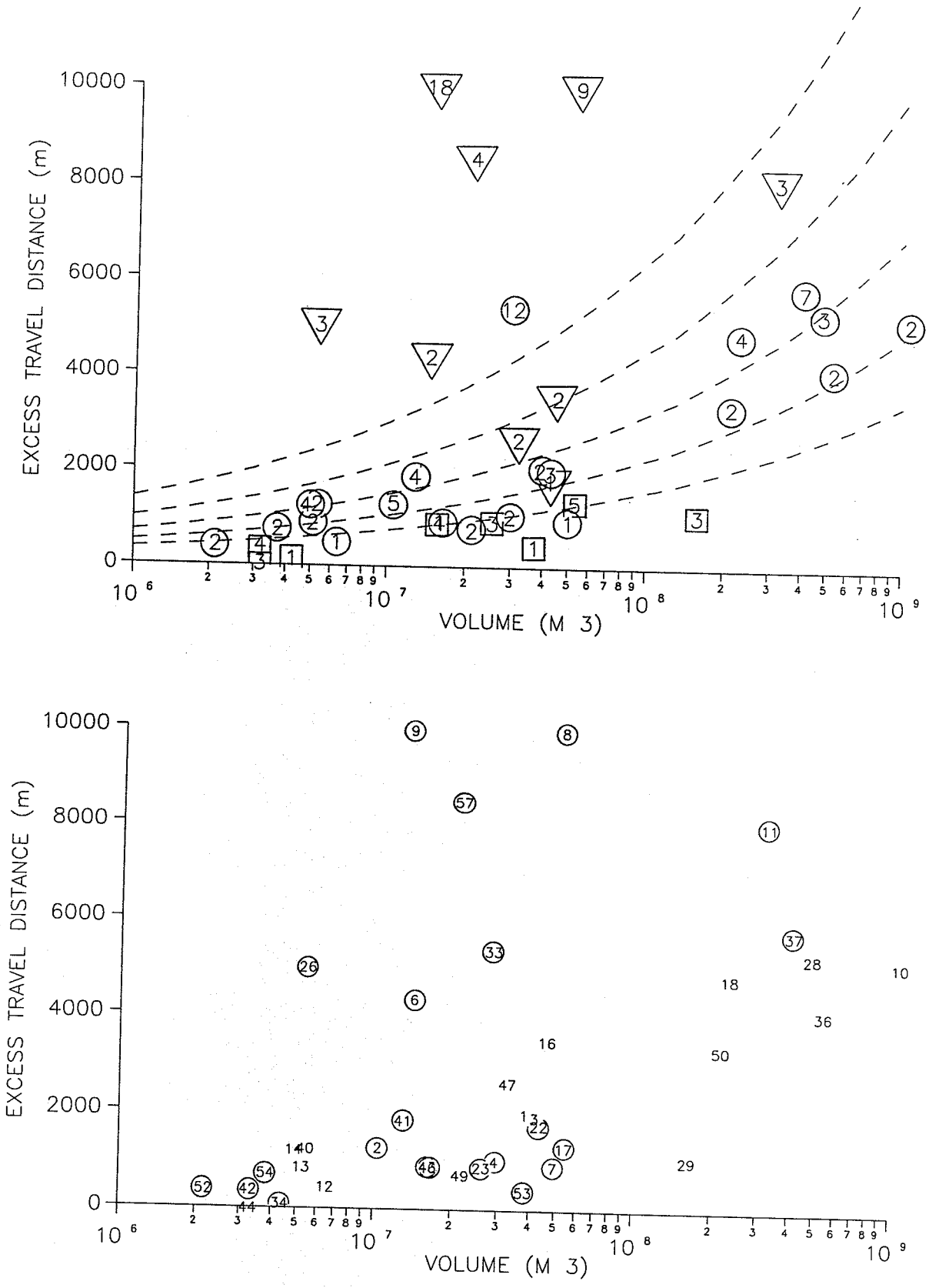

Figure 4.11

Excess travel distance versus volume
a) compared to Eqn 5, b) numbers of events listed on Figure 4.10.

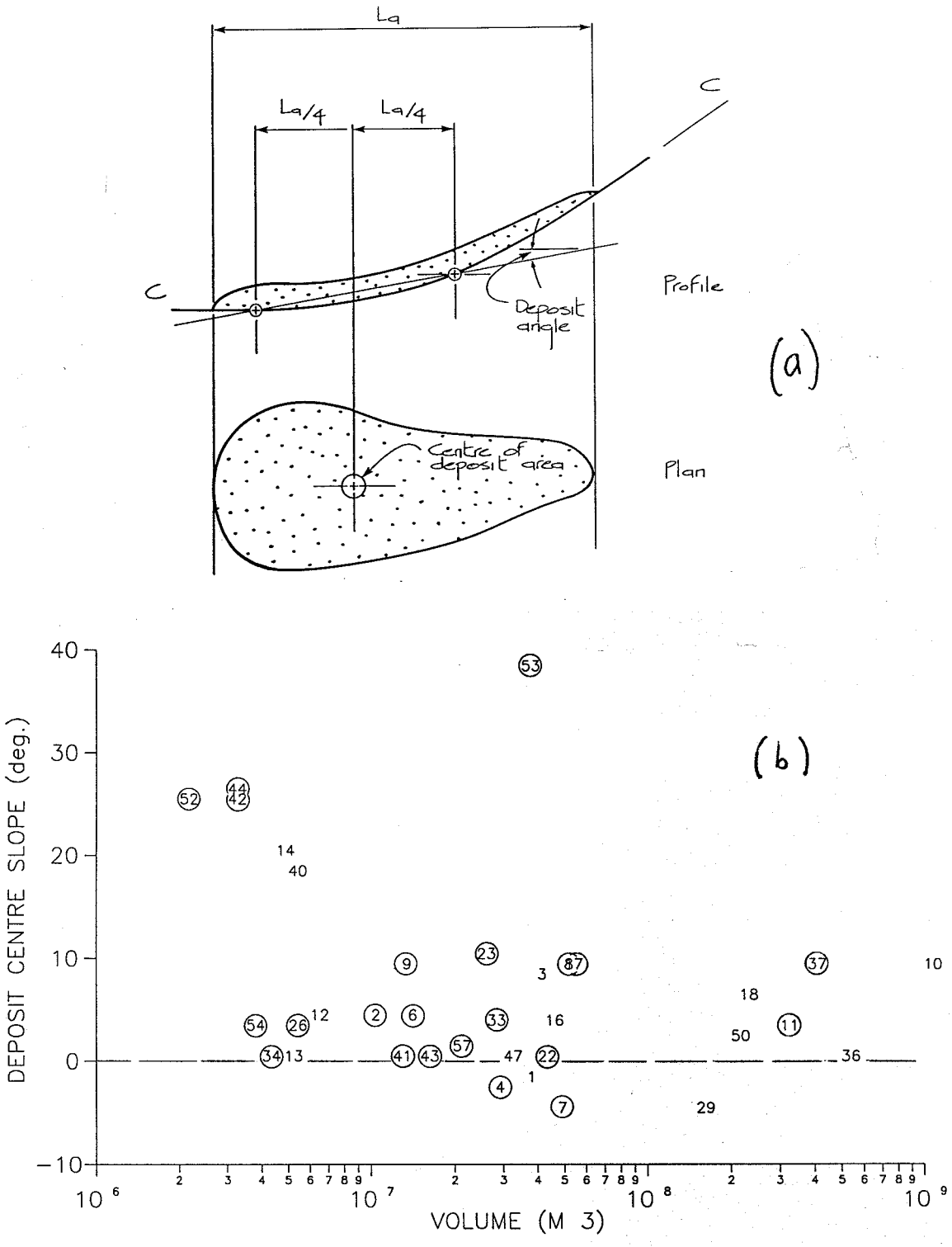

Figure 4.12

a) Definition of the deposit center slope angle.
b) Its relation to deposit volume.

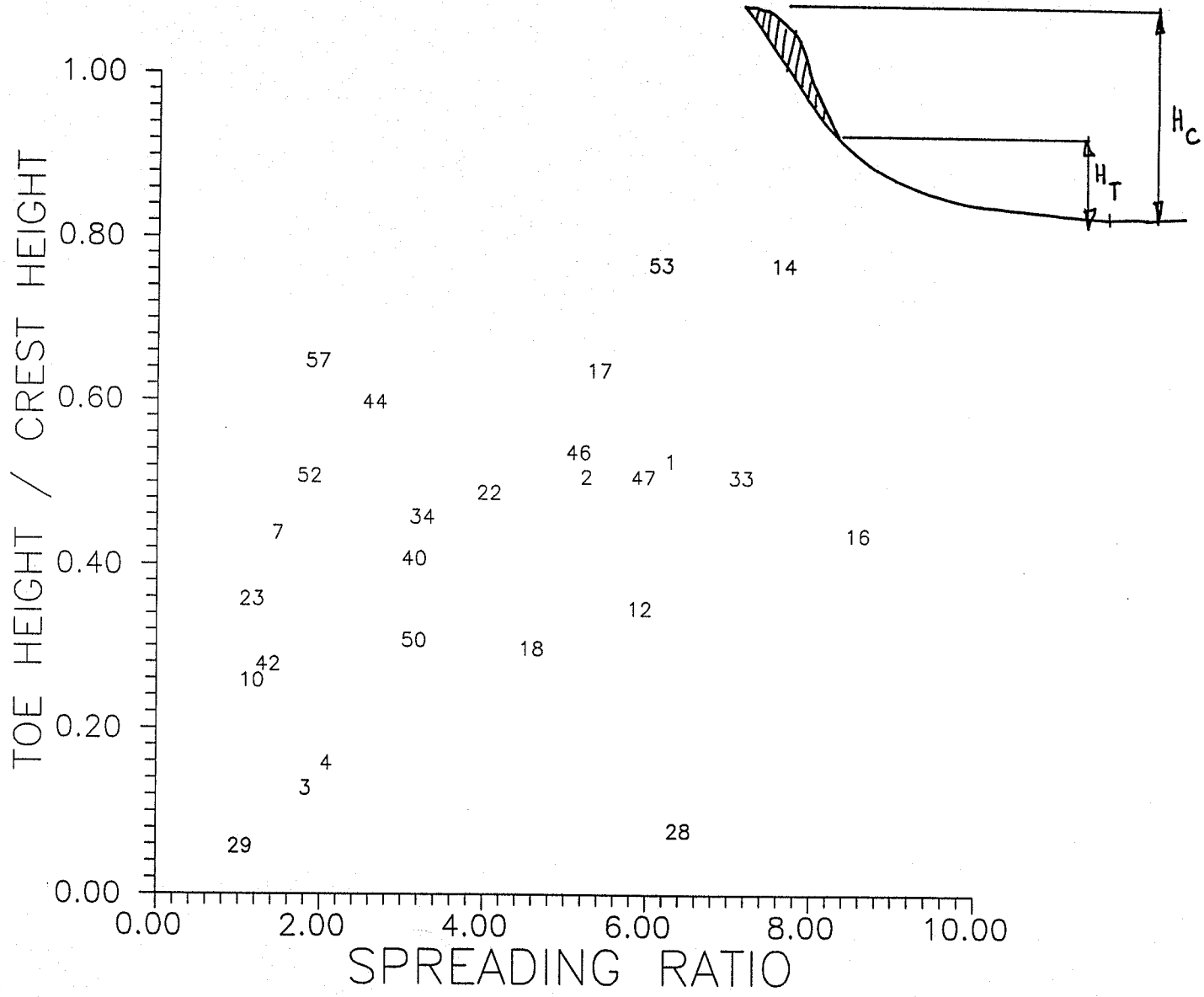

Figure 4.13

Spreading ratio vs. normalized toe height.

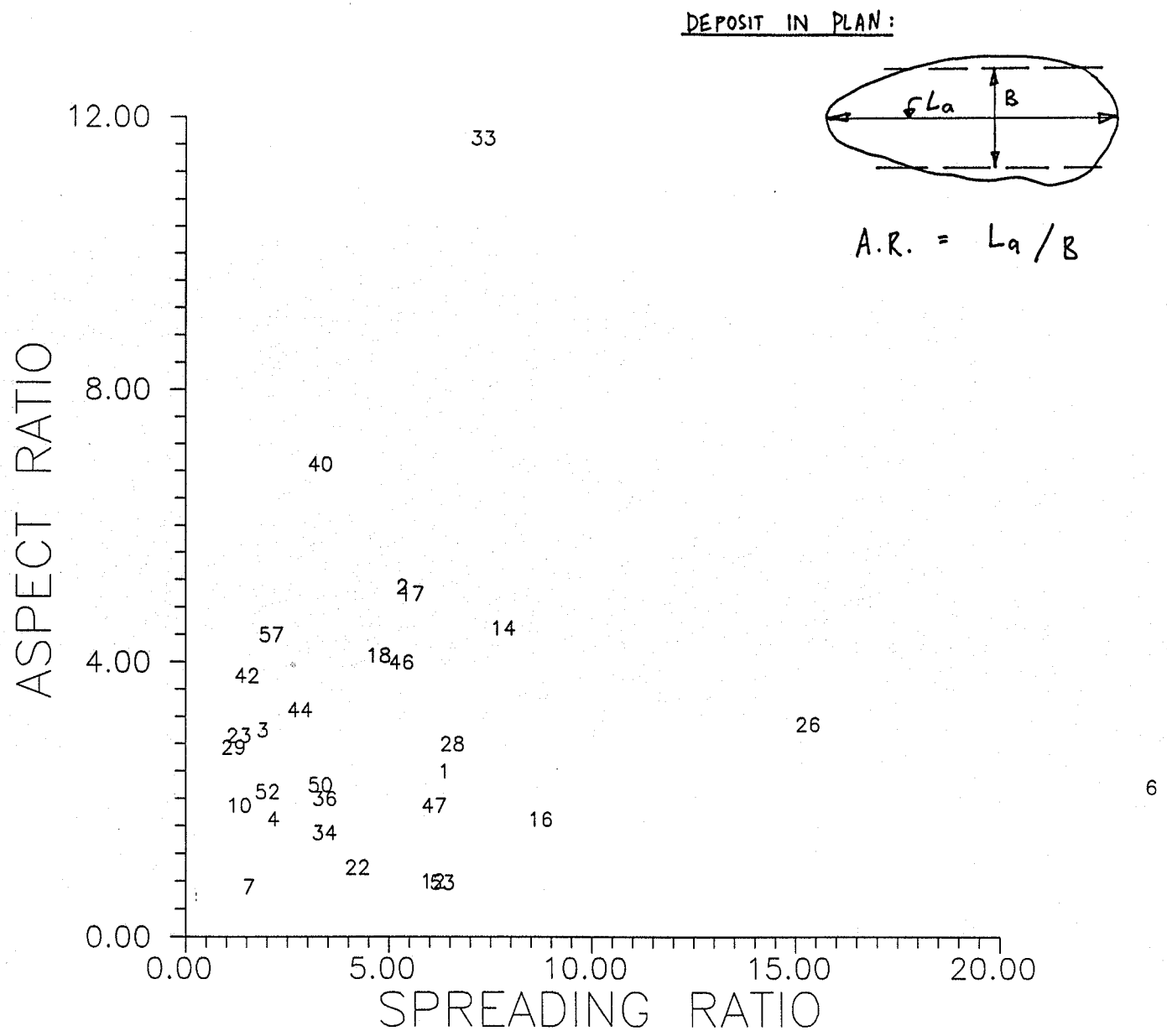

Figure 4.14

Spreading ratio vs. deposit confinement.

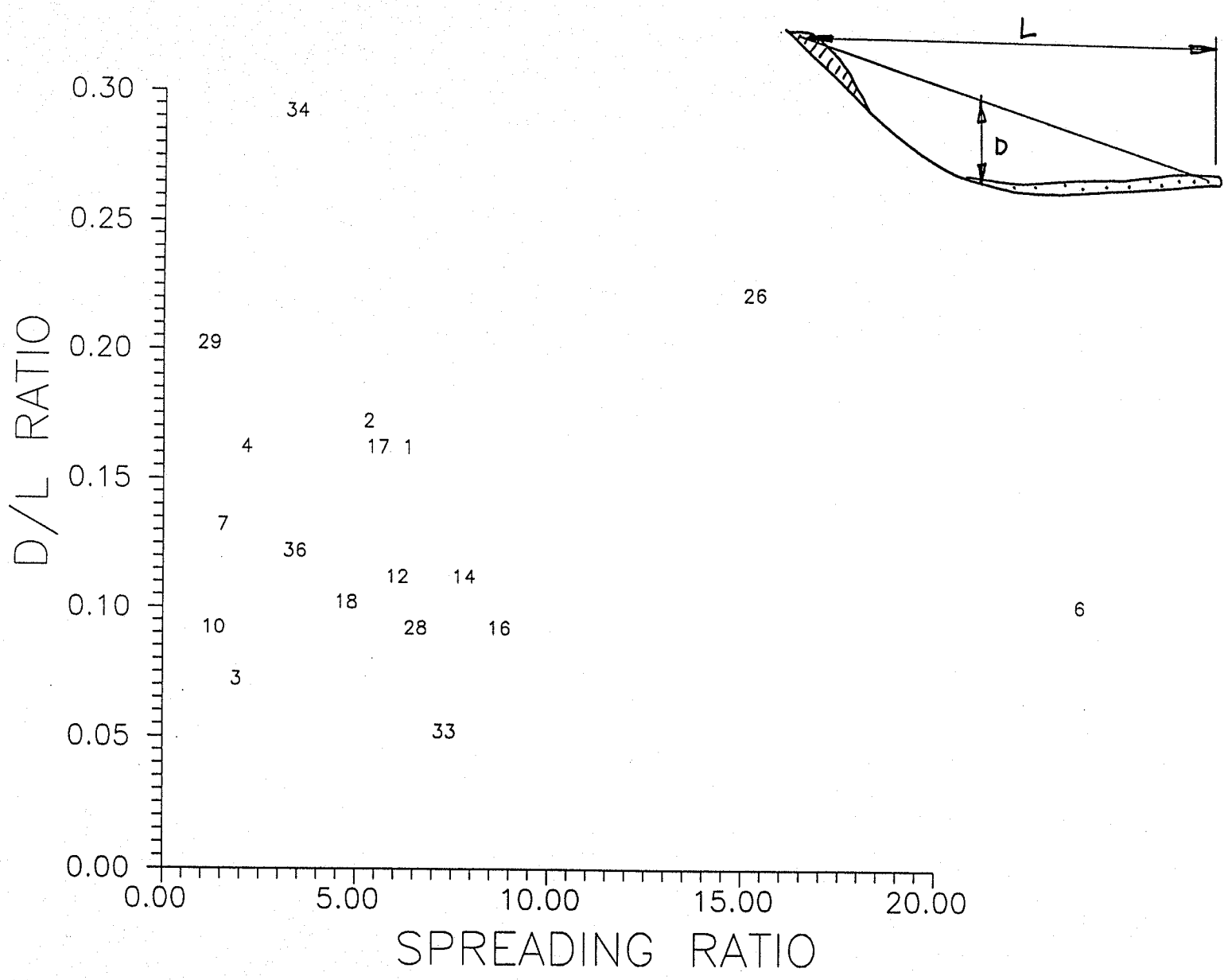

Figure 4.15

Spreading ratio vs. path curvature.

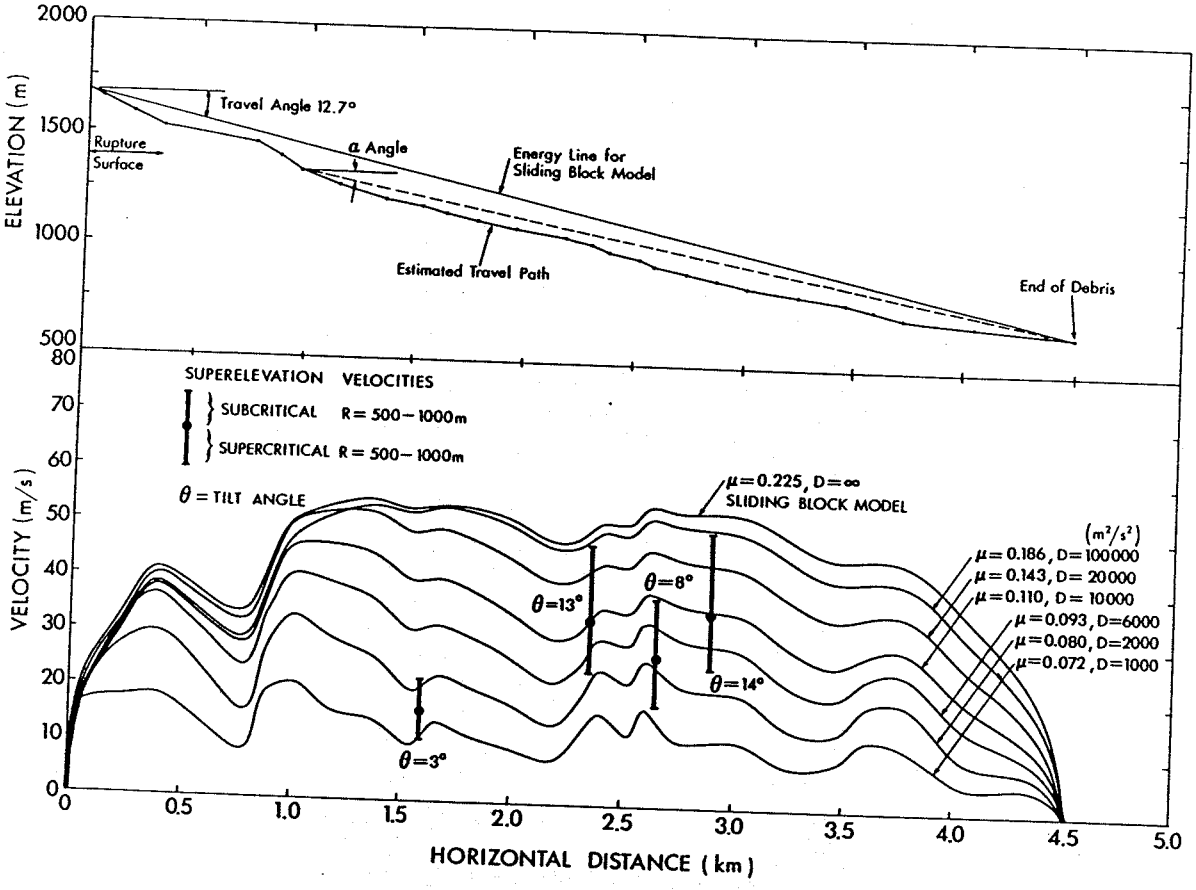

Figure 4.16

Example Koerner analysis (McLellan & Kaiser, 1984).

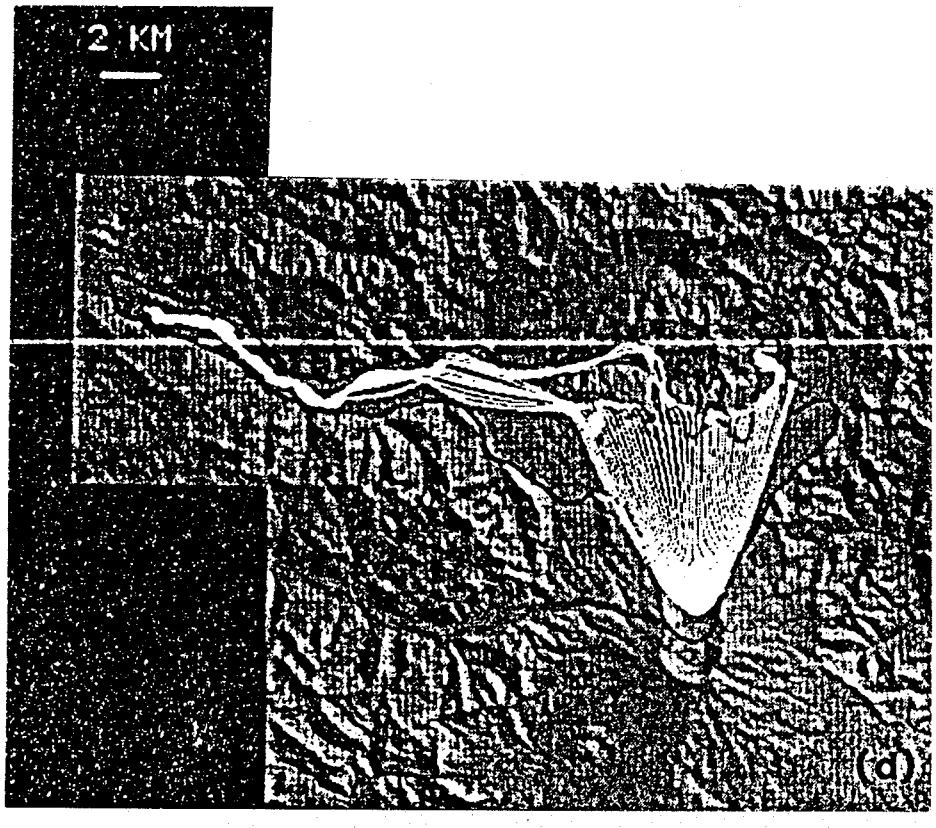

Figure 4.17

Multi-particle 3D analysis of the Mt. St. Helens rock avalanche (McEwen & Malin, 1989).

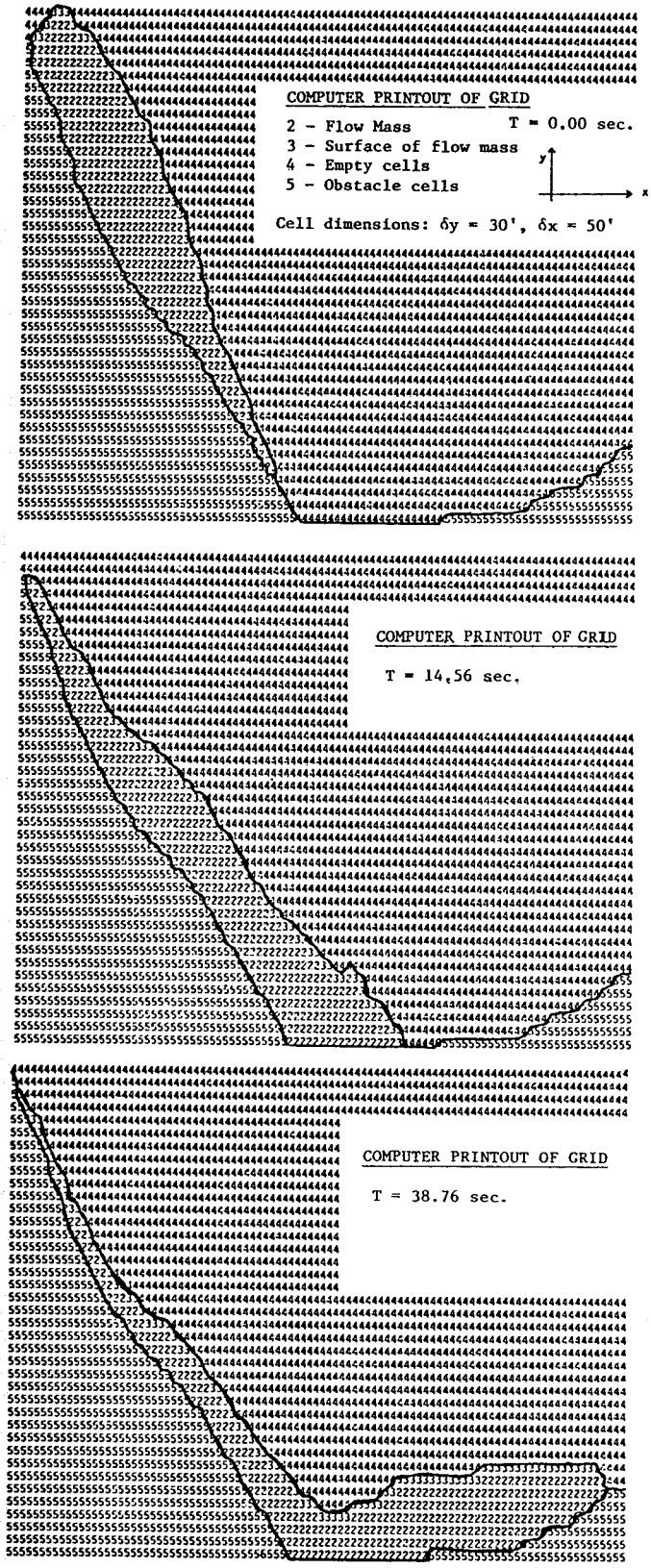

Fig. 4.18 Two-dimensional fluid dynamics analysis of a profile of the Madison Canyon slide (Trunk et al., 1986)

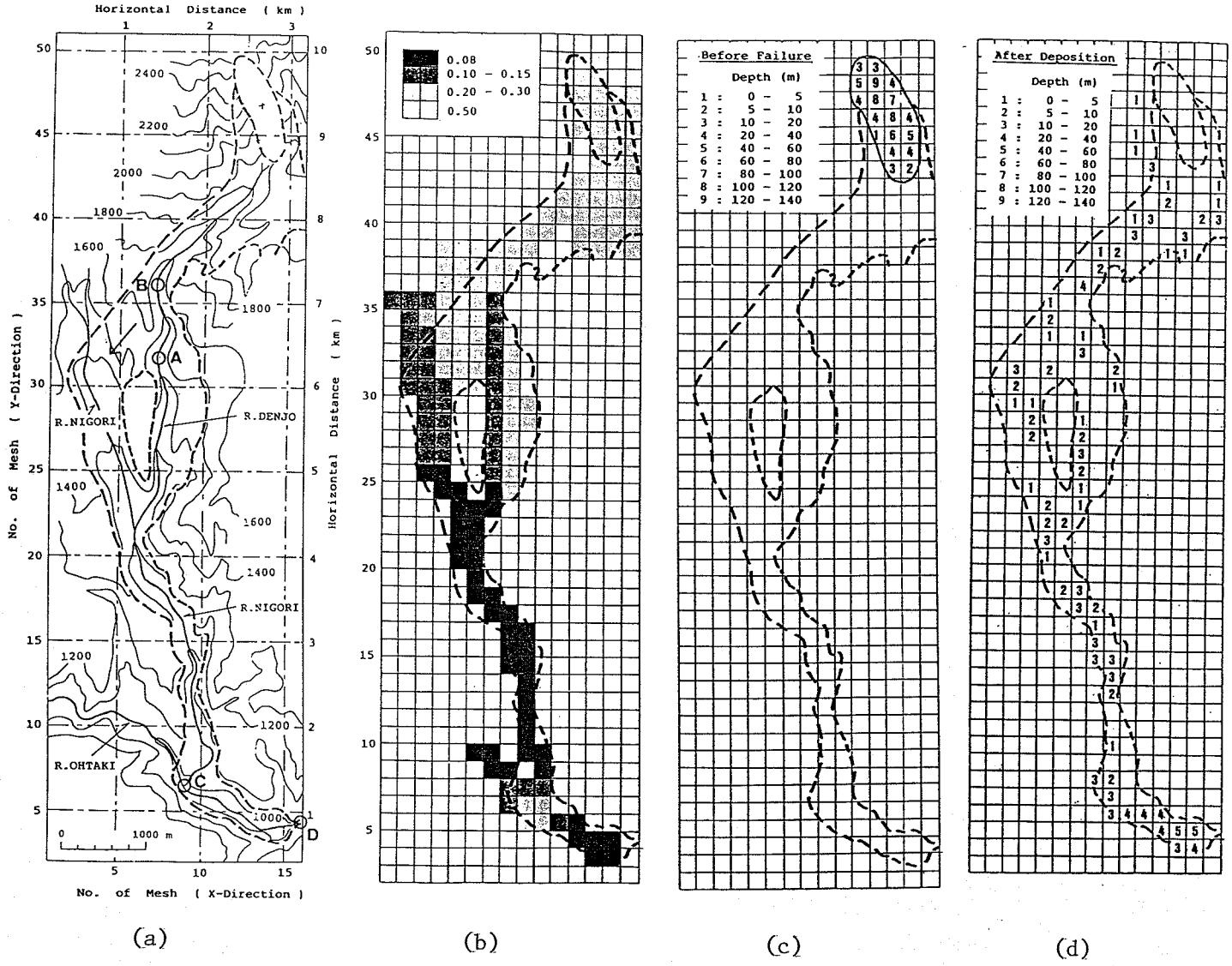

Figure 4.19

Three-dimensional analysis of the Mt. Ontake rock avalanche by Sassa (1988). a) topography, b) assumed distribution of the apparent friction coefficient (including pore pressure effects), c) source area, d) final deposits.

5. SUMMARY OF CONCLUSIONS AND RECOMMENDATIONS

5.1 Conclusions from the Present Study

A comprehensive review study of the failure behaviour of large rockslides has been completed. The following is a summary of the main results:

1) Large rockslides exhibit a wide range of failure velocities, from barely perceptible creep movements to catastrophic rock avalanching. Recognition of the "capability" of a potential slide to develop catastrophic movement rates (over 1 m/sec) is important.

2) Costs of large rockslides in terms of both life and economic losses are poorly indicated by averaging of records. Certain individual cases in the past had the nature of major catastrophes, exceeding the average damage trends by an order of magnitude.

3) Frequencies of occurrence of major catastrophic rock avalanches range from 0.0002 to 0.002 cases per year per 10000 km^2 of mountainous terrain, being the highest in mountains formed of sedimentary and volcanic rocks (see Table 2.1). Approximate frequency-magnitude curves have been constructed, as shown in Figures 2.1 and 2.2.

4) Data available from the European Alps are contrary to the hypothesis that the rates of major rock avalanche occurrence have been decreasing during post-glacial time.

5) To estimate the probability of failure at a given site, it is necessary to update the average probabilities subjectively, based on symptoms such as the occurrence of previous failures, and signs of deformation and cracking.

6) The amount of displacement is a poor indicator of impending failure, as there are cases of catastrophic detachment following more than 100 m of slow displacement (see Case 10 in Appendix C).

7) The best indicator for failure prediction appears to be the rate change of displacement, deformation or another parameter (e.g. micro-seismic activity). The inverse velocity method developed by Fukuzono (1985) provides an excellent means of recording rate changes. A parameter S_f, being the reciprocal of the slope of the inverse velocity-time curve with the dimension of length, is a convenient index. Critical values of the index preceding failure of large rockslides are less than 1000 mm.

8) The inverse velocity method cannot be used for long term predictions (beyond one or two months). It also cannot be used to predict earthquake triggered events (cf. Mt. St. Helens, Voight, 1989).

9) The capability of a large rockslide to develop catastrophic movements depends on:

- Failure mechanism (self-stabilizing or not).
- Brittleness of the sliding surface in all its components.
- Internal brittleness of the sliding body, unless the failure is rotational or translational.
- Velocity dependence of shear strength (viscous or rate-softening).

10) There are no means at present to analyze the above parameters and their interaction quantitatively. Assessment of capability must therefore rely on empirical means, comparing a given situation with available precedents.

11) A data base of physical attributes of large rockslides has been established, with the purpose of facilitating selection of prototype case histories for assessment of rockslide behaviour. The data base (Appendix A) reflects the complexity of rockslide failure mechanisms, which involve diverse geometries, rock mass strength, anisotropy and

fabric, as well as major structures (faults or weak surfaces). A number of quantitative indices have been devised, in order to provide a complete check list of parameters capable of influencing rockslide behaviour. The main criterion was to make all the parameters accessible to quantitatively defined queries, using computerized data base technology. Fifty-seven case histories have been compiled to date. The data base is designed so as to be usable by other workers and it is intended to distribute copies in return for additional data.

12) A classification of rockslide detachment mechanisms has been developed, based on the influence of structural control (Figure 3.2). Typical parameters of the detachment mechanisms are listed in Tables 3.1 to 3.10 derived from the data base.

13) Only two of the nine classes appear to produce exclusively non-catastrophic failures:

- Rotational slumps across the fabric in weak rocks, without structural controls (Type A).

- Flexural topples, involving relatively weak and highly anisotropic rock masses (Type H).

Compound slides involving the presence of a covered weak surface beneath the centre of the source area ("centre slide", Type F) also appear to be predominantly slow, although this may be due to a lack of a case history involving steeper slope and stronger rock.

Collapse failures of steep slopes in strong rock (Type B), which are unrelated to the rock fabric but controlled by random, non-persistent joints and intact rock failure, are always catastrophic. They tend to involve relatively low volumes.

Rock glides (Type C) and compound slides (Type D) are fully under the control of the rock fabric and/or major structures. These failures involve the largest magnitudes and are usually catastrophic,

except in case of very weak rocks, combined with moderate slopes and very flat structural dips.

Compound slides involving the presence of a weak surface in the toe area (Type E) or crest area (Type G) approximate to the behaviour of Types A or B (i.e. slow or catastrophic), depending on the nature and relative importance of the cross-fabric segment of the sliding surface. Such failures are probably the most difficult to assess in terms of capability.

Block topples (Type I) are distinguished from Type H by involving moderately anisotropic rocks, the anisotropy being of structural origin rather than a rock property. The stability of a series of blocks is derived largely from the equilibrium of the base of relatively thick columns, rather than from the friction between column faces. The failure mechanism is brittle and the failure is catastrophic, although it may involve relatively small volumes, or gradual piecemeal detachment scenarios.

14) Some aspects of failure behaviour of rockslides within the framework of the above classification are illustrated by the reports of sites visited in course of this project, Appendix C.

15) A brief review of the several competing hypotheses of rock avalanche motion is given in Section 4.2. The recently favoured hypotheses include:

- Lubrication by saturated subgrade material in the slide path, liquefied by rapid undrained loading.

- Acoustic fluidization of dry rock fragments, due to vibrations induced by the slide path roughness or by prolonged earthquake shaking.

Both of these hypotheses can be studied only in the context of full scale events, not by small scale or laboratory testing.

16) Existing methods of velocity and runout prediction for rock avalanches have been reviewed, in the categories of empirical models, single or multiple block models and algorithms based on the principles of fluid mechanics.

17) Existing empirical correlations for runout prediction suffer from wide scatter, due to the neglect of the multi-dimensional nature of the problem. An improved correlation which accounts for the influence of lateral confinement of the deposit as well as volume has been developed using the data base (Figure 4.11). A substantial scatter remains, however, partly as a result of incorrect volume estimates but mainly due to the influence of the nature of subgrade material in the slide path.

18) The fieldwork carried out in course of the present research project included a detailed re-examination of the Avalanche Lake rockslide in the Mackenzie Mountains, N.W.T. An account of the results is given as Case 13 in Appendix C. We established conclusively that the rock avalanche deposit was emplaced in the valley as found and not modified by glacier movements as proposed previously. This conclusion has important consequences on the calibration of dynamic models for rock avalanche runout.

Avalanche Lake is an ideal site for calibration, as it involves two large debris lobes, emplaced simultaneously on two dramatically different profiles (Appendix C): The "shelf lobe" was deposited against a steep adverse slope and produced the highest runup of any known rock avalanche case (Evans, 1989). The "south lobe" of approximately the same size, ran for four km along a nearly horizontal floor of a valley. An opinion was expressed that the emplacement of the two deposits cannot be accounted for by a dynamic model (Kaiser and Simmons, 1989).

19) Block models in current use are incorrectly referenced to the extreme ends of the rock avalanche path. An application of such a model to the Avalanche Lake case history showed that the reference

point must be the centre of gravity of the failing mass. With such a provision, it is possible to model both of the slide lobes with a single set of parameters (Figure 14, Case 13, Appendix C).

20) A new two-dimensional fluid mechanics model was developed during this project (Appendix B). Its application to the shelf lobe of Avalanche Lake showed that rock avalanche debris cannot be modelled as a fluid. Fluid material would lack the internal coherence required to achieve the observed runup of the shelf lobe (Figure 4, Appendix B). The new model is capable of accounting for the internal rigidity of granular debris and provides a simulation of the observed runup (Figure 5, Appendix B).

5.2 Recommendations for Further Work

Some of the more promising topics for further research in connection with large rockslide hazards are listed in the following:

1) Place additional data in the rockslide data base. We intend to distribute the data base at cost to interested researchers in Canada and abroad, in return for their supplying case history data.

2) Assemble further inventories of rock avalanche occurrence in Canada, to improve the collection of frequency data.

3) Compile additional pre-failure displacement records of large rock failures in open pit mines, to improve our understanding of failure prediction.

4) Develop improved means of displacement rate calculations for use with the inverse velocity method. This should be based on advanced curve-fitting techniques.

5) Improve the Mass-Referenced Flow Model (Appendix B) and provide rigorous calibration.

APPENDIX A

DATABASE USER'S MANUAL

PHYSICAL ATTRIBUTES OF LARGE ROCKSLIDES

Authors: Oldrich Hungr
Thurber Engineering Ltd.
200 - 1445 West Georgia Street
Vancouver, B.C.
V6G 2T3

S. G. Evans
Terrain Sciences Division
Geological Survey of Canada
601 Booth Street
Ottawa, Ontario
K1A 0E8

Note: This manual forms Appendix A of the report "Failure Behaviour of Large Rockslides".

Thurber Engineering Ltd.
Vancouver, B.C.

File: 16-11-6
August 23, 1990

1. INTRODUCTION

1.1 Purpose

Large rockslides are relatively rare, but can be extremely damaging both by their direct impact and indirect effects such as damming of streams or creation of waves in lakes or reservoirs. Single major rapid rockslides have caused life losses in the tens of thousands and material damage in hundreds of millions of dollars.

The failure behaviour of rockslides is determined by a complex and time-dependent balance between the driving and resisting forces. The purpose of this data base is to compile quantitative factors which are considered important in controlling the failure mechanisms and which may prove useful for prediction of the failure scenario. The data base further contains factors describing the failure behaviour itself such as displacements, velocities and various accompanying symptoms.

Two types of usage of the data base are intended. Firstly, it should serve as a means of retrieval of case histories with particular attributes which may be of current interest to the user. For example, the user may wish to review case histories involving a certain lithology or structure of the source area. Secondly, it is a repository of quantitative parameters which can be retrieved and combined in certain ways in order to examine their relationships and trends.

1.2 Scope

The data base covers well-defined gravitational movements of slopes in rock (or predominantly in rock), the volume of which exceeds approximately one million m^3 or those whose deposits cover areas exceeding 0.1 km^2 (cf. Abele, 1974, p. 5). The geographic range is unlimited, because well documented case histories are few even in the worldwide context.

Cases which should not be included are:

- Slope deformations of uncertain origin or immature development (double crests, saggings). Only recognized landslide areas with distinct and connected upslope and lateral boundaries should be included.

- Landslides and collapses concurrent with volcanic eruptions.

- Slides in which rock is not the dominant material (less than 50% in terms of volume, e.g. glacier collapses or overburden slides).

1.3 Implementation

The data may originate from direct observations, engineering or geological reports, maps or published case histories. Space is provided for identification of the data sources.

The data base is implemented using the dBase IV program for IBM and compatible microcomputers. Three data base (.DBF) files contain the actual data records. Other files contain input, output and query formats. The main files are described in Table 1. These files are fundamental to the operation of the data base. The user may generate other files using the dBase IV facilities, to set up queries, rearrange records and prepare tables or reports. Some additional files are created automatically by dBase IV for backup and sorting purposes.

1.4 System Setup and Operation

The files are grouped in two Catalogs (REFS.CAT and ROCKS.CAT), each of which is distributed on a separate diskette.

The first catalog is built around the file of bibliographic information REFS.DBF (reference list and coding). The second catalog contains the two files describing the rockslide case histories: ROCKSL.DBF which is concerned with the source area and STURZS.DBF which summarizes data about failure and post-failure behaviour.

In order to transfer the two catalogs into your dBase IV system, copy all the files into your dBase subdirectory using the global DOS commands:

```
Copy A:REF.*.*
Copy A:ROCKS.*.*
Copy A:STURZ.*.*
```

(Replace A: with B: in the above if your floppy disk drive is designated B).

Once the files are copied, start dBase IV and use the Catalog menu to create Catalog REFS and Catalog ROCKS. The data base will then become accessible through the dBase IV control centre and menu system. Only a very basic knowledge of the dBase IV software system is required to review and input data. Somewhat greater facility is needed in order to set up queries and prepare output reports.

1.5 Data Base File Review, Input and Output

Input and review of data can be carried out using screen forms listed in Tables 14, 15, 17, 18, 20 and 21 and described in the subsequent sections. The user may wish to design his own custom input forms as well.

To access one of the three data base files for review, input or correction, open the required file from the Control Centre and select one of the four screen formats (Forms) which display the content of the data records in an easy to review, commented format (Table 1). Move from record to record using the dBase IV menu appearing on top of the screen. (Press Alt. and a letter indicating the desired function.)

The input screens are largely self-explanatory. Two types are available, a "full" screen which addresses the full range of parameters and a "short form" screen where the number of parameters is reduced to the essentials. The user can create his own screens to access parts of the data base in which he is interested. Detailed definitions of the various parameters contained in them are given in the following sections. These definitions should be followed carefully, in order to ensure consistency of the data base.

2. THE BIBLIOGRAPHY FILE

2.1 General

To access the bibliography file, use the dBase IV Control Centre menu to select Catalog REFS. Data input and review is conducted using two screens, one to enter the basic bibliographic information and the other to furnish keywords, locations and utility codes.

New references are entered sequentially after the last existing record and provided with an I.D. number which need not correspond to the record number, but must be unique.

The query file REF_S.QBE controls output selection and sorting of reference lists. It is initially set up so that the references are listed alphabetically and that only those items selected using the PRINT variable on the REF_CDE screen (see below) are printed. To print a reference list, run the program REF_PRIN provided in the Catalog.

A list of variables used in the REFS.DBF file is given in Table 13.

2.2 Screen REF_IN, Bibliographic Reference

This screen, listed in Table 14, is self explanatory. The following variables are entered:

IDD	The sequential I.D. number of the reference assigned by the user. This number is used to connect the bibliographic records to the ROCKS database file.
FIRST_AUTH	Last name of the first author (no comma or period).
INITIALS	Initials of the first author.
SECOND_AUT	Last name of the second author.
SND_INIT	Initials of the second author.
OTHERS	Last names and initials of other authors, separated by commas, but no comma or period at the end.

YEAR	Year of publication (no period).
TITLE	Title of an article, followed by a period. If the reference is a book, leave this blank.
TITLE_CONT	Continuation of the title, if required.
PUBLIC	Title of publication (e.g. Canadian Geotechnical Journal), no period.
PUBL_2	Continuation of the publication title, if required (no period).
EDITOR	Name of editor(s), if available.
VOLUME	Volume (zero if not available).
NUMBER	Issue number (or zero).
PUBLISHER	Publisher or source organization (no period).
CITY	City of Publisher's office (if available).
PAGES	Page range, if an article (example: 99-105) or number of pages if a book (example: 505).
LANGUAGE	Language, if not English.

As far as possible, no abbreviations should be used in titles or names of organizations. This is consistent with the requirements of most journal editors at the present time.

2.3 Screen REF_CDE, Bibliographic Coding (Table 15)

This screen should not be used to create new records. Its purpose is to add keywords and other coding to existing bibliographic records.

The variables are described in the order of appearance on the screen:

PRINT — This is a yes (Y) or no (N) character specifying whether the particular record is to be included in the next printed listing of references. It defaults to N. To activate the process of selection, there should be a Y in Column PRINT in the REF_S query file. If this column is left blank, all references will be printed, regardless of the character PRINT..

The next five lines of the screen display the I.D. number, authors' names, title and publication of the reference under consideration. This data is merely passed over from screen REF_IN. It is not accessible for editing from this screen.

TYPE — This is a two-character code designating the type of the article:

- CA — Case history (single case).
- MC — Multiple case history.
- RC — Regional collection of case histories.
- TH — A theoretical model, concerning either the detachment mechanism (stability), or failure or post-failure dynamics.
- EM — Empirical model or correlation.
- SA — State of the art or a review article.
- CO — An article describing a constitutive model for static (strength) or (deformation) or dynamic (deformation or flow) behaviour of the slide material.
- RD — An article describing remedial stabilization or protection measures or works.

The type code may remain blank.

CODE — Contents code number. This is a three digit number designated by the user according to his/her own code list or classification of the references.

KEYWORDS — Key words assigned by the user, separated by commas.

COPY — Yes (Y) or No (N) character, depending on whether a copy of the article is available in the User's library or project files.

LOC1 — Two alternative locations where the article

LOC2	can most easily be found (e.g. library, personal files, etc.).
DETAIL	How detailed is the article (classify subjectively on a scale of 1 to 5) (5 is the most detailed).
USEFUL	How useful is the article (classify 1 to 5, from the User's subjective viewpoint).
COM	This is a memo field, which may contain various comments, or a short abstract of the article. The memo is opened by pressing CNTRL-HOME and closed by CNTRL-END.

3. THE ROCKSLIDES DATA BASE FILES

3.1 General

Each record of the Rockslides data base potentially represents a detailed quantitative report on a case history. Due to the large number of variables required, the data base had to be divided into two parts. The first part (ROCKSL.DBF) contains information on the geometry, geology and structure of the rockslide source area. The second part (STURZS.DBF) describes the failure event, the travel path, the deposit and associated damage.

For the purposes of this data collection, failure is defined as the most rapid past movement episode of the rockslide event. In those cases where full catastrophic detachment has already occurred, the failure period is easily defined. Where it has not, the fastest movements observed so far may or may not be exceeded in the future. The data base does not require a prediction of future behaviour. Only factual past behaviour is recorded in it.

In case of incomplete detachment, it is not necessary to record variables concerning the slide path and deposit.

3.2 Data Preparation

In order to measure the required geometrical variables, it is necessary to obtain several cross-sections and plans of the rockslide. Copies of these should be deposited in a project file for future reference. It is suggested to use an accurate reducing/enlarging photocopy machine to change the drawings to a metric scale, preferably larger than 1:25,000. The following drawings are required:

1) Plan of the rockslide, including the source area, path and deposit, preferably with contours. The centreline of the movement trajectory of the rockslide should be drawn on the plan (Fig. 1).

2) Reconstructed profile of the slope prior to the rockslide (Section A-A, Fig. 2). The profile should be constructed along a straight line drawn through the planimetric centre of the source area, in a direction perpendicular to the contours. The profile should extend from the lowest point in the valley to the highest point of the ridge.

3) Longitudinal profile of the source area (Section X-Y, Fig. 3 and 4). The profile is drawn through Point X, being the lowest topographic elevation on the detachment surface. It is constructed along a straight line parallel with the average direction of sliding so that the downhill direction is to the left. Point Y lies where the profile intersects the crest of the head scarp of the rockslide. Point Z is the point where the sliding surface is deepest with respect to a straight line connection between X and Y (Fig. 4).

4) Lateral cross-section of the source area (Section B-B), Fig. 3 and 5). This cross-section is drawn through Point Z (see previous paragraph), in a direction perpendicular to that of the longitudinal profile, looking downslope.

5) Path centreline profile (Section C-C, Fig. 1 and 6). This is a profile drawn along the line drawn through the planimetric centres of the source area and deposit, following approximately the direction of the predominant flow lines. The pre-slide ground profile should be reconstructed on the centreline profile as well as possible (Fig. 6).

3.3 General Rules for Input, Precision

3.3.1 The P-Number System

Many quantitative variables in the data base are recorded using two values. The first is the value of the variable itself in specified units, such as a length or an angle. The second is a single digit number between 1 and 5, designating the precision of the estimate using the scale defined in Table 2. It is referred to as the P-number.

The P-number system allows approximate data to be incorporated into the data base, but to be separated from the more accurate measurements in course of query operations.

3.3.2 Blank and Zero Fields

Whenever a data field is left blank or zero, this implies that the value is unknown. An exception to this rule is when a zero value is specified, alongside a

non-zero P-number. In that case, the parameter is implied to be known and have zero value. A P-number equal to zero always means that the parameter value is unknown.

3.3.3 Source Selection Priority

Quantity estimates given by the authors of the source reference should be accepted, unless: 1) better estimates are available from later (or better informed) sources, or 2) the user has a means of making his own reliable estimate (e.g. from maps or direct observations).

3.3.4 Value Ranges

Where a source gives a quantity as a range, the mid-point value of the range should be entered and the width of the range should be used to calculate the P-number.

3.4 Screen ROCKSL, Source Area Description

The ROCKS screen is a multi-page form designed for formatted access to the entire range of variables in the ROCKSL.DBF file. The screen format is shown in Table 17. "Short form" screens, with a reduced number of parameters for each record, are shown in Table 18. The variables are listed in Table 16. Detailed definition of the variables on each page is given in the following paragraphs.

PAGE 1. IDENTIFICATION

SIG	Last modification of this record (enter initials and date).
ID	Case identification number (assigned consecutively).
LOCALITY	Name of locality
CONTINENT	Continent: NA North America SA South and Central America EU Europe AS Asia AF Africa AU Australia, Oceania
COUNTRY	Country.
LATITUDE	Latitude (to the nearest hundredth of a degree, positive north of equator).
LONGITUDE	Longitude (as above, positive west of Greenwich).

REFERENCES List of identification numbers of references in the Bibliography file (separated by commas).

SOURCES List of relevant source publications not in the Bibliography, reports, organizations or individuals.

PAGE 2. SLOPE GEOMETRY PRIOR TO SLIDE (see Fig. 2)

Notes:

1) The following data are measured along the straight central profile of the rockslide, oriented down the fall line of the pre-failure slope, from the centre of the source area in plan (Section A-A, Fig. 2).

2) All slope angles in the following items should be measured as mean angles of slope segments not less than 100 m high. Minor undulations of the profile should be neglected.

S_AZIMUTH Azimuth angle of the profile.

S_BOTTOM Valley bottom elevation (m).

S_TOE Slope toe elevation (lowest point of bedrock dominated slope, or the point where slope angle becomes less than 10° (whichever is steeper). Bedrock slopes covered by soil veneer or talus should be considered as bedrock dominated.

S_CREST Slope crest elevation. The crest is the point on the profile where the most prominent change in slope occurs (Fig. 2a). In case of rounded slopes, it is the point of maximum curvature in the profile, neglecting local undulations (Fig. 2b).

S_CR_ANGLE Crest angle (°): difference between slope angles immediately below and above the crest, zero for a rounded slope).

S_MEAN_SL Slope of a straight line between the crest and toe points.

S_MAX_SL Slope of steepest major segment between toe and crest (The segment must be at least 100 m high.

S_PROFILE Type of slope profile between toe and crest:
CX - Convex
LN - Linear
CV - Concave
ST - Stepped

S_TOP — Top of slope elevation (highest point in profile).

S_TOP_SL — Mean slope angle between crest and top (°).

S_RADIUS — Approximate radius (in plan) of contours drawn through the center of the rockslide source area. Positive if the area is convex (a ridge), negative if a re-entrant. Enter 10000 if a straight slope (see Fig. 1).

PAGE 3. SOURCE AREA GEOMETRY

R_TYPE — Type of source mechanism (Fig. 7):

A - Rock Slump
B - Collapse
C - Glide
D - Compound slide
E - Toe slide
F - Centre slide
G - Crest slide
H - Flexural topple
I - Block topple

Notes: The large-scale shape of the source area should be considered, neglecting local irregularities. The distinction between Types C and E is that the back scarp in the former is essentially a tension feature, contributing no shear resistance.

Variables concerning the longitudinal profile (Fig. 4):

R_HEAD — Elevation, crest of head scarp (m).

R_TOE — Elevation, toe of the source area (m). This will often be concealed by slide deposits or talus and an approximation must be made.

R_LENGTH — Length of source area in plan (m).

R_D_FACTOR — Depth Factor H/L, as defined in Fig. 4.

R_LONG_SYM — Longitudinal Symmetry Index (Fig. 4).

Variables concerning the lateral profile (Fig. 5):

R_WIDTH — Width of source area at the deepest point (m).

R_LAT_DF — Lateral Depth Factor, H/B (Fig. 5).

R_LAT_SYM — Lateral Symmetry Index, b_1/B (Fig. 5).

R_LAT_AN — Lateral inclination angle. Slope of a line connecting the margins of the lateral section (Fig. 5).

R_H_MAX Maximum vertical thickness of the slide mass. (The point of max. thickness need not coincide with the section locations).

Other variables:

R_AREA Plan area of the source scar (m^2).

R_VOLUME Estimated volume exclusive of bulking (m^3). The volume of the deposit is not to be entered here.

R_MOV_AZ Mean azimuth of slide movement direction in the source area (°).

PAGE 4. SOURCE AREA GEOLOGY AND STRUCTURE

G_LITHO Dominant lithological group:

IN - Igneous, intrusive
VO - Igneous volcanic
SC - Sedimentary, clastic
CA - Sedimentary, carbonate
MH - High or medium grade metamorphic
ML - Low grade metamorphic

Rock Mass (RM) units: The data base allows for recording the characteristics of three major units of rock mass: RM1 is the most abundant unit in the failed volume. RM2 is the unit considered strongest in terms of rock mass strength, estimated in the strongest direction. RM3 is the weakest unit with mass strength estimated in the weakest direction, but not considering distinct weak structures (e.g. faults), which are recorded separately later. The RM units are characterized by reasonably uniform rock mass quality; they need not be homogeneous in terms of lithology.

Each of the RM units should be sufficiently abundant, or strategically placed, to play a major role in the slide mechanics. Each RM unit should be at least 5m thick. If thinner, it should be recorded as a major structure (weak bed). The purpose of these definitions is to record average and range of rock mass strength in the source area, irrespective of the macro-structure.

If either RM2 or RM3 is not significantly different from RM1, leave all parameters for such a unit blank.

G_RM1 Percent of failed volume represented by Unit RM1.

G_RM2 Percent represented by RM2 (the strongest unit).

G_RM3 Percent represented by RM3 (the weakest unit).

G_ARCH "Architecture" of the source area - relationship between the RM units:

RT - Randomly interbedded, in thick zones (typical spacing between unit boundaries >25 m).
RI - Randomly interbedded, in thin zones
HD - Strongest rock mass concentrated in the head area
CE - Strongest rock concentrated in the centre one third.
TO - Strongest rock in the toe area
SU - Strongest rock concentrated near slope surface
AS - Rock mass strength varies in the lateral direction (asymmetric condition)
OT - other

PAGE 5, DESCRIPTION OF THE MAIN ROCK MASS UNITS

Description of each of the three main rock mass units (RM1, RM2 and RM3):

RM1_ROCK Dominant rock type (use a simple name).

Rock Mass Quality parameters (based on the CSIR rock mass classification system). The variables are to be estimated from a typical vertical section of the source rock mass belonging to the given unit:

RM1_STR Intact strength class (1 to 7, see Table 3).

In case of strength variation (e.g. interbedded stronger and weaker layers), estimate the average strength and express the variation using the P-number

RM1_WEA Mean degree of weathering (Table 4).

RM1_SPAC Typical discontinuity spacing estimated from a vertical section (m). RQD values measured in a vertical drill hole can be converted to joint spacing using Fig. 8.

RM1_JOINTS Condition of joints (1 to 5, Table 5).

RM1_WATER Groundwater (1 to 4, Table 6).

Other parameters:

RM1_SETS	Number of major joint sets.
RM1_ANIS	Rock substance (intact rock) strength anisotropy (1 to 5, see Table 7).
RM1_STRUCT	Structural anisotropy (indicate degree to which rock mass strength is controlled by bedding or a dominant joint set, scale 1 to 5, see Fig. 9).
RM1_CAUSE	Geological cause of strength or structural anisotropy (examples: BEDDING, FOLIATION, SCHISTOSITY, FISSILITY, DOMINANT JOINT SET, CLAY INTERBEDS).
RM1_AXES	Character of anisotropy axes (1-5, see Table 8).
RM1_DIP	Mean dip of the weakest plane.
RM1_DIP_LO	Minimum dip angle in case of curvature (negative if opposite to the mean dip).
RM1_DIP_HI	Maximum dip angle in case of curvature.
RM1_AZIM	Mean dip direction azimuth.
RM1_FI	Estimated minimum friction angle of the rock mass (in the weakest direction).
RM1_FIDS	Estimated minimum friction angle on planes dipping down in the direction of movement.

PAGE 6, MAJOR INDIVIDUAL STRUCTURES

Three major structures MS1 - MS3 (important joints, weak beds or faults, influencing the failure mechanism) A weak bed or rubbly zone should be considered as a structure if it is thinner than 5 m. If thicker, it should be described as an RM unit:

MS1_TYPE Type of structure:

JT - Joint
FT - Fault, sheared zone
WB - Weak bed, seam or lens (must be thinner than 5m)
CT - Contact
RB - Crushed or rubbly zone (must be thinner than 5m)
OT - Other

MS1_CURV Character of the surface (1-5, see Table 8).

MS1_DIP	Mean dip.
MS1_DIP_LO	Minimum dip angle in case of curvature (negative if opposite to the mean dip).
MS1_DIP_HI	Maximum dip angle in case of curvature.
MS1_AZIM	Mean dip direction azimuth.
MS1_FI	Estimated friction angle parallel with the dip.
MS1_THICK	Mean Thickness (m).

PAGE 7, THE DETACHMENT SURFACE

Percentage of the plan area of the detachment surface:

SL_MS1	Located on Major Structure MS1.
SL_MS2	Located on MS2.
SL_JOINTS	Controlled by a series of joints.
SL_WEAK	Located along the weak direction of Rock Mass RM1 (as described above, must be anisotropic to some degree in terms of strength or structure).
SL_W_RM3	Located along the weak direction of Rock Mass RM3.
SL_MASS	Through rock mass, not in the weakest direction.
SL_TOE	Toe Index (See Fig 10a). This index is required for detachment surfaces containing a structurally controlled planar segment. It is defined as a ratio between the distance from the planar segment to the toe of the source scar and the length of the scar, measured on Profile X-Y as defined in Par. 3.2 above. If the planar segment daylights in the toe of the scar, the index is zero (only the P-number should be non-zero).
SL_CU_MIN	Minimum curvature radius in m of Profile X-Y (Fig. 10b). Should be recorded only if the detachment surface profile has a well defined curvature. For stepped or segmented profiles, enter 10000 (Fig. 10c).
SL_CU_MAX	Maximum curvature radius of the same profile. In case of rotational slides, the two radii should be the same.
G_WATER	Evidence of groundwater presence on the detachment surface (1 to 4, use scale in Table 6).

Note:
The groundwater evidence may originate from piezometric measurements where available, but in most cases will have to be estimated from clues such as the presence of springs in the head scarp, reports of water in the tension cracks or in the slope toe prior to failure, or by evident climatic control on the time of failure.

TOPPLING	Is there evidence of toppling displacements prior or during failure? Indicate the estimated percentage of the source volume affected by significant rotations.
G_COMMENT	Comments on source area geology or failure mechanism.
F_VELOCITY	Velocity class of the most rapid known or inferred past movement episode (see Table 9).

3.5 Screen STURZS - Failure, Path & Deposit Description

This is another multi-page form, which is used for formatted access to the entire range of variables in the STURZS.DBF file. The screen format is shown in Table 20. A "short form" screen with a reduced number of parameters for each record is listed in Table 21. The variables are listed in Table 18. Detailed definition of the variables on each page is given in the following paragraphs.

PAGE 1. FAILURE DESCRIPTION

SIG	Last modification of this record (initials, date).
ID_2	I.D. Number, matching the ID variable in file ROCKS.DBF.
LOC	Locality, to match file Rocks.DBF.
F_DATE	Failure date (Day, Month, Year) (for failure definition see Par. 3.1).
F_NUMBER	How many failures (including this one) are known to have occurred at the same location.
F_PREVIOUS	Date of the previous failure (if unknown, give the latest possible date. If only year known, give date as Dec. 31))
F_PREV_VOL	Volume of the previous failure
F_OTHER_SL	Dates and approximate volumes of other previous failures
F_CREEP	Is or was the area known as a disturbed or creeping slope ? (Y/N)

F_SYM_TIME	How many days prior to failure were symptoms of instability first noticed?
F_OBS_TIME	How many days prior to failure was evidence of active movements first observed (e.g. fresh cracks, positive movement observations, increased rockfall activity, other active changes)?
F_EST_DISP	Maximum estimated pre-failure displacement (m).
F_MEAS_DIS	Maximum measured displacement (m).
F_RATE	Maximum observed pre-failure displacement rate (mm/day).

PAGE 2, PRE-FAILURE SYMPTOMS AND CAUSES

Observed pre-failure symptoms (Y/N):

F_T_CRACKS	Tension Cracks
F_FALLS	Minor precursory falls
F_BULGE	Pressure ridges or bulging
F_DRAINAGE	Drainage disruption
F_NOISE	Noise
F_ANIMALS	Animal behaviour
F_OTHER_SY	Other (specify)

Nearest recorded earthquake prior to failure:

EQ_DATE	Date (Day, Month, Year)
EQ_PRIOR	Time period prior to failure (Hours)
EQ_MAG	Richter Magnitude
EQ_DIST	Distance to epicentre (km)
EQ_DEPTH	Hypocentral depth (km)

Precipitation data (classify on a scale of 1 to 3, defined as follows:

0	Not known
1	No significant or unusual precipitation
2	Moderate or average precipitation
3	Above average precipitation

PR_DAY	Precipitation within 24 hours preceding the failure (1-3).
PR_SHORT	Short term precipitation during one week prior to failure (1-3).
PR_MED	Medium term precipitation (2 months, 1-3)
PR_SEAS	Seasonal precipitation during the preceding year (1-3).
PR_SNOW	Snowpack during preceding winter (1-3).

HUM_INTER	Human intervention as a possible cause of failure (0 - Unknown, 1 - None, 2 - Moderate, 3 - Major)
HUM_TYPE	Type of intervention (specify)
F_COMMENT	Comments regarding failure symptoms and causes (memo).

PAGE 3, SLIDE PATH DURING FAILURE (STURZSTROM PATH

Notes:

1) The slide path is considered to extend from the toe of the source area to the distal rim of the deposit.

2) Should the slide split into two or more distinct paths and deposits, fill out Pages 3 and 4 for each major branch, as separate records, leaving the preceding sections blank.

Total vertical (H) and horizontal (L) distances and the maximum depth of the profile, D (Measured on Profile C-C, Fig. 6):

a) Between crest of scar and the most distant point of deposit ("Fahrboschung" parameters)

P_H	H	(m)
P_L	L	(m)
P_D	D	(m)

b) Between the centres of gravity of the source and deposit (if known)

P_HC	H_c	(m)
P_LC	L_c	(m)
P_DC	D_c	(m)

c) Between points on the post-failure ground surface, corresponding to the centres of gravity of the plan areas of the source and deposit

P_HA	H_a	(m)
P_LA	L_a	(m)
P_DA	D_a	(m)

P_WIDTH Mean width of the slide path (measure at five points and average, m)

P_ENTRAIN	Estimated net volume of material entrained (or lost, if negative) along the path between the source scar and the deposition area.
P_CROSS	Maximum flow cross-section (vertical) of the slide along the path (assume straight line top surface m^2).
P_DURATION	Duration of the main displacement in minutes
P_VELOCITY	Mean flow velocity at a specific point in the path. (Note:if there are more than one velocity estimate, record the most reliable one here and the remainder under comments below. Do not record average velocity here, as it can be determined from duration).
P_VEL_METH	Indicate method by which the above velocity estimate was obtained (e.g. SUPERELEVATION, RUNUP, EYEWITNESS ESTIMATE etc.).
P_V_CROSS	Vertical flow cross-section area at the point where velocity measurement was taken (to determine discharge, m^2)
P_RUNUP	Maximum runup of the debris (Maximum height of upwards vertical displacement of any part of the debris, m)
P_COMMENT	Comments on the flow behaviour of the slide.

PAGE 4, DEPOSIT

D_AREA	Plan area of the deposit (m^2).
D_VOLUME	Estimated total volume of the deposit (m^3).

Note: Some slides form "projection" deposits, narrow, long trains of debris extending outside the regular outline of the main deposit. If narrower than 10 % of the maximum width of the deposit, the projection should be excluded when estimating the following four parameters. Also, if the deposit is split into two or more well detached parts along the direction of travel, please collect the following for the largest part only.

D_LENGTH	Length of the deposit in plan, measured in the direction of movement (m).

D_WIDTH	Maximum plan width of the deposit, measured perpendicular to the movement direction.
D_THICK	Maximum estimated vertical thickness of the deposit (m).
D_SLOPE	Average slope angle of the central part of the deposit, measured along the fall line (not necessarily in a straight line). The definition of this angle is given in Figure 11.
D_PROJECT	Length of projection deposit (zero if there is none)
D_PART	If the deposit is split into parts, indicate the percentage of total deposit area represented by the main part (100 % if no split).
D_GRAIN	Modal (most abundant in terms of volume) grain size observed on the surface of the main part of the deposit.
D_GRADING	Grading: NO - None identified, although there are exposures available IN - Inverse (coarser towards the top) NR - Normal (coarser towards the base)
D_SPLASH	Percent of total deposit area represented by the "splash" of fine grained material outside the margins of the main coarse deposits.
D_PS_ORIG	Has the splash material been identified as originating from soils entrained along the path of the rockslide? F - Fully P - Partly N - No (it is probably derived from the source scar)

Indicate the presence or absence of the following symptoms (Enter Y or N or blank if not known):

D_BASE	Presence of entrained material near the base of the deposit, visible in exposures.
D_RIMS	Raised rims.
D_MOLARDS	Molards, conical features on the deposit.
D_LONG_RID	Longitudinal ridges (in direction of motion).

D_LAT_RIDG	Lateral ridges.
D_ESC_STR	Sand boils, mud volcanoes, other escape structures.
D_COMMENT	Comments and additional information regarding the deposit.

PAGE 4 SLIDE PATH SUBGRADE AND DAMAGE DATA

The slide path begins at the toe of the source area and ends at the distal rim of the deposit. The following variables record the percentage of the path length, represented by various types of subgrade.

S_BEDROCK	Bedrock, possibly with a thin veneer of colluvium or talus.
S_RESIDUAL	Residual soil.
S_TALUS	Extensive and deep talus deposits.
S_MORAINE	Glacial till.
S_TERRACE	River terrace deposits (granular)
S_RIVER	Alluvial sand and gravel.
S_LACUSTR	Lacustine deposits or fine-grained (silt or clay) alluvium from a large stream.
S_SHALL	Shallow water (less than 10m deep).
S_DEEP	Deep water (>10m).
S_ICE	Glacial ice.

Indirect damage:

I_DAM	Has a landslide dam been created?
I_WAVE_H	Maximum runup height of a landslide-caused wave in a body of water (m).
I_WAVE_LEN	Length of shoreline affected by the landslide wave (Km).

Damage cost summary:

M_LIVES	Number of lives lost in the landslide.
M_INJURIES	Number of persons injured.
M_HOUSES	Number of dwellings destroyed by the landslide (not counting non-inhabitable buildings).
M_OTHER	Other major damage (specify, give cost figures if available).
D_COMMENT	Comments and additional information concerning the failure behaviour or damage.

Table 1

LIST OF dBASE IV FILES

a) Catalog REFS.CAT, Bibliography

REFS.DBF	Bibliography file, containing authors, titles, publications as well as keywords, reference locations and utility codes.
REF_IN.SCR	Screen format file for input of bibliography.
REF_CDE.SCR	Screen format file for input of keywords and utility codes for references.
REF_LIST.FRO	Report file for printing sequential list of references.
REF_PRIN.PRG	dBase program for printing reference lists.
REF_S.QBE	Query file for sorting of reference lists.

b) Catalog ROCKS.CAT, Large Rockslides Data Base

ROCKSL.DBF	Parameters describing the source area of the rockslide (location, dimensions, geology, structure).
ROCKSL.SCR	Screen format for input of the above.
ROCK_SH.SCR	"Short form" screen format.
STURZS.DBF	Parameters describing the failure and post-failure behaviour (dates, displacements, velocities, travel path, deposit, damage statistics).
STURZS.SCR	Screen format for input of failure data.
STURZ_SH	"Short form" screen format for failure data.

Table 2

PRECISION CODE

P-Number	Estimated precision of the given value	
0	Value unknown	
1	Very High	(± 5%)
2	High	(±10%)
3	Moderate	(±20%)
4	Low	(±50%)
5	Very Low	(guess)

*Note: In case of elevation values, the percentage deviation should be calculated with respect to the relative elevation difference of concern (e.g. the difference between crest and toe of the source area).

Table 6

ROCK STRENGTH IDENTIFICATION

(After Jennings & Robertson, 1969)

Class	Designation	Description	Uniaxial Compressive Strength (MPa)
1	extremely weak rock	Indented by thumbnail	0.25 - 1.0
2	very weak rock	Crumbles under firm blow with point of geological hammer, can be peeled by a pocket knife	1.0 - 5.0
3	weak rock	Can be peeled by a pocket knife with difficulty, shallow indentations made by firm blow with point of geological hammer	5.0 - 25
4	medium strong rock	Cannot be scraped or peeled with a pocket knife, specimen can be fractured with single firm blow of geological hammer	25 - 50
5	strong rock	Specimen requires more than one blow of geological hammer to fracture it	50 - 100
6	very strong rock	Specimen requires many blows of geological hammer to fracture it	100 - 250
7	extremely strong rock	Specimen can only be chipped by geological hammer	> - 250

Table 7

WEATHERING DESCRIPTION

(After Geological Soc. of London, 1970)

Term	Grade Symbol	Diagnostic Features
Fresh	W1	Parent rock showing no discolouration, loss of strength or any other weathering effects.
Slightly weathered	W2	Rock may be slightly discoloured, particularly adjacent to discontinuities, which may be open and will have slightly discoloured surfaces, the rock material is not noticeably weaker than the fresh rock.
Moderately weathered	W3	Rock is discoloured, discontinuities may be open and will have discoloured surfaces with alteration starting to penetrate inwards, rock material is noticeably weaker, as determined in the field, than the fresh rock. (The ratio should be estimated where possible).
Highly weathered	W4	Rock is discoloured, discontinuities may be open and have discoloured surfaces, and the original fabric of the rock near to the discontinuities may be altered, alteration penetrates deeply inwards, but corestones are still present. (The ratio of original rock to weathered rock should be estimated where possible).
Completely weathered	W5	Rock is discoloured and changed to a soil but original fabric is mainly preserved. There may be occasional small corestones. The properties of the soil depend in part on the nature of the parent rock.
Residual soil	W6	Rock is discoloured and completely changed to a soil in which original rock fabric is completely destroyed. There is a large change in volume. (Genesis should be determined where possible).

Table 8

DISCONTINUITY CONDITION

(After Bieniawski, 1976)

Class	Description
1	Very rough surfaces Not continuous No separation Hard joint wall rock
2	Slightly rough surfaces Separation <1 mm Hard joint wall rock
3	Slightly rough surfaces Separation <1 mm Soft joint wall rock
4	Slickensided surfaces or Gouge <5 mm thick or Joints open 1 - 5 mm Continuous joints
5	Soft gouge >5 mm thick or Joints open >5 mm Continuous joints

Table 9

GROUNDWATER IN THE ROCK MASS

(After Bieniawski, 1976)

Class	Description	Ratio Water Pressure to Overburden Stress
1	Dry	0
2	Moist	0 - 0.2
3	Water under moderate pressure	0.2 - 0.5
4	Water under high pressure	>0.5

Table 10

ROCK SUBSTANCE STRENGTH ANISOTROPY CLASSES

Class	Designation	Description	Typical Examples
1	Isotropic	Same strength in all directions.	Granite, limestone
2	Moderately Anisotropic	Banded or weakly foliated rock, slightly weaker in one direction.	Gneiss, banded sandstone or carbonate
3	Slightly Fissile	Contains thin weak partings oriented in one direction. Strength Anisotropy Index* 3-5.	Gneiss with shistose partings Sandstone or carbonate with thin shaley layers.
4	Fissile	Rock substantially weaker in one direction due to parallel orientation of platy particles. Strength Anisotropy Index* over 5.	Shale, Schist
5	Highly Fissile	No coherence in the weak direction, smooth fissility planes.	Slate, Phyllite

* Strength Anisotropy Index = Strength ratio (compressive, shear or tensile) between strongest and weakest directions.

Table 11

CHARACTER OF INDIVIDUAL MAJOR DISCONTINUITIES, OR OF ROCK ANISOTROPY AXES

Curvature Class	Description	Range of Radii of Curvature (m)
1	Planar	Infinity
2	Nearly planar	>2,000 m
3	Widely curved	500 - 2,000 m
4	Wavy	100 - 500 m
5	Contorted	<100 m

Table 12

FAILURE VELOCITY CLASSES

(After Varnes, 1978)

Class	Description	Maximum Velocity
1	Extremely slow	<0.06 m/year
2	Very slow	0.06 - 1.5 m/year
3	Slow	1.5 - 18 m/year
4	Moderate	18 - 550 m/year
5	Rapid	550 m/year - 0.005 m/sec
6	Very rapid	0.005 - 3 m/sec
7	Extremely rapid	>3 m/sec

Table 13, List of Parameters, File REFS.DBF

Structure for database: C:\DBASE\REFS.DBF
Number of data records: 248
Date of last update : 05/24/91

Field	Field Name	Type	Width	Dec	Index
1	IDD	Numeric	4		N
2	FIRST_AUTH	Character	15		N
3	INITIALS	Character	6		N
4	SECOND_AUT	Character	15		N
5	SND_INIT	Character	6		N
6	OTHERS	Character	72		N
7	YEAR	Numeric	4		N
8	TITLE	Character	72		N
9	TITLE_CONT	Character	72		N
10	PUBLIC	Character	72		N
11	PUBL_2	Character	72		N
12	EDITOR	Character	34		N
13	VOLUME	Numeric	3		N
14	NUMBER	Numeric	2		N
15	PUBLISHER	Character	40		N
16	CITY	Character	15		N
17	PAGES	Character	12		N
18	LANGUAGE	Character	10		N
19	TYPE	Character	5		N
20	CODE	Numeric	3		N
21	KEYWORDS	Character	70		N
22	COPY	Character	1		N
23	LOC1	Character	20		N
24	LOC2	Character	20		N
25	DETAIL	Numeric	1		N
26	USEFUL	Numeric	1		N
27	PRINT	Character	1		N
28	COM	Memo	10		N
** Total **			659		

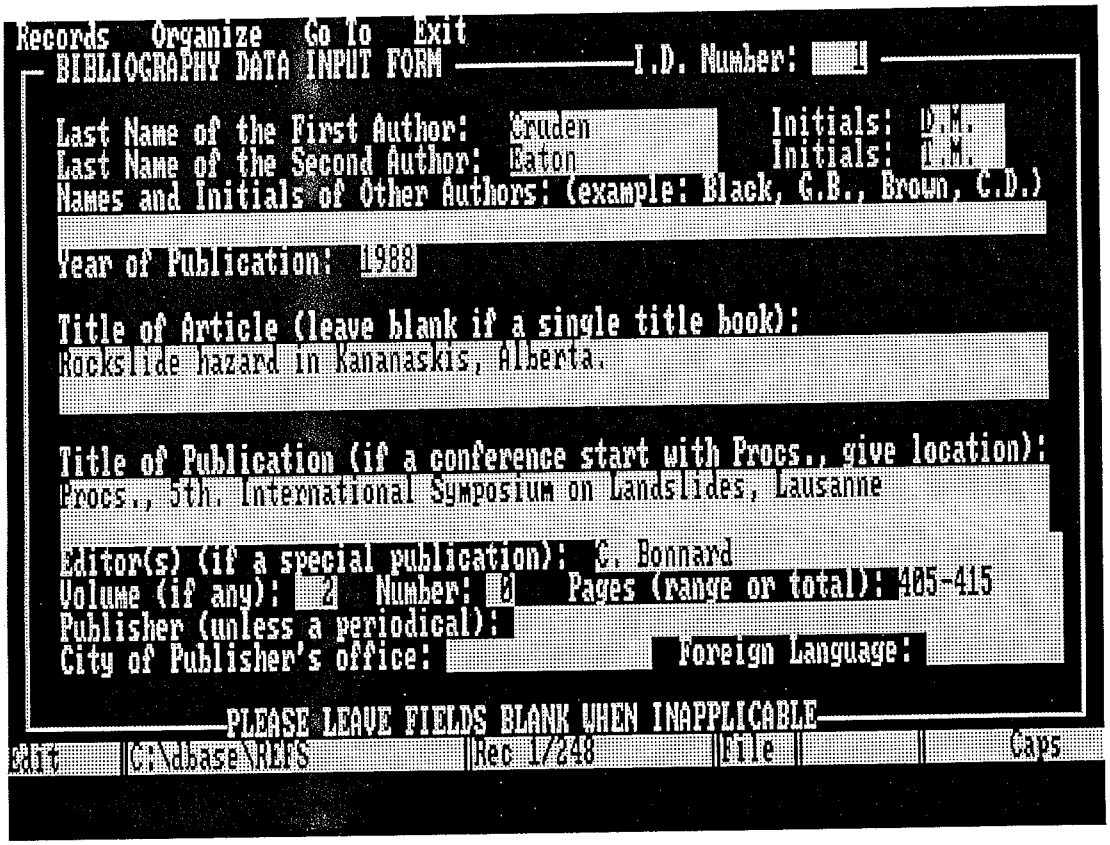

Table 14. Bibliography input screen REF__IN.

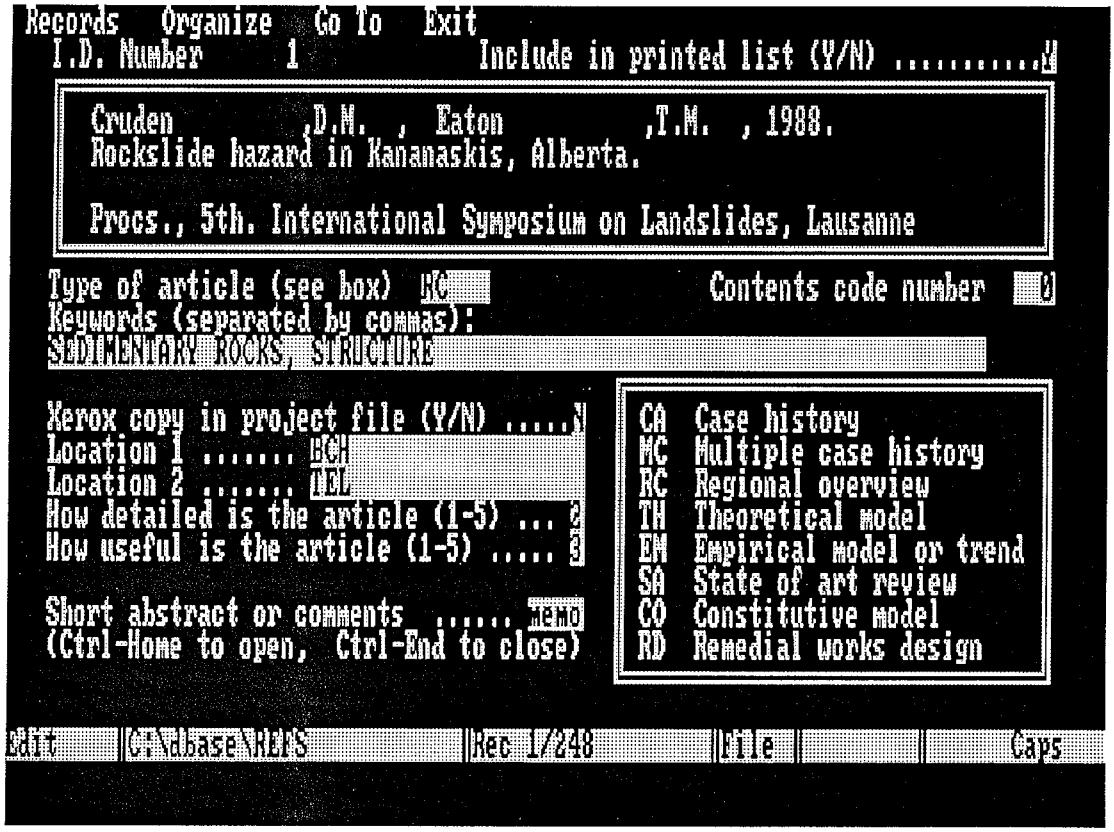

Table 15. Bibliography coding screen REF__CDE.

Table 16, List of Parameters, File ROCKSL.DBF

Page # 1

Structure for database: C:\DBASE\ROCKSL.DBF
Number of data records: 57
Date of last update : 05/22/91

Field	Field Name	Type	Width	Dec	Index
1	ID	Numeric	4		N
2	LOCALITY	Character	20		N
3	CONTINENT	Character	2		N
4	COUNTRY	Character	20		N
5	LATITUDE	Float	6	2	N
6	LONGITUDE	Float	6	2	N
7	REFERENCES	Character	50		N
8	SOURCES	Memo	10		N
9	S_AZIMUTH	Float	4		N
10	S_BOTTOM	Numeric	4		N
11	S_TOE	Numeric	4		N
12	S_CREST	Numeric	4		N
13	S_CR_ANGLE	Float	4	1	N
14	S_MEAN_SL	Float	4	1	N
15	S_MAX_SL	Float	4	1	N
16	S_PROFILE	Character	2		N
17	S_TOP	Numeric	4		N
18	S_TOP_SL	Float	4	1	N
19	S_RADIUS	Numeric	5		N
20	R_TYPE	Character	2		N
21	R_HEAD	Numeric	4		N
22	P1	Numeric	1		N
23	R_TOE	Numeric	4		N
24	P2	Numeric	1		N
25	R_LENGTH	Numeric	4		N
26	P3	Numeric	1		N
27	R_D_FACTOR	Float	4	2	N
28	P4	Numeric	1		N
29	R_LONG_SYM	Float	4	2	N
30	P5	Numeric	1		N
31	R_H_MAX	Float	5	1	N
32	P6	Numeric	1		N
33	R_WIDTH	Numeric	4		N
34	P7	Numeric	1		N
35	P8	Numeric	1		N
36	R_LAT_SYM	Float	4	2	N
37	P9	Numeric	1		N
38	R_AREA	Numeric	9		N
39	P10	Numeric	1		N
40	R_VOLUME	Numeric	12		N
41	P11	Numeric	1		N
42	R_MOV_AZ	Float	4		N
43	P12	Numeric	1		N
44	G_LITHO	Character	2		N
45	G_RM1	Numeric	3		N
46	P13	Numeric	1		N
47	G_RM2	Numeric	2		N
48	P14	Numeric	1		N
49	G_RM3	Numeric	2		N
50	P15	Numeric	1		N

Table 16, continued

51	G_ARCH	Character	2		N
52	RM1_ROCK	Character	15		N
53	RM1_STR	Numeric	1		N
54	P16_1	Numeric	1		N
55	P17_1	Numeric	1		N
56	RM1_SPAC	Float	4	1	N
57	P18_1	Numeric	1		N
58	RM1_JOINTS	Numeric	1		N
59	P19_1	Numeric	1		N
60	RM1_WATER	Numeric	1		N
61	P20_1	Numeric	1		N
62	RM1_SETS	Numeric	1		N
63	RM1_ANIS	Numeric	1		N
64	RM1_STRUCT	Numeric	1		N
65	RM1_CAUSE	Character	15		N
66	RM1_AXES	Numeric	1		N
67	RM1_DIP	Float	4	1	N
68	P21_1	Numeric	1		N
69	RM1_DIP_LO	Float	5	1	N
70	RM1_DIP_HI	Float	4	1	N
71	RM1_AZIM	Float	5	1	N
72	P22_1	Numeric	1		N
73	RM1_FI	Float	4	1	N
74	P23_1	Numeric	1		N
75	RM1_FIDS	Float	4	1	N
76	P24_1	Numeric	1		N
77	RM2_ROCK	Character	15		N
78	RM2_STR	Numeric	1		N
79	P16_2	Numeric	1		N
80	P17_2	Numeric	1		N
81	RM2_SPAC	Float	4	1	N
82	P18_2	Numeric	1		N
83	RM2_JOINTS	Numeric	1		N
84	P19_2	Numeric	1		N
85	RM2_WATER	Numeric	1		N
86	P20_2	Numeric	1		N
87	RM2_SETS	Numeric	1		N
88	RM2_ANIS	Numeric	1		N
89	RM2_STRUCT	Numeric	1		N
90	RM2_CAUSE	Character	15		N
91	RM2_AXES	Numeric	1		N
92	RM2_DIP	Float	4	1	N
93	P21_2	Numeric	1		N
94	RM2_DIP_LO	Float	5	1	N
95	RM2_DIP_HI	Float	4	1	N
96	RM2_AZIM	Float	4		N
97	P22_2	Numeric	1		N
98	RM2_FI	Float	4	1	N
99	P23_2	Numeric	1		N
100	RM2_FIDS	Float	4	1	N
101	P24_2	Numeric	1		N
102	RM3_ROCK	Character	15		N
103	RM3_STR	Numeric	1		N
104	P16_3	Numeric	1		N
105	P17_3	Numeric	1		N

Table 16, continued

Page # 3

106	RM3_SPAC	Float	4	1	N
107	P18_3	Numeric	1		N
108	RM3_JOINTS	Numeric	1		N
109	P19_3	Numeric	1		N
110	RM3_WATER	Numeric	1		N
111	P20_3	Numeric	1		N
112	RM3_SETS	Numeric	1		N
113	RM3_ANIS	Numeric	1		N
114	RM3_STRUCT	Numeric	1		N
115	RM3_CAUSE	Character	15		N
116	RM3_AXES	Numeric	1		N
117	RM3_DIP	Float	4	1	N
118	P21_3	Numeric	1		N
119	RM3_DIP_LO	Float	5	1	N
120	RM3_DIP_HI	Float	4	1	N
121	RM3_AZIM	Float	4		N
122	P22_3	Numeric	1		N
123	RM3_FI	Float	4	1	N
124	P23_3	Numeric	1		N
125	RM3_FIDS	Float	4	1	N
126	P24_3	Numeric	1		N
127	MS1_TYPE	Character	2		N
128	MS1_CURV	Numeric	1		N
129	MS1_DIP	Float	4	1	N
130	P25_1	Numeric	1		N
131	MS1_DIP_LO	Float	5	1	N
132	MS1_DIP_HI	Float	4	1	N
133	MS1_AZIM	Float	4		N
134	P26_1	Numeric	1		N
135	MS1_FI	Float	4	1	N
136	P27_1	Numeric	1		N
137	MS1_THICK	Float	4	1	N
138	P28_1	Numeric	1		N
139	MS2_TYPE	Character	2		N
140	MS2_CURV	Numeric	1		N
141	MS2_DIP	Float	4	1	N
142	P25_2	Numeric	1		N
143	MS2_DIP_LO	Float	5	1	N
144	MS2_DIP_HI	Float	4	1	N
145	MS2_AZIM	Float	4		N
146	P26_2	Numeric	1		N
147	MS2_FI	Float	4	1	N
148	P27_2	Numeric	1		N
149	MS2_THICK	Float	4	1	N
150	P28_2	Numeric	1		N
151	SL_MS1	Numeric	3		N
152	P29	Numeric	1		N
153	SL_MS2	Numeric	3		N
154	P30	Numeric	1		N
155	SL_JOINTS	Numeric	3		N
156	P31	Numeric	1		N
157	SL_WEAK	Numeric	3		N
158	P32	Numeric	1		N
159	SL_MASS	Numeric	3		N
160	P33	Numeric	1		N

Table 16, continued

Page # 4

161	G_WATER	Numeric	1		N
162	P34	Numeric	1		N
163	TOPPLING	Numeric	3		N
164	P341	Numeric	1		N
165	G_COMMENT	Memo	10		N
166	F_VELOCITY	Numeric	1		N
167	P78	Numeric	1		N
168	P79	Numeric	1		N
169	PGE1	Numeric	2		N
170	SIG	Character	14		N
171	R_LAT_DF	Float	4	2	N
172	R_LAT_AN	Float	5	1	N
173	RM1_WEA	Numeric	1		N
174	RM2_WEA	Numeric	1		N
175	RM3_WEA	Numeric	1		N
176	P74	Numeric	1		N
177	SL_W_RM3	Numeric	3		N
178	P75	Numeric	1		N
179	SL_TOE	Float	4	2	N
180	P76	Numeric	1		N
181	SL_CU_MIN	Numeric	5		N
182	P77	Numeric	1		N
183	SL_CU_MAX	Numeric	5		N
184	P_78	Numeric	1		N
185	P_79	Numeric	1		N
186	P80	Numeric	1		N
** Total **			629		

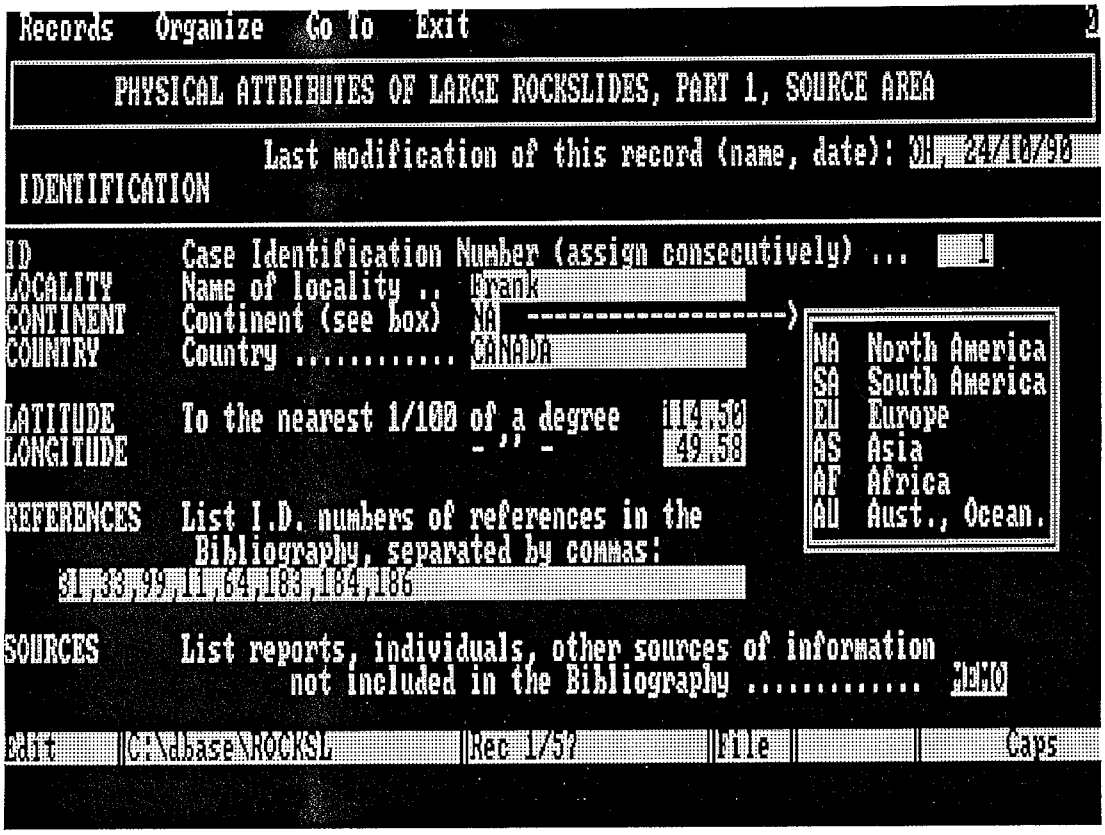

Table 17. Rockslide Data Base, source data screen ROCKSL.

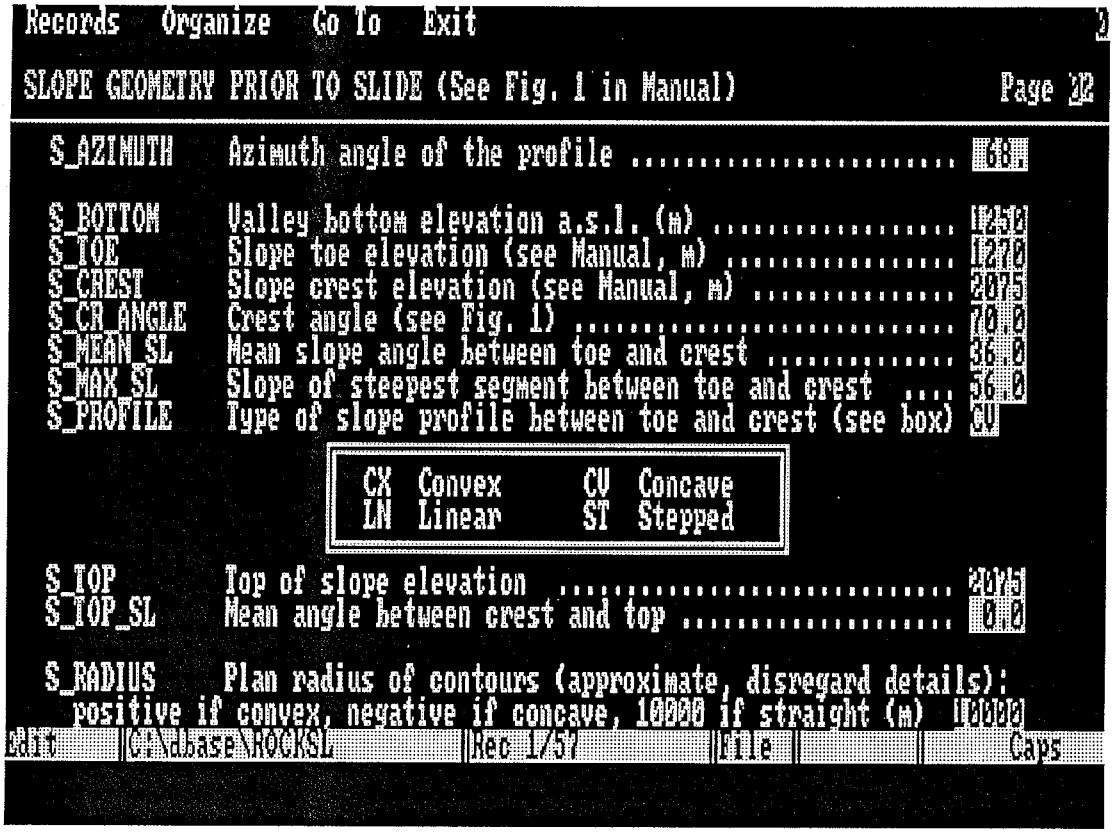

Table 17, continued

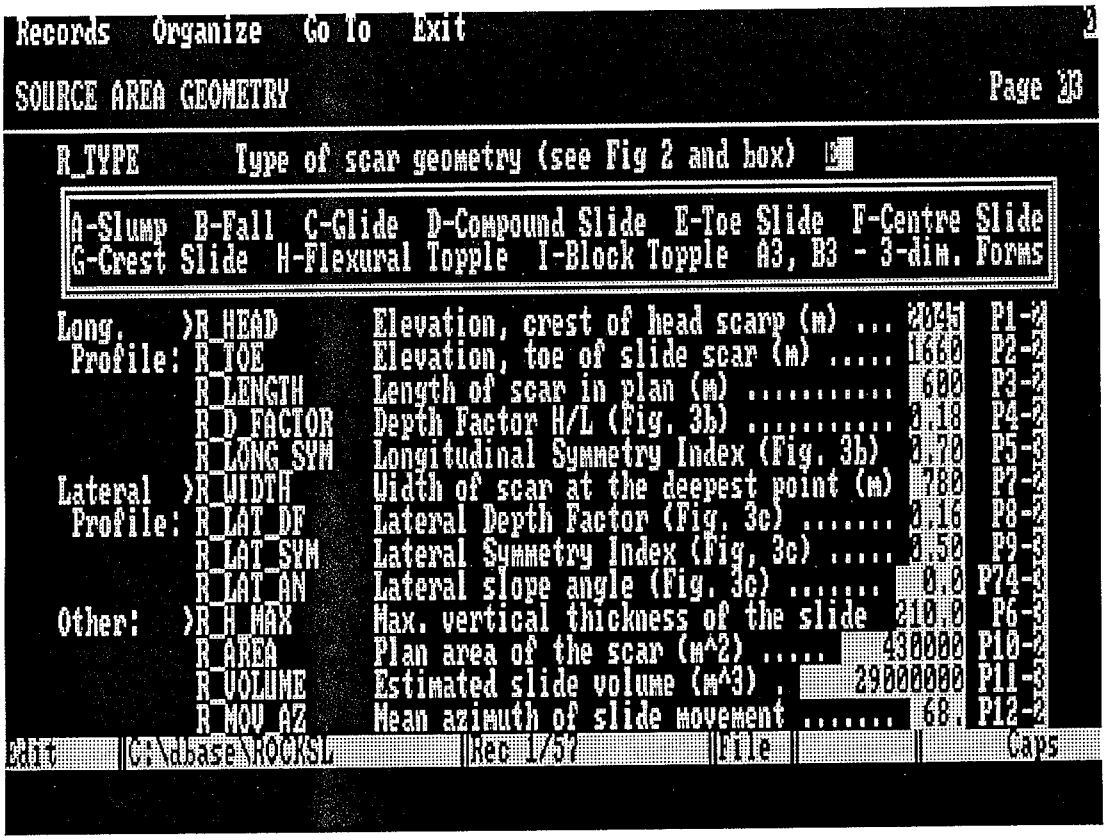

Table 17, continued

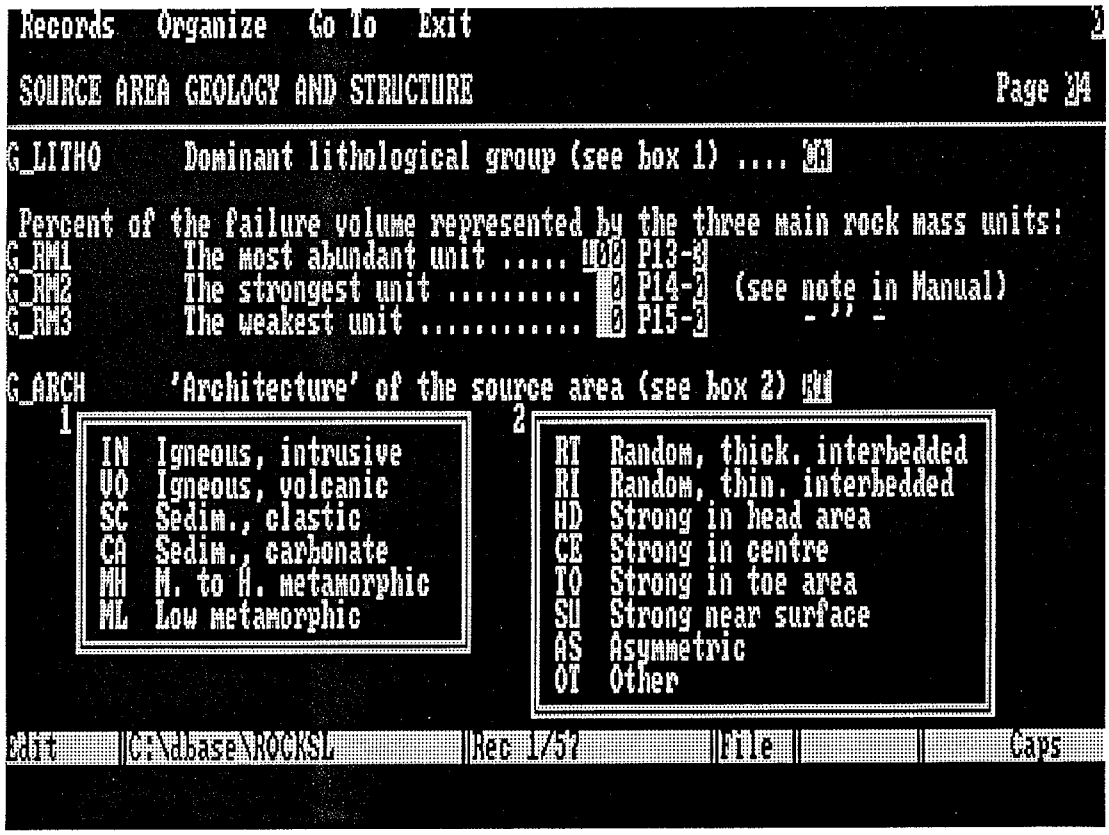

Table 17, continued

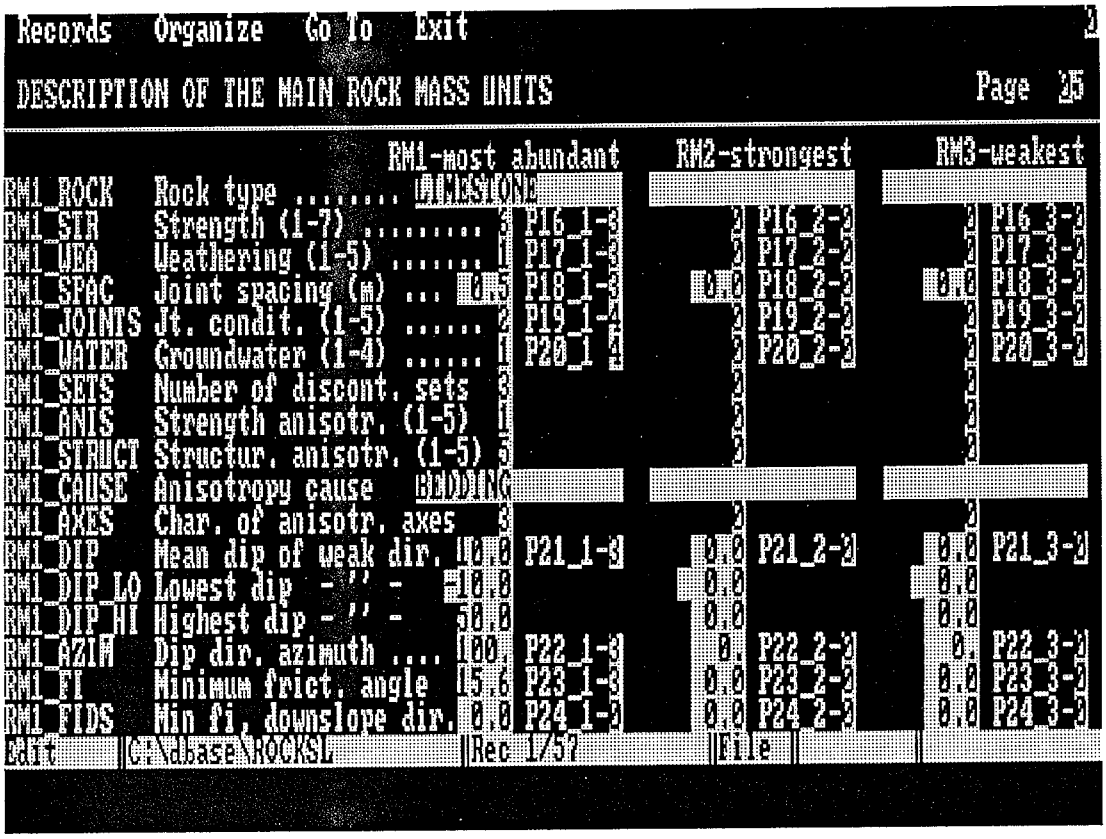

Table 17, continued

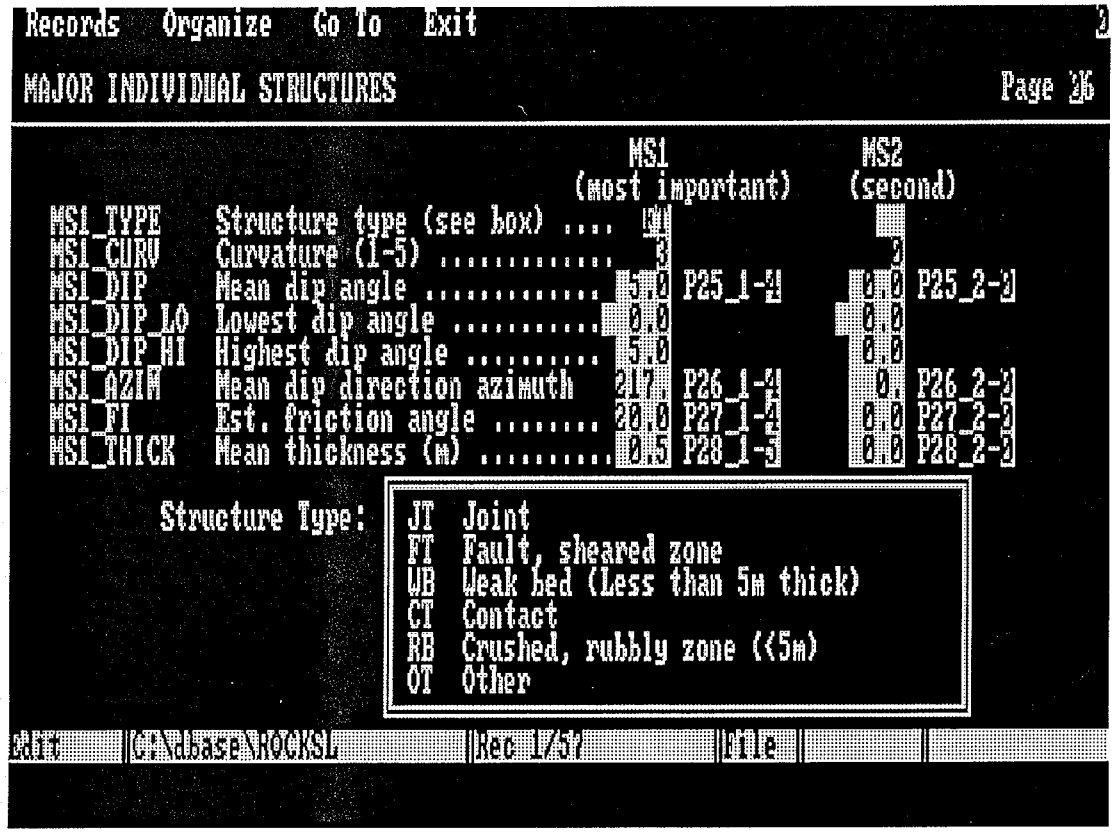

Table 17, continued

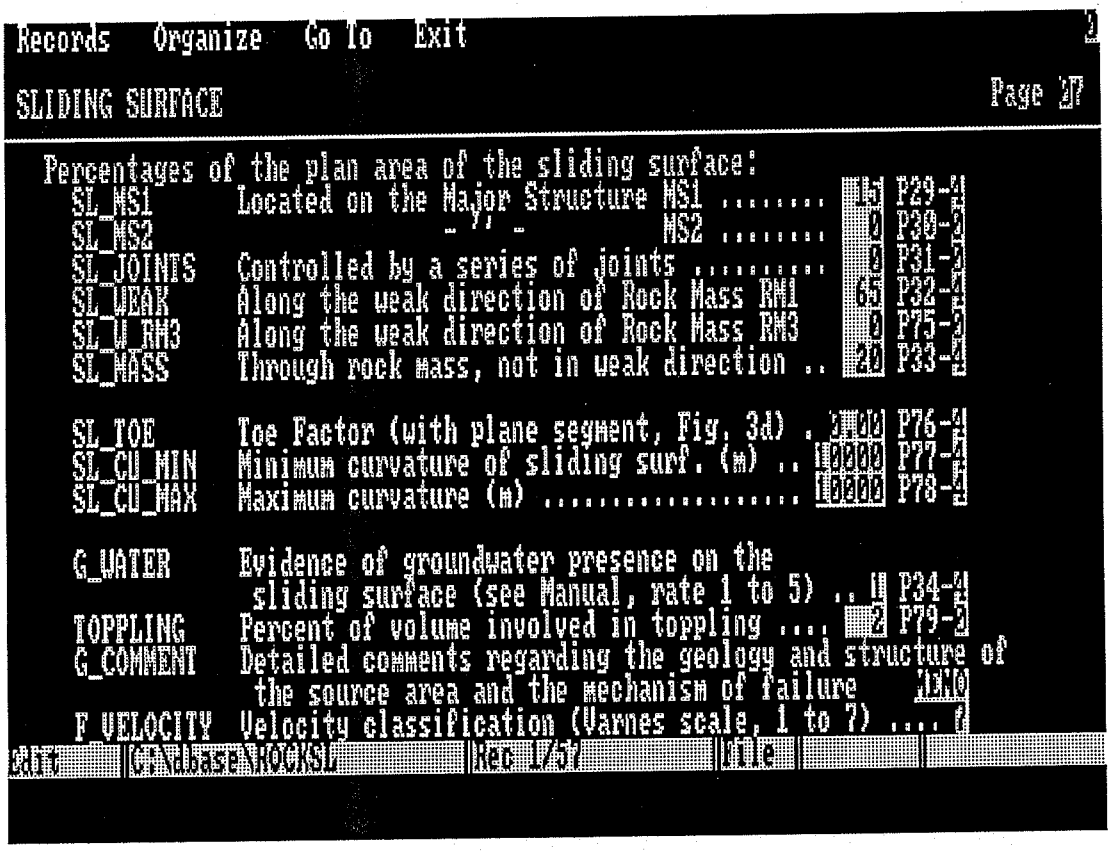

Table 17, continued

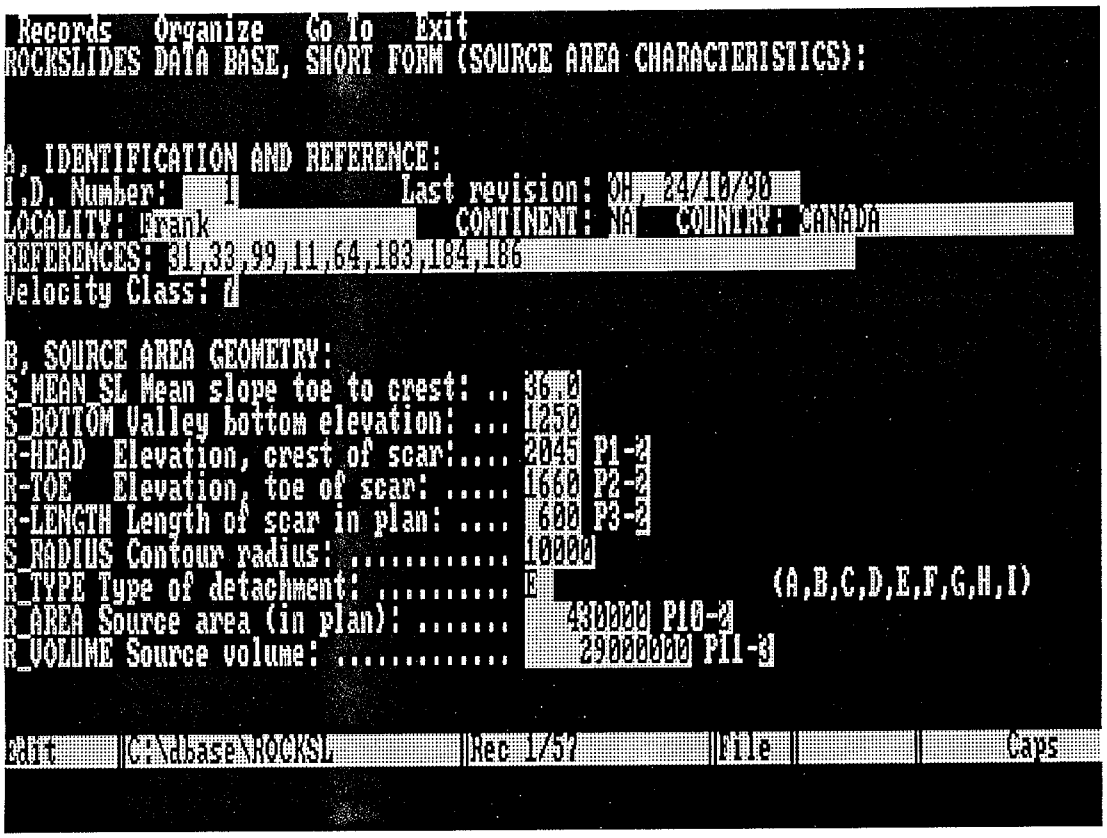

Table 18. Source area data, short form screen ROCK__SH.

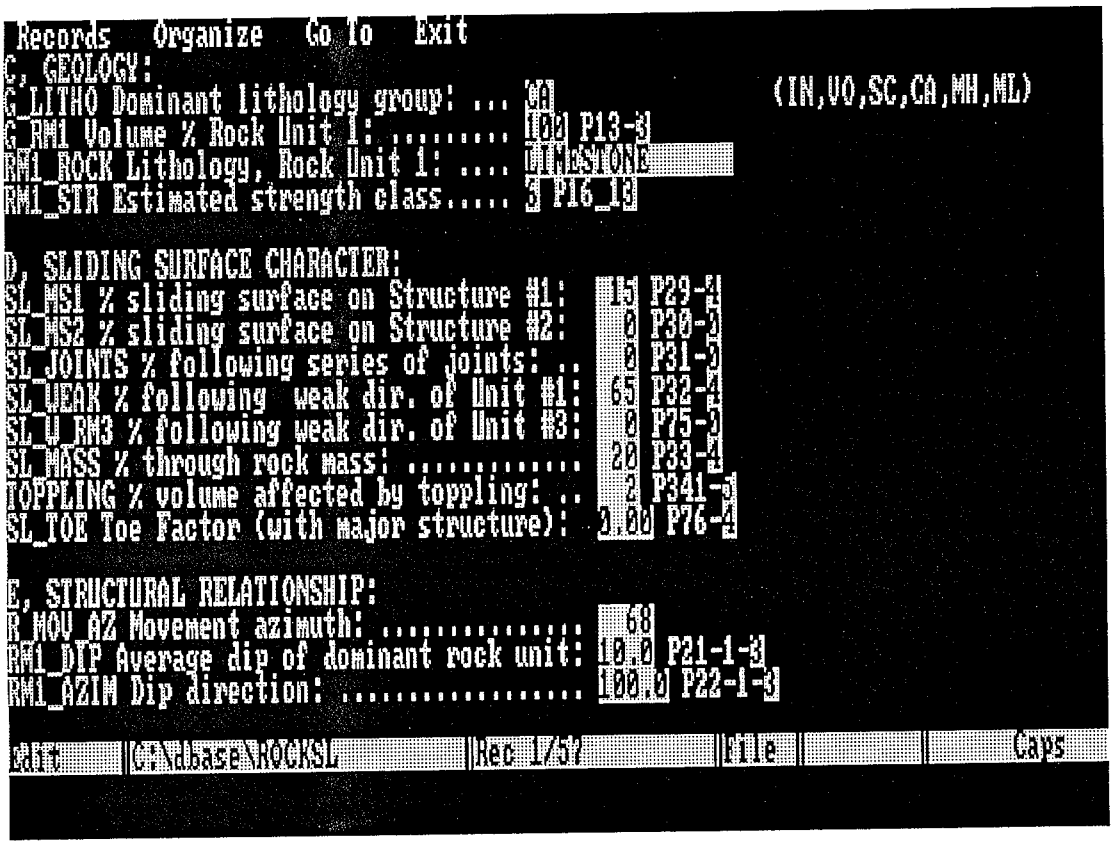

Table 18, continued

Table 19, List of Parameters, File STURZS.DBF

Structure for database: C:\DBASE\STURZS.DBF
Number of data records: 57
Date of last update : 04/17/91

Field	Field Name	Type	Width	Dec	Index
1	ID_2	Numeric	4		N
2	F_DATE	Date	8		N
3	F_NUMBER	Numeric	3		N
4	F_PREVIOUS	Date	8		N
5	F_PREV_VOL	Numeric	10		N
6	F_OTHER_SL	Character	70		N
7	F_CREEP	Character	1		N
8	F_SYM_TIME	Numeric	7		N
9	P35	Numeric	1		N
10	F_OBS_TIME	Numeric	7		N
11	P36	Numeric	1		N
12	F_EST_DISP	Float	5	2	N
13	P37	Numeric	1		N
14	F_MEAS_DIS	Float	5	2	N
15	P38	Numeric	1		N
16	F_RATE	Float	10	6	N
17	P39	Numeric	1		N
18	F_T_CRACKS	Character	1		N
19	F_FALLS	Character	1		N
20	F_BULGE	Character	1		N
21	F_DRAINAGE	Character	1		N
22	F_NOISE	Character	1		N
23	F_ANIMALS	Character	1		N
24	F_OTHER_SY	Character	70		N
25	EQ_DATE	Date	8		N
26	EQ_PRIOR	Float	6	2	N
27	EQ_MAG	Float	4	1	N
28	EQ_DIST	Float	5	1	N
29	EQ_DEPTH	Float	5	1	N
30	PR_DAY	Numeric	1		N
31	PR_SHORT	Numeric	1		N
32	PR_MED	Numeric	1		N
33	PR_SEAS	Numeric	1		N
34	PR_SNOW	Numeric	1		N
35	HUM_INTER	Numeric	1		N
36	HUM_TYPE	Character	40		N
37	F_COMMENT	Memo	10		N
38	P_H	Numeric	5		N
39	P50	Numeric	1		N
40	P_L	Numeric	5		N
41	P51	Numeric	1		N
42	P_D	Numeric	5		N
43	P52	Numeric	1		N
44	P_HC	Numeric	5		N
45	P53	Numeric	1		N
46	P_LC	Numeric	5		N
47	P54	Numeric	1		N
48	P_DC	Numeric	5		N
49	P55	Numeric	1		N
50	P_HA	Numeric	5		N

Table 19, continued

Page # 2

51	P56	Numeric	1		N
52	P_LA	Numeric	5		N
53	P57	Numeric	1		N
54	P_DA	Numeric	5		N
55	P58	Numeric	1		N
56	P_WIDTH	Numeric	5		N
57	P59	Numeric	1		N
58	P_ENTRAIN	Numeric	8		N
59	P60	Numeric	1		N
60	P_CROSS	Numeric	8		N
61	P61	Numeric	1		N
62	P_DURATION	Float	4	1	N
63	P62	Numeric	1		N
64	P_VELOCITY	Float	4	1	N
65	P63	Numeric	1		N
66	P_V_CROSS	Numeric	8		N
67	P64	Numeric	1		N
68	P_RUNUP	Numeric	4		N
69	P65	Numeric	1		N
70	P_COMMENT	Memo	10		N
71	D_AREA	Numeric	10		N
72	P66	Numeric	1		N
73	D_VOLUME	Numeric	12		N
74	P67	Numeric	1		N
75	D_LENGTH	Numeric	8		N
76	P68	Numeric	1		N
77	D_WIDTH	Numeric	8		N
78	P69	Numeric	1		N
79	D_THICK	Numeric	4		N
80	P70	Numeric	1		N
81	D_SLOPE	Float	4	1	N
82	P71	Numeric	1		N
83	D_PROJECT	Numeric	5		N
84	D_PART	Numeric	3		N
85	D_GRAIN	Numeric	6		N
86	P72	Numeric	1		N
87	D_GRADING	Character	2		N
88	D_SPLASH	Numeric	3		N
89	P73	Numeric	1		N
90	D_PS_ORIG	Character	1		N
91	D_BASE	Character	1		N
92	D_RIMS	Character	1		N
93	D_MOLARDS	Character	1		N
94	D_LONG_RID	Character	1		N
95	D_LAT_RIDG	Character	1		N
96	D_ESC_STR	Character	1		N
97	D_COMMENT	Memo	10		N
98	PG1	Numeric	2		N
99	PG2	Numeric	2		N
100	PG3	Numeric	2		N
101	PG4	Numeric	2		N
102	PG5	Numeric	2		N
103	PG6	Numeric	2		N
104	S_ICE	Numeric	3		N
105	S_DEEP	Numeric	3		N

Page # 3

106	S_SHALL	Numeric	3		N
107	S_LACUSTR	Numeric	3		N
108	S_RIVER	Numeric	3		N
109	S_TERRACE	Numeric	3		N
110	S_MORAINE	Numeric	3		N
111	S_TALUS	Numeric	3		N
112	S_RESIDUAL	Numeric	3		N
113	S_BEDROCK	Numeric	3		N
114	I_DAM	Character	1		N
115	I_WAVE_H	Float	5	1	N
116	I_WAVE_LEN	Numeric	5		N
117	M_LIVES	Numeric	6		N
118	M_INJURIES	Numeric	6		N
119	M_HOUSES	Numeric	5		N
120	M_OTHER	Character	60		N
121	SIG	Character	14		N
122	LOC	Character	20		N
123	P_VEL_METH	Character	14		N
** Total **			684		

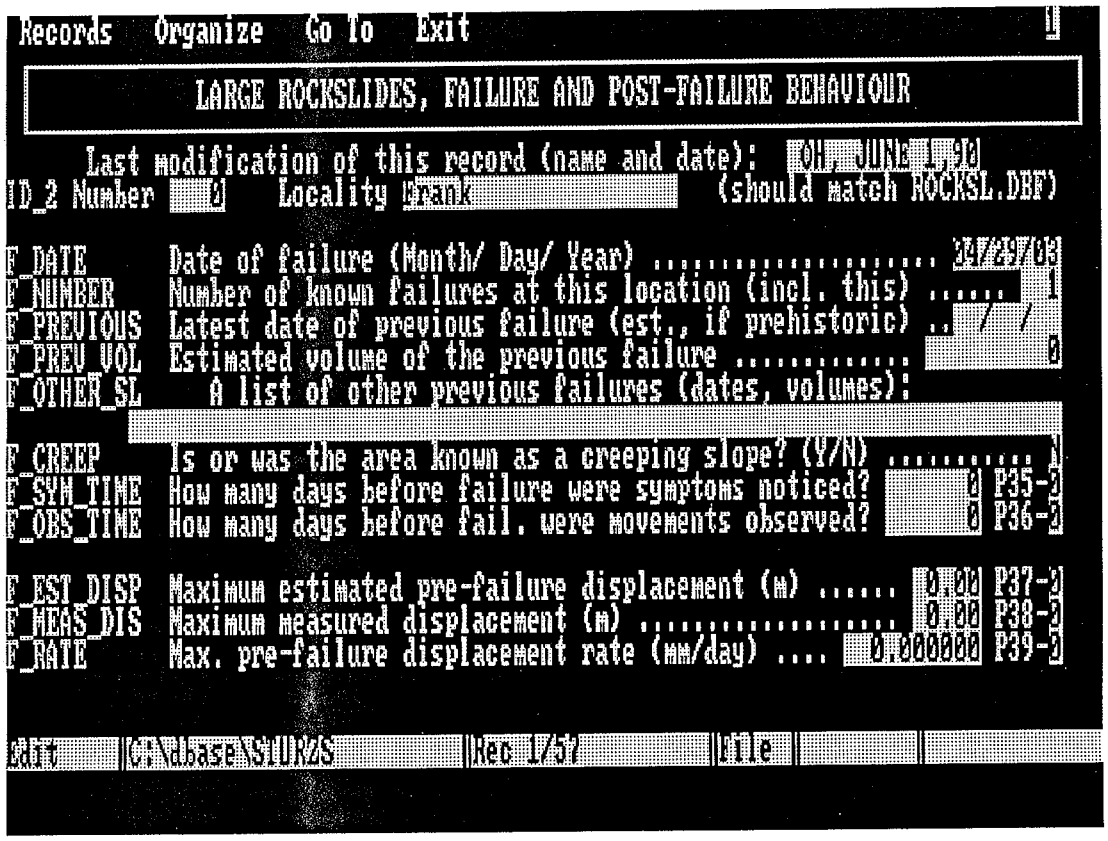

Table 20. Failure data screens STURZS

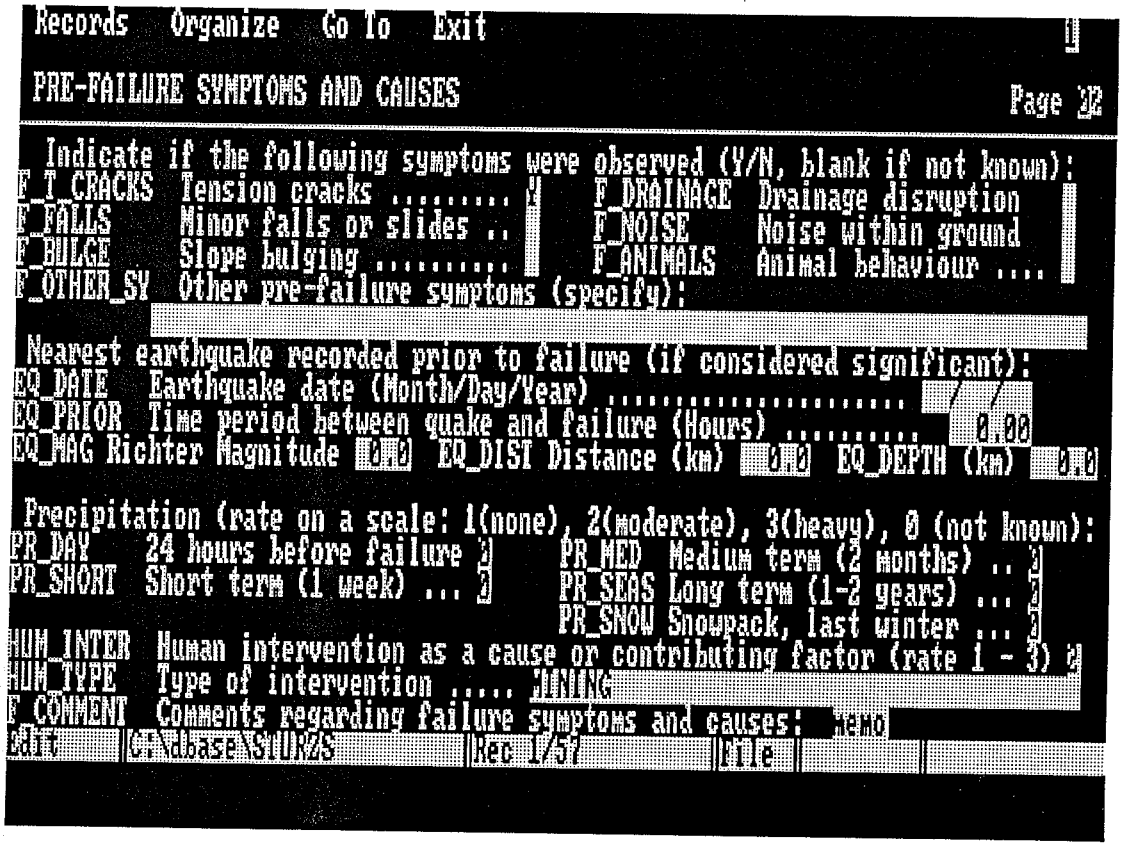

Table 20, continued

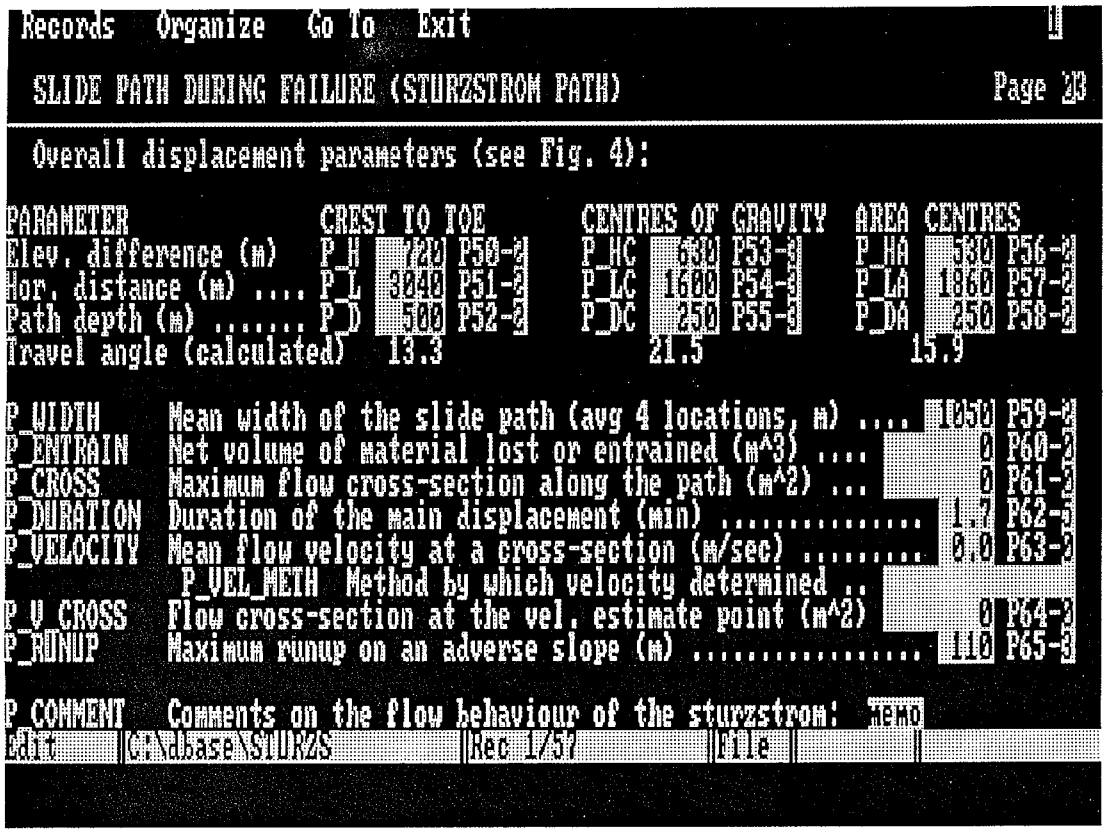

Table 20, continued

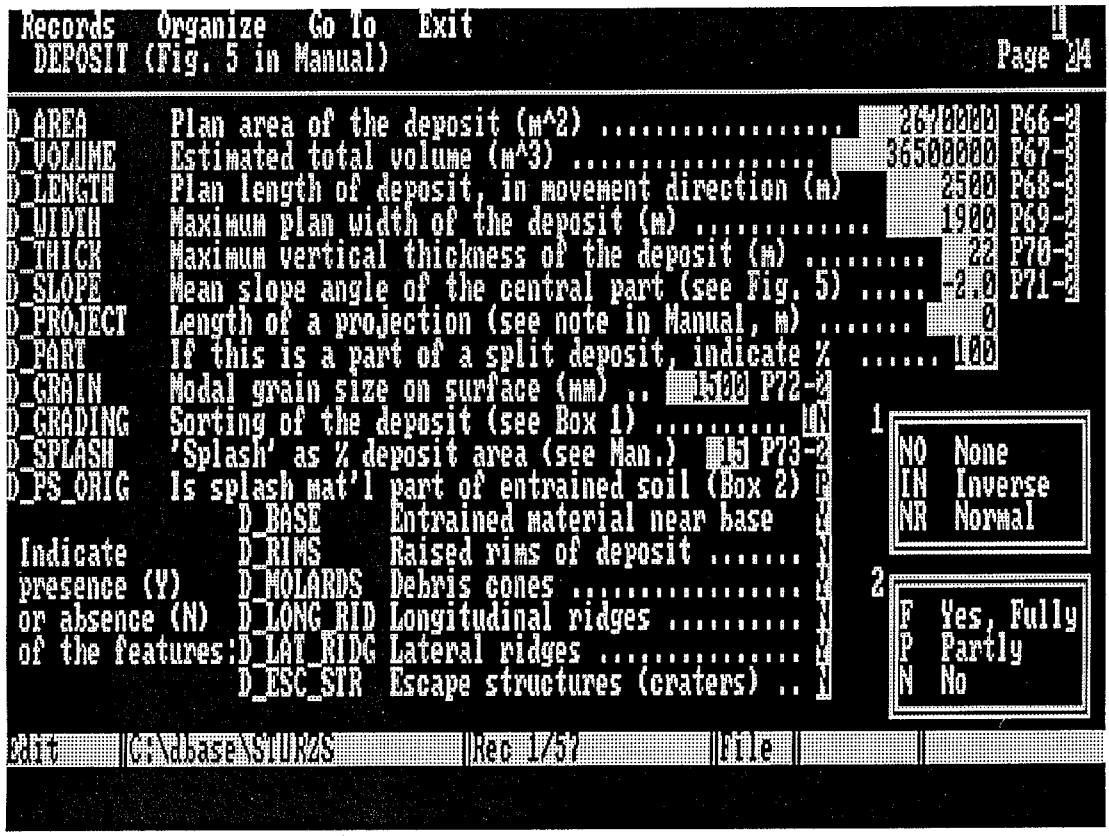

Table 20, continued

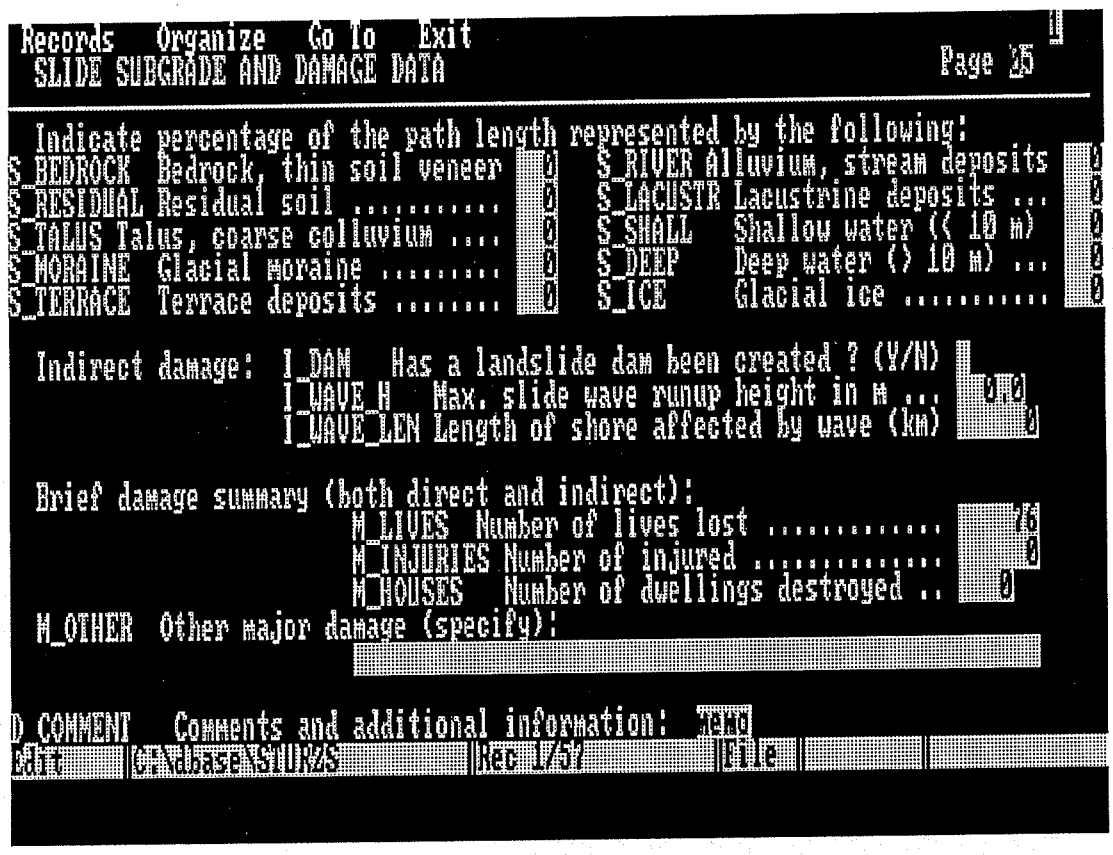

Table 20, continued

Table 21. Failure data, short form screen STURZ__SH

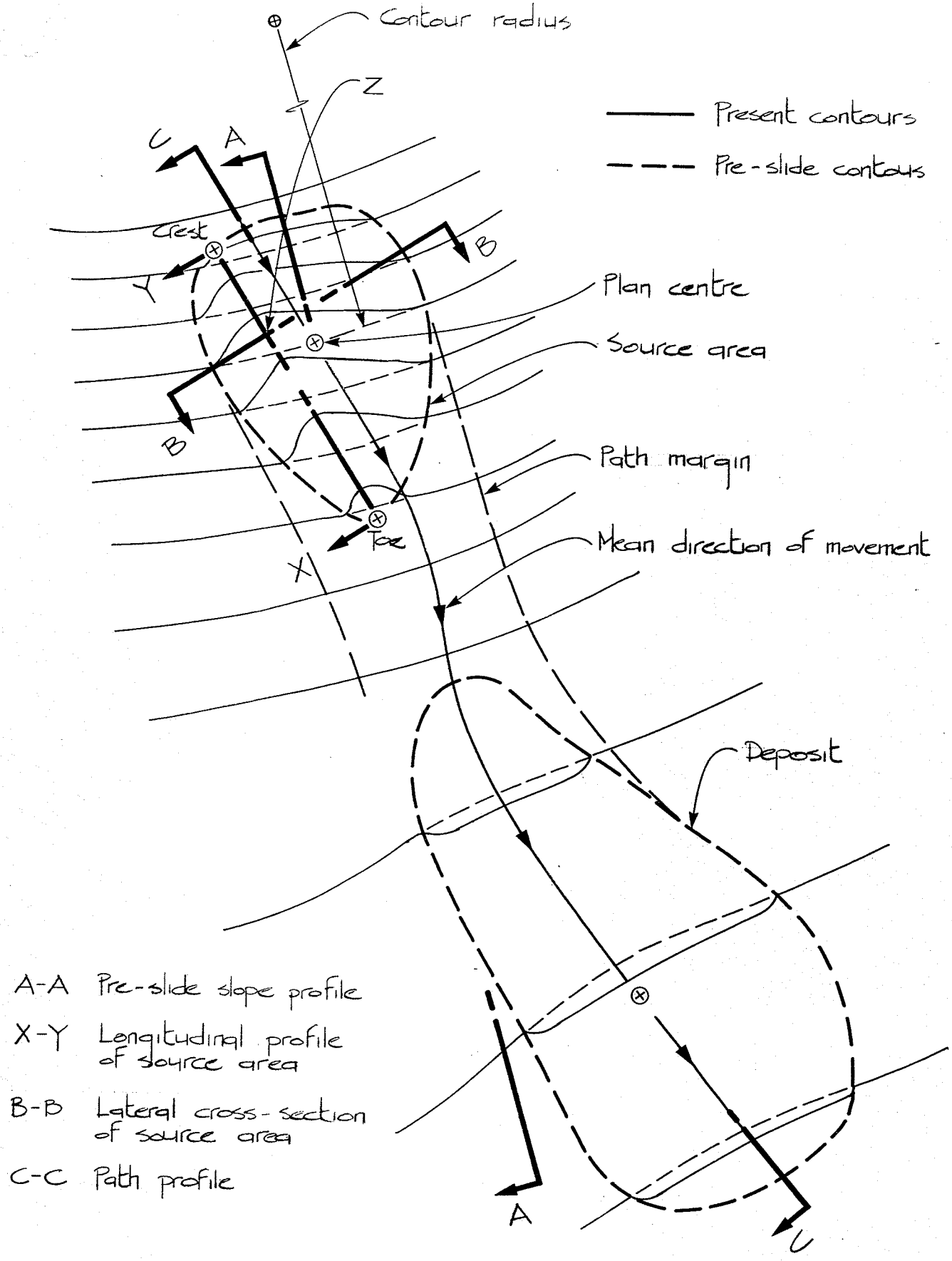

Figure 1 - Plan of the rockslide site

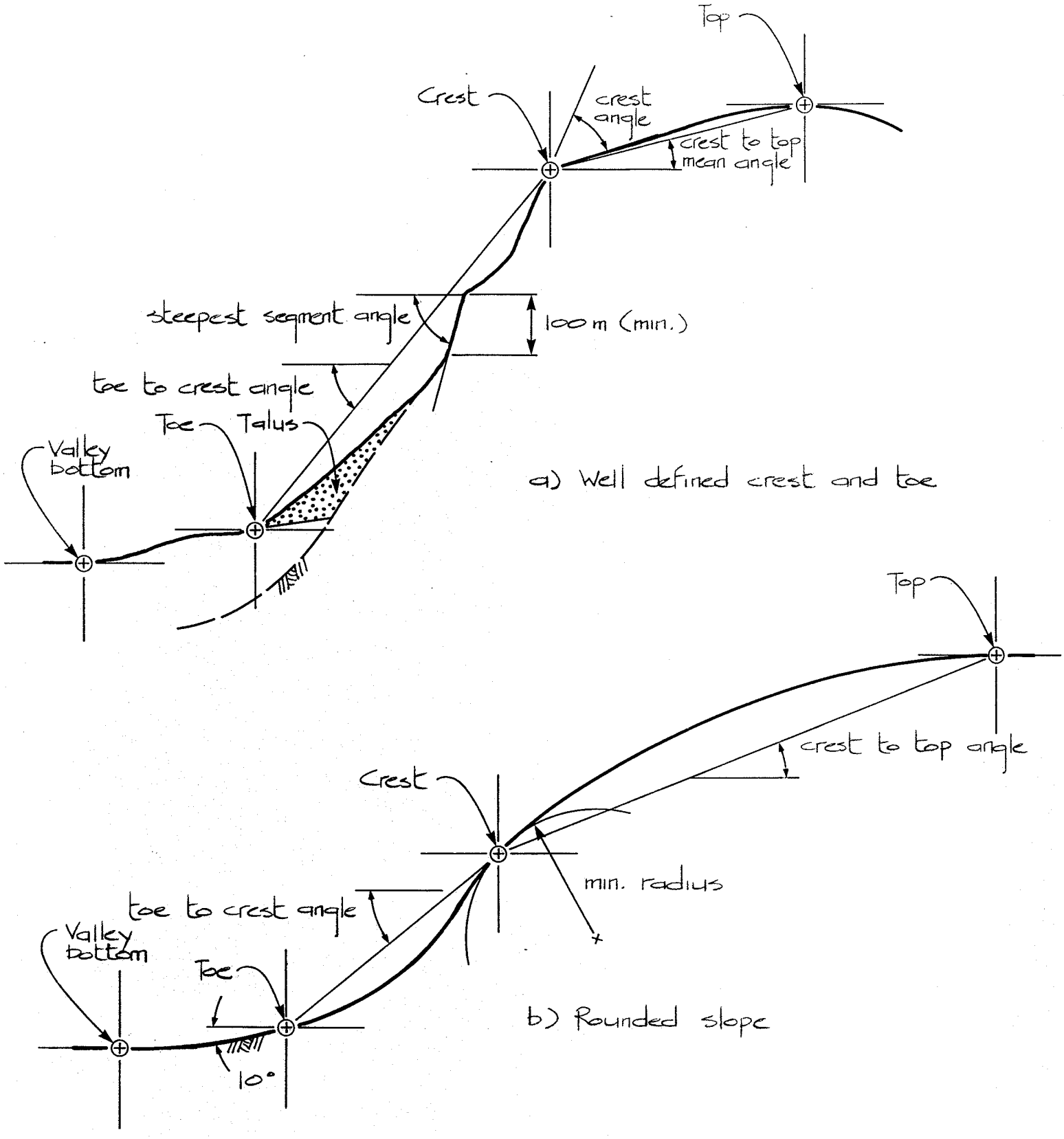

Figure 2 - Reconstructed slope profile (Profile A-A)

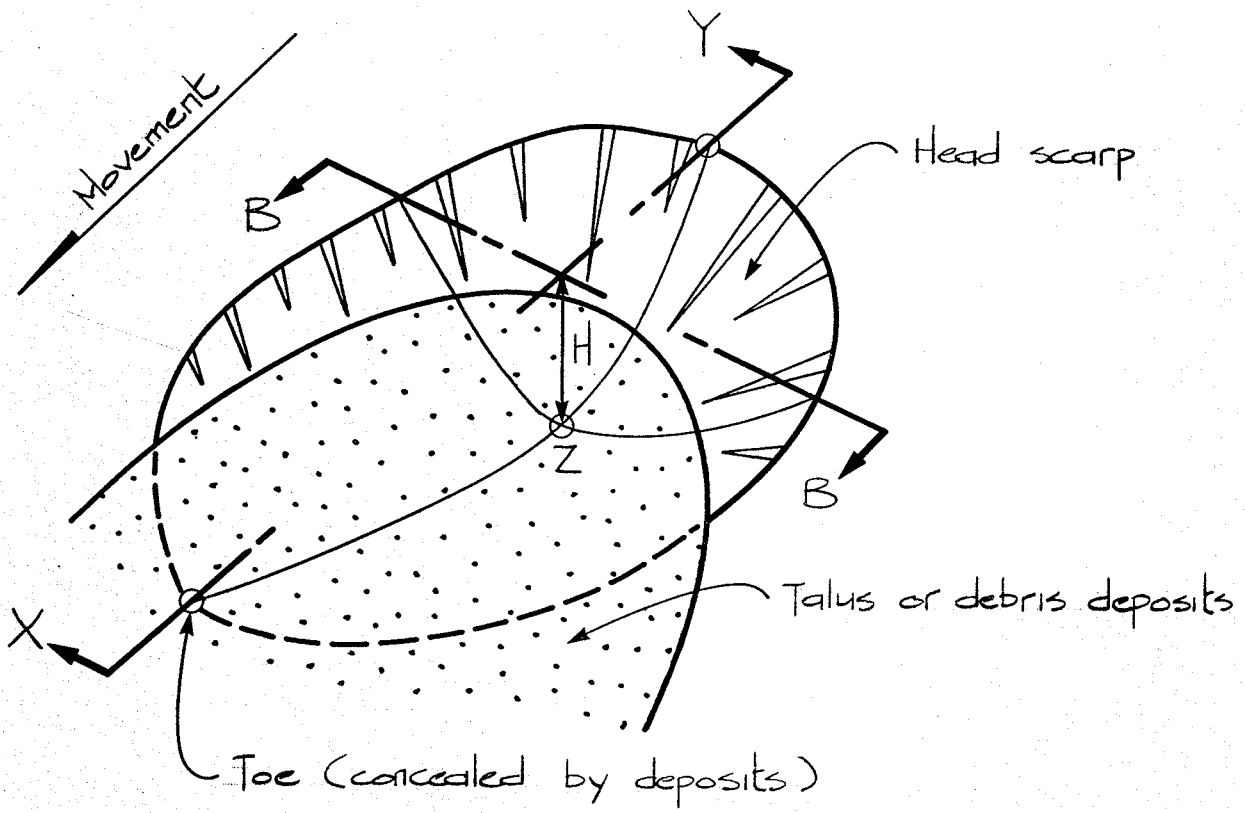

Figure 3 - Isometry of the source area, showing the longitudinal profile X-Y and traverse cross-section B-B

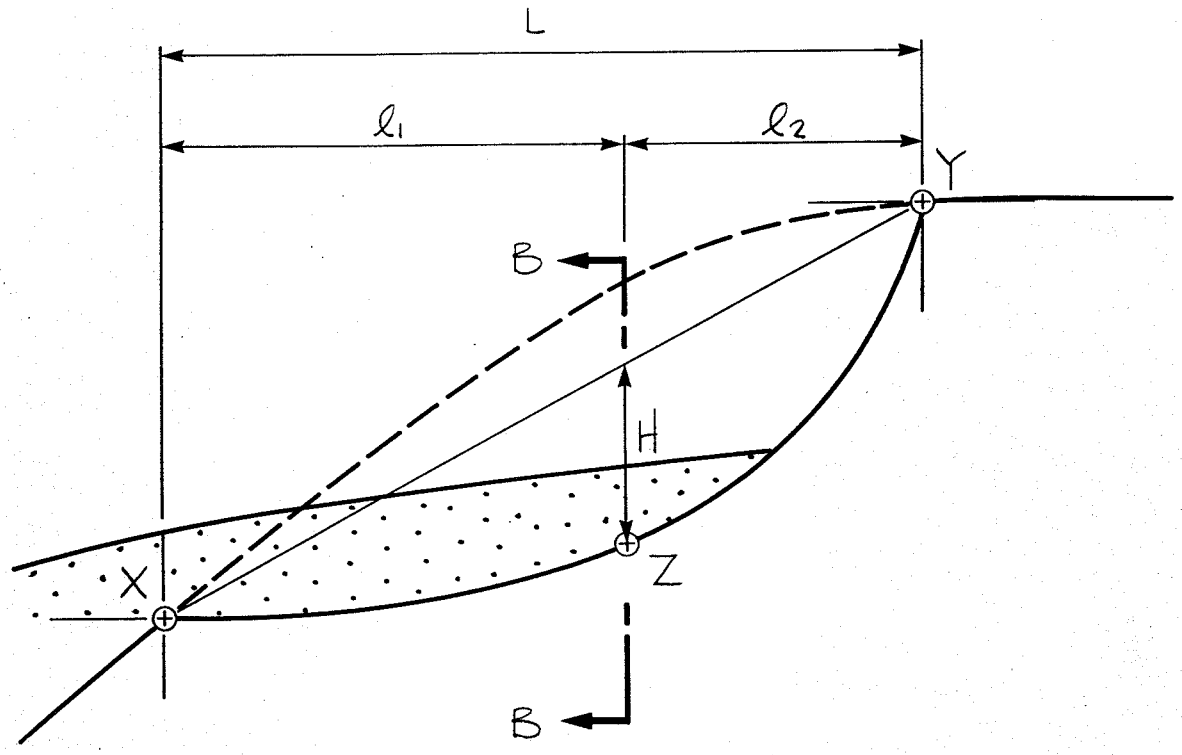

L = Length of source area

H/L = Depth Factor

ℓ_1/L = Longitudinal Symmetry Index

Figure 4 - Longitudinal profile of the source area (Profile X-Y)

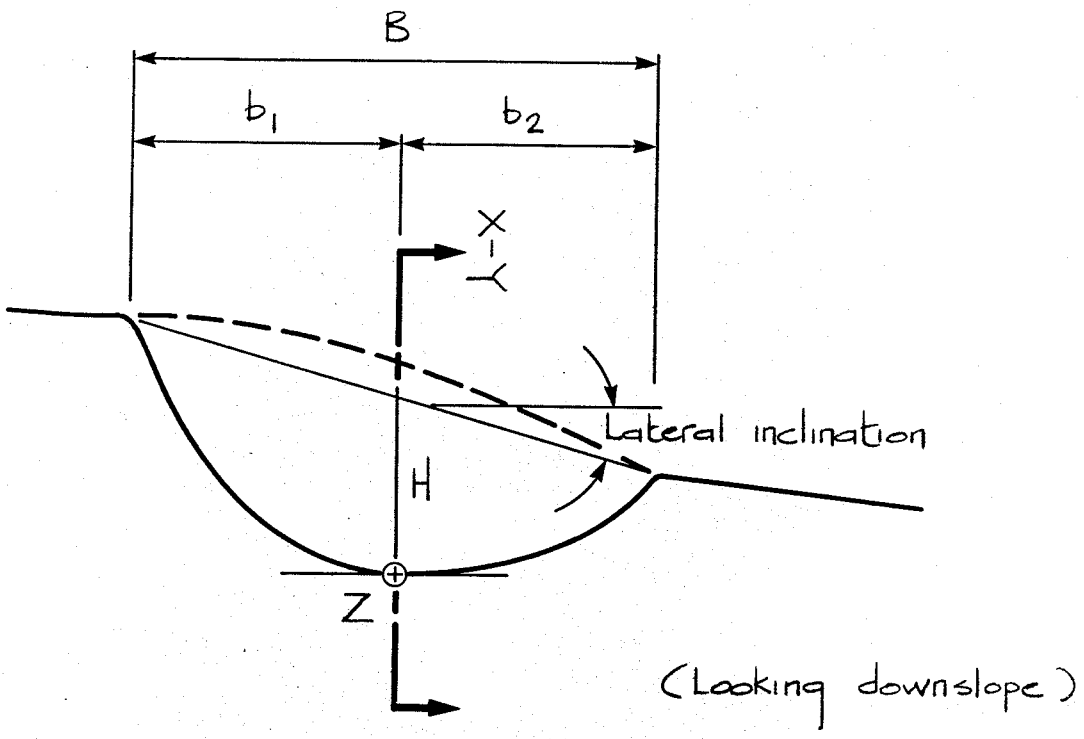

B = Source area width

H/B = Lateral Depth Factor

b_1/B = Lateral Symmetry Index

Figure 5 - Lateral cross-section of the source area (B-B

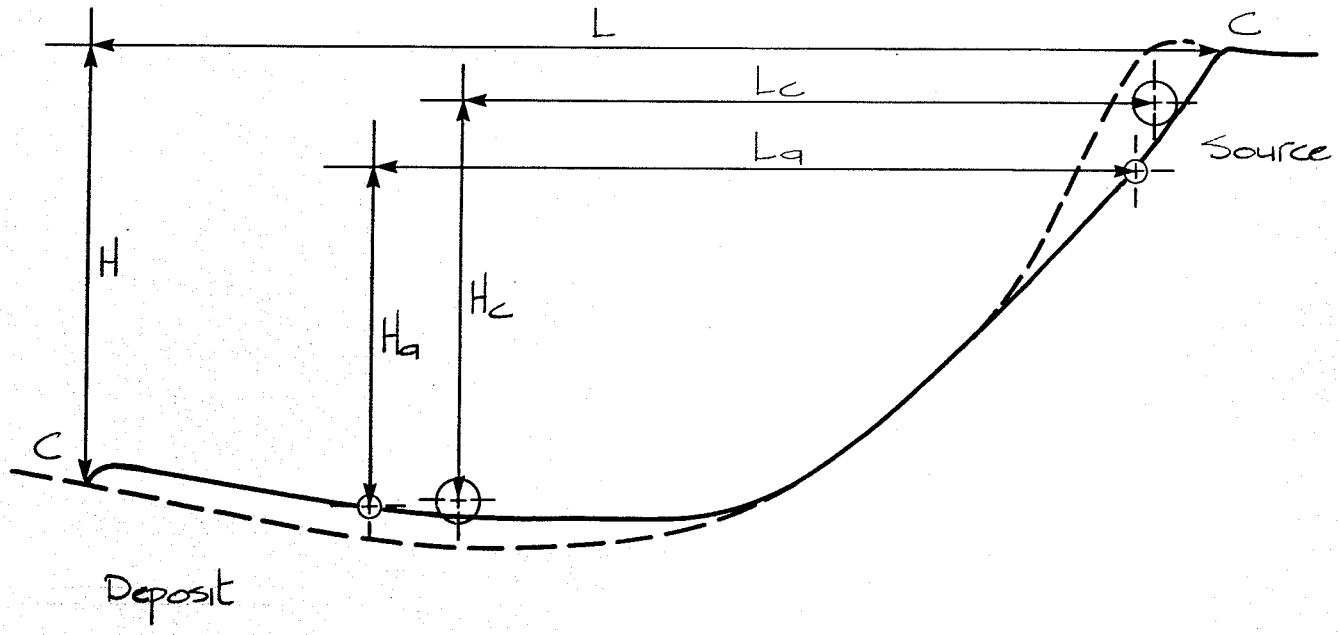

Centre of gravity of the mass

Centre of gravity of the plan area

Figure 6 - Parameters characterizing rockslide profile (Section C-C)

TYPE	A	B	REST	TOPPLING	
	NO STRUCTURAL CONTROL	RAND DISC TINUI		FLEXURAL	BLOCK
	A	B		H	I
	SLUMP	COLL IDE		FLEX. TOPPLE	BLOCK TOPPLE
CATASTROPHIC (>3 m/sec) (Stronger rock, steep slope)		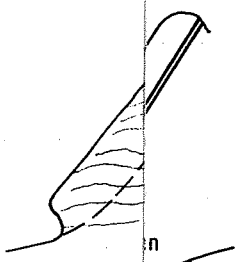 2. Eln  dison			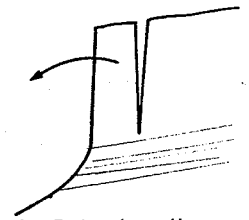 19. Pulverhorndl 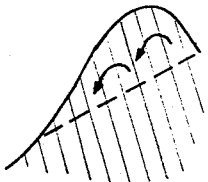 20. Elk Ridge
NON-CATASTROPHIC (Weaker rock, gentle slope)	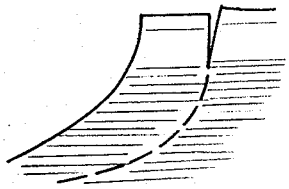 1. Massif de Plate	 ek		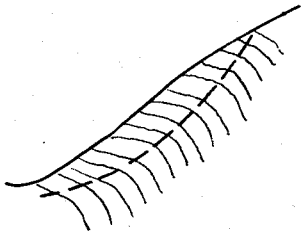 17. Clapiére 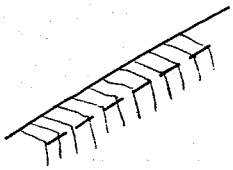 18. Glen Pean	

LEGEND : ═══ Wea surface developed h the rock mass

Note - references for case histor
10- Heim (1932). 4- Hungr &
8- nil. 9- Cruden & Krahn (1 ation of rockslide detachment
history references provided in the text)

13. AVALANCHE LAKE (TYPE C)

LOCATION: Mackenzie Mountains, Northwest Territories, (127° 15'W, 62° 15'N).

DATA BASE ENTRY: No.

PUBLISHED INFORMATION: 34, 194, 196.

NOTE:

The detailed description and analysis of this landslide area formed a special subject in the framework of this research. The results are summarized in a paper recently submitted to the Canadian Geotechnical Journal.

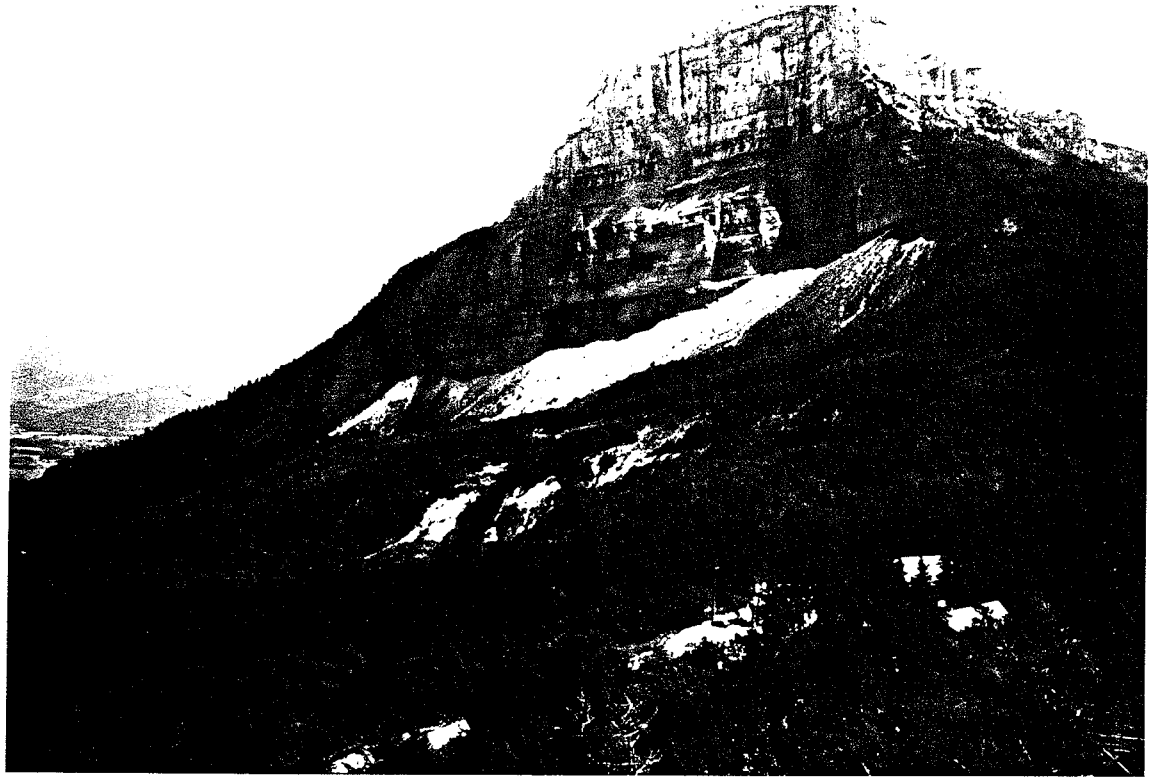

Figure C.1

Mont Granier Slide. (a) View of the slide scar, (b) Exposure of the Vallanginian marls near the sliding surface.

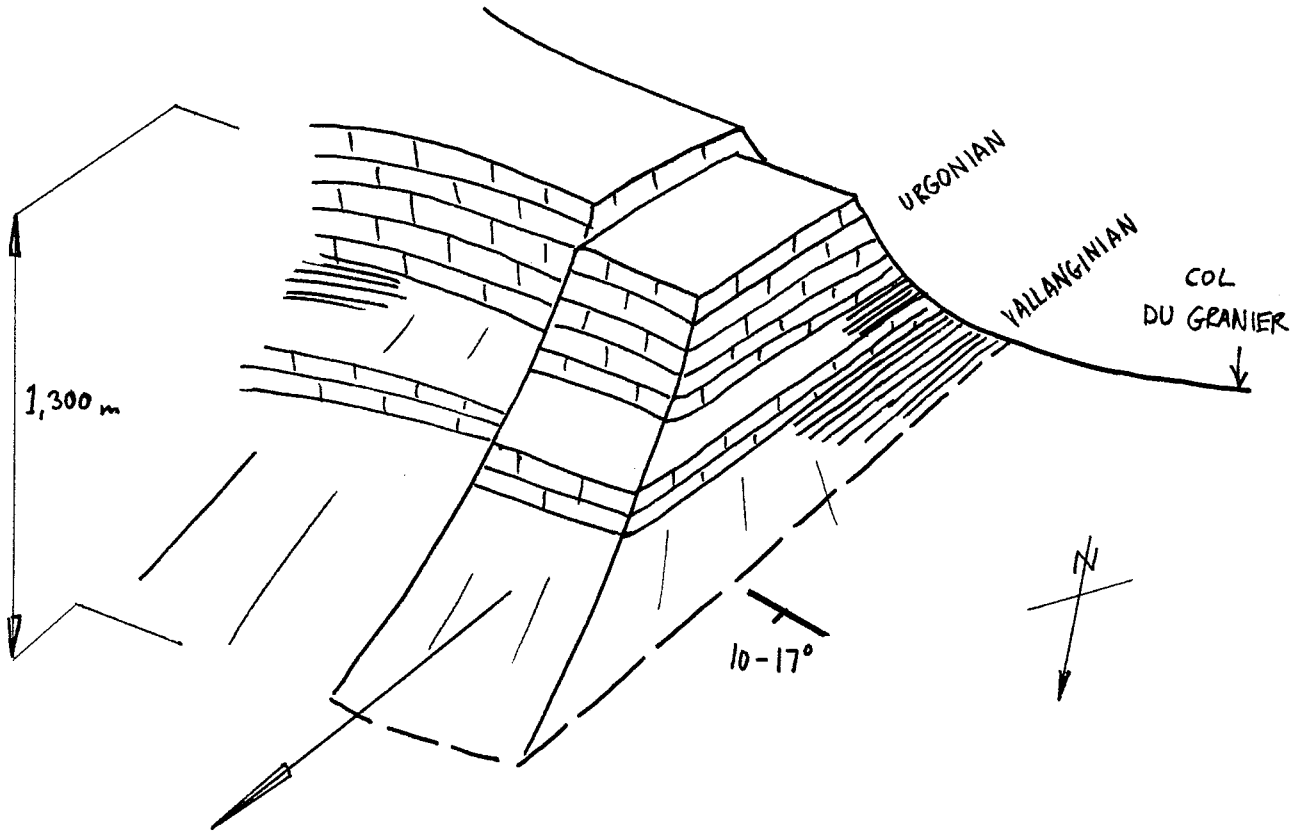

Figure C.2

Schematic diagram of the Mont Granier Slide (not to scale).

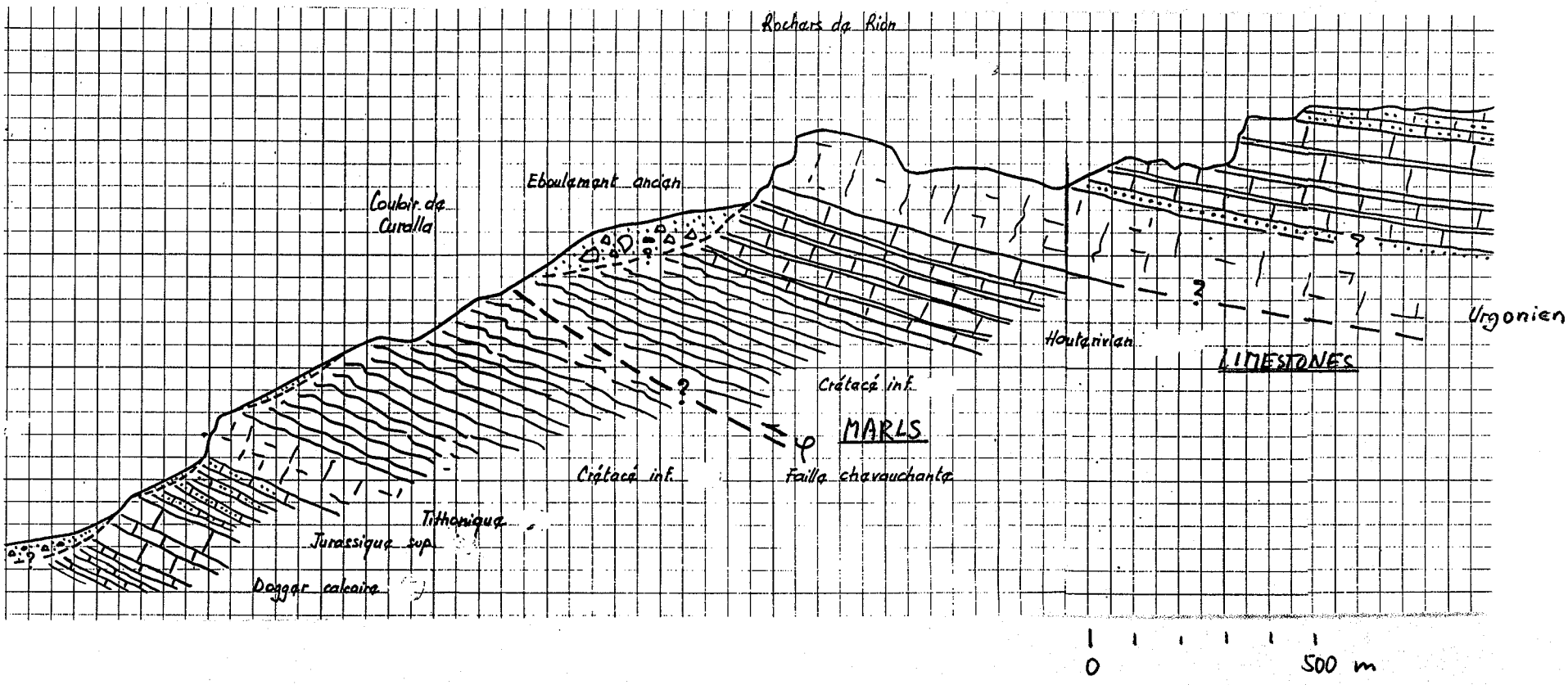

Figure C.3.

Sketch of a typical cross-section through the edge of Massif de Plate (drawn by Dr. A. Malatrait of B.R.G.M., Lyon, 1990).

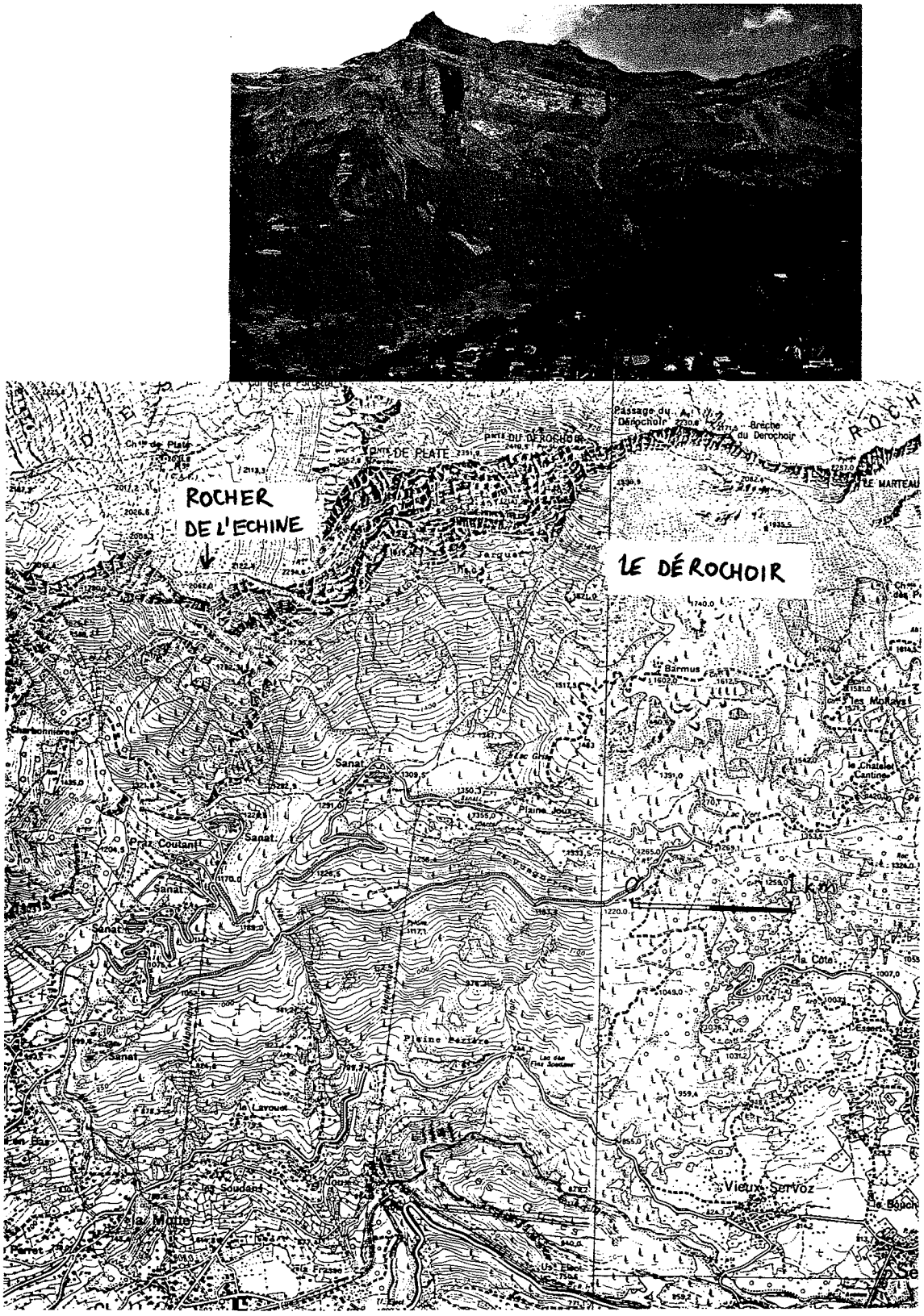

Figure C.4.

Massif de Plate, view of the Derochoir (above), plan (below).

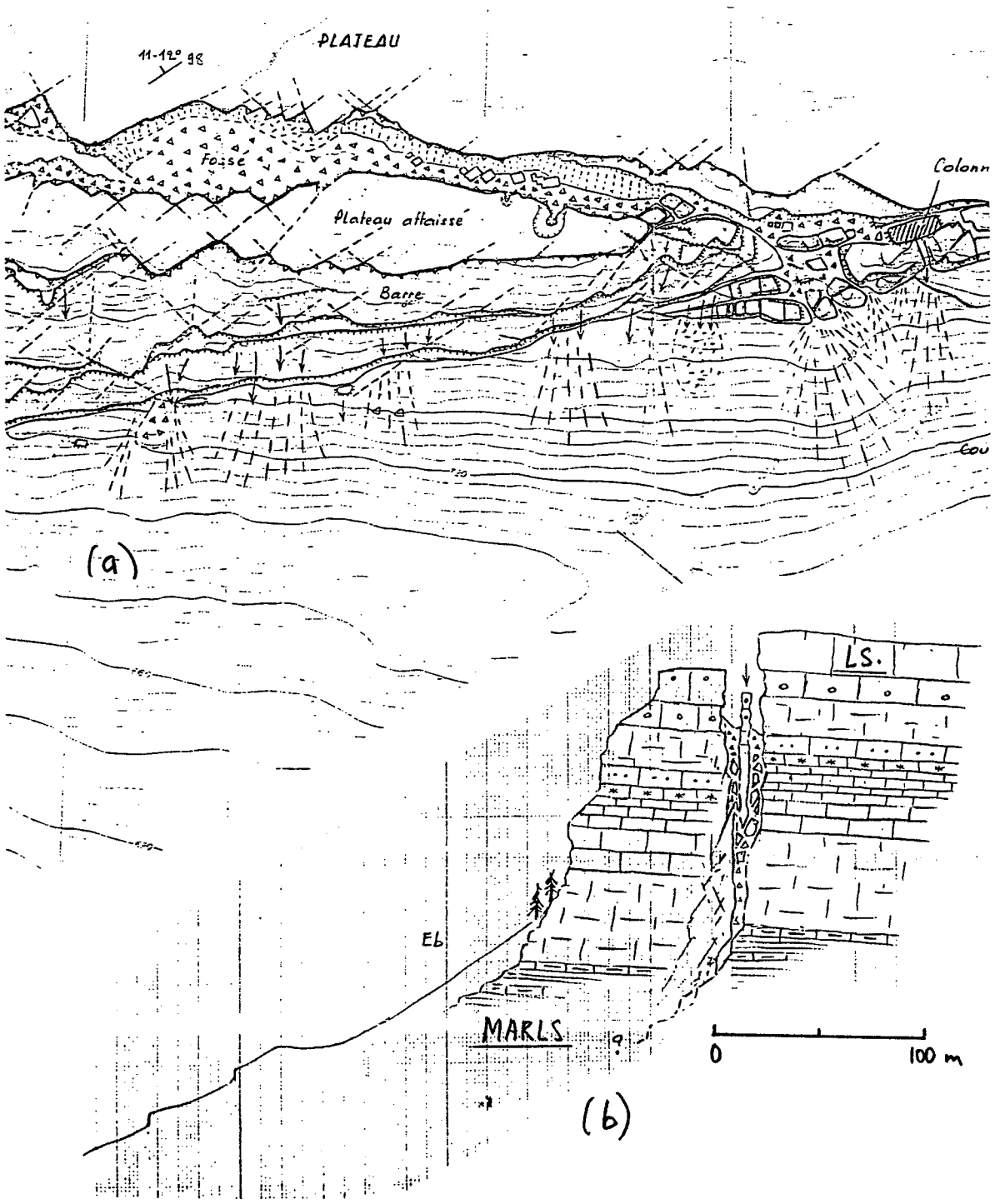

Figure C.5.

Barre des Fecles, Nantua. a) partial plan, b) typical cross-section (sketches by B.R.G.M., Lyon).

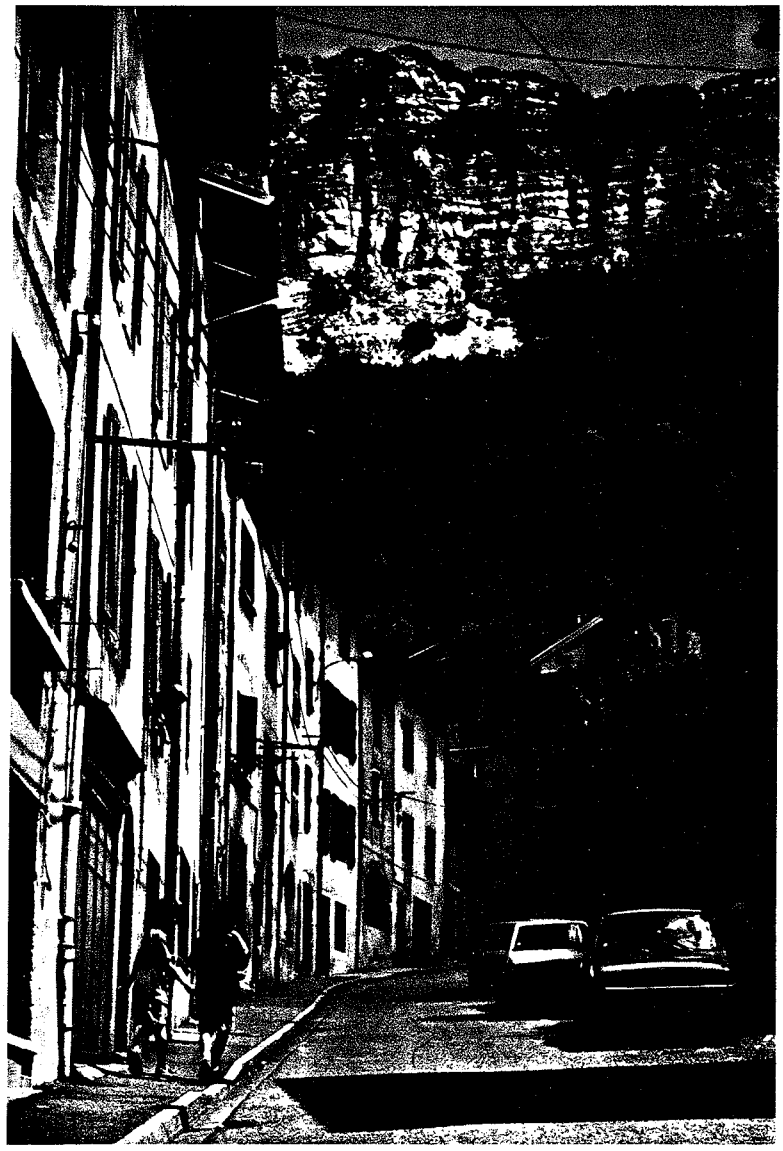

Figure C.6.

Barre des Fecles
a) Overall view (the moving block extends the full width of the photo).
b) View from a street in Nantua.

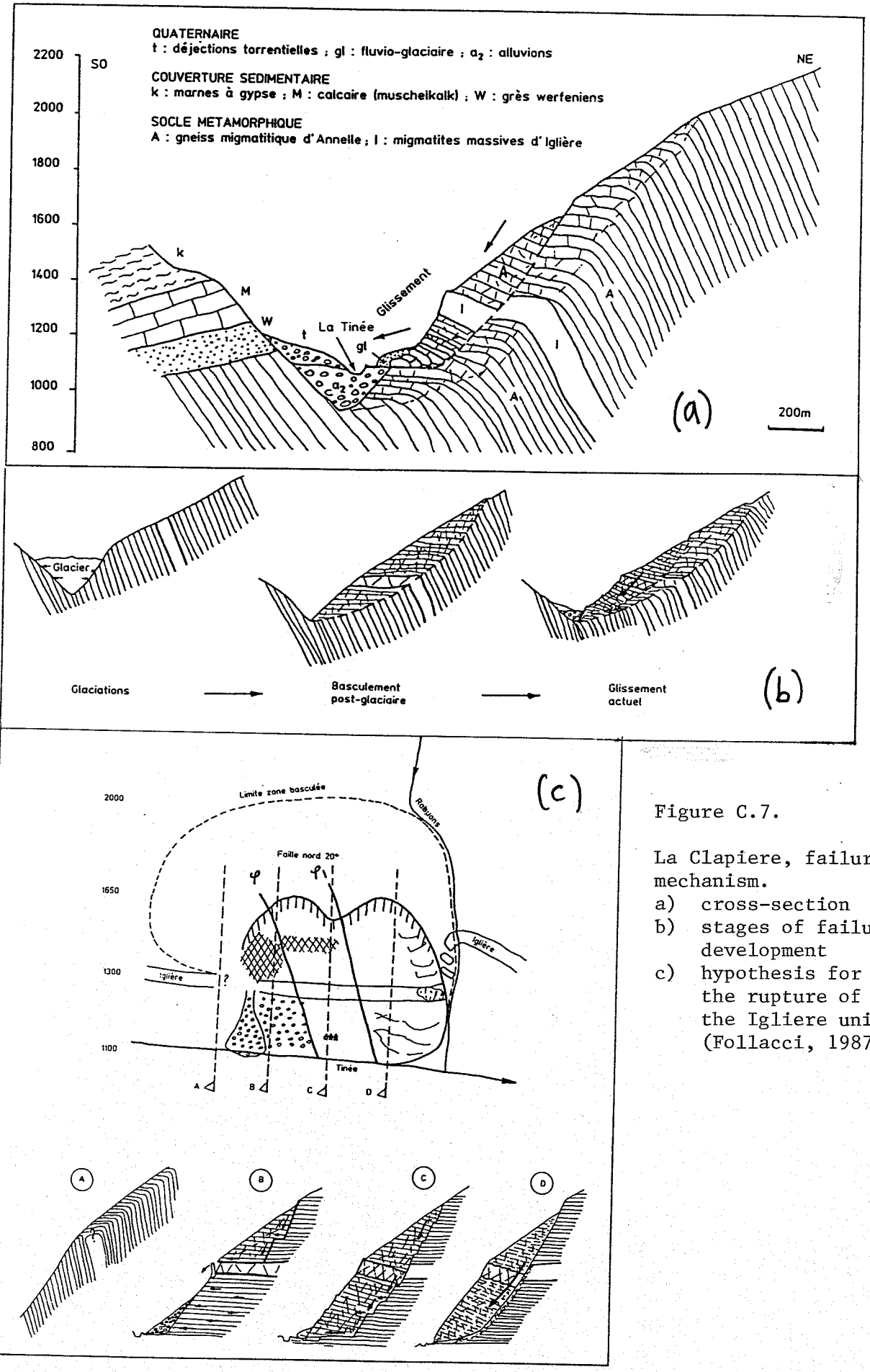

Figure C.7.

La Clapiere, failure mechanism.

a) cross-section
b) stages of failure development
c) hypothesis for the rupture of the Igliere unit (Follacci, 1987)

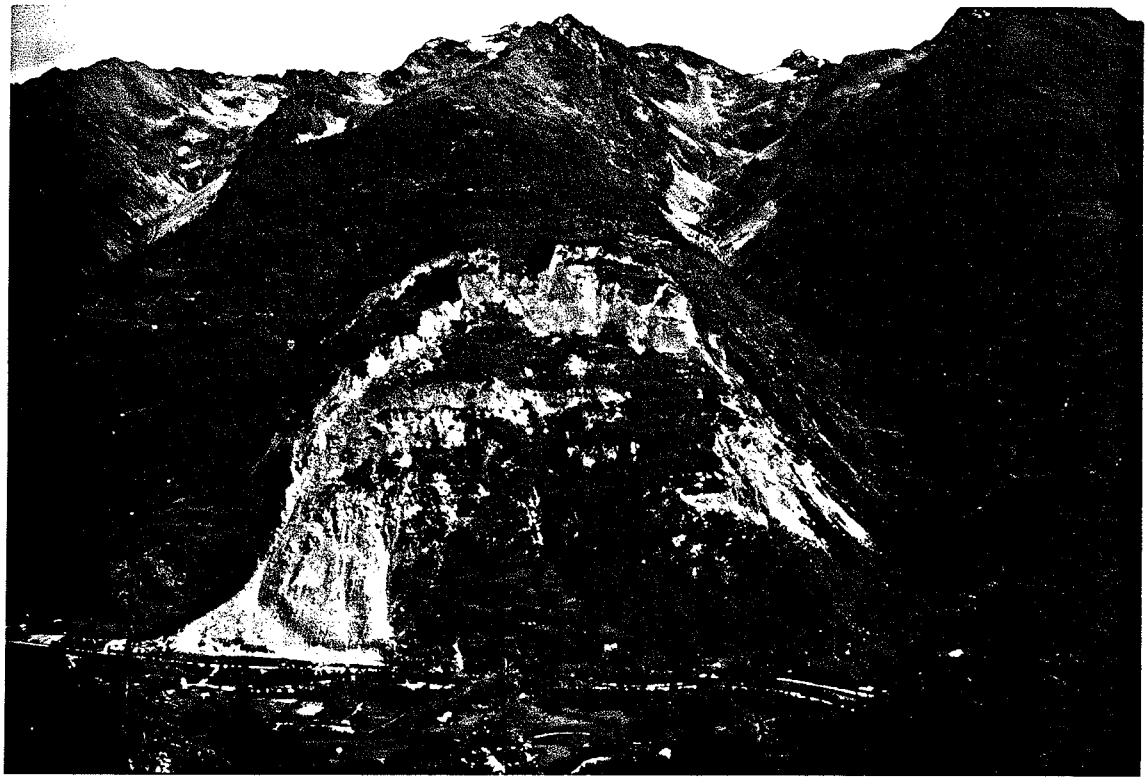

Figure C.8.

La Clapiere. a) Overall view, b) detail of the head area, showing the developing sliding surface.

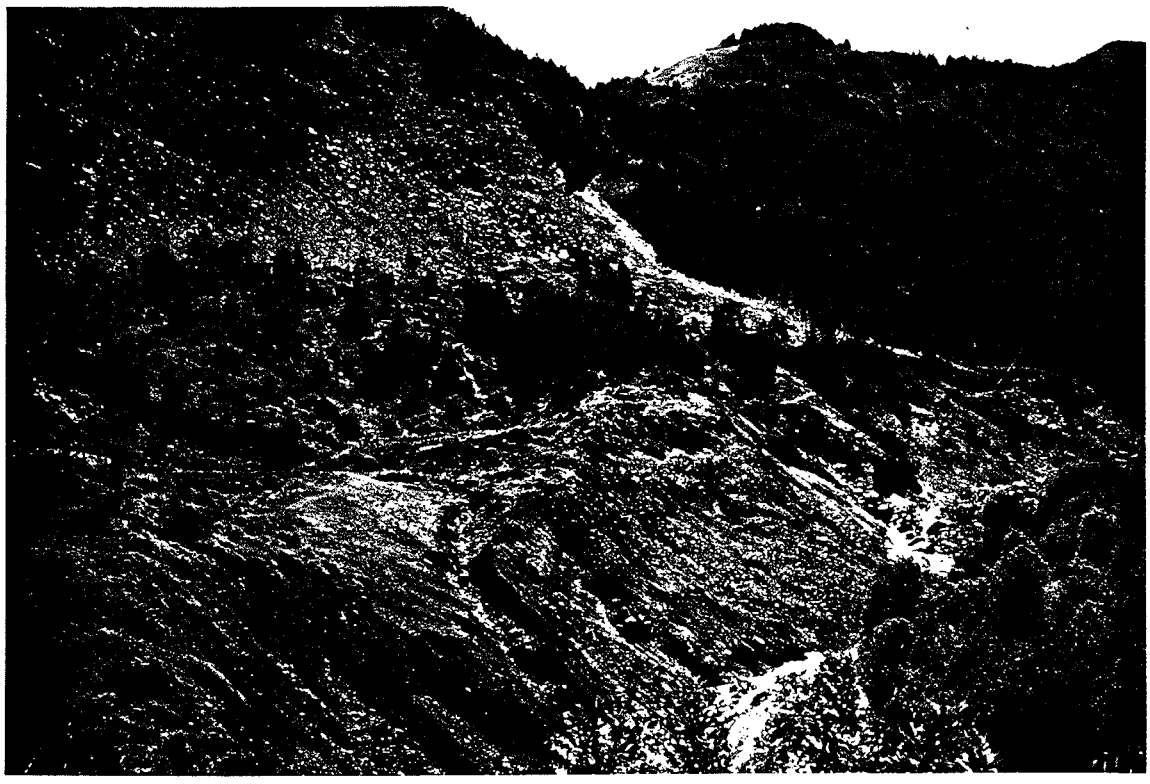

Figure C.9.

The Torregio Slide. a) Detail of toppled schist beds in the left side scarp, b) View of the slide area.

Figure C.10.

Spriana Slide. a) Gneiss strata affected by flexural toppling, b) Overall view of the slide area.

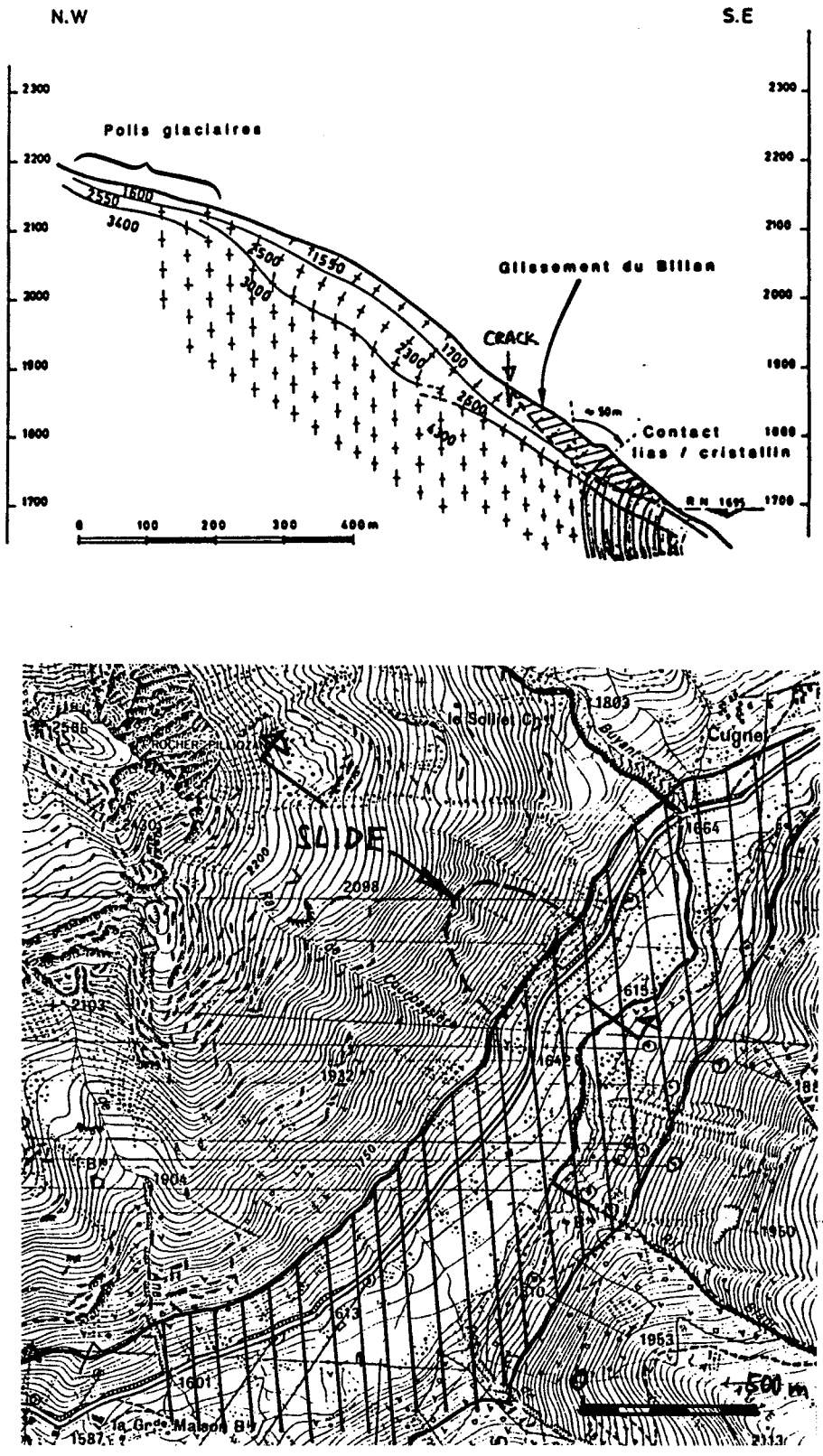

Figure C.11.

Billan landslide, Grande Maison reservoir. a) Profile with seismic velocities, b) plan (Dubie et al., 1988).

Figure C.12.

Billan Slide. a) Overall view, b) Toppled schist near the centre of the slide area.

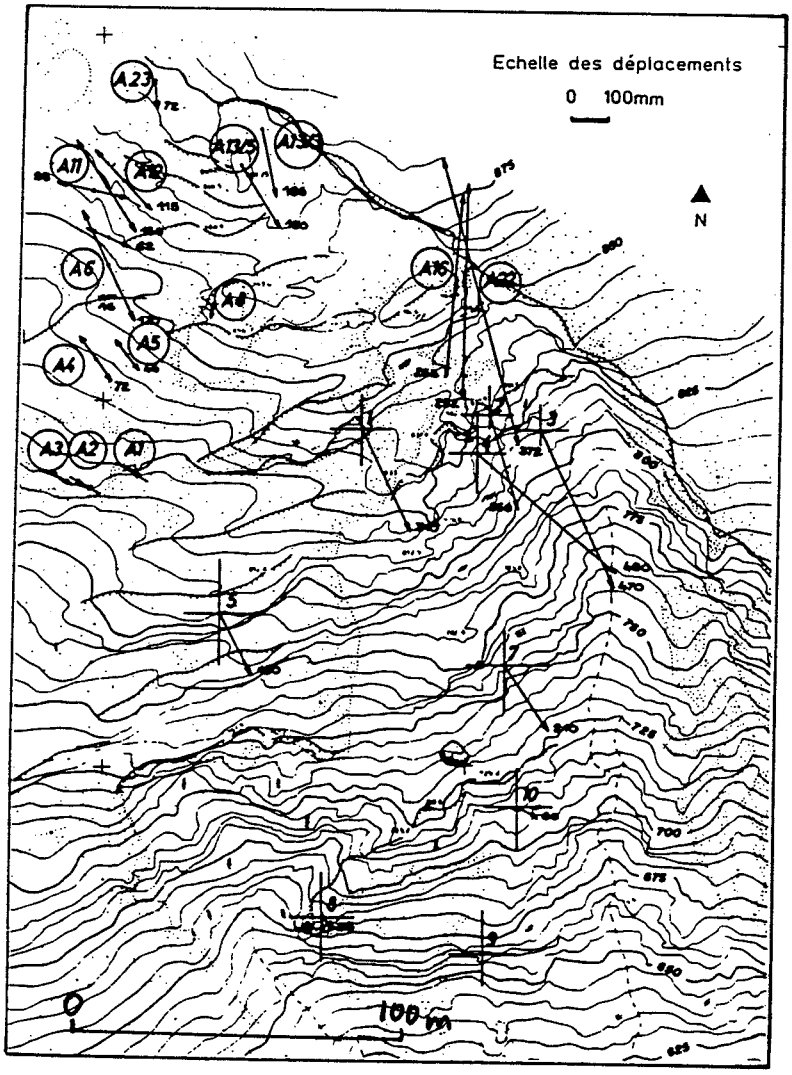

(a)

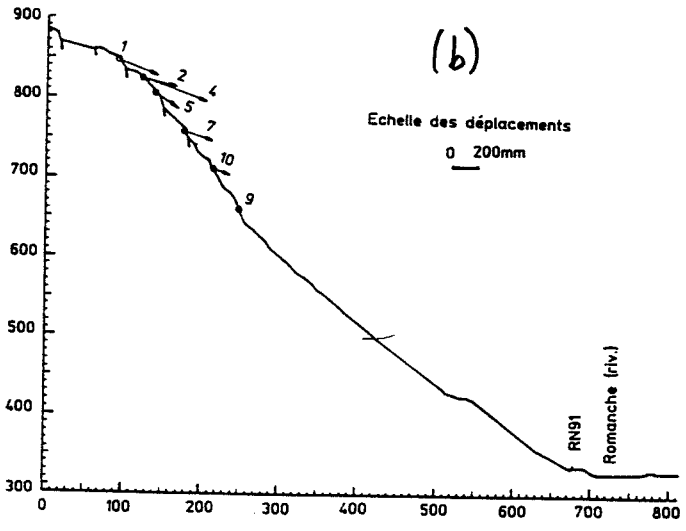

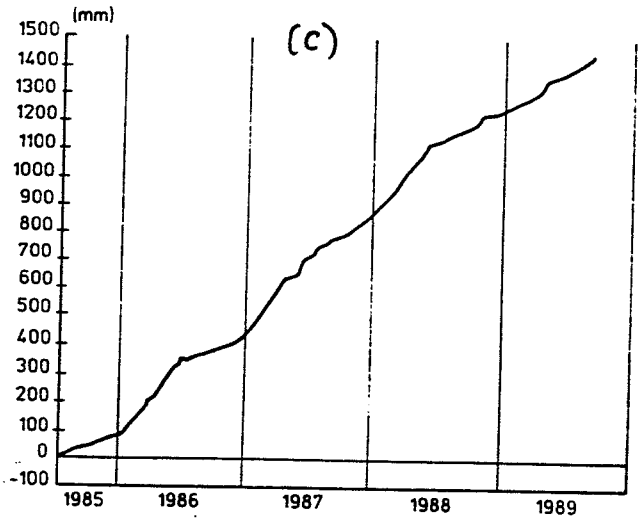

Figure C.13.

Sechillienne Slide. a) Crest area of the active segment of the slope, showing displacement vectors, b) profile, c) extensometer record A22. (Antoine et al., 1987, Evrard et al., 1990).

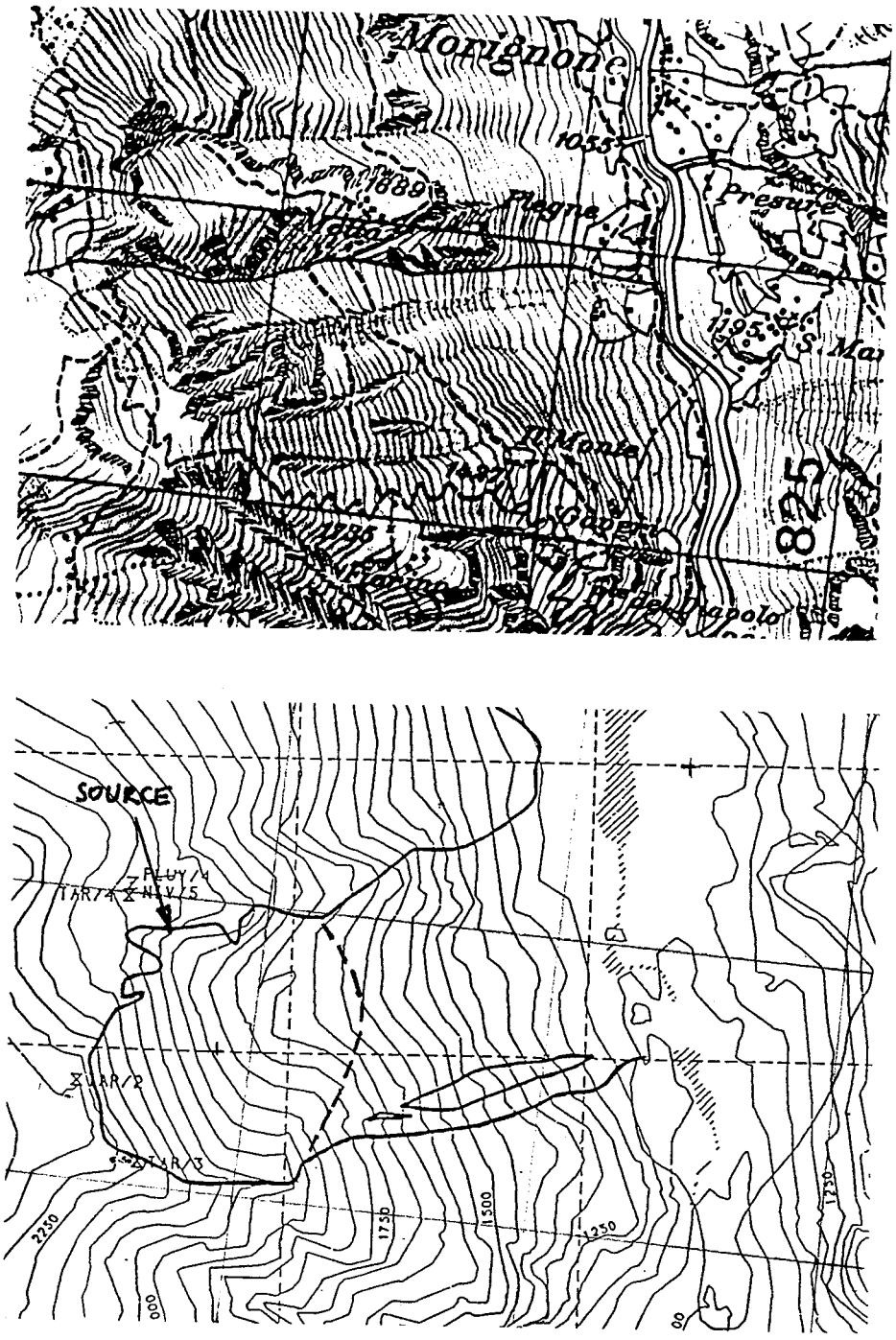

Figure C.15.

Val Pola Slide. a) Topography before slide (notice crown scarp). b) After slide. Scale 1:25,000. The full grid lines are coincident.

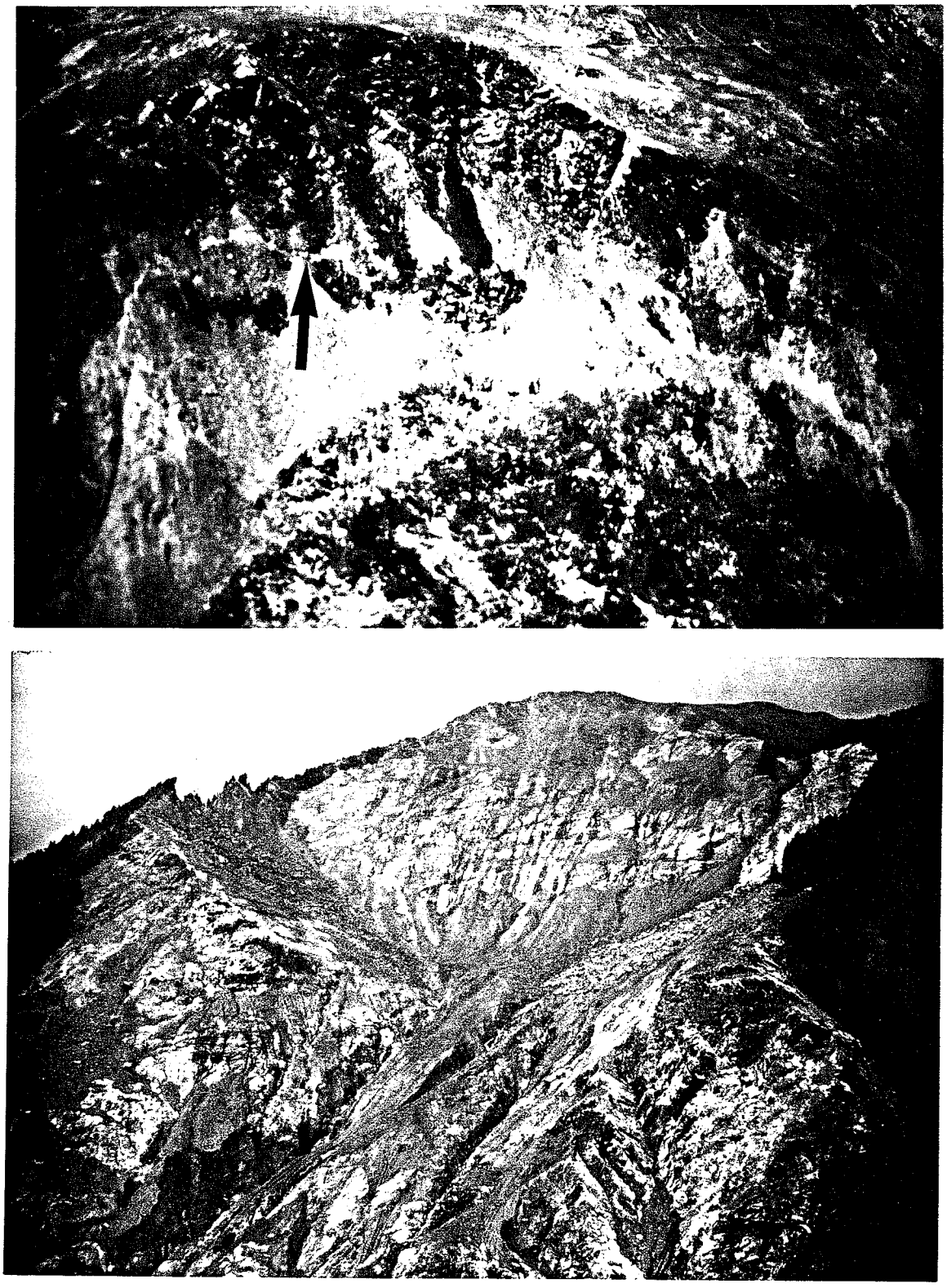

Figure C.16.

Val Pola Slide. a) Crown scarp 3 days before failure (arrow shows fresh crack), b) failure surface in 1990.

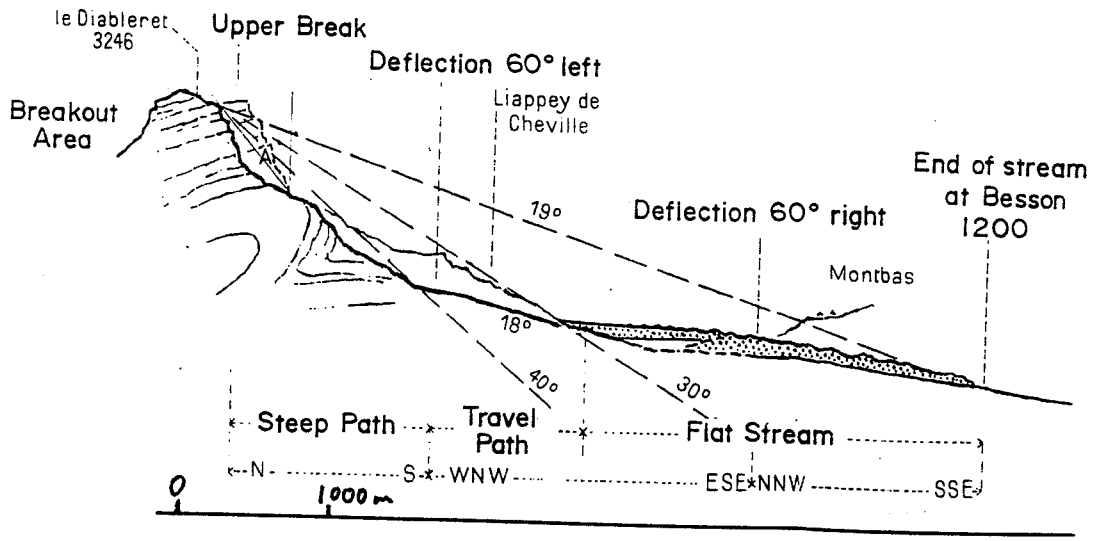

Figure C.17.

Diablerets Slide. a) Profile by Heim (1932). b) View towards the source area (the source niche is the area in shadows).

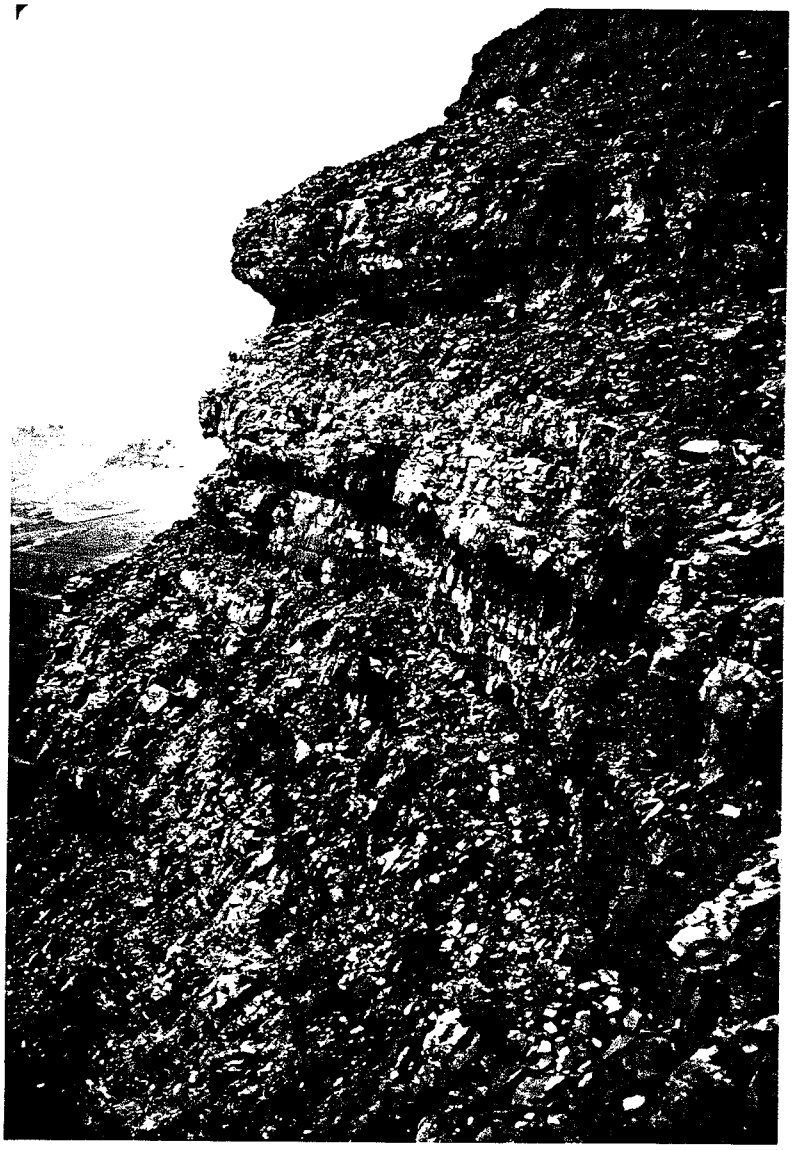

Figure C.18.

Rockslide Pass.
a) Small slide adjacent to the main detachment. The view is taken looking in the direction of movement from the crown of the slide scar.
b) Exposure of carbonaceous beds 500 m behind the main slide, corresponding to the location of the sliding surface.

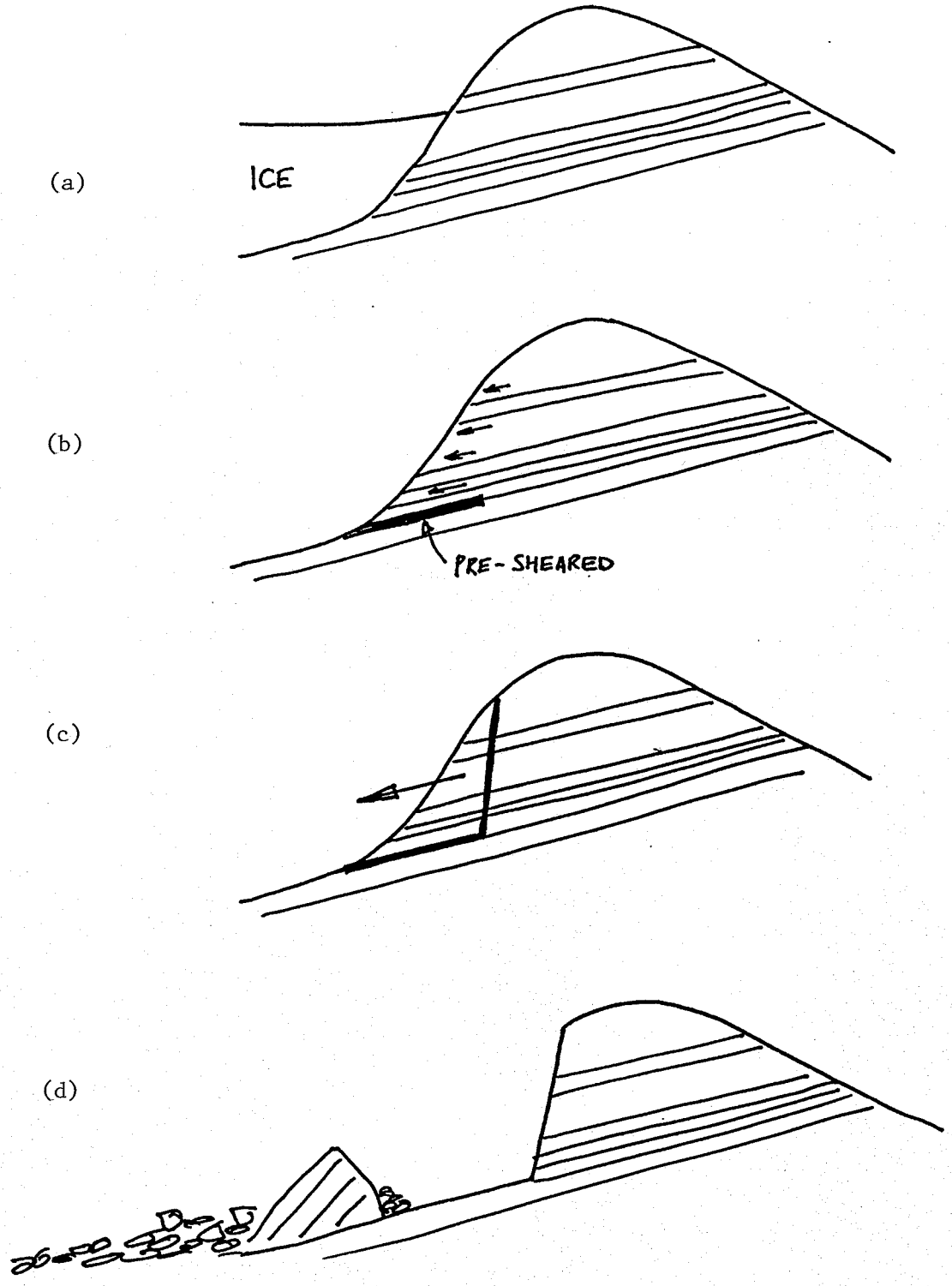

Figure C.19.

Possible sequence of development of the Rockslide Pass slide. a) Glacier erosion, b) stress relief following deglaciation, c) failure (earthquake?), d) present condition.

APPENDIX D

BIBLIOGRAPHY

(SEQUENTIAL AND ALPHABETIC LISTING)

BIBLIOGRAPHY, NUMERICAL LISTING

I.D. No.	First and Second Author		Year	Code*
1	Cruden	Eaton	1988	RC
2	Goguel	Pachoud	1981	CA
3	Bovis		1990	CA
4	Einstein		1988	TH
5	DeFreitas	Watters	1973	MC
6	Follacci	Guardia	1988	CA
7	Heim		1932	MC
8	Goodman	Bray	1976	TH
9	Hoek	Brown	1981	SA
10	Hutchinson		1988	SA
11	Hungr		1981	SA
12	Nemcok		1982	RC
13	Radbruch-Hall	Varnes	1976	RC
14	Radbruch-Hall		1978	SA
15	Riemer	Locher	1988	MC
16	Tabor		1971	MC
17	Anon.		1977	RC
18	Wetmiller	Evans	1989	CA
19	Zischinski		1968	MC
20	Bagnold		1954	CO
21	Baltzer		1875	RC
22	Banks	Strohm	1974	TH
23	Eisbacher	Clague	1984	RC
24	Broadbent	Ko	1972	TH
25	Browning		1973	CA
26	Bruce	Cruden	1977	CA
27	Buss	Heim	1881	CA
28	Campbell		1978	MC
29	Chowdhury		1978	CA
30	Golder Assoc.		1987	RC
31	Cruden	Krahn	1978	CA
32	Anon.		1981	TH
33	Daly	Miller	1912	CA
34	Eisbacher		1979	MC
35	Govi		1989	CA
36	Erismann		1979	TH
37	Fahnestock		1978	CA
38	Francis	Baker	1977	EM
39	Goguel	Pachoud	1972	CA
40	Govi		1977	RC
41	Griggs		1920	CA
42	Habib		1975	TH
43	Hadley		1964	MC
44	Hamel		1972	CA
45	Hamel		1976	CA
46	Hammett		1974	TH
47	Hardy	Morgenstern	1978	MC
48	Harrison	Falcon	1938	CA
49	Hoek	Bray	1977	SA

50	Hsu		1975	EM
51	Hsu		1978	CA
52	Johnson		1978	CA
53	Kennedy	Niermeyer	1971	CA
54	Kenney		1967	CA
55	Kent		1966	TH
56	Koerner		1976	TH
57	Koerner		1977	TH
58	Kojan	Hutchinson	1978	CA
59	Krahn		1974	CA
60	Lachenbruch		1980	TH
61	Lucchitta		1978	CA
62	Marangunic		1972	CA
63	Mathews	McTaggart	1969	CA
64	McConnell	Brock	1904	CA
65	McSaveney		1978	CA
66	Melosh		1979	TH
67	Mencl		1966	CA
68	Mollard		1977	RC
69	Morgenstern		1978	MC
70	Mueller		1964	CA
71	Mueller		1968	CA
72	Palmer		1977	MC
73	Pautre	Sabarly	1974	TH
74	Piteau	Mylrea	1978	CA
75	Plafker	Ericksen	1978	MC
76	Romero	Molina	1974	TH
77	Saito		1965	EM
78	Scheidegger		1973	EM
79	Schumm	Chorley	1964	CA
80	Sharpe		1938	SA
81	Shreve		1966	CA
82	Shreve		1968	CA
83	Shreve		1968	TH
84	Simmons	Cruden	1980	CA
85	Skempton		1966	TH
86	Skempton	Hutchinson	1969	SA
87	Solonenko		1977	RC
88	Terzaghi		1950	SA
89	Varnes		1978	SA
90	Voellmy		1955	TH
91	Voight		1978	CA
92	Voight	Kennedy	1978	EM
93	Watson	Wright	1967	CA
94	Zaruba	Mencl	1969	SA
95	Zischinski		1966	MC
96	Mears		1980	TH
97	Bjerrum	Jorstad	1968	RC
98	Skermer		1980	SA
99	Cruden	Hungr	1986	EM
100	Yarnold	Lombard	1989	EM
101	McEwen		1989	CA
102	Jackson, Jr.	Isobel	1990	MC
103	Evans		1987	CA

104	Evans		1987	CA
105	Wyllie	Munn	1978	CA
106	Evans	Aitken	1987	CA
107	Cruden		1982	CA
108	Cruden		1976	MC
109	Eisbacher		1900	RC
110	Naranjo	Francis	1987	CA
111	Trunk	Dent	1986	TH
112	Keefer		1984	EM
113	Keefer		1984	EM
114	Follacci		1987	CA
115	Whitehouse	Griffiths	1983	RC
116	Coates	Yu	1978	SA
117	Bovis		1982	MC
118	Mokievsky-Zubok		1977	CA
119	Baillarge		1900	CA
120	Slingerland	Voight	1978	SA
121	McEwen	Malin	1989	CA
122	Cassie	Van Gassen	1988	EM
123	Li-Tianchi		1983	EM
124	Perla	Cheng	1980	TH
125	Kobayashi	Kagawa	1987	TH
126	Eppler	Fink	1987	CA
127	Evans		1989	CO
128	Ui		1983	EM
129	Ui	Yamamoto	1986	EM
130	Lee	Duncan	1975	CA
131	Rochet		1987	TH
132	Hadj-Hamou	Kavazanjian,Jr.	1985	TH
133	Evrard	Gouin	1990	CA
134	Moore	Clague	1989	MC
135	Sassa		1984	EM
136	Bovis	Mears	1976	EM
137	Lin	Whitman	1986	TH
138	Machida		1984	
139	Bonnard		1985	SA
140	Schneider	Gailen	1939	CA
141	Schuster	Fleming	1986	SA
142	Clague	Evans	1989	RC
143	Hadley		1978	CA
144	Mathews	McTaggart	1978	CA
145	Anon		1987	CA
146	Crandell	Fahnestock	1965	CA
147	Marangunic	Bull	1968	CA
148	Anon.		1986	CA
149	Alexander		1988	CA
150	McLellan	Kaiser	1984	EM
151	Bock		1977	CA
152	Butler	Oelfke	1986	MC
153	Anon.		1990	CA
154	Chowdhury		1980	TH
155	Cruden		1980	EM
156	Cruden		1980	EM
157	Davies		1981	EM

158	Dawson	Matthews	1986	CA
159	Erismann		1988	
160	Anon.		1987	CA
161	Fauque	Strecker	1988	CA
162	Fukuoka	Yoshida	1977	
163	Gordon	Birnie	1978	
164	Heuberger	Masch	1984	
165	Hoyer		1971	
166	Huang	Wang	1988	CA
167	Hungr		1989	EM
168	Hungr	Morgenstern	1984	CA
169	Hutchinson		1986	TH
170	Korner		1980	
171	Dubie	Benefice	1988	CA
172	Melosh		1987	TH
173	Ouchi	Mizuyama	1989	CA
174	Plafker		1968	CA
175	Porter	Orombelli	1981	
176	Porter	Orombelli	1980	
177	Sassa		1988	TH
178	Van Gassen	Cruden	1990	TH
179	Voight	Faust	1982	TH
180	Clague	Evans	1987	MC
181	Clague	Souther	1982	CA
182	Cruden		1985	SA
183	Cruden		1986	CA
184	Cruden	Beaty	1987	
185	Cruden	Eaton	1987	RC
186	Cruden	Krahn	1973	CA
187	Eisbacher		1982	SA
188	Eisbacher		1971	RC
189	Evans		1983	MC
190	Evans		1983	CA
191	Evans		1989	CA
192	Evans		1986	MC
193	Evans	Clague	1989	CA
194	Kaiser	Simmons	1989	MC
195	Keefer	Wilson	1985	
196	McLellan		1983	MC
197	Moore	Mathews	1978	CA
198	Patton		1976	CA
199	Peterson	Sego	1988	CA
200	Piteau		1977	RC
201	Wetmiller	Horner	1988	
202	Terzaghi		1962	SA
203	Hendron	Patton	1985	CA
204	Lemos	Skempton	1984	
205	Wilson	Keefer	1985	
206	Barton		1977	
207	Follaci		1984	RC
208	King		1987	CA
209	King	Loveday	1985	CA
210	Courel	Delaunay	1980	RC
211	Montandon		1933	RC

212	Cruden	Antoine	1984	CA
213	Abele		1974	SA
214	Pautre	Schneider	1973	CA
215	Smith		1971	CA
216	Ryder	Bovis	1990	CA
217	Mahr		1977	MC
218	Malatrait		1975	RC
219	McLellan	Kaiser	1984	CA
220	Keefer	Tannaci	1981	
221	Anon		1988	CA
222	Hu		1987	CA
223	Vibert	Arnould	1988	CA
224	Antoine	Camporota	1987	CA
225	Goguel		1980	
226	Hungr	Gerath	1984	CA
227	Lutton	Banks	1979	MC
227	Schultz	Southworth	1989	MC
229	Howard		1973	
230	Moriwaki	Yazaki	1985	
231	De Matos		1987	
232	Anon.		1981	
233	Hungr	Evans	1991	
234	Norem	Locat	1991	
235	Fukuzono		1985	
236	Salt		1988	
237	Zavodni	Broadbent	1980	
238	Miller		1982	
239	Voight		1989	
240	Hungr	Salgado	1989	
241	Inokuchi		1985	
242	Cruden	Hu	1991	
243	Braun	Gillmeister	1989	
244	Fukuzono		1990	
245	Gardner		1980	
246	Hsu		1983	
247	Inokuchi		1988	
248	Barkan		1962	EM
249	DeMatos		1987	
250	Brawner	Stacey	1975	
251	King	Loveday	1989	
252	Evans		1989	
253	Evans		1989	

* Reference Code:
- CA - Case History
- MC - Multiple Case History
- RC - Regional Case History
- TH - Theoretical Model
- EM - Empirical Model
- SA - State of the Art Review
- CO - Constitutive Model
- RD - Remedial Design

BIBLIOGRAPHY, ALPHABETIC LISTING

Abele, G., 1974. Bergsturze in den Alpen. Wissenschaftliche Alpenvereinshefte , Number 25 , Munich, (in German).

Alexander, D., 1988. Valtellina landslide and flood emergency, Northern Italy, 1987. Disasters. , Vol. 12 Number 3 , pp. 212-222.

Anon, , 1987. Downie Slide report, Columbia Gorge, Revelstoke Project. British Columbia Hydro and Power Authority , unpublished.

Anon, , 1988. Note illustrative della frana di val pola. Lombardy Regional Government , unpublished, (in Italian).

Anon., , 1981. Peace River Development, Site C Project, report on reservoir slopes. Internal report by the B. C. Hydro Generation Projects Division, No. H1361, , Vancouver.

Anon., , 1986. Lake of the Woods Slide, Hope, B.C. Thurber Consultants Ltd., unpublished report to the Regional District of Fraser - Cheam, .

Anon., , 1987. The Katz Landslide, Agassiz, B.C. Thurber Consultants Ltd., unpublished report to the Regional District of Fraser - Cheam, .

Anon., , 1990. Mount Breakenridge Slide, Phase II Study. Thurber Consultants Ltd., unpublished report to the Regional District of Fraser - Cheam, .

Anon., , Washington Public Power Supply System, 1977. Preliminary Safety Analysis Report, WPPSS Nuclear Project No. 1 , unpublished.

Anon., ., 1981. Peace River Development, Site C. Report on reservoir slopes. B.C. Hydro and Power Authority , upublished.

Antoine, P., Camporota, P. ,Giraud, A., Rochet, L., 1987. La menace d'ecroulement aux ruines de Sechilliene (Isere). Bulletin liaison de Laboratoire des Ponts et Chausees , Vol. 150 , pp. 55-63, (in French).

Bagnold, R.A., 1954. Experiments on a gravity-free dispersion of large solid spheres in a Newton fluid under shear. Proceedings, Royal Society of London, Ser. A , Vol. 225 , pp. 49-63.

Baillarge, C., 1900. The Quebec land slide of September 19, 1889. Procs., Institution of Civil Engineers , , London, pp. 141-152.

Baltzer, A., 1875. Uber die Bergsturze in den Alpen. Jahrbuch, Scheweizer Alpenclub, Bern , Vol. 10 , pp. 409-456, (in German).

Banks, D.C., Strohm, W.E. ,1974. Calculations of rock-slide velocities. Procs., 3rd. Congress ISRM, Denver , Vol. 2 , pp. 839-847.

Barkan, D.D., 1962. Dynamics of Bases and Foundations , Mc Graw Hill, New York, pp. 400.

Barton, M.E., 1977. Landsliding along bedding planes. Bull., Assoc. Int. Geol. Ingenieur. , Vol. 16 , pp. 5-7.

Bjerrum, L., Jorstad, A.J. ,1968. Stability of rock slopes in Norway. Norwegian Geotechnical Institute, Publication , Number 79 , pp. 91-11.

Bock, C.G., 1977. Martinez Mountain rock avalanche. Geological Society of America, Reviews in Engineering Geology , Vol. 3 , pp. 155-168.

Bonnard, C., 1985. Detection et utilisation des terrains instables. Raport General, Ecole Polytechnique Federale de Lausanne , , (in French).

Bovis, M., 1990. Rock slope deformation at Affliction Creek, British Columbia. Pre-print , .

Bovis, M.J., 1982. Uphill-facing (antislope) scarps in the Coast Mountains, southwest, B.C. Bulletin, Geological Soc. of America , Vol. 93 , pp. 804-812.

Bovis, M.J., Mears, A.I. ,1976. Statistical prediction of snow avalanche runout from terrain variables in Colorado. Arctic and Alpine Research. , Vol. 8 Number 1 , pp. 115-120.

Braun, D.D., Gillmeister, N.M. ,1989. Post-glacial to historic dip slope bedrock slides in northeastern Pennsylvania. G.S.A. Special Paper 236 , A.P. Schultz, R.W. Jibson Ed., , pp. 75-95.

Brawner, C.O., Stacey, P. ,Stark, R., 1975. A successfull application of mining with pitwall movement. Canadian Institute of Mining and Metallurgy Bulletin , .

Broadbent, C.D., Ko, K.C. ,1972. Rheological aspects of rock slope failures. Proc., 13th. U.S. Symposium on Rock Mechanics, Urbana, Ill , , pp. 579-593.

Browning, J.M., 1973. Catasatrophic rock slide, Mount Huascaran, north-central Peru. Bulletin, Am. Assoc. Petroleum Geologists , Vol. 57 , pp. 1335-1345.

Bruce, I., Cruden, D. ,1977. The dynamics of the Hope Slide. Bulletin, International Assoc. Engineering Geology , Number 16 , pp. 94-98.

Buss, E., Heim, A. ,1881. Der Bergsturz von Elm. , Worster, Zurich, pp. 133, (in German).

Butler, D.R., Oelfke, J.G. ,Oelfke, L.A., 1986. Historic rockfall avalanches, Northeastern Glacier National Park. Montana,U.S.A. Mountain Research and Development , Vol. 6 Number 3 , pp. 261-271.

Campbell, D.B., 1978. Performance of a waste rock dump on moderate to steeply sloping foundations. Procs., Symposium on the Stability in Coal Mining, Vancouver , , pp. 396-405.

Cassie, J.W., Van Gassen, W. ,Cruden, D.M., 1988. Laboratory analogue of the formation of molards, cones of rock-avalanche debris. Geology , Vol. 16 , pp. 735-738.

Chowdhury, R., 1978. Analysis of the Vajont Slide - a new approach. Rock Mechanics , Vol. 11 , pp. 29-38.

Chowdhury, R.N., 1980. Landslides as natural hazard - mechanisms and uncertainties. Geotechnical Engineering. , Vol. 11 , pp. 135-180.

Clague, J.J., Evans, S.G. ,1987. Rock avalanches. Canadian Geographer. , Vol. 31 , pp. 278-282.

Clague, J.J., Evans, S.G. ,1989. Catastrophic natural hazards in the Northern Coast Mountains near Stewart, British Columbia. Mining Review, November/December. , , pp. 23-28..

Clague, J.J., Souther, J.G. ,1982. The Dusty Creek landslide on Mount Caley, British Columbia. Canadian Journal of Earth Sciences. , Vol. 19 , pp. 524-539.

Coates, D.R., Yu, Y.S. ,1978. Block flow slope instability. Canmet Report , Canada Centre for Mineral & Energy Tech., pp. 1-12.

Courel, M.F., Delaunay, J. ,1980. Les eboulements d'extension catastrophique. Service Geologique National, B.R.G.M., Orleans, France, unpublished , , pp. 86.

Crandell, D.R., Fahnestock, R.K. ,1965. Rockfalls and avalanches from Little Tahoma Peak on Mt. Rainier, Washington.
B Bulletin 1221-A , U.S. Geological Survey, pp. 30.

Cruden, D.M., 1976. Major rock slides in the Rockies. Canadian Geotechnical Journal , Vol. 13 Number 1 , pp. 8-20.

Cruden, D.M., 1980. The anatomy of landslides. Canadian Geotechnical Journal , Vol. 17 Number 2 , pp. 295-300.

Cruden, D.M., 1980. A large landslide on Mars: Discussion and reply. Geological Society of America Bulletin. , Vol. 1 Number 91 , pp. 64-64.

Cruden, D.M., 1982. The Brazeau Lake slide, Jasper National Park, Alberta. Canadian Journal of Earth Sciences , Vol. 19 Number 5 , pp. 975-981.

Cruden, D.M., 1985. Rock slope movements in the Canadian Cordillera. Canadian Geotechnical Journal. , Vol. 22 , pp. 528-540.

Cruden, D.M., 1986. Monitoring the south peak of Turtle Mountain, 1980-1985. Alberta Environment, Research Management Division. , Vol. 86 Number 37 , pp. 70.

Cruden, D.M., Antoine, P. ,1984. The slide from Mt. Granier, Isere and Savoie, France on Nov. 24, 1248. Procs. 4th International Symposium of Landslides, Toronto , Vol. 1 , pp. 475-481.

Cruden, D.M., Beaty, C.B. ,1987. The Frank slide, southwestern Alberta. Geological Society of America, Centennial Field Guide, Rocky Mountain Section., , pp. 15-18.

Cruden, D.M., Eaton, T.M. ,1987. Reconnaissance of rockslide hazrds in Kananaskis County, Alberta. Canadian Geotechnical Journal. , Vol. 24 , pp. 414-429.

Cruden, D.M., Eaton, T.M. ,1988. Rockslide hazard in Kananaskis, Alberta. Procs., 5th. International Symposium on Landslides, Lausanne , C. Bonnard Ed., Vol. 2 , pp. 405-415.

Cruden, D.M., Hu, X.Q. ,1991. Some recent developments in the analysis of rock slope movements in the Rockies. Landslide Hazards in the Canadian Cordillera , S.G. Evans Ed., in Press.

Cruden, D.M., Hungr, O. ,1986. The debris of the Frank Slide and theories of rockslide- avalanche mobility. Canadian Journal of Earth Sciences , Vol. 23 , pp. 425-432.

Cruden, D.M., Krahn, J. ,1973. A reexamination of the geology of the Frank slide. Canadian Geotechnical Journal. , Vol. 10 , pp. 581-591.

Cruden, D.M., Krahn, J. ,1978. Frank Rockslide, Alberta, Canada. Rockslides and Avalanches , Voight, B., Ed., Vol. 1 Elsevier, pp. 97-112.

Daly, R.A., Miller, W.G. ,Rice, G.S., 1912. Report of the Commission appointed to investigate Turtle Mountain, Frank, Alberta. Geological Survey of Canada Memoir No. 27 , .

Davies, T.R.H., 1981. Spreading of rock avalanche debris by mechanical fluidization. Rock Mechanics , Vol. 15 , pp. 9-24.

Dawson, A.G., Matthews, J.A. ,Shakesby,R.A., 1986. A catastrophic landslide (Sturzstrom) in Verkilsdalen, Rondane National Park, Southern Norway. Geografiska Annaler , Vol. 68 , pp. 77-87.

De Matos, M., 1987. A sliding-consolidation model for rapid flow slides. Ph. D. Thesis, Univ. of Alberta , , Edmonton.

DeFreitas, M.H., Watters, R.J. ,1973. Some examples of toppling failure. Geotechnique , Vol. 23 , pp. 495-514.

DeMatos, M., 1987. A sliding-consolidation model for rapid flow-slides. Ph.D. Thesis, University of Alberta, Edmonton , (Unpublished).

Dubie, J.Y., Benefice, P. ,Guitton, C., 1988. Teletransmission de l'auscultation d'un glissement: retenue de Grand'Maison, glissement du Billan. Procs., 5th Int. Symposium on Landslides , C. Bonnard Ed., Vol. 1 , Lausanne, pp. 399-403, (in French).

Einstein, H.H., 1988. Landslide risk assessment procedure. Procs. 5th International Symposium on Landslides, Lausanne , C.Bonnard Ed., Vol. 2 , pp. 1075-1090.

Eisbacher, G., Clague, J.J. ,1984. Destructive mass movements in high mountains: hazard and management. Geological Survey of Canada, Paper 84-16 , , pp. 230.

Eisbacher, G.H., 1900. First-order regionalization of landslide characteristics in the Canadian Cordillera. Geoscience Canada , Vol. 6 Number 2 , pp. 69-79.

Eisbacher, G.H., 1971. Natural slope failure, northeastern Skeena Mountains. Canadian Geotechnical Journal. , Vol. 8 , pp. 384-390.

Eisbacher, G.H., 1979. Cliff collapse and rock avalanches (sturzstroms) in the Mackenzie Mountains, northwestern Canada. Canadian Geotechnical Journal , Vol. 16 , pp. 309-334.

Eisbacher, G.H., 1982. Slope stability and land use in mountain valleys. Geoscience Canada. , Vol. 9 , pp. 14-27.

Eppler, D.B., Fink, J. ,Fletcher, R., 1987. Rheologic properties and kinematics of emplacement of the Chaos Jumbles rockfall avalanche, Lassen Volcanic National Park, California Journal of Geophysical Research , Vol. 92 Number 5 , pp. 3623-3633.

Erismann, T.H., 1979. Mechanism of large landslides. Rock Mechanics , Vol. 12 , pp. 15-46.

Erismann, T.H., 1988. Modes and consequences of first rock fracture in landslides. Zeitschrift fur Geomorphologie , Vol. 32 Number 3 , pp. 257-272.

Evans, S.G., 1983. The Enderby Cliffs landslide British Columbia. In Current Research, Part B, Geological Survey of Canada. , 423-427, pp. Paper 89-1B:.

Evans, S.G., 1983. Landslides in layered volcanic successions with particular reference to Tertiary basalt successions of South Central B.C. Ph.D. Thesis, University of Alberta, Edmonton, Alberta , , pp. 350.

Evans, S.G., 1986. Landslide damming in the Corillera of Western Canada; in Landslide Dams Processes, Risk and Mitigation. American Society of Civil Engineers, Special Geotechnical Publication , Vol. 3 , pp. 111-130.

Evans, S.G., 1987. A rock avalanche from the peak of Mount Meager, B.C. Current Research, Part A, Paper 87-1A. , Geological Survey of Canada, Ottawa, pp. 929-934.

Evans, S.G., 1987. Surface displacement and massive toppling on the northeast ridge of Mount Currie, B.C. Current Research, Part A, Paper 87-1A , Geological Survey of Canada, Ottawa, pp. 181-189.

Evans, S.G., 1989. The 1946 Mount Colonel Foster rock avalanche and associated displacement wave, Vancouver Island, B.C. Canadian Geotechnical Journal , Vol. 26 , pp. 447-452.

Evans, S.G., 1989. Rock avalanche run-up record. Nature , Vol. 340 , pp. 271.

Evans, S.G., 1989. , .

Evans, S.G., 1989. The 1946 Mt. Colonel Foster rock avalanche and associated displacement wave, Vancouver Island, British Columbia Can. Geotechnical Journal , Vol. 26 , pp. 447-452.

Evans, S.G., Aitken, J.D. ,Wetmiller, R.J., Horner, R.B., 1987. A rock avalanche triggered by the October 1985 North Nahanni earthquake, District of Mackenzie, N.W.T. Canadian Journal of Earth Sciences , Vol. 24 Number 1 , pp. 176-184.

Evans, S.G., Clague, J.J. ,Woodsworth, G.J., Hungr, O., 1989. The Pandemonium Creek rock avalanche, British Columbia. Canadian Geotechnical Journal , Vol. 26 , pp. 427-446.

Evrard, H., Gouin, T. ,Benoit, A., Duranthon, J.P., 1990. Sechilienne, risques majeurs d'eboulements en masse. Bull. Liaison Labo. Ponts et Chausees, Paris , Vol. 165 , pp. 7-16, (in French).

Fahnestock, R.K., 1978. Little Tahoma Peak rockfalls and avalanches, Mount Rainier. Rockslides and Avalanches , Voight, B. Ed., Vol. 1 Elsevier, pp. 181-197.

Fauque, L., Strecker, M.R. ,1988. Large rock avalanche deposits (Sturzstrome) at Sierra Aconguija, northern Sierras Pampeanas, Argentina. Ecolgae Geologicae Helvetiae , Vol. 81 Number 3 , pp. 579-592.

Follacci, J.P., 1987. Les mouvements du versant de la Clapiere a Saint Etienne de Tinee (Alpes Maritimes). Bull. Liaison Labo. Ponts et Chausees , Vol. 151 , Paris, pp. 39-54.

Follacci, J.P., Guardia, P. ,Ivaldi, J.P., 1988. Le Glissement de la Clapiere dans son cadre dynamique. Procs., 5th International Symposium on Landslides, Lausanne , C. Bonnard Ed., Vol. 2 , pp. 1323-1328, (in French).

Follaci, J.P., 1984. Cretes doubles et perturbations de versants dans un domaine de montague alpine (Mercantour et ses bordures). Documents du B.R.G.M. , Vol. 83 , pp. 533-542.

Francis, P.W., Baker, M.W. ,1977. Mobility of pyroclastic flows. Nature , Vol. 270 , pp. 164-165.

Fukuoka, M., Yoshida, Y. ,Masuda, T., 1977. Kinetic friction in landslides. Proceedings of the 9th Conference on Soil Mechanics and Foundation Engineering., Vol. 2 , pp. 71-74.

Fukuzono, T., 1985. A new method for predicting the failure time of slope. Procs., 4th Int. Conference and Field Workshop on Landslides , , Tokyo, pp. 145-150.

Fukuzono, T., 1990. Recent studies on time prediction of slope failure. Landslide News , Number 4 , Tokyo, pp. 9-12.

Gardner, J.S., 1980. Frequency, magnitude and spatial distribution of rockfalls and rockslides, Highwood Pass area, Alberta, Canada. Thresholds in Geomeorphology , Coates, D.R. and Vitek, J.D. Ed., Allen & Unwin, pp. 267-295.

Goguel, J., 1980. Les risques de grands eboulements. Le Recherche , Vol. 11 , pp. 620-628, (in French).

Goguel, J., Pachoud, A. ,1972. Geology and dynamics of the rockfall of the Granier Range which occurred in November 1248. Bulletin, Bureau de Recherches Geologiques et Minieres, Hydrogeologie , Vol. 1 , Lyon, pp. 29-38.

Goguel, J., Pachoud, A. ,1981. Les mouvements de terrain du versant sud du Massif de Plate, Haute-Savoie, France. Bull. Liaison Laboratoire Central de Ponts et Chaussees, Special No. 10, , pp. 15-26, (in French).

Golder Assoc., , 1987. Regional study of coal mine waste dumps in British Columbia. Report to the Federal Panel on Energy R.& D. , Supply and Services Canada Ed., (unpublished).

Goodman, R.E., Bray, J.W. ,1976. Toppling of rock slopes. Rock Engineering, Geotechnical Eng. Division Conference, Boulder , Vol. 2 ASCE, pp. 201-237.

Gordon, J.E., Birnie, R.V. ,Timmis, R., 1978. A major rockfall and debris slide on the Lyell Glacier, South Georgia. Arctic and Alpine Research , Vol. 10 Number 1 , pp. 49-60.

Govi, M., 1977. Photo-interpretation and mapping of the landslides triggered by the Friuli earthquake (1976). Bulletin, International Assoc. Engineering Geology , Number 15 , pp. 67-72.

Govi, M., 1989. The 1987 landslide on Mount Zandilla in the Valtellina, Northern Italy. Landslide News , Number 3 Japan Landslide Society, Tokyo, pp. 1-3.

Griggs, E., 1920. Great Mageik Slide, Alaska. Ohio Journal of Science , Vol. 20 , pp. 325-354.

Habib, P., 1975. Production of gaseous pore pressure during rock slides. Rock Mechanics , Vol. 7 , pp. 193-197.

Hadj-Hamou, T., Kavazanjian,Jr., E. ,1985. Seismic stability of gentle infinite slopes Journal of Geotechnical Engineering. , Vol. 3 Number 6 ASCE, pp. 681-697.

Hadley, J.B., 1964. Landslides and related phenomena accompanying the Hebgen Lake earthquake of August 17, 1959. U.S. Geological Survey, Prof. Paper 435-K , , pp. 107-138.

Hadley, J.B., 1978. Madison Canyon Rockslide, Montana, U.S.A. Rockslides and Avalanches , Voight, B. Ed., Vol. 1 Elsevier, pp. 167-180..

Hamel, J.V., 1972. The slide at Brilliant Cut. Procs., 13th U.S. Symposium on Rock Mechanics , ASCE, pp. 487-510.

Hamel, J.V., 1976. Libby Dam left abutment rock wedge stability. Rock Engineering for Foundations and Slopes Conf., Boulder, Colo. , ASCE, pp. 361-385.

Hammett, R.D., 1974. A study of the deformation of a discontinuous rock mass. Ph.D. thesis, James Cook University of North Queensland , , Australia.

Hardy, R.M., Morgenstern, N.R. ,Patton, F.D., 1978. The Garibaldi Advisory Panel Report. Dept. of Highways, Provincial Govt. of British Columbia. , (unpublished).

Harrison, J.V., Falcon, N.L. ,1938. An ancient landslip at Sairdmarreh in south- western Iran. Journal of Geology , Vol. 46 , pp. 296-309.

Heim, A., 1932. Landslides and human lives (Bergsturz und Menchenleben). , N. Skermer Ed., Bi-Tech Publishers, Vancouver, B.C., pp. 196.

Hendron, A.J., Patton, F.D. ,1985. The Vaiont Slide, a geotechnical analysis based on how geologic observations of the failure surface. U.S. Army Corps. of Eng.,Tech.Report. , Vol. 85 Number 5 , pp. 104.

Heuberger, H., Masch, L. ,Preuss, E., Schrocker,A., 1984. Quaternary landslides and rock fussion in cental Nepal and in the Tyrolean Alps. Mountain Research and Development , Vol. 4 Number 4 , pp. 345-362.

Hoek, E., Bray, J.V. ,1977. Rock slope engineering , Inst. Min. Met., London, pp. 309.

Hoek, E., Brown, J. ,1981. Underground excavations in rock. , Inst. of Mining & Metallurgy, London, pp. 526.

Howard, K., 1973. Avalanche mode of motion: implication from lunar examples. Science , Vol. 180 , pp. 1052-1055.

Hoyer, M.C., 1971. Puget Peak avalanche, Alaska. Geological Society of America Bulletin , Vol. 82 , pp. 1267-1284.

Hsu, K.J., 1975. Catastrophic debris streams (sturzstorms) generated by rock falls. Bulletin, Geological Society of America , Vol. 86 , pp. 129-140.

Hsu, K.J., 1978. Albert Heim, observations on landslides and relevance to modern interpretations. Rockslides and Avalanches , Voight, B. Ed., Vol. 1 Elsevier, pp. 71-92.

Hsu, K.J., 1983. Actualistic catastrophism. Sedimentology , Vol. 30 , pp. 3-9.

Hu, G., 1987. Multiple stroke of high speed landslides. Procs., International Symposium on Engineering Geological Environment in Mountainous Areas, , Beijing, pp. 441-456.

Huang, R.Q., Wang, S.T. ,1988. Rolling friction mechanism for the high speed motion of a large scale landslide. Proceedings of the 5th International Symposium on Landslides. , C. Bonnard Ed., , pp. 187-191.

Hungr, O., 1981. Dynamics of rock avalanches. Ph. D. Thesis , University of Alberta, pp. 500.

Hungr, O., 1989. Mobility of rock avalanches. Bulletin, National Research Center for Disaster Prevention , Tsukuba, Japan, pp. 1-13.

Hungr, O., Evans, S.G. ,1991. Prediction of the failure behaviour of large rockslides. GAC Special Paper - Landslide Hazards in the Cordillera , S.G. Evans Ed., in prep..

Hungr, O., Gerath, R.F. ,Morgan, G.C., 1984. Landslides of the Scatter River area, northeastern British Columbia. Procs., 37th Canadian Geotechnical Conference , , Toronto, pp. 113-118.

Hungr, O., Morgenstern, N.R. ,1984. Experiments on the flow behavior of granular materials at high velocity. Geotechnique , Vol. 35 , pp. 383-385.

Hungr, O., Salgado, F. ,Byrne, P.M., 1989. Evaluation of a three-dimensional method of slope stability analysis. Can. Geotechnical Journal , Vol. 26 Number 4 , pp. 679-686.

Hutchinson, J.N., 1986. A sliding-consolidation model for flow slides. Canadian Geotechnical Journal , Vol. 23 Number 2 , pp. 115-126.

Hutchinson, J.N., 1988. General report: Morphological and geotechnical parameters of landslides in relation to geology and hydrogeology. Procs., 5th International Symposium on Landslides, Lausanne , C. Bonnard Ed., Vol. 1 , pp. 3-35.

Inokuchi, T., 1985. The Ontake rock slide and debris avalanche, caused by the Naganoken Seibu Earthquake, 1984. Procs., 4th. Int. Conference and Field Workshop on Landslides , , Tokyo, pp. 329-338.

Inokuchi, T., 1988. Gigantic landslides and debris avalalanches on volcanoes in Japan. Unpublished report, Nat. Research Center for Disaster Prevention , , Tsukuba, pp. 6.

Jackson, Jr., L.E., Isobel, J.S. ,1990. Rock Avalanches in the Pelly Mountains, Yukon Territory Current Research, Part E, Paper 90-1E , Geological Survey of Canada, Ottawa, pp. 263-269.

Johnson, B., 1978. Blackhawk Landslide, California. Rockslides and Avalanches , Voight, B. Ed., Vol. 1 Elsevier, pp. 481-504.

Kaiser, P.K., Simmons, J.V. ,1989. A reassessment of transport mechanisms of some rock avalanches in the Northwest Territories, Cananda. Canadian Geotechnical Journal , Vol. 27 , pp. 129-144.

Keefer, D.K., 1984. Landslides caused by earthquakes. Bulletin, Geological Society of America , Vol. 95 , pp. 46-421.

Keefer, D.K., 1984. Rock avalanches caused by earthquakes: Source characteristics. Science , Vol. 223 , pp. 1288-1290.

Keefer, D.K., Tannaci, N.E. ,1981. Bibliography on landslides, soil liquefaction and related ground failure in selected historic earthquakes U.S.G.S. Open File Report. , , pp. 81-572.

Keefer, D.K., Wilson, R.C. ,Harp, E.L., Lips, E.W., 1985. The Borah Peak, Idaho Earthquake of October 28, 1983 - Landslide. Earthquake Spectra. , Vol. 2 , pp. 91-125.

Kennedy, B.A., Niermeyer, K.E. ,1971. Slope monitoring systems used in the prediction of major slope failure at the Chiquicamata Mine, Chile. Planning Open Pit Mines, Johannesburg Symposium , , pp. 215-225.

Kenney, T.C., 1967. Stability of the Vaiont valley slope. Rock Mechanics and Engineering Geology , Vol. 5 , pp. 10-16.

Kent, P.E., 1966. The transport mechanism in catastrophic rock falls. Journal of Geology , Vol. 74 , pp. 79-83.

King, J., 1987. The breaching of the Bairaman Dam, East New Britain Province. Geological Survey Paper 85/9, New Guinea , .

King, J., Loveday, I. ,1985. Preliminary Geological report on the effects of the earthquake of May 11 1985, centered near Bialla, W. New Britain. Geological Survey Paper 85/12, New Guinea. , .

King, J., Loveday, I. ,Schuster, R.L., 1989. The 1985 Bairaman landslide dam and resulting debris flow, Papua New Guinea. Quarterly Journal of Engineering Geology , Vol. 22 , London, pp. 257-270.

Kobayashi, Y., Kagawa, T. ,1987. The prediction of hazards from debris avalanches and rockfalls with the aid of computer simulations. Int. Symp. of Eng. Geological Environment in Mountainous areas, Beijing. , , pp. 567-572.

Koerner, H.J., 1976. Reichweite und Geschwindigkeit von Bergsturzen und Fliesschneelawinen. Rock Mechanics , Vol. 8 , pp. 225-256.

Koerner, H.J., 1977. Flow mechanisms and resistances in the debris streams of rock slides. Bulletin, International Assoc. Engineering Geology , Number 16 , pp. 101-104.

Kojan, E., Hutchinson, J.N. ,1978. Mayunmarca rockslide and debris flow, Peru. Rockslides and Avalanches , Voight, B. Ed., Vol. 1 Elsevier, pp. 351-361.

Korner, H.J., 1980. The energy-line method in the mechanics of avalanches. Journal of Glaciology. , Vol. 26 Number 94 , pp. 501-505.

Krahn, J., 1974. Rock slope stability with emphasis on the Frank Slide. Ph.D. thesis , University of Alberta.

Lachenbruch, A.H., 1980. Frictional heating, fluid pressure and the resistance to fault motion. Journal of Geophysical Research , Vol. 85 , pp. 6097-6112.

Lee, K.L., Duncan, J.M. ,1975. Landslide of April 25, 1974 on the Mantaro River, Peru. Report to the National Research Council, Nat. Academy of Sciences, Washington, (npublished), pp. 70.

Lemos, L., Skempton, A.W. ,Payton, P.R., 1984. Earthquake loading of shear surfaces in slopes. Procs. 11th ICSMFE. , Vol. 6 , pp. 1955-1958.

Li-Tianchi, , 1983. A mathematical model for predicting the extent of a major rockfall. Zeitschrift fur Geomorphologie , Vol. 27 Number 4 Borntraeger, Berlin, pp. 473-482.

Lin, J., Whitman, R.V. ,1986. Earthquake induced displacements of sliding blocks. Journal of Geotechnical Engineering , Vol. 112 Number 1 , pp. 44-59.

Lucchitta, B.K., 1978. A large landslide on Mars. Bulletin, Geological Society of America , Vol. 89 , pp. 1601-1609.

Lutton, R.J., Banks, D.C. ,Strohm, W.E., 1979. Slides in Gaillard Cut, Panama Canal Zone. Rockslides and Avalanches , B. Voight Ed., Vol. 2 Elsevier, Amsterdam, pp. 151-224.

Machida, H., 1984. Large-scale rockslides, avalanches and related phenomena. Transactions, Japanese Geomorphological Union , Vol. 5 Number 3 , pp. 155-178.

Mahr, T., 1977. Deep-reaching gravitational deformations of high mountain slopes. Int. Asc. Eng. Geol. Bull. , Number 16 , pp. 121-127.

Malatrait, N., 1975. Analyse et classement des mouvements gravitaires, Feuille St. Jean-de- Maurienne. Thesis, L'Universite Scientifique et Medicale de Grenoble , , pp. 219.

Marangunic, C., 1972. Effects of a landslide on Sherman Glacier, Alaska. Inst. of Polar Studies Report No. 30 , Ohio State University, Columbus, Ohio.

Marangunic, C., Bull, C. ,1968. The landslide on the Sherman Glacier. The Great Alaska Earthquake of 1964, Part A, Hydrology. Publication 1603 , National Academy of Science, Washington, pp. 383-394.

Mathews, W.H., McTaggart, K.C. ,1969. The Hope Landslide, B.C. Procs., Geological Association of Canada , Vol. 20 , pp. 65-75.

Mathews, W.H., McTaggart, K.C. ,1978. Hope Rockslides, British Columbia, Canada. Rockslides and Avalanches , Voight, B. Ed., Vol. 1 Elsevier, pp. 259-275..

McConnell, R.G., Brock, R.W. ,1904. The great landslide at Frank, Alberta Canadian Parliament Sessional Paper, No. 25 , Dept. of the Interior, Ottawa.

McEwen, A.S., 1989. Mobility of large rock avalanches: Evidence from Valles Marineris, Mars Geology , Vol. 17 , pp. 1111-1114.

McEwen, A.S., Malin, M.C. ,1989. Dynamics of Mount St. Helens' 1980 pyroclastic flows, rockslide - avalanche, lahars, and blast. Journal of Volcanology and Geothermal Researach. , Vol. 37 Elsevier, Amsterdam, pp. 205-231.

McLellan, P.J., Kaiser, P.K. ,1984. Application of a two-parameter model to rock avalanches in the Mackenzie Mountains. Procs., 4th International Symposium on Landslides , Vol. 1 , Toronto, pp. 559-565.

McLellan, P.J., Kaiser, P.K. ,1984. The Rockslide Pass rock avalanche, Mackenzie Mountains, N.W.T. Procs., 4th Int. Symposium on Landslides, Toronto , Vol. 1 , pp. 135-140.

McLellan, P.J.A., 1983. Investigation of some rock avalanches in the MacKenzie Mountains. M.Sc. Thesis, University of Alberta, Edmonton, Alberta , , pp. 281.

McSaveney, M.J., 1978. Sherman Glacier rock avalanche, Alaska. Rockslides and Avalanches , Voight, B. Ed., Vol. 1 Elsevier, pp. 197-258.

Mears, A.I., 1980. A fragment-flow model of dry-snow avalanches. Journal of Glaciology , Vol. 26 Number 94 International Glaciological Society, Cambridge, Eng., pp. 153-163.

Melosh, H.J., 1979. Acoustic fluidization: a new geologic process? Journal of Geophysical Research , Vol. 84 , pp. 7513-7520.

Melosh, H.J., 1987. The mechanics of large rock avalanches. Geological Society of America, Reviews in Engineering Geology. , Vol. 7 , pp. 41-49.

Mencl, V., 1966. Mechanics of landslides with non- circular slip surfaces with special reference to the Vaiont slide. Geotechnique , Vol. 16 , pp. 329-337.

Miller, V.J., 1982. The northeast Tripp Slide at Kennecott's Nevada Mine division. Strability in Surface Mining , C.O. Brawner Ed., A.I.M.M.P.E., New York.

Mokievsky-Zubok, O., 1977. Glacier-caused slide near Pylon Peak, B.C. Canadian Journal of Earth Sciences , Vol. 14 , pp. 2657-2662.

Mollard, J.D., 1977. Regional landslide types in Canada. Landslides, Reviews in Engineering Geology , Coates, D.R. Ed., Vol. 3 Geological Soc. of America, pp. 29-56.

Montandon, F., 1933. Chronologie des grands eboulements alpins du debut de l'ere chretienne a nos jours. Materiaux pour l'Etude des Calamities, Societe de geographie, Geneve, Vol. 32 .

Moore, D.P., Mathews, W.H. ,1978. The Rubble Creek landslide, southwestern British Columbia. Canadian Journal of Earth Sciences , Vol. 15 , pp. 1039-1052.

Moore, J.G., Clague, D.A. ,Holcomb, R.T., Lipman, P.W., Normark, W.R., Torresan, M.E., 1989. Prodigious submarine landslides on the Hawaiian Ridge. Journal of Geophysical Research. , Vol. 94 Number 12 , pp. 465-484.

Morgenstern, N.R., 1978. Mobile soil and rock flows. Geotechnical Engineering , Vol. 9 , pp. 123-141.

Moriwaki, H., Yazaki, S. ,Oyagi, N., 1985. A gigantic debris avalanche and its dynamics at Mt. Ontake caused by the Naganoken-Seibu earthquake, 1984. Procs., 4th Int. Conference and Field Workshop on Landslides , , Tokyo, pp. 359-364.

Mueller, L., 1964. The rock slide in the Vaiont Valley Felsmechanik und Ingenieur Geologie , Vol. 2 , pp. 189-212.

Mueller, L., 1968. New considerations on the Vaiont Slide. Felsmechanik und Ingenieur Geologie , Vol. 6 , pp. 1-91.

Naranjo, J.A., Francis, P. ,1987. High velocity debris avalanche at Lastarria volcano in the north Chilean Andes. Bulletion of Volcanology , Number 49 , pp. 509-514.

Nemcok, A., 1982. Zosuvy v Slovenskych Karpatoch. , Veda, Bratislava, (in Slovak).

Norem, H., Locat, J. ,1991. A dynamic model for rock avalanches. GAC Special Paper - Landslide Hazards in the Cordillera , S.G. Evans Ed., in prep..

Ouchi, S., Mizuyama, T. ,1989. Volume and movement of Tombi landslide in 1858, Japan. Transactions, Japaneese Geomorphological Union. , Vol. 10 Number 1 , pp. 27-51.

Palmer, L., 1977. Large rockslides of the Columbia River gorge, Oregon & Washington. Landslides, Reviews in Engineering Geology , Coates, D.R. Ed., Vol. 3 Geological Soc. of America, pp. 69-83.

Patton, F.D., 1976. The Devastation Glacier slide (abstract). Geological Association of Canada, Cordilleran Section, 1976 Annual Symposium, Program and Abstracts, , pp. 26-27.

Pautre, A., Schneider, B. ,1973. Les consequences de l'avalanche rocheuse du Huascaran, Perou, 1970. Symp. Nat. S.S.S.C. Cannes. , Vol. 1 , pp. 194-201.

Pautre, A.F., Sabarly, F. ,Schneider, B.,, 1974. L'effet d'echelle dans les ecroulements de falaise. Procs., 3rd Congress ISRM, Denver , Vol. 2 , pp. 859-864, (in French).

Perla, R., Cheng, T.T. ,McClung, D.M., 1980. A two-parameter model of snow-avalanche motion. Journal of Glaciology , Vol. 26 Number 94 , pp. 197-207.

Peterson, A.E., Sego, D.C. ,Cruden, D.M., Evans, S.G., 1988. The English Chief Rockslide. Proceedings, Annual Conference of Canadian Society for Civil Engineering , Vol. 3 , pp. 85-111.

Piteau, D.R., 1977. Regional slope-stability controls and engineering geology of the Fraser Canyon, B.C. Landslides, Geological Society of America, Reviews in Eng. Geology., Vol. 3 D.R. Coates, pp. 85-111.

Piteau, D.R., Mylrea, F.H. ,Blown, I.G.,, 1978. Downie Slide, Columbia River, British Columbia. Rockslides and Avalanches , Voight, B. Ed., Vol. 1 Elsevier, pp. 365-392.

Plafker, G., 1968. The great Alaska earthquake of 1964: Source areas of the Shattered Pear and Pyramid Peak landslides at Sherman Glacier. National Research Council, Publication 1603 , 374-382, Washington.

Plafker, G., Ericksen, G.E. ,1978. Nevados Huascaran avalanches, Peru. Rockslides and Avalanches , Voight, B. Ed., Vol. 1 Elsevier, pp. 277-314.

Porter, S.C., Orombelli, G. ,1980. Catastrophic rockfall of September 12, 1717 on the Italian flank of the Mt. Blanc. Zeitschrift fur Geomorphologie N.F. , Vol. 24 Number 2 , pp. 200-218.

Porter, S.C., Orombelli, G. ,1981. Alpine rockfall hazards. American Scientist, January-February Issue , Vol. 69 , pp. 69-75.

Radbruch-Hall, D.H., 1978. Gravitational creep of rock masses on slopes. Rockslides and Avalanches , B. Voight Ed., Vol. 1 Elsevier, Amsterdam, pp. 607-657.

Radbruch-Hall, D.H., Varnes, D.J. ,Savage, W.Z., 1976. Gravitational spreading of steep-sided ridges ("Sackung") in western United States. Bulletin, International Assoc. of Engineering Geology , Vol. 14 , pp. 23-35.

Riemer, W., Locher, T. ,Nunez, I., 1988. Mechanics of deep seated gravitational movements in metamorphic rocks in Ecuador. Procs., 5th Int. Symposium on Landslides, Lausanne , C. Bonnard Ed., Vol. 2 , pp. 307-310.

Rochet, L., 1987. Developpement des modeles numeriques dans l'analyse de la propagation de eboulements rocheux. Procs., 6th. Congress ISRM , Vol. 1 , pp. 479-484, (in French).

Romero, S.U., Molina, R. ,1974. Kinematic aspects of Vaiont Slide. Procs., 3rd Congress ISRM, Denver , 2 Ed., Vol. 2 , pp. 865-870.

Ryder, J.M., Bovis, N.J. ,Church, M., 1990. Rock avalanches at Texas Creek, British Columbia. Submitted to Cen. Journal of Earth Sciences , .

Saito, M., 1965. Forecasting the time of occurrence of a slope failure. Procs., Int. Conf. Soil Mech. Foundation Engineering, Montreal. , Vol. 6 , pp. 537-541.

Salt, G., 1988. Landslide mobility and remedial measures. Procs., 5th. International Symposium on Landslides , C. Bonnard Ed., Vol. 1 , pp. 757-762.

Sassa, K., 1984. The mechanism starting liquefied landslides and flows. Procs., 4th Int. Symposium on Landslides , Vol. 2 , Torornto, pp. 349-354.

Sassa, K., 1988. Special Lecture: Geotechnical model for the motion of landslides. Proceedings of the 5th International Symposium of Landslides. , Vol. 1 C. Bonnard, pp. 37-55.

Scheidegger, A.E., 1973. On the prediction of the reach and velocity of catastrophic landslides. Rock Mechanics , Vol. 5 , pp. 231-236.

Schneider, V.J., Gailen, U.S. ,1939. Der Felssturz am Gspaltenberg (Gemeinde Flums). Strasse und Verkehr , Vol. 1 , pp. 1-13., (in German).

Schultz, A.P., Southworth, C.S. ,1989. Large bedrock landslides of the Appalachian Valley and Ridge Province of eastern North America. U.S. Geological Survey Special Paper 236 , , pp. 57-74.

Schumm, S.A., Chorley, R.J. ,1964. The fall of Threatening Rock. American Journal of Science , Vol. 262 , pp. 1041-1054.

Schuster, R.L., Fleming, R.W. ,1986. Economic losses and fatalities due to landslides. Bulletin, Assoc. Engineering Geologists , Vol. 23 , pp. 11-28.

Sharpe, C.F.S., 1938. Landslides and related phenomena , Columbia University Press, pp. 137.

Shreve, R.L., 1966. Sherman Landslide, Alaska. Science , Vol. 154 , pp. 1639-1643.

Shreve, R.L., 1968. The Blackhawk Landslide Geological Soc. of America, Special Paper No. 108 , .

Shreve, R.L., 1968. Leakage and fluidization in air-layer lubricated avalanches. Bulletin, Geological Soc. of America , Vol. 79 , pp. 653-658.

Simmons, J.V., Cruden, D.M. ,1980. A rock labyrinth in the Front Ranges of the Rockies, Alberta. Canadian Geotechnical Journal , Vol. 17 , pp. 1300-1309.

Skempton, A.W., 1966. Bedding plane slip, residual strength and the Vaiont Landslide. Geotechnique , Vol. 16 , pp. 82-84.

Skempton, A.W., Hutchinson, J. ,1969. Stability of natural slopes and embankment foundations. Procs., Int. Conf. Soil Mech. Foundation Engineering, Mexico , , pp. 291-340.

Skermer, N.A., 1980. Alpine landslides - a lesson for British Columbia? The BC Professional Engineer , , pp. 19-24.

Slingerland, R.L., Voight, B. ,1978. Occurences, properties, and predictive models of landslide-generated water waves. Rockslides and Avalanches , B. Voight Ed., Vol. 2 .

Smith, R.H., 1971. A study of a prehistoric landslide surface at Cheaux Lake, east of Chilliwack, B.C. B.A.Sc. Thesis, University of British Columbia , , pp. 24.

Solonenko, V.P., 1977. Landslides and collapses in seismic zones and their prediction. Bulletin, International Assoc. Engineering Geology , Number 15 , pp. 4-8.

Tabor, R.W., 1971. Origin of ridge-top depressions by large-scale creep in the Olympic Mountains, Washington. Bulletin, Geological Society of America , Vol. 82 , pp. 1811-1822.

Terzaghi, K., 1950. Mechanics of landslides. Berkey Volume , Geological Society of America, New York, pp. 83-124.

Terzaghi, K., 1962. Stability of slopes in hard, unweathered rock. Geotechnique , Vol. 12 , pp. 251-270.

Trunk, F.J., Dent, J.D. ,Lang, T.E., 1986. Computer modeling of large rock slides. Journal of Geotechnical Engineering , Vol. 112 Number 3 ASCE, pp. 348-361.

Ui, T., 1983. Volcanic dry avalanche deposits-identification and comparison with nonvolcanic debris stream deposits. Journal of Volcanology and Geothermal Research , Number 18 Elsevier, Amsterdam, pp. 135-150.

Ui, T., Yamamoto, H. ,Suzuki-Kamata, K., 1986. Characterization of debris avalanche deposits in Japan J. Volcanology and Geothermal Energy , Number 29 , pp. 231-243.

Van Gassen, W., Cruden, D.M. ,1990. Momentum transfer and friction in the debris of rock avalanches. Canadian Geotechnical Journal. , Vol. 26 , pp. 1-23.

Varnes, D.J., 1978. Slope movement types and processes. Landslides, Analysis and Control, Transportation Res. Board Spec. Report , Schuster, R.L. & Krizek, R.J. Ed., , pp. 11-33.

Vibert, Ch., Arnould, M. ,Cojean, R., LeCleach, J.M., 1988. Essai de prevision de rupture d'un versant montagneux. Procs., 5th. International Symposium on Landslides, Lausanne , C. Bonnard Ed., Vol. 1 , pp. 789-792, (in French).

Voellmy, A., 1955. Uber die Zerstorungskraft von Lawinen. Schweizerische Bauzeitung , Vol. 73 , pp. 159-285, (in German).

Voight, B., 1978. Lower Gros Ventre Slide, Wyoming. Rockslides and Avalanches , Voight, B. Ed., Vol. 1 Elsevier, pp. 113-166.

Voight, B., 1989. Materials science law applies to time forecasts of slope failure. Landslide News , Number 3 Japan Landslide Society, Tokyo, pp. 8-10.

Voight, B., Faust, C. ,1982. Frictional heat and strength loss in some rapid landslides. Geotechnique. , Vol. 33 , pp. 243-273.

Voight, B., Kennedy, B.A. ,1978. Slope failure of 1967-1969, Chiquicamata Mine, Chile. Rockslides and Avalanches , Voight, B. Ed., Vol. 2 Elsevier, pp. 595-632.

Watson, R.A., Wright, H.E. ,1967. The Saidmarreh Landslide, Iran. Geological Society of America Special Paper 123. , , pp. 115-139.

Wetmiller, R.J., Evans, S.G. ,1989. Analysis of the earthquakes associated with the 1964 Hope landslide and their effects on slope stability at the site. Canadian Geotechnical Journal , Vol. 26 , pp. 484-490.

Wetmiller, R.J., Horner, R.B. ,Hasegawa, H.S., North, R.G., Lamontagne, M., Weichert, D.H., Evans, S.G., 1988. An analysis of the 1985 Nahanni Earthquakes. Bulletin, Seismological Society of America , , pp. 590-616.

Whitehouse, I.E., Griffiths, G.A. ,1983. Frequency and hazard of large rock avalanches in the central Southern Alps, New Zealand. Geology , Vol. 11 , pp. 331-334.

Wilson, R.C., Keefer, D.K. ,1985. Prediction of areal limits of earthquake induced landsliding. Evaluating earthquake hazards in the L.A. region USGS. USGS Prof. Paper 1360, , pp. 317-365.

Wyllie, D.C., Munn, F.J. ,1978. The use of movement monitoring to minimize production losses due to pit slope failures. Stability in Coal Mining, Vancouver Symposium , CIM.

Yarnold, J.C., Lombard, J.P. ,1989. A facies model for large rock-avalanche deposits formed in dry climates. Conglomerates in Basin Analysis: A.O. Woodford Symposium , Colburn,I.,Patrick,L.,Minch,J. Ed., Vol. 62 , pp. 9-31.

Zaruba, Q., Mencl, V. ,1969. Landslides and their control. , Elsevier, Amsterdam, pp. 205.

Zavodni, Z.M., Broadbent, C.D. ,1980. Slope failure kinematics. C.I.M. Bulletin , Vol. 73 Number 16 .

Zischinski, U., 1966. On the deformation of high slopes. Procs., 1st Congress ISRM, Lisbon , Vol. 2 , pp. 179-185.

Zischinski, V., 1968. Uber Sackungen. Rock Mechanics , Vol. 1 , pp. 30-52, (in German).

APPENDIX E

GLOSSARY

ROCKSLIDE	A failure of a large mass of rock from a slope. In the context of this report it should involve more than 1 million m^3 of material (predominantly bedrock), or create a deposit covering more than 0.1 km^2. It should also involve a well-defined complete or incipient detachment, with a distinct head scarp and lateral boundaries. The movement mechanism may not necessarily be sliding.
ROCK AVALANCHE	A rapidly moving rockslide, involving disintegration of the moving mass to form a stream of fragments.
STURZSTROM	A stream of fragments resulting from a rock avalanche.
DEPOSIT	Rockslide debris which has deposited after failure.
SOURCE AREA	The area from which a rockslide mass originated - where it was located prior to failure.
SOURCE SCAR	Synonym for detachment surface.
DETACHMENT SURFACE	Surface along which a rockslide mass separated from the surrounding and underlying stable rock. The surface may be a displacement (shear or tension) discontinuity, or a distinct shear strain discontinuity (hinge surface) in case of advanced toppling deformation.
HEAD SCARP	Exposed part of the detachment surface in the upper part of the source area.
SIDE SCARPS	Exposed parts of the detachment surface at the lateral margins of the source area.

PATH	The path of the rockslide or rock avalanche, which extends from the lower edge (toe) of the source area to the distal rim of the deposit.
TOPPLING	Rotation of rock masses or blocks in the downslope direction.
FLEXURAL TOPPLING	Rotation of an anisotropic rock mass, without the development of a distinct hinge surface.
HINGE SURFACE	A distinct shear strain discontinuity at the base of a strongly toppled rock mass.
BLOCK TOPPLING	Rotation of a blocky rock mass, with a well developed hinge surface.
FAILURE	The most significant displacement event in the development of a rockslide, involving the formation of a continuous detachment surface. In the data base, velocities and displacements pertaining to the most significant past displacement event are arbitrarily designated as failure parameters, even though the case may not yet have reached the failure stage.
BRITTLENESS	Propensity for the reduction of strength with increasing displacement, due to destruction of material bridges, roughness and asperitives, modification of contact surfaces or positive changes in pore pressure.
DILATION	Increase of volume with strain.

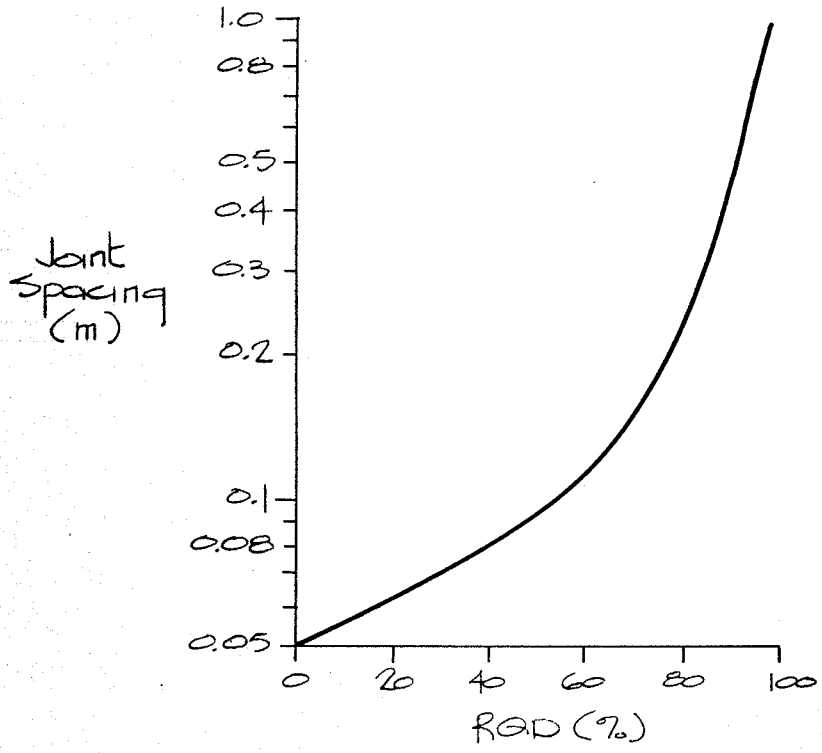

Figure 8 - Approximate relationship between Joint Spacing and RQD

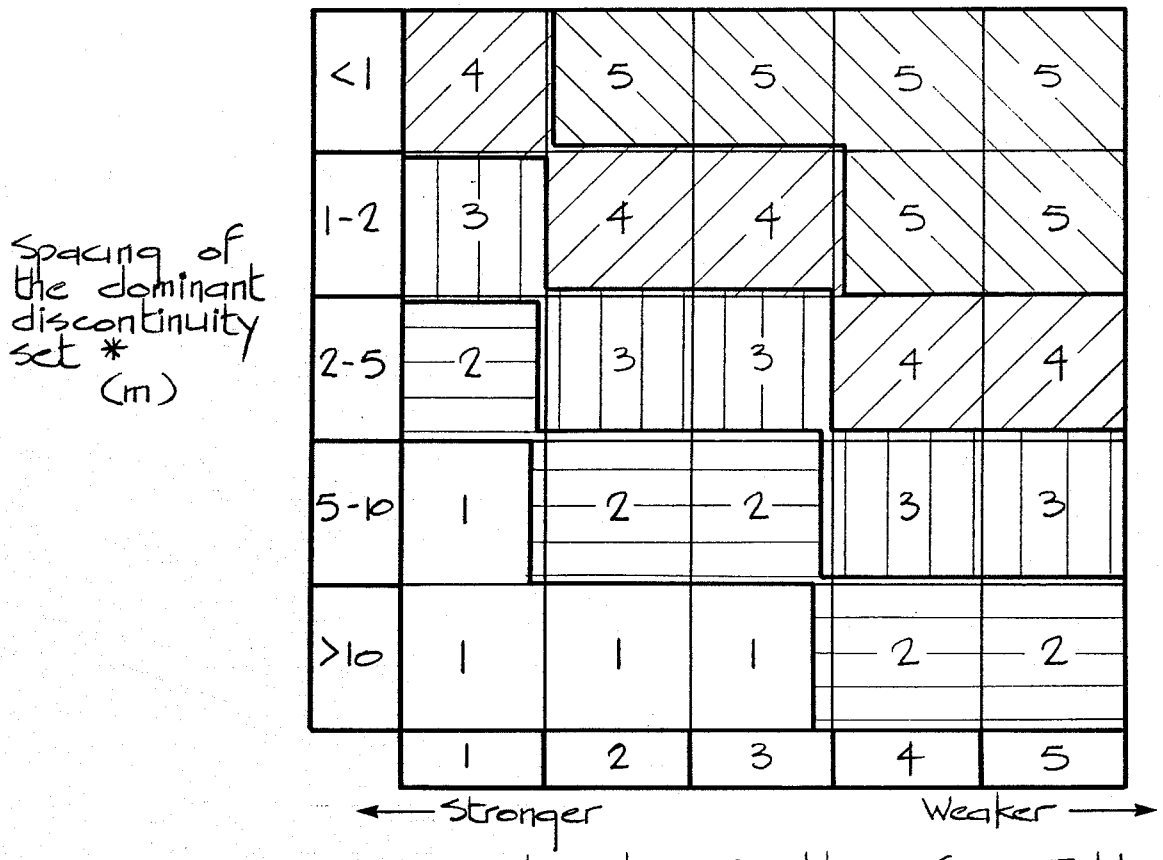

Class	Description
1.	Non-directional rock mass
2.	Weakly bedded or directionally jointed
3.	Moderately bedded or directionally jointed
4.	Strongly bedded or directionally jointed
5.	Very strongly bedded or directionally jointed

* The dominant discontinuity set must consist only of relatively straight, persistent joints (e.g. bedding joints) (persistence > 20m, curvature radius > 50m)

Figure 9 – Definition of Structural Anisotropy Classes

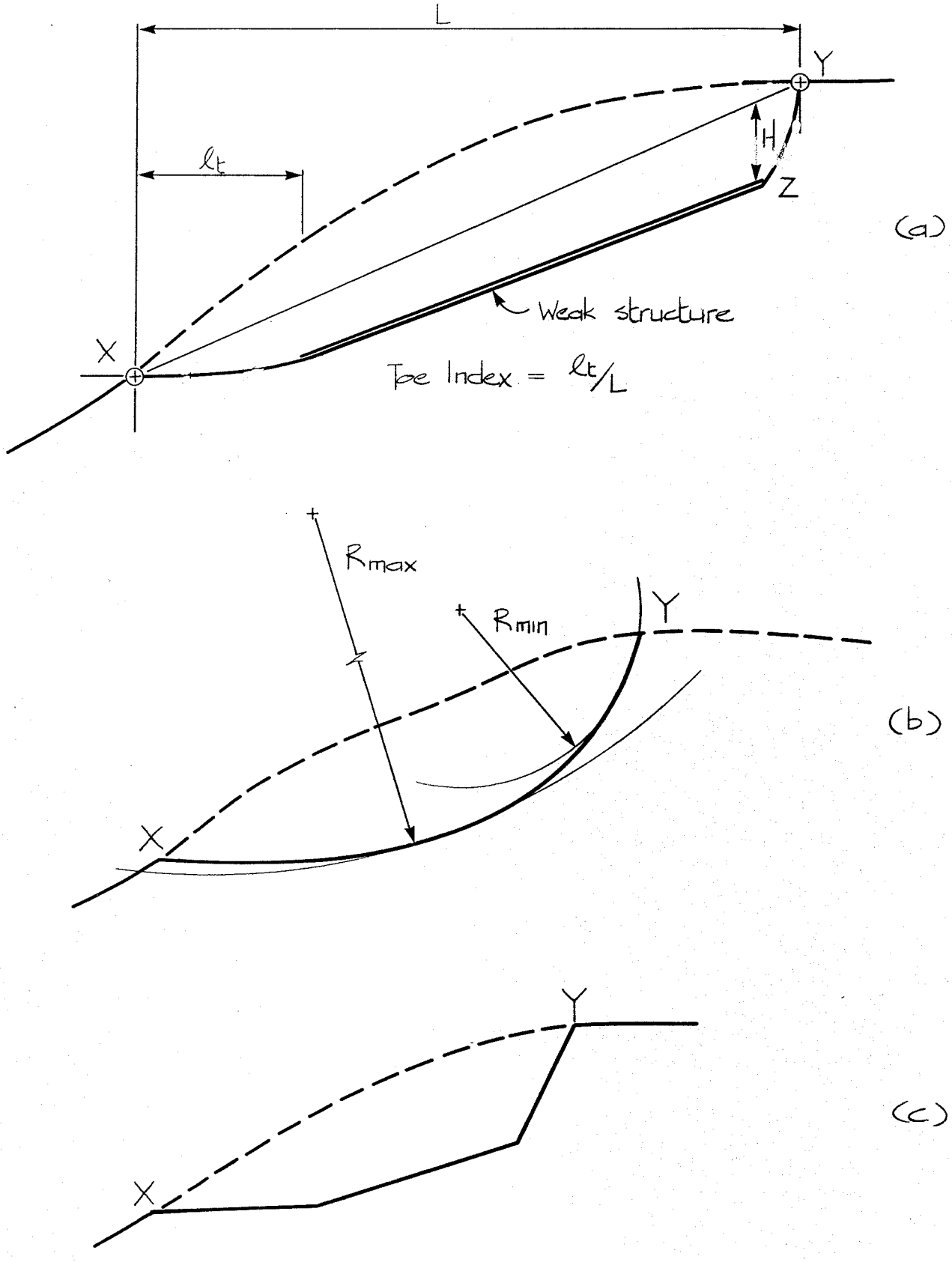

Figure 10 – (a) Toe Index definition
(b) Maximum and minimum curvature
(c) A segmented profile, curvature radius = 10,000

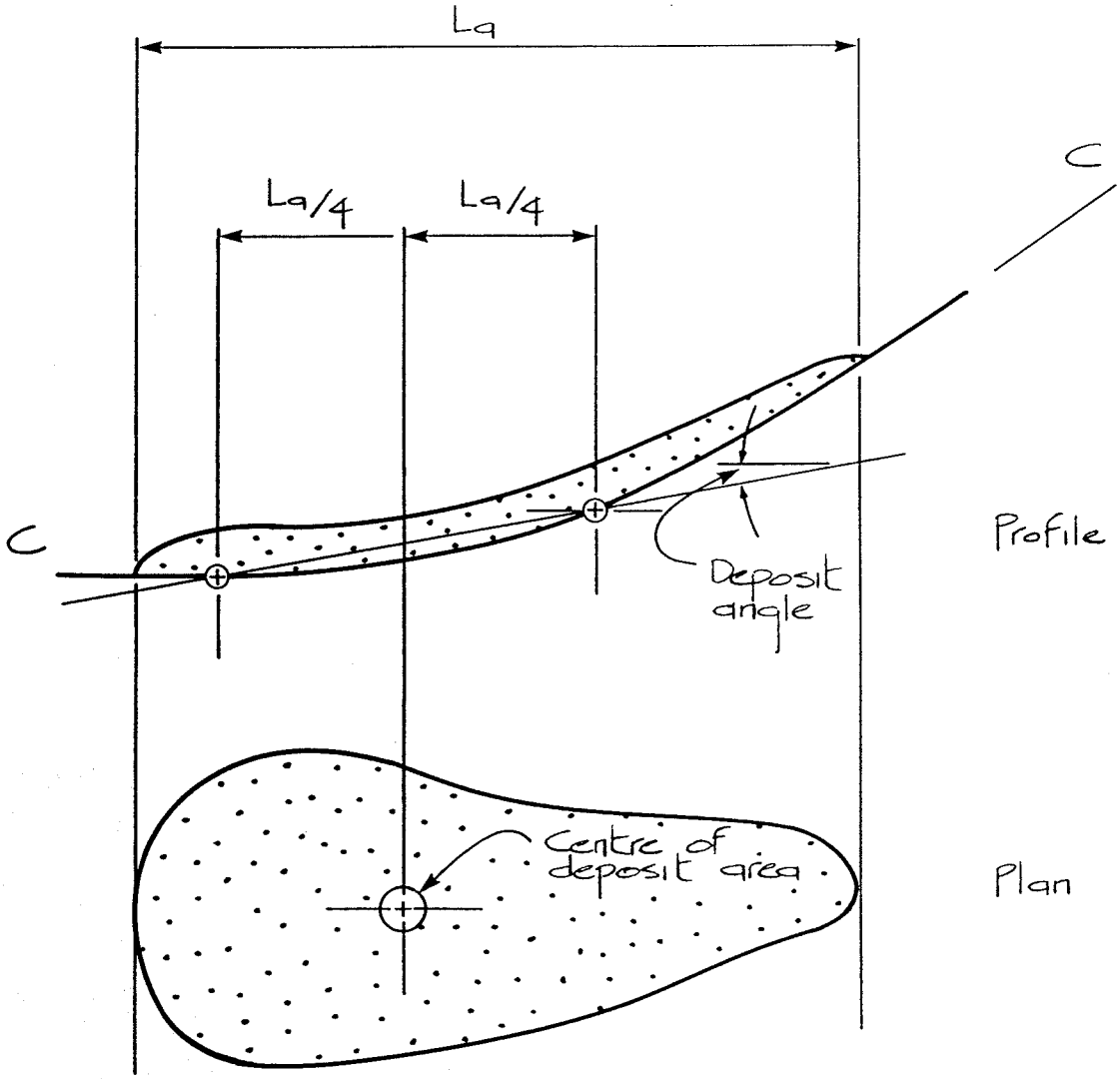

Figure 11 - Central angle of the deposit

APPENDIX B

MASS-REFERENCED FLOW MODEL FOR DYNAMIC SIMULATION OF FLOW SLIDES

1. MODEL DERIVATION

The mass-referenced flow model uses the standard equation of motion based on momentum conservation. The slide mass is divided into cells of a given volume. The motion equation is referenced to the moving centre of gravity of each cell. The cells are free to deform, but each maintains a constant volume during motion.

The forces acting on each cell are illustrated in Figure 1. They include:

- Gravity force (weight).
- Base shear resistance force T, which includes a constant (frictional) term, a linear (viscous) term and a square (turbulent) term.
- Lateral thrust forces P_1 and P_2. These forces are determined as hydrostatic pressures, if the material is considered to be a fluid. They are determined from the Rankine earth pressure theory if the material is a frictional medium:

$$P = \frac{\gamma h^2 k}{2} \qquad (1)$$

where k varies between an active earth pressure coefficient (typically 0.2 to 0.5) and passive coefficient (2 to 5), depending on the strain in the given cell. The change in the k coefficient is linearly related to strain through a pair of stiffness coefficients S (Figure 2).

The solution proceeds in small time steps. At the onset of each time step, the resultant of all forces on each cell is evaluated and the resulting acceleration calculated. Double numerical integration is used to determine the velocity and displacement of each element at the end of the time step.

The flow depths are adjusted at the end of the time step to maintain continuity. Lateral strains are determined and the corresponding k-coefficients calculated as shown in Figure 2. A set of new force resultants is then determined for the next time step.

2. MODEL APPLICATION

Figure 3 shows an application of the model to the classic dam break problem in perfect fluid. The Ritter's Solution, obtained by the Method of Characteristics, gives an estimate of the discharge at the site of the "dam", which remains unchanged for a long period of time, while waves progress both downstream and up into the reservoir. The computer model as shown provides an excellent simulation of the shape of the dam break wave and a nearly-exact estimate of the discharge.

An application of the model to the "shelf lobe" of the Avalanche Lake rockslide (Case 13 in Appendix C) is shown in Figure 4. The fluid resistance is calculated using the method of Koerner (1976), with a frictional and turbulent resistance term. The numerical values were chosen on the basis of a block model analysis.

The analysis shown in Figure 4 assumes the material to be a fluid, i.e. the k-coefficients always equal to 1.0. As could be expected, the moving mass spreads out rapidly while descending the slope, with waves extending from both the front and tail. At 26 seconds, the slide front reaches the mid-point of the runup slope and effectively halts there, as the material piles upon itself in the form a standing wave. No further progress of the slide is possible and the model becomes unstable after 30 seconds.

An equivalent result was obtained in a subsequent run, using perfect (inviscid) fluid. Thus, the fluid-based model cannot simulate the observed runup, as the moving mass lacks the internal rigidity required to mount the adverse slope.

Figure 5 shows the same analysis, repeated with equivalent resistance parameters. The material is in

this case assumed to be a frictional medium, with an internal friction angle equal to 45° and Rankine k-coefficients of 0.2 and 5.8 for the active and passive states respectively. The variation in the applicable earth pressure coefficients, depending on the level of strain in the successive cells, is also shown in the Figure.

The sliding mass shows much less longitudinal spreading than before. At 23 seconds, the frontal part reaches the passive condition due to its contact with the adverse slope, while the tail part remains in an active condition. At 29 seconds, most of the sliding body is compressing, as the leading front is hurled onto the shelf. At 39 seconds, the main part of the sliding body begins to fall back from the runup slope, while the leading front still continues to flow over the surface of the shelf.

These results at least qualitatively simulate all aspects of the observed runup.

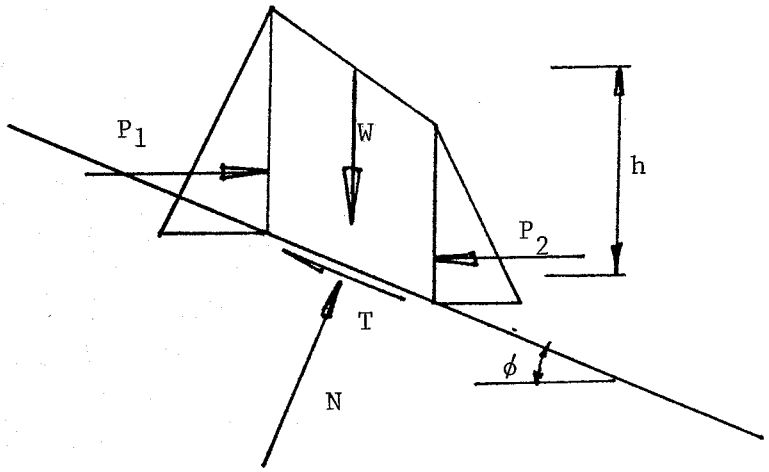

Figure 1, Forces acting on a single cell.

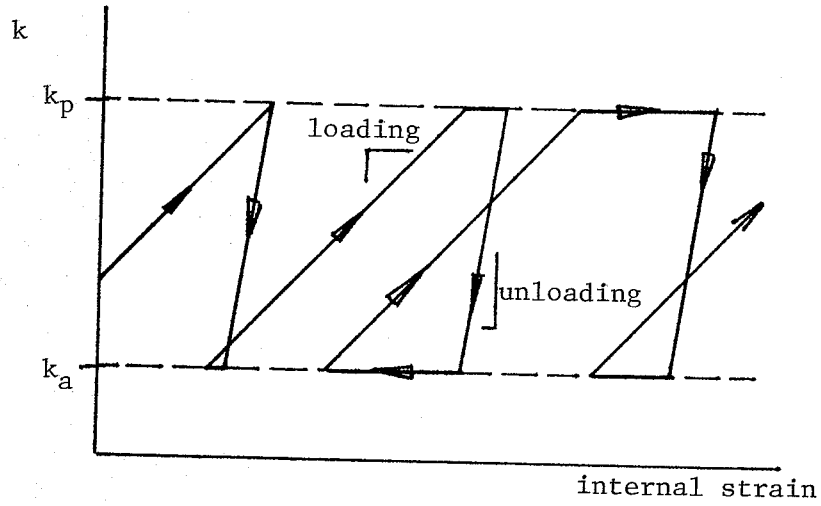

Figure 2, Relationship between lateral-pressure coefficient k and strain (compression positive).

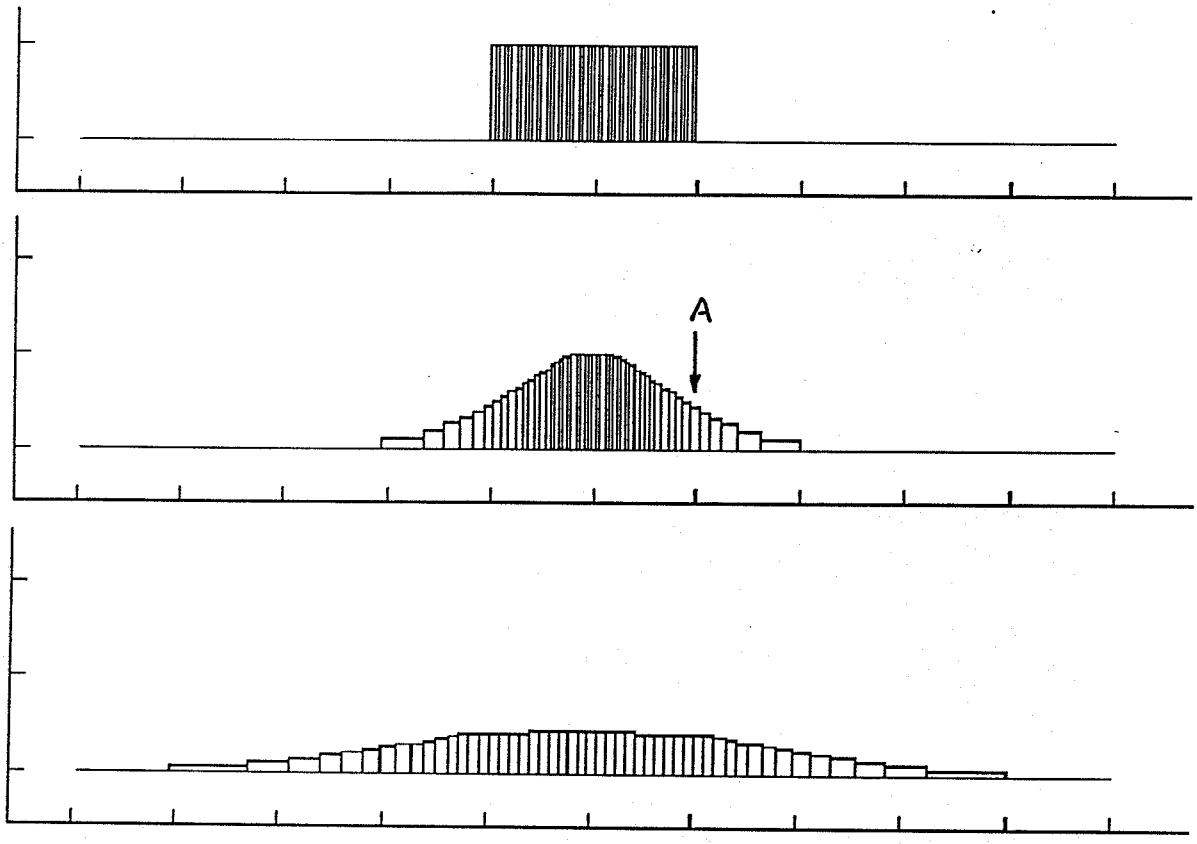

Figure 3 Dam break problem in a perfect fluid. One division equals 100 m. Discharge at Point A is 927 $m^3/sec/m$.

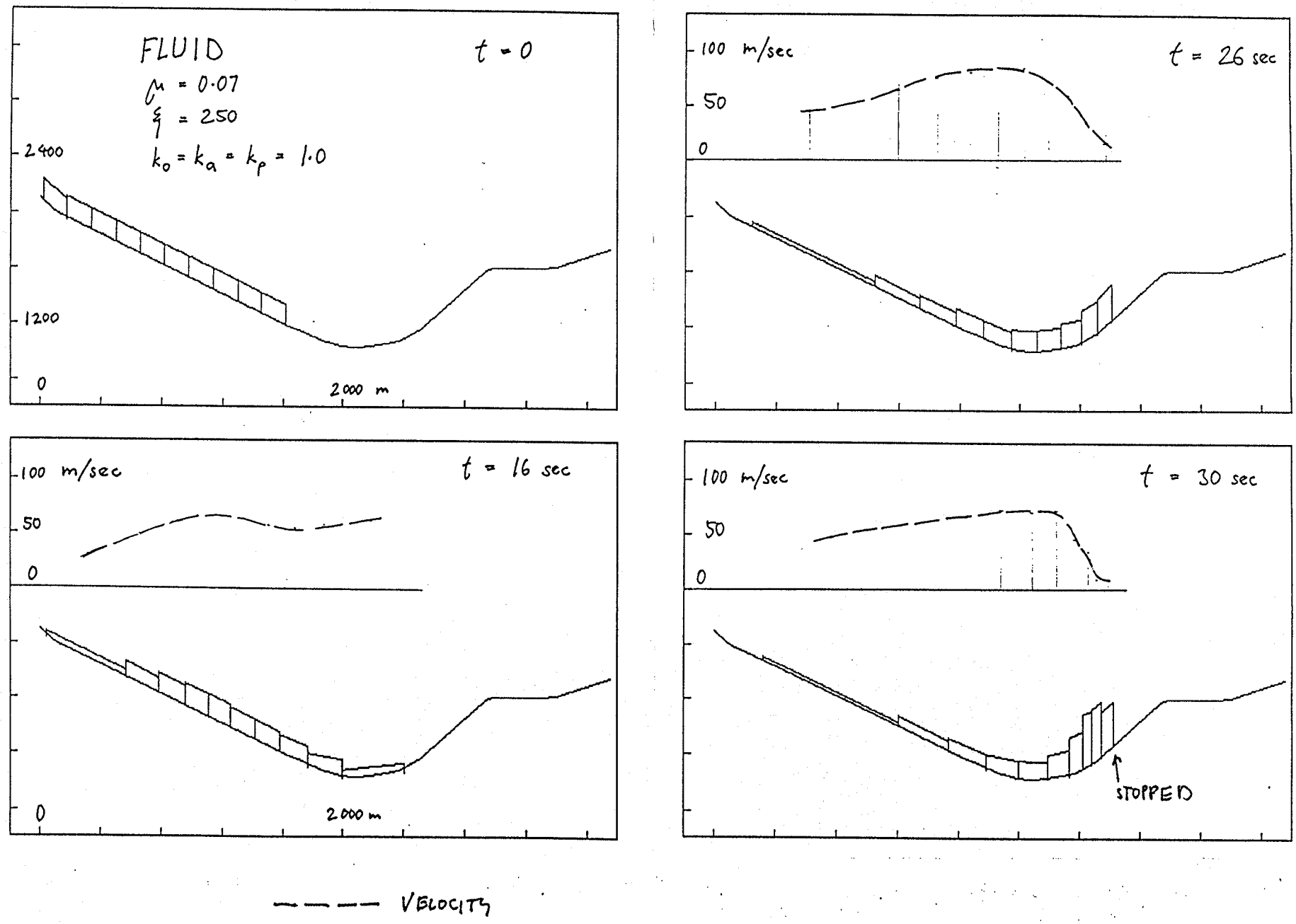

Figure 4 Avalanche Lake, shelf lobe, dynamic analysis using fluid properties.

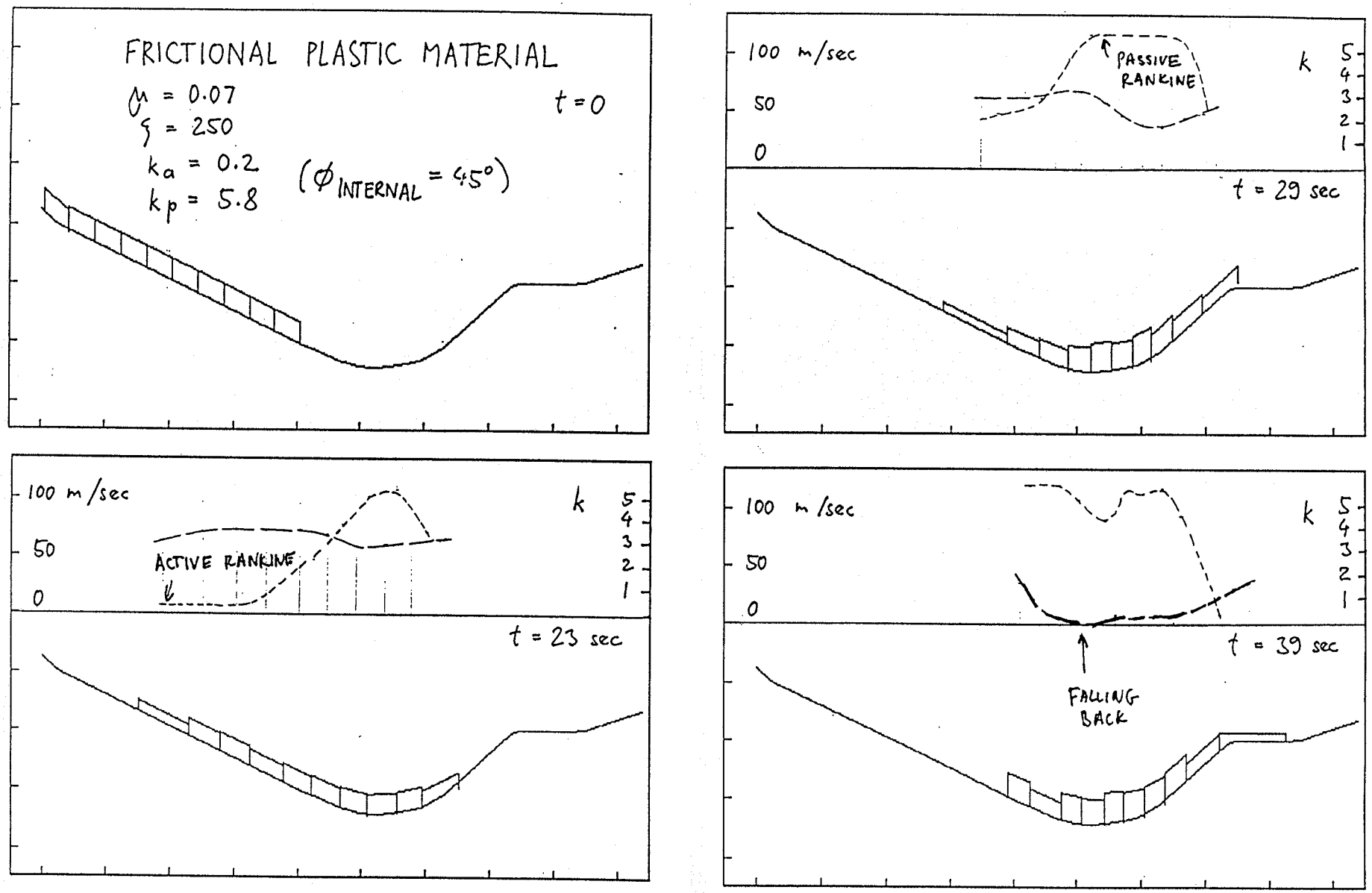

Figure 5 Avalanche Lake, shelf lobe, dynamic analysis using plastic model.

APPENDIX C

REPORTS FROM SITE VISITS

TABLE OF CONTENTS

1. MOUNT GRANIER (TYPE C)

LOCATION: Col du Granier, Isere Valley, 70 km east of Grenoble, France.

DATA BASE ENTRY: No. 18

PUBLISHED INFORMATION*: 7, 23, 39, 212, 213

OTHER INFORMATION AVAILABLE:

Topography 1:25,000, photos, rock samples.

GEOLOGY:

Gently folded beds of Cretaceous marls and limestones dip at 10 to 17° to the north, in the direction of movement. The upper part of the source mass was made up partly of limestones, including the massive Urgonian unit (Figure C.1). The lower two-thirds were mostly argillaceous units with the frequency of limestone interbeds decreasing downwards. A generalized cross-section of the equivalent Cretaceous sequence from the Massif de Plate site (70 km to the north-west) is shown in Figure C. The character of the rock mass in this sequence is uniform throughout the French Alps and the Jura Mountains (Dr. P. Antoine, pers. comm.).

The basal sliding surface was seated in the Vallanginian marly units, a good cross-section of which can be seen some 100 m east of the Col access road, near Elevation 800 m (Figure C.1b). The rock forms rhythmically alternating layers 10 to 20 cm thick, between buff coloured marl and greyish, stronger argillaceous limestone. The marl rock can be easily peeled with a pocket knife - very weak strength (U_c about 1 Mpa). It is slightly weathered (discoloured). The more carbonaceous layers are somewhat stronger. The bedding planes are tight, planar and

---

* Reference to record numbers in the Bibliography file, Appendix D.

slightly rough, coated with clay and silt particles. Apart from this coating, no clay fillings have been observed. The bedding dips 14° to the north. There are two or three non-persistent and tight vertical joint sets.

ORIGINAL SLOPE:

The slide detached from a large buttress, formed by the north-east edge of the frontal ridge of Massif de la Chartreuse. Goguel and Pachoud (1972) suggested a reconstruction of the original slope in the form of a pyramid. More likely, the detachment formed a block as shown schematically in Figure C.2, so that the original slope may have been as steep as the present back slope of the scar, which forms a near-vertical cliff over 600 m high.

FAILURE MECHANISM:

The most probable interpretation of the failure mechanism is a simple translational failure along a bedding plane in the Vallanginian marls (Cruden and Antoine, 1984 and Figure C.2). The sliding surface can still be found close to the present ground surface over a large area of the scar, although it is generally covered by a thin veneer of debris. An exposure of the sliding surface can be seen in the bed of a stream.

Judging from the extreme steepness of the eastern side scarp, it probably represents tensile detachment, from which the slide mass moved away in course of its glide down the bedding plane. Its contribution to the resisting forces was therefore minimal. The transverse width of the source area is unknown and, as a result, volume estimates range from 200 to 600 millions m^3.

No estimates of the velocity of the 1248 rock avalanche are available, but it was undoubtedly great, as the debris ran for more than 5 km over near horizontal ground.

The deposit is heavily cultivated by vineyards. The debris appears to have the predominant character of a mixture of clay, silt, sand and gravel with some small boulders. Large boulders derived from the Urgonian are rare on the surface. The boulders have been mined for construction stone since the Middle Ages and many may have disappeared as a result. Nevertheless, there is a remarkable contrast between the deposit of this slide and that of rock avalanches made up of stronger and more durable rock, such as the Frank Slide.

2. MASSIF DE PLATE (TYPE A)

LOCATION: Town of Servoz, 10 km west of Chamonix, France

DATA BASE ENTRY: No. 21

PUBLISHED INFORMATION: 23, 225

OTHER INFORMATION:

Topography 1:25,000 and 1:2,000 photos, airphotos, monitoring results.

GEOLOGY:

The same Cretaceous sequence as described in connection with Mont Granier. A generalized geological cross-section through the crest of the slope is shown in Figure C.3. The strata dip at 15 to 20° north (into the slope). The weak marly units are covered by colluvium and no exposures have been observed, except for prominent cliffs of the calcareous units.

ORIGINAL SLOPE:

The southern slope of Massif de Plate falls about 1,400 m towards the Arve River, at a mean angle of 21°. The upper part of the slope is topped by vertical cliffs of the Urgonian Limestone. The cliffs show many signs of subsidence and slumping, with local downward displacements of more than several hundred metres.

FAILURE MECHANISM:

Bedding and all other large structures in the slope dip into the slope and therefore do not participate in instability. Failure apparently occurs by deep rotational slumping of the slope crest under the weight of the Urgonian strata. Many such slumps can be observed in various stages of development.

The largest single failure on this slope is the Derochoir above Servoz (Figure C.4). The Derochoir is a semi-circular niche 1.5 km wide and 500 m deep in plan. Beneath it is a 15 to 20° slope covered by deep colluvium, which continues down into the river channel. Several villages, including Servoz are situated on the slide debris.

The summer, 1751 failure of the Derochoir was graphically described by an eyewitness (Donati), quoted by Eisbacher and Clague (1984, page 142). It is likely that the source area involved previously displaced terrain. After a winter of heavy snow, the slide began to subside and continued for over a month. It is clear from the description that the overall rate of failure was only moderate, perhaps some metres per hour. Rapid movements occurred only locally, due to toppling of slabs of the Urgonian, tilted by the underlying movements.

The displacements added to the colluvial masses on the lower slopes and may have lead to a gradual constriction of the river channel, as did similar movements a thousand years before. But no rock avalanche occurred. If there was a reservoir in the valley during the failure, it would not have been seriously affected.

The B.R.G.M. (Lyon) maintains instrumentation across tension cracks on the Rocher des Echines, a slightly subsided block west of the Derochoir. The movements have not exceeded 1 mm since 1983 but they have a steady trend and indicate gradual tilting of the block.

3. NANTUA (TYPE A)

LOCATION: Town of Nantua, Jura Mountains, 120 km north-east of Lyon, France.

DATA BASE ENTRY: Nil

PUBLISHED INFORMATION: 225

OTHER INFORMATION:

Unpublished geological sketches by the B.R.G.M. (Lyon). Photographs, monitoring data.

GEOLOGY:

The same Cretaceous sequence as described in connection with Mont Granier, consisting of calcareous marls surmounted by massive limestone. The bedding dips gently into the slope.

ORIGINAL SLOPE:

The town of Nantua lies in a U-shaped valley, cut some 400 m below the surface of the surrounding plateau. The slopes are talus covered, with angles of 30 to 35°, surmounted by a vertical cliff 100 m high.

FAILURE MECHANISM:

A segment of the limestone cliff 500 m long and up to 100 m wide, called Barre des Fecles has now subsided by a total of approximately 18 m vertically, and moved towards the valley by about 5 m, to open a system of cracks (Figure C.5). A volume of more than 5 million m^3 of rock is in motion, directly above the heavily populated centre of the town. The subsidence rate amounted to 40 mm per year in 1986, decreasing to about 10 mm in the following years. The failure mechanism inferred from the direction of the movement vectors is a rotational slump, as indicated in Figure C.5b.

The B.R.G.M. maintains a monitoring system by means of precise triangulation survey of permanent monuments. The surveys are conducted annually. Remedial measures include only rockfall control, as it is assumed that the large scale movements will remain slow.

4. CLAPIÉRE (TYPE H)

LOCATION: Near town of St. Étienne de Tinée, Maritime Alps, south-west France.

DATA BASE ENTRY: No. 19

PUBLISHED INFORMATION: 6, 114, 223

OTHER INFORMATION: Photographs, rock samples, monitoring data, unpublished reports.

GEOLOGY:

The valley of the Tinée River defines the boundary between Mesozoic sediments and the crystalline and metamorphic basement. The Clapiére landslide occurs in the metamorphic rocks of the north-east valley wall.

Most of the rock is a muscovite schist, weak to medium strong and highly fissile. Some layers exhibit higher percentage of amorphous minerals and could classify as gneiss. A prominent cliff-forming migmatite unit passes through the centre of the slide area (Barre d'Igliére).

The schistosity and relict bedding dips at 60° to 70° into the slope. However, immediately in and around the slide area, the dips are reduced to near horizontal by widespread flexural toppling.

ORIGINAL SLOPE:

The original slope rises to a relative elevation of about 1,500 m above the Tinée, sloping at about 20°. The lowest 800 m of the slope is oversteepened by glacial erosion, to an average angle of about 40°. The toppled segment of the slope coincides with the oversteepening.

FAILURE MECHANISM:

An interpretation of the failure mechanism was compiled by the Department of Public Works regional research office in Nice, on the basis of surficial mapping and monitoring (Follacci, 1987). The main elements of this interpretation are shown in Figure C.7. Figure C.7a is a cross-section of the valley, showing the main lithological units and structural attitudes. The position of the sliding surfaces is inferred. A hypothesis of failure development due to Follacci (1987) is summarized in Figure C.7b. The three stages include oversteepening of the toe by glacier, widespread flexural toppling and, finally, the development of discrete sliding surfaces.

The strong Iglière unit is discontinuous across the slide area. A hypothetical explanation of this is shown in Figure C.7c. This assumes that the main displacement discontinuity at the base of the sliding mass exploits breaks in the Iglière rock developed by toppling.

The toppling displacements are ancient and the Clapiére slope was stable throughout the historical period, although it was traversed by a series of step-like scarps. Active movements began in the early nineteen-eighties with the development of multiple fresh scarps and cracks in the slope. The movements accelerated to a worrisome extent by 1987, and a catastrophic failure was anticipated (see Figure 2.5 in the main report text). Today, the recent displacements total more than 100 m and a distinct back-scarp is visible (Figure C.8). However, the movement velocities have decreased substantially in recent years. Bulging of Quaternary sediments at the foot of the slope indicates that the failure surface passes under the valley floor.

The slope is being monitored by electronic distance and angle measuring devices. The Wild robot theodolite system was installed in 1990 and is now in use. Data are being transmitted to a central monitoring station in Lyon.

A dynamic analysis of a potential catastrophic failure was carried out by L. Rochet (1987). Based on the results, some houses on the valley floor and a road were relocated. Two drainage tunnels were designed, to prevent upstream flooding due to the potential damming of the Tinée. The first tunnel, 2,600 m long and 10 m^2 in cross-section is being completed. A second tunnel, about twice as long and large, is being planned but may not be built, as the decreased velocities brought about an impression of reduced urgency of the hazard.

5. TORREGGIO (TYPE H)

LOCATION: Val Malenco, 8 km north of Sondrio, northern Italy.

DATA BASE ENTRY: No. 35

PUBLISHED INFORMATION: Nil

OTHER INFORMATION: Topography at 1:50,000, rock samples, photographs.

GEOLOGY:

Muscovite schist with gneissic interbeds. The rock is weak to moderately strong, highly fissile and moderately weathered. The original schistosity dipped steeply into the slope. However, the present attitude of the schistosity is flatter, as a result of widespread flexural toppling. The toppling process lead to disturbance of the rock fabric, creating closely spaced fractures, many of which are open or infilled by a silty gouge (Figure C.9a).

ORIGINAL SLOPE:

The original slope rises about 1,200 m above the narrow channel of the Torreggio Torrent. The slide took place in the lowermost 600 m of the slope, which has an inclination of approximately 36°.

FAILURE MECHANISM:

The mechanism of the failure is equivalent to that of the Clapiére, as shown in Figure C.7b. The oversteepened valley wall failed by flexural toppling, which gradually developed into a slump based below the stream bed (Figure C.9b). The gradual cumulative displacements built up to many tens of metres by 1987. The major storm which affected the Valtellina Region in July 1987 caused a substantial sudden displacement of the slide mass.

This constricted the Torreggio channel, already under flooding conditions, and the subsequent rapid erosion of the slide debris triggered a major debris flow resulting in severe destruction in Val Malenco, as far as Sondrio.

Although sudden, the slide displacement probably did not involve catastrophic velocities. The stream channel was constricted gradually, not dammed up, and there was no runup on the opposite bank.

The slopes surrounding the slide scar are being monitored by ISMES (Bergamo). The lower channel of the Torreggio and the Mallero downstream of the slide are being provided by debris flow passage channellization and check dams. No remedial measures are being implemented at the slide site, probably due to poor foundation conditions for check dams.

6. SPRIANA (TYPE H)

LOCATION: Val Malenco, 4 km north of Sondrio, northern Italy.

DATA BASE ENTRY: Nil

PUBLISHED INFORMATION: Nil

OTHER INFORMATION: Topography 1:50,000 photographs, rock samples

GEOLOGY:

Gneiss and muscovite schist, moderately strong, fissile (Monte Canale Formation), lenses of dolomitic limestone. Schistosity dips steeply into the slope, but is affected by widespread flexural toppling.

ORIGINAL SLOPE:

36° to 1,200 m above the channel of the Mallero Torrent.

FAILURE MECHANISM:

This appears to be a complex flexural toppling displacement in relatively strong, but highly anisotropic rock (Figure C.10a). The slope is moderately steep and has been stable during the historic period: there are several small villages directly on the slide (now abandoned)(Figure C.10b). An acceleration of movements took place possibly as a result of toe undermining by the Mallero, during the July 1987 storm. The overall recent displacement is very small, however. Stone buildings on the slide have not been disturbed. The current movement rates are negligible.

7. BILLAN (TYPE H)

LOCATION: North-west bank of the Grande Maison reservoir, 1.5 km upstream from the dam, Isére, France.

DATA BASE ENTRY: Nil

PUBLISHED INFORMATION: 171

OTHER INFORMATION: Topography, 1:20,000, monitoring results, photographs, rock samples.

GEOLOGY:

Schists and greenstones in the upper part of the slope, calcareous shale (Lias) near the toe. Schistosity as well as the contact of the two units dip near vertically into the slope. However, the beds are rotated outwards by flexural toppling, to lie at a mean dip of about 35 to 45°. The maximum depth of toppling was determined by seismic profiling as less than 100 m (Figure C.11).

The schists are moderately strong to strong, moderately fissile and heavily fractured, with cleavage joints spaced typically at less than 10 cm. The Lias is weak and highly fissile.

ORIGINAL SLOPE:

30° average to a relative elevation of 1,000 m above the reservoir bottom. The lowermost 400 m are oversteepened to 38°.

FAILURE MECHANISM:

This is another example of a slope affected by large scale flexural toppling (Figure C.12).

During filling of the reservoir, in May 1986, a crack appeared above a bulge in the slope. A road traversing the centre of the bulge just above the Lias contact subsided by 240 mm over a period of one month.

During the following summer, Electricite de France constructed an 850 m long drainage gallery with a total of 1,300 m of drain holes. The movement rates were reduced to acceptable levels. The peak drainage flow rate from the gallery was 150 lps in the spring of 1987. A comprehensive permanent monitoring system is being maintained on the slide and is described in Dubie et al. (1988).

8. SECHILLIENNE (TYPE B)

LOCATION: Romanche Valley, 6 km east of Vizille, Isére, France.

DATA BASE ENTRY: No. 20

PUBLISHED INFORMATION: 133,224

OTHER INFORMATION: Topography at 1:20,000, rock samples, photographs.

GEOLOGY:

Alternating sericite schists and amphibolites. Schistosity is sub-vertical and strikes approximately perpendicular to the contours. The schist units are weak to medium strong, very fissile and often tightly folded or contorted. The amphibolite units, which appear to be predominant in surface exposures, are very strong and non-fissile, moderately jointed. There are several families of joints and minor faults, although none dip towards the valley.

ORIGINAL SLOPE:

The lower 600 m of the slope above the Romanche are oversteepened to an average angle of 40°. The top 500 m range from 10 to 30°.

FAILURE MECHANISM:

The crest of the steep lower segment of the slope underwent substantial displacements in prehistoric times, as shown by the existence of a complex system of depressions, scarps and pinnacles (hence the local name "Les Ruines"). Fresh movements developed gradually in the early nineteen-eighteens and were manifested in increasing intensity of rockfall from the "ruins". Great intensification of such activity occurred in the spring of 1985 and multiple tension cracks opened in the crest area (Figure C. 13).

The movement mechanism is obviously very complex, being controlled by several sets of non-pervasive joints and minor faults.

A monitoring system (wire extensometers, optical targets) was installed by the Department of Public Works. Some fissures opened by 1.5 m in four years at a relatively steady rate, except for yearly acceleration in the spring (Figure C.14). The dominant movement direction is oblique by about 45° to the slope line. Many of the tension cracks are near vertical, dipping opposite to the oblique movement direction, indicating that the movements have a toppling component. The toppling is not associated with the schistosity but is controlled by sub-vertical joint set. There is no indication of a sliding surface.

The most significant movements are concentrated in an area of approximately 300 x 300 m at the crest of the steep slope segment. An order of magnitude smaller movement rates have been registered over a large area reaching nearly to the summit of the slope.

The major movement rates have reduced during the last two years to 20 to 100 mm per year. The crest of the active zone has now lost several tens of thousands m^3 of material by means of continuing rockfall. Nevertheless, a partial collapse of the slope crest is expected and a protective berm has been built on the valley floor, to reduce the probability of a landslide dam being created. The berm was designed to contain a rock avalanche of up to 3.5 millions m^3 in magnitude.

9. DEFILE DE MAUPAS (TYPE B)

LOCATION:

DATA BASE ENTRY: Nil

PUBLISHED INFORMATION: Nil

OTHER INFORMATION: Topography at 1:20,000, photographs.

GEOLOGY: Granodiorite of the crystalline basement, very strong, massive, randomly jointed.

ORIGINAL SLOPE:

Ridge, 1,100 m in total height, the lower 500 m of height averages 52° (Figure C.14.b).

FAILURE MECHANISM:

Collapse of an irregular mass of rock along a series of random joints, possible minor faults (Figure C.14). No dominant structure can be identified. The slide scar is diamond shaped. Failure was sudden but runout was limited due to confinement of the valley and the small volume. The volume of the failure is approximately 1 million m^3. It occurred in 1989 and caused relocation of a road.

10. VAL POLA (TYPE D)

LOCATION: Val Tellina, 9 km south of Bormio, Northern Italy.

DATA BASE ENTRY: No. 22.

PUBLISHED INFORMATION: 35, 149, 221

OTHER INFORMATION:

Topography at 1:50,000, 1:20,000, rock samples, photographs.

GEOLOGY:

Diorite, gabbro, ortho-quartzite, lesser amounts of gneiss. Typical rock fragments in the deposit are very strong. Rock in the source area must have been heavily fractured and weathered, judging by the small size of the debris fragments and widespread brown discoloration. The source area has a set of bedding joints dipping 32° at Azimuth 10°, i.e. 60° counterclockwise of the slope direction. Major faults traverse the slope. A fault plane dipping at 40° at Azimuth 70° (downslope direction) formed the back scarp of the side. Another fault, coinciding with the heavily eroded Val Pola ravine, formed the northern margin of the slide.

ORIGINAL SLOPE:

A ridge between two hanging valleys of the Mount Zandilla Massif. The average slope was 32° to an elevation 1300 m above the Adda River valley. The slope was deeply incised by the Val Pola ravine just north of the source area. The source area toe was 500 m above the floor of the valley. The source was an ancient slide mass which had subsided by about 100 m in prehistoric time. The back scarp of this slide mass was sufficiently well defined to be mapped on the 1:50,000 Swiss topographic map (Figure C.15a).

FAILURE MECHANISM

The slide mechanism is fully determined by major structures: a major fault in the back scarp, another fault to the north and relict bedding/schistosity planes in the south. The resulting shape is a remarkably regular compound wedge (Figure C.15b). The slide mass had to deform internally to be able to slide from the scar.

The failure occurred during the July 1987 Valtellina storm which caused catastrophic damage in the region through flooding, landsliding and erosion. The course of events leading to the failure is described by Govi (1989). The Adda Valley was devastated by flooding during the first few days of the storm. On July 25, 1987, a 600 m long fissure opened along the base of the crown scarp of the Val Pola Slide mass. Debris flows and rockfalls occurred with increasing frequency over the next two days (the main precipitation event ended on July 22). The failure of the Val Pola Slide occurred on July 28. The rock mass initially shifted slowly towards the north, parallel with the dip direction of the bedding joints. Subsequently, it collapsed towards the valley, forming a rock avalanche. The debris deposit contains an estimated 45 million m^3, compared with 32 to 33 million removed from the scar (Anon., 1988).

The slide debris, observed in 1990 following extensive earthworks to stabilize the slide dam, consists of fragments with a modal size of only about 50 - 100 mm and 30 to 50% sandy matrix. Only a few boulder sized particles can be seen. This contrasts strongly with the bouldery nature of debris at the Hope Slide or Frank.

The Italian government carried out an impressive reconstruction scheme including temporary pumping of the Adda discharge followed by the construction of a permanent drainage tunnel, reshaping of the debris deposit and the construction of a spillway reinforced by concrete sills and erosion-resisting grids. The total cost of the slide is said to have been $200 M, but this is only a fraction of the total damage caused by the Valtellina storm.

11. DIABLERETS (TYPE E)

LOCATION:

DATA BASE ENTRY: No. 17.

PUBLISHED INFORMATION: 7, 23

OTHER INFORMATION: Rock samples, photographs.

GEOLOGY:

Urgonian Limestone, overlying calcareous slate. This is a similar stratigraphic sequence as described at Mount Granier and Massif de Plate, but slightly metamorphosed. The limestone is very strong and massive, the slate is sandy, medium strong and moderately fissile. The strata dip gently into the slope. Heim (1932) shows the hinge of a minor anticline coinciding with the face of the slope. The curvature of the bedding due to the fold results in a segment of rock dipping towards the valley at the face of the slope.

ORIGINAL SLOPE

The original surface of the source area is a sharp ridge sloping at 50° in two directions and over 1,000 m high.

FAILURE MECHANISM

The failure scar is a narrow rectangular niche in the ridge, with a flat base. Most of the sliding surface appears to have cut through the rock mass nearly perpendicular to bedding in a manner similar to that of the back scarp of the Frank Slide (Figure C.17). There is no sign of any weak surfaces (faults, major joints) in the back and side scarps of the source area. Failure may have been triggered by a forward slip of the base of the source block along bedding planes.

The failure created a rock avalanche involving about 30 million m^3 which streamed first across the valley and then along its axis. The overall displacement is rather limited, possibly because of lack of loose saturated material in the slide path.

12. ROCKSLIDE PASS (TYPE C)

LOCATION: Mackenzie Mountains, Northwest Territories, (127° 45'W, 63° 20'N).

DATA BASE ENTRY: No. 28.

PUBLISHED INFORMATION: 34, 194, 196, 219

OTHER INFORMATION:

Topography at 1:50,000, samples of clay gouge, photographs.

GEOLOGY:

Dolomite with siltstone interbeds in the lower part of the section. The rock is generally strong to very strong, thinly bedded to massive. Monocline, dipping uniformly at 11 to 13° in the direction of sliding. The bedding planes are moderately rough and very planar and straight. They are generally tight and unweathered. An exception is a thin clay seam located at the base of sliding, as described below.

ORIGINAL SLOPE

The original slope was a major buttress marking the end of a ridge. Its front was probably nearly 45° steep and approximately 800 m high.

FAILURE MECHANISM

The failure mechanism appears identical to that of Mount Granier shown in Figure C.2. The 600 m high breakaway scarp resembles that of Granier, although it is situated behind the unstable mass, rather than to the side of it as in the European example. The failure occurred by gliding along the gently inclined basal plane, which daylighted just above the valley floor at the toe of the slope.

The basal shear plane must have been exceptionally weak, as it facilitated not only the main detachment of some 450 millions m^3, but also a small adjacent slide situated a short distance south of the main scar (Figure C.18a). This slide is a reduced "copy" of the main detachment. It contains a volume of only approximately 200,000 m^3. The unstable block, 20 m thick on average, slid over the same horizon as the main slide, dipping 12° and displaced about 200 m to the toe of the slope, then broke up and steamed a short distance along the valley floor.

We attempted to find the weak layer. The sliding surface exposed on the main slide scar is covered by a carbonaceous siltstone broken up by frost action to sand and gravel sizes and underlain some tens of centimetres deep by a hard, rough intact rock surface. There are no traces of slickensides or clay. We were not successful in locating the weak surface in exposures behind the slide scar. One of these exposures is shown in Figure C.18b. Careful inspection of a complete 20 m stratigraphic column centered on the basal sliding surface revealed no layer weaker than moderately strong siltstone and no clay.

We made an excavation at the uphill margin of the small slide scar (the location of persons in Figure C.18a) and found a bedding plane containing infilling of moderately plastic clay 5 to 20 mm thick, aligned precisely with the sliding surface. The clay was enclosed between moderately rough walls of strong siltstone rock. There were no traces of slickensiding in the wall rock.

The best explanation of the above findings is that the failure surface exploited a bedding plane in siltstone rock, which was pre-sheared for a certain distance behind the valley wall due to stress relief. This hypothesis is illustrated in Figure C.19. Earthquake trigger for the failure is very likely, and may explain the high mobility of the smaller slide.

The distribution of debris gives a strong impression that the rock mass travelled initially as a coherent block, only disintegrating after contacting the valley floor. After disintegration, the frontal part of the slides developed into a rock avalanche.